Midwest Pooled Fund Research Program
Fiscal Year 2019 (Year 30)
Research Project Number TPF-5(430) Supplement 1
NDOT Sponsoring Agency Code RPFP-20-MGS-2

EVALUATION OF MIDWEST GUARDRAIL SYSTEM WITH REDUCED EMBEDMENT AND REDUCED POST SPACING FOR LOW-FILL CULVERTS AND OTHER APPLICATIONS

Submitted by

Tewodros Yosef, Ph.D.
Post-Doctoral Research Associate

Mojdeh Asadollahi Pajouh, Ph.D., P.E.
Research Assistant Professor

Robert Bielenberg, M.S.M.E.
Research Engineer

Ronald K. Faller, Ph.D., P.E.
Research Professor & MwRSF Director

MIDWEST ROADSIDE SAFETY FACILITY
Nebraska Transportation Center
University of Nebraska-Lincoln

Main Office
Prem S. Paul Research Center at Whittier School
Room 130, 2200 Vine Street
Lincoln, Nebraska 68583-0853
(402)472-0965

Outdoor Test Site
4630 N.W. 36th Street
Lincoln, Nebraska 68524

Submitted to

MIDWEST POOLED FUND PROGRAM
Nebraska Department of Transportation
1500 Nebraska Highway 2
Lincoln, Nebraska 68502

MwRSF Research Report No. TRP-03-468-23

April 24, 2023

TECHNICAL REPORT DOCUMENTATION PAGE

1. Report No. TRP-03-468-23	**2. Government Accession No.**	**3. Recipient's Catalog No.**
4. Title and Subtitle Evaluation of Midwest Guardrail System with Reduced Embedment and Reduced Post Spacing for Low-Fill Culverts and Other Applications		**5. Report Date** April 24, 2023 **6. Performing Organization Code**
7. Author(s) Yosef, T., Asadollahi Pajouh, M., Bielenberg, R.W., and Faller, R.K.		**8. Performing Organization Report No.** TRP-03-468-23
9. Performing Organization Name and Address Midwest Roadside Safety Facility (MwRSF) Nebraska Transportation Center University of Nebraska-Lincoln Main Office: Prem S. Paul Research Center at Whittier School Room 130, 2200 Vine Street Lincoln, Nebraska 68583-0853 Outdoor Test Site: 4630 N.W. 36th Street Lincoln, Nebraska 68524		**10. Work Unit No.** **11. Contract** TPF-5(430) Supplement #1
12. Sponsoring Agency Name and Address Midwest States Pooled Fund Program Nebraska Department of Roads 1500 Nebraska Highway 2 Lincoln, Nebraska 68502		**13. Type of Report and Period Covered** Final Report: 2020-2023 **14. Sponsoring Agency Code** RPFP- 20-MGS-2

15. Supplementary Notes
Prepared in cooperation with U.S. Department of Transportation, Federal Highway Administration

16. Abstract

The objective of this research effort was to evaluate the use of the Midwest Guardrail System (MGS) with reduced post embedment and potentially with reduced post spacing to satisfy *Manual for Assessing Safety Hardware* (MASH) Test Level 2 (TL-2) and TL-3 criteria when installed over low-fill culverts. The goal was to identify the shallowest post configuration that would meet TL-2 and TL-3 criteria, focusing on MGS post embedment depths between 28 and 40 in.

A series of bogie tests, test nos. LFCB-1 through LFCB-6, were performed on a steel W6x8.5 post embedded in MASH strong soil at 36, 32, and 28-in. embedment depths. These tests did not provide the desired data regarding the soil response due to yielding of the posts and relatively stiff soil. As such, three additional bogie tests, test nos. LFCB-7 through LFCB-9, were conducted on W6x16 steel posts with 40, 34, and 28-in. embedment depths. A W6x16 steel post was used to eliminate the possibility of post yielding for soil calibration purposes only. Next, the test results were used to develop simplified numerical modeling of the soil-post system under impact. The updated soil spring models were used in LS-DYNA models to replicate W6x8.5-post bogie tests (i.e., test nos. LFCB-1 through LFCB-6). Modifications were incorporated into the LS-DYNA models for a better prediction of overall post behavior. The validated soil spring models were incorporated into the full MGS model. A series of LS-DYNA simulations were conducted on the MGS with the shallowest embedment of 28 in. and standard embedment of 40 in. at TL-2 and TL-3 impact conditions, with full-, half-, and quarter-post spacings. Also, considering the variability of soil strength and its effect on soil-post behavior, a lower bound and an upper bound were adopted for the soil strength curve. In all simulations, the 2270P vehicle model was captured safely and all MASH criteria were met. Based on the simulation results, it was found that the MGS with the shallow embedment depth of 28 in. and half-post spacing would have dynamic deflection and working width similar to the baseline MGS with a 40-in. embedment depth and full post spacing at TL-2 and TL-3 impact conditions with no transition required. Thus, this MGS configuration was recommended for further full-scale crash testing under MASH test designation no. 3-11.

17. Key Words Highway Safety, Crash Test, Roadside Appurtenances, Compliance Test, MASH 2016, Component Test, Reduced Post Embedment, MGS, Reduced Post Spacing, LS-DYNA.		**18. Distribution Statement** No restrictions. This document is available through the National Technical Information Service. 5285 Port Royal Road, Springfield, VA 22161	
19. Security Classification (of this report) Unclassified	**20. Security Classification (of this page)** Unclassified	**21. No. of Pages** 221	**22. Price**

Form DOT F 1700.7 (8-72) Reproduction of completed page authorized

DISCLAIMER STATEMENT

This material is based upon work supported by the Federal Highway Administration, U.S. Department of Transportation and the Midwest Pooled Fund Program under TPF-5(430) Supplement 1. The contents of this report reflect the views and opinions of the authors who are responsible for the facts and the accuracy of the data presented herein. The contents do not necessarily reflect the official views or policies of the University of Nebraska-Lincoln, state highway departments participating in the Midwest Pooled Fund Program nor the Federal Highway Administration, U.S. Department of Transportation. This report does not constitute a standard, specification, or regulation. Trade or manufacturers' names, which may appear in this report, are cited only because they are considered essential to the objectives of the report. The United States (U.S.) government and the State of Nebraska do not endorse products or manufacturers.

UNCERTAINTY OF MEASUREMENT STATEMENT

The Midwest Roadside Safety Facility (MwRSF) has determined the uncertainty of measurements for several parameters involved in standard full-scale crash testing and non-standard testing of roadside safety features. Information regarding the uncertainty of measurements for critical parameters is available upon request by the sponsor and the Federal Highway Administration.

ACKNOWLEDGEMENTS

The authors wish to acknowledge several sources that made a contribution to this project: (1) the Midwest Pooled Fund Program funded by the California Department of Transportation, Florida Department of Transportation, Georgia Department of Transportation, Hawaii Department of Transportation, Illinois Department of Transportation, Indiana Department of Transportation, Iowa Department of Transportation, Kansas Department of Transportation, Kentucky Department of Transportation, Minnesota Department of Transportation, Missouri Department of Transportation, Nebraska Department of Transportation, New Jersey Department of Transportation, North Carolina Department of Transportation, Ohio Department of Transportation, South Carolina Department of Transportation, South Dakota Department of Transportation, Utah Department of Transportation, Virginia Department of Transportation, Wisconsin Department of Transportation, and Wyoming Department of Transportation for sponsoring this project; and (2) MwRSF personnel for constructing the barriers and conducting the component tests, and (3) the Holland Computing Center at the University of Nebraska, which receives support from the Nebraska Research Initiative, for providing computational resources. Acknowledgment is also given to the following individuals who contributed to the completion of this research project.

Midwest Roadside Safety Facility
J.C. Holloway, M.S.C.E., Research Engineer & Assistant Director –Physical Testing Division
K.A. Lechtenberg, M.S.M.E., Research Engineer
S.K. Rosenbaugh, M.S.C.E., Research Engineer
C.S. Stolle, Ph.D., Research Assistant Professor
J.S. Steelman, Ph.D., P.E., Associate Professor
B.J. Perry, M.E.M.E., Research Associate Engineer
A.T. Russell, B.S.B.A., Testing and Maintenance Technician II
E.W. Krier, B.S., Former Engineering Testing Technician II
D.S. Charroin, Engineering Testing Technician II

Midwest Roadside Safety Facility, Cont.
R.M. Novak, Engineering Testing Technician II
S.M. Tighe, Engineering Testing Technician I
T.C. Donahoo, Engineering Testing Technician I
J.T. Jones, Engineering Testing Technician I
C. Charroin, Temporary Engineering Construction Testing Technician I
T. Shapland, Temporary Engineering Construction Testing Technician I
E.L. Urbank, B.A., Research Communication Specialist
Z.Z. Jabr, Engineering Technician
Undergraduate and Graduate Research Assistants

California Department of Transportation
Bob Meline, Chief, Roadside Safety Research Branch
David Whitesel, P.E., Transportation Engineer
John Jewell, P.E., Senior Transportation Engineer, Specialist

Florida Department of Transportation
Derwood C. Sheppard, Jr., P.E., Design Standards Publication Manager, Roadway Design Engineer

Georgia Department of Transportation
Christopher Rudd, P.E., State Design Policy Engineer
Frank Flanders IV, P.E., Assistant State Design Policy Engineer

Hawaii Department of Transportation
James Fu, P.E., State Bridge Engineer
Dean Takiguchi, P.E., Engineer, Bridge Design Section
Kimberly Okamura, Engineer, Bridge Design Section

Illinois Department of Transportation
Filiberto Sotelo, P.E., Engineering Policy Unit Chief
Martha Brown, P.E., Safety Evaluation Unit Chief

Indiana Department of Transportation
Katherine Smutzer, P.E., Standards Engineer
Elizabeth Phillips, P.E., Highway Design Director

Iowa Department of Transportation
Chris Poole, P.E., Roadside Safety Engineer
Daniel Harness, P.E., Transportation Engineer Specialist
Stuart Nielsen, P.E., Transportation Engineer Administrator, Design

Kansas Department of Transportation
Ron Seitz, P.E., Director of Design
Scott King, P.E., Road Design Bureau Chief
Brian Kierath Jr., Engineering Associate III, Bureau of Road Design

Kentucky Department of Transportation
Jason J. Siwula, P.E., Assistant State Highway Engineer
Kevin Martin, P.E., Transportation Engineer Specialist
Gary Newton, Engineering Tech III, Design Standards

Minnesota Department of Transportation
Michael Elle, P.E., Design Standards Engineer
Michelle Moser, P.E., Assistant Design Standards Engineer

Missouri Department of Transportation
Sarah Kleinschmit, P.E., Policy and Innovations Engineer

Nebraska Department of Transportation
Phil TenHulzen, P.E., Design Standards Engineer
Jim Knott, P.E., Construction Engineer
Mick Syslo, P.E., State Roadway Design Engineer
Brandon Varilek, P.E., Materials and Research Engineer & Division Head
Mark Fischer, P.E., PMP, Research Program Manager
Lieska Halsey, Research Project Manager
Angela Andersen, Research Coordinator
David T. Hansen, Internal Research Coordinator
Jodi Gibson, Former Research Coordinator

New Jersey Department of Transportation
Hung Tang, P.E., Principal Engineer, Transportation
Joseph Warren, Assistant Engineer, Transportation

North Carolina Department of Transportation
Neil Mastin, P.E., Manager, Transportation Program Management – Research and Development
D. D. "Bucky" Galloway, P.E., CPM, Field Operations Engineer
Brian Mayhew, P.E., State Traffic Safety Engineer
Joel Howerton, P.E., Plans and Standards Engineer

Ohio Department of Transportation
Don Fisher, P.E., Roadway Standards Engineer

South Carolina Department of Transportation
J. Adam Hixon, P.E., Design Standards Associate
Mark H. Anthony, P.E., Letting Preparation Engineer
Henry Cross, P.E., Design Standards Engineer
Jason Hall, P.E., Engineer

South Dakota Department of Transportation
David Huft, P.E., Research Engineer
Randy Brown, P.E., Standards Engineer

Utah Department of Transportation
Shawn Debenham, Traffic and Safety Specialist
Glenn Blackwelder, Operations Engineer

Virginia Department of Transportation
Charles Patterson, P.E., Standards/Special Design Section Manager
Andrew Zickler, P.E., Complex Bridge Design and ABC Support Program Manager

Wisconsin Department of Transportation
Erik Emerson, P.E., Standards Development Engineer
Rodney Taylor, P.E., Roadway Design Standards Unit Supervisor

Wyoming Department of Transportation
William Wilson, P.E., Architectural and Highway Standards Engineer

Federal Highway Administration
David Mraz, Division Bridge Engineer, Nebraska Division Office

SI* (MODERN METRIC) CONVERSION FACTORS

APPROXIMATE CONVERSIONS TO SI UNITS

Symbol	When You Know	Multiply By	To Find	Symbol
		LENGTH		
in.	inches	25.4	millimeters	mm
ft	feet	0.305	meters	m
yd	yards	0.914	meters	m
mi	miles	1.61	kilometers	km
		AREA		
in^2	square inches	645.2	square millimeters	mm^2
ft^2	square feet	0.093	square meters	m^2
yd^2	square yard	0.836	square meters	m^2
ac	acres	0.405	hectares	ha
mi^2	square miles	2.59	square kilometers	km^2
		VOLUME		
fl oz	fluid ounces	29.57	milliliters	mL
gal	gallons	3.785	liters	L
ft^3	cubic feet	0.028	cubic meters	m^3
yd^3	cubic yards	0.765	cubic meters	m^3
		NOTE: volumes greater than 1,000 L shall be shown in m^3		
		MASS		
oz	ounces	28.35	grams	g
lb	pounds	0.454	kilograms	kg
T	short ton (2,000 lb)	0.907	megagrams (or “metric ton”)	Mg (or "t")
		TEMPERATURE (exact degrees)		
°F	Fahrenheit	5(F-32)/9 or (F-32)/1.8	Celsius	°C
		ILLUMINATION		
fc	foot-candles	10.76	lux	lx
fl	foot-Lamberts	3.426	candela per square meter	cd/m^2
		FORCE & PRESSURE or STRESS		
lbf	poundforce	4.45	newtons	N
lbf/in^2	poundforce per square inch	6.89	kilopascals	kPa

APPROXIMATE CONVERSIONS FROM SI UNITS

Symbol	When You Know	Multiply By	To Find	Symbol
		LENGTH		
mm	millimeters	0.039	inches	in.
m	meters	3.28	feet	ft
m	meters	1.09	yards	yd
km	kilometers	0.621	miles	mi
		AREA		
mm^2	square millimeters	0.0016	square inches	in^2
m^2	square meters	10.764	square feet	ft^2
m^2	square meters	1.195	square yard	yd^2
ha	hectares	2.47	acres	ac
km^2	square kilometers	0.386	square miles	mi^2
		VOLUME		
mL	milliliter	0.034	fluid ounces	fl oz
L	liters	0.264	gallons	gal
m^3	cubic meters	35.314	cubic feet	ft^3
m^3	cubic meters	1.307	cubic yards	yd^3
		MASS		
g	grams	0.035	ounces	oz
kg	kilograms	2.202	pounds	lb
Mg (or "t")	megagrams (or “metric ton”)	1.103	short ton (2,000 lb)	T
		TEMPERATURE (exact degrees)		
°C	Celsius	1.8C+32	Fahrenheit	°F
		ILLUMINATION		
lx	lux	0.0929	foot-candles	fc
cd/m^2	candela per square meter	0.2919	foot-Lamberts	fl
		FORCE & PRESSURE or STRESS		
N	newtons	0.225	poundforce	lbf
kPa	kilopascals	0.145	poundforce per square inch	lbf/in^2

*SI is the symbol for the International System of Units. Appropriate rounding should be made to comply with Section 4 of ASTM E380.

TABLE OF CONTENTS

LIST OF FIGURES

LIST OF TABLES

1 INTRODUCTION

1.1 Problem Statement

Roadside safety hardware requires special consideration at culverts. Soil fill is often provided over culverts, but the depth is not generally sufficient to install standard 6-ft long Midwest Guardrail System (MGS) posts. Inadequate post embedment can adversely affect the guardrail's performance. Various methods have been developed to enable post attachment to culvert structures. However, it may be desirable to use more closely spaced posts at a reduced embedment rather than introduce new hardware to state maintenance inventories. Since the performance of the MGS with post embedment depths less than 35 in. has not been evaluated, a need exists to determine the potential for using reduced post embedment and/or reduced post spacing with the MGS to span low-fill culverts under *Manual for Assessing Safety Hardware* (MASH) Test Level 2 (TL-2) and Test Level 3 (TL-3) impact conditions [1].

1.2 Background

Three types of guardrail systems are generally used to treat culverts: (1) long-span guardrail systems [1]; (2) strong-post guardrail systems anchored to the top slab of the culvert [3-6]; and (3) weak-post guardrail systems mounted to the outer face of the culvert headwall (e.g., weak-post, guardrail system bridge railing) [7, 8] or weak posts anchored to the top of the slab using socketed connections [9, 10]. Long-span guardrail systems are simpler to install but are limited by the maximum feasible span. Mechanical connections introduce additional installation complexity and maintenance (e.g., a narrow shoulder roadway may require a lane to be closed for a day or more to complete repair depending on the depth of the connection), but also permit unlimited system lengths.

A study performed in Texas in the late 1980s found that reduced embedment depths did not perform satisfactorily with W-beam mounted on timber posts [11]. Standard post embedment depths were 38 in. at the time of this study. Reduced embedment depths of 18 in. and 27 in. were evaluated with full-scale crash testing. The 18-in. embedment depth resulted in failure by the vehicle vaulting over excessively rotated posts. Similarly, the 27-in. embedment resulted in failure by complex vehicle-barrier interactions, including rotation of the posts out of the soil and tearing of the W-beam. Based on those observations, the researchers recommended against using shallow embedment depths, and instead advocated a direct mechanical connection by bolting steel W-shape posts with welded based plates to the top slabs of box culverts.

In 2012, the Midwest Roadside Safety Facility (MwRSF) performed a series of bogie tests on MGS posts with reduced embedment depths [12]. The standard 40-in. embedment cases resulted in post yielding approximately 10 in. below the ground line. Alternative bogie tests were performed with embedment reduced to 36 in., and bogie impact height of 24⅞ in., matching that used for the standard 40-in. embedment depth tests, and increased to 28⅞ in. Post resistance decreased with reduced embedment depths by about 12 percent for the lower impact height and about 20 percent for the higher impact height. The posts did not form plastic hinges in any reduced embedment bogie test.

Both MwRSF and the Texas A&M Transportation Institute (TTI) have developed top-mounted strong post anchorage systems for culverts [3-6]. The MwRSF system used W6x9

posts at half-post spacing (37½ in.) and satisfied National Cooperative Highway Research Program (NCHRP) Report No. 350 and MASH criteria in full-scale crash testing [3-5, 13-1]. The TTI system expanded to full post spacing (75 in.) and satisfied MASH criteria [6, 14]. System repair and replacement following a vehicle impact also requires temporary removal of soil fill to access the post mounting hardware. MwRSF recently investigated alternative socketed connections with either a side-mounted connection at culvert headwalls [7, 8] or top-mounted sockets on culverts [9, 10], but research on these alternative connection methods has so far been limited to weak post MGS designs.

In another related research effort, full-scale crash testing under MASH test designation no. 3-10 performed by MwRSF satisfied all MASH criteria for MGS systems with top rail mounting heights of 34 in. and 36 in. (reduced embedment depths of 37 in. and 35 in., respectively) [15-16]. These tests were performed to investigate the potential for vehicle underride and wheel snag, but the MGS was found to perform acceptably in both shallower embedment cases. Full-scale crash test designation no. 3-11 was never conducted part of this study, so the expected increases in working width and deflection associated with reduced embedment depths were never quantified.

1.3 Objective

The objective of this research effort is to evaluate the use of the MGS with reduced post embedment and potentially with reduced post spacing to satisfy TL-2 and TL-3 criteria of MASH 2016 [1], when installed over low-fill culverts. The goal was to identify the shallowest post configuration with the potential to meet MASH TL-2 and TL-3 criteria when installed over low-fill culverts. The investigation considered post embedment depths between 28 in. and 40 in. Analytical modeling examined potential dynamic deflections for reduced embedment MGS, as well as the need for transitions to standard MGS at the ends of the reduced embedment system. Full-scale crash testing may be performed in a supplementary phase of work.

1.4 Scope

The research objective was achieved through the completion of several tasks. A series of dynamic bogie tests were performed on reduced post embedment depths to quantify the effect of reduced embedment on post-soil behavior. Bogie test results were analyzed, evaluated, and documented. Next, computer simulation analyses with LS-DYNA were conducted to determine feasibility and recommend potential reduced post embedment configurations capable of meeting MASH TL-2 and TL-3 criteria. Analysis of the recommended MGS configurations with reduced post embedment was conducted to determine if any stiffness transitioning was required. Finally, recommendations were made pertaining to full-scale crash testing of the configurations of MGS with reduced post embedment depths in future research.

2 COMPONENT TESTING CONDITIONS

2.1 Purpose

Several standard W6x8.5 and W6x16 steel posts with various embedment depths were evaluated with dynamic component tests to gather dynamic soil-post data with shallower embedment depths, which could eventually allow evaluation of the MGS at reduced post embedment depths and/or reduced post spacings.

2.2 Scope

The first six bogie tests, test nos. LFCB-1 through LFCB-6, included W6x8.5 steel posts with embedment depths of 36, 32, and 28 in. These tests did not provide the desired data regarding soil response due to the post yielding at 36- and 32-in. embedment depths. As such, three additional bogie tests, test nos. LFCB-7 through LFCB-9, were conducted on W6x16 steel posts at 40, 34, and 28-in. embedment depths, respectively. A stronger (i.e., W6x16 steel post) was used to eliminate the possibility of post yielding for soil calibration purposes only. It was desired that the post would not yield and only rotate, which isolates the soil resistance from the post resistance during an impact event. In total, nine bogie tests were conducted on W6x8.5 and W6x16 steel posts at various embedment depths, as shown in Table 1.

Test nos. LFCB-1 and LFCB-2 were conducted with posts embedded 36 in. Test nos. LFCB-3 and LFCB-4 used an embedment depth of 32-in., and test nos. LFCB-5 and LFCB-6 used an embedment depth of 28 in. Test nos. LFCB-7 through LFCB-9 were conducted on W6x16 steel posts with embedment depths of 40, 34, and 28 in., respectively. The target impact conditions for all tests were a speed of 20 mph and an angle of 90 degrees, creating a classic “head-on” or full-frontal impact and strong axis bending. The posts were impacted 24⅞ in. above the ground line perpendicular to the front face of the post. The test setup is shown in Figures 1 through 4. Material specifications, mill certifications, and certificates of conformity for the (test component description, e.g., post) are shown in Appendix A.

A compacted, coarse, crushed limestone material, alternatively classified as well-graded gravel by the Unified Soil Classification System, that met American Association of State Highway and Transportation Officials (AASHTO) standard soil designation M147 Grade B, as recommended by MASH 2016, was utilized for all tests [1]. MASH 2016 adheres to the general philosophy that testing longitudinal barriers in stiff soil results in higher impact and barrier loads, increased occupant risk values, and increased propensity for rail rupture, pocketing, and snag. Therefore, MASH 2016 has established a minimum post-soil resistance force to ensure systems are installed in strong, stiff soil.

Table 1. Dynamic Bogie Testing Matrix

Test No.	Post Type	Post Length (in.)	Embedment Depth (in.)	Impact Axis	Target Impact Velocity (mph)	Impact Height (in.)
LFCB-1	W6x8.5	68	36	Strong Axis	20	24⅞
LFCB-2	W6x8.5	68	36	Strong Axis	20	24⅞
LFCB-3	W6x8.5	64	32	Strong Axis	20	24⅞
LFCB-4	W6x8.5	64	32	Strong Axis	20	24⅞
LFCB-5	W6x8.5	60	28	Strong Axis	20	24⅞
LFCB-6	W6x8.5	60	28	Strong Axis	20	24⅞
LFCB-7	W6x16	72	40	Strong Axis	20	24⅞
LFCB-8	W6x16	66	34	Strong Axis	20	24⅞
LFCB-9	W6x16	60	28	Strong Axis	20	24⅞

Test Quantity	Post Type	Post Length 'X' (in.)	Post Grade	Embedment Depth 'Y' (in.)	Bogie No.	Load Height (in.)	Impact Speed (mph)	Impact Direciton (deg)	Soil Intallation Method
2	a1	68	A36	36	3	24 7/8	20	90	3' Hole – HE8
2	a2	64	A36	32	3	24 7/8	20	90	3' Hole – HE8
2	a3	60	A36	28	3	24 7/8	20	90	3' Hole – HE8

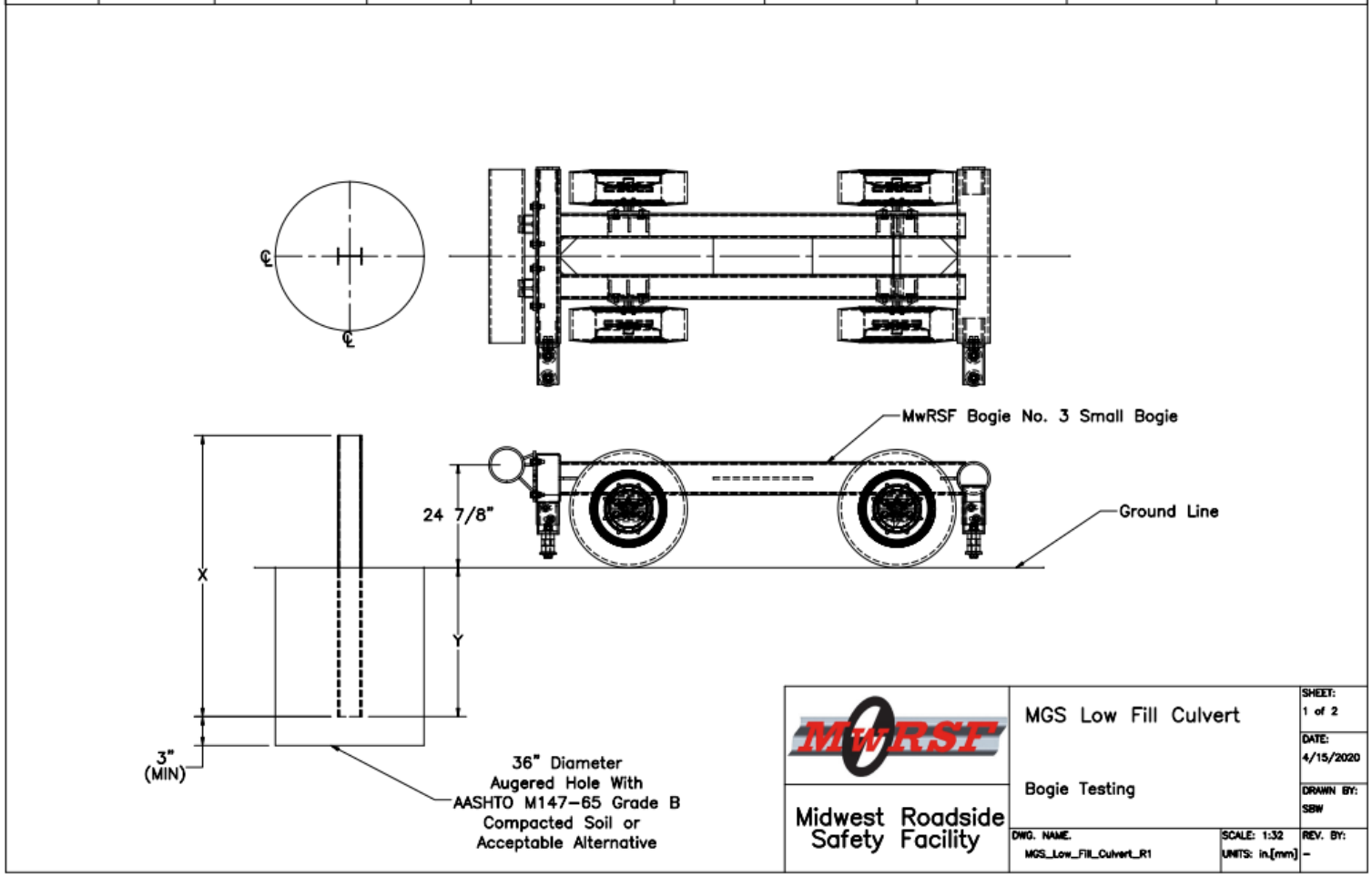

Figure 1. Bogie Testing Matrix and Setup, Test Nos. LFCB-1 through LFCB-6

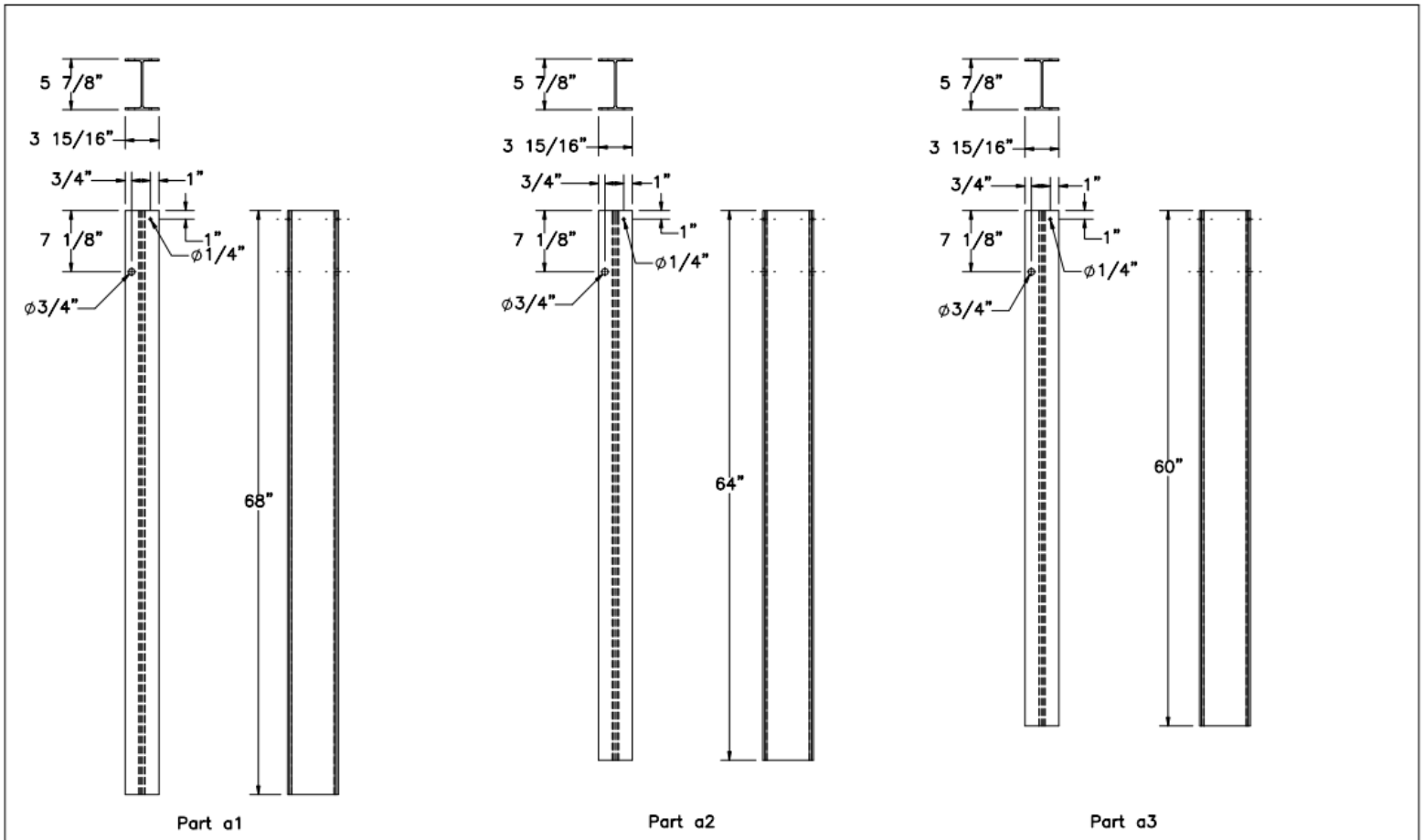

Item No.	QTY.	Description	Material Specification	Hardware
a1	2	W6x8.5, 68" Long Steel Post	ASTM A992	–
a2	2	W6x8.5, 64" Long Steel Post	ASTM A992	–
a3	2	W6x8.5, 60" Long Steel Post	ASTM A992	–

Midwest Roadside Safety Facility

MGS Low Fill Culvert

Post Details

SHEET: 2 of 2
DATE: 4/15/2020
DRAWN BY: SBW
REV. BY: –
DWG. NAME. MGS_Low_Fill_Culvert_R1
SCALE: 1:16
UNITS: in.[mm]

Figure 2. W6x8.5 Steel Post Details, Test Nos. LFCB-1 through LFCB-6

Test No.	Post Type	Post Length 'X' (in.)	Post Grade	Embedment Depth 'Y' (in.)	Bogie No.	Load Height (in.)	Impact Speed (mph)	Impact Direciton (deg)	Soil Intallation Method
LFCB–7	a1	72	A992	40	3	25	20	90	3' Hole – HE8
LFCB–8	a2	66	A992	34	3	25	20	90	3' Hole – HE8
LFCB–9	a3	60	A992	28	3	25	20	90	3' Hole – HE8

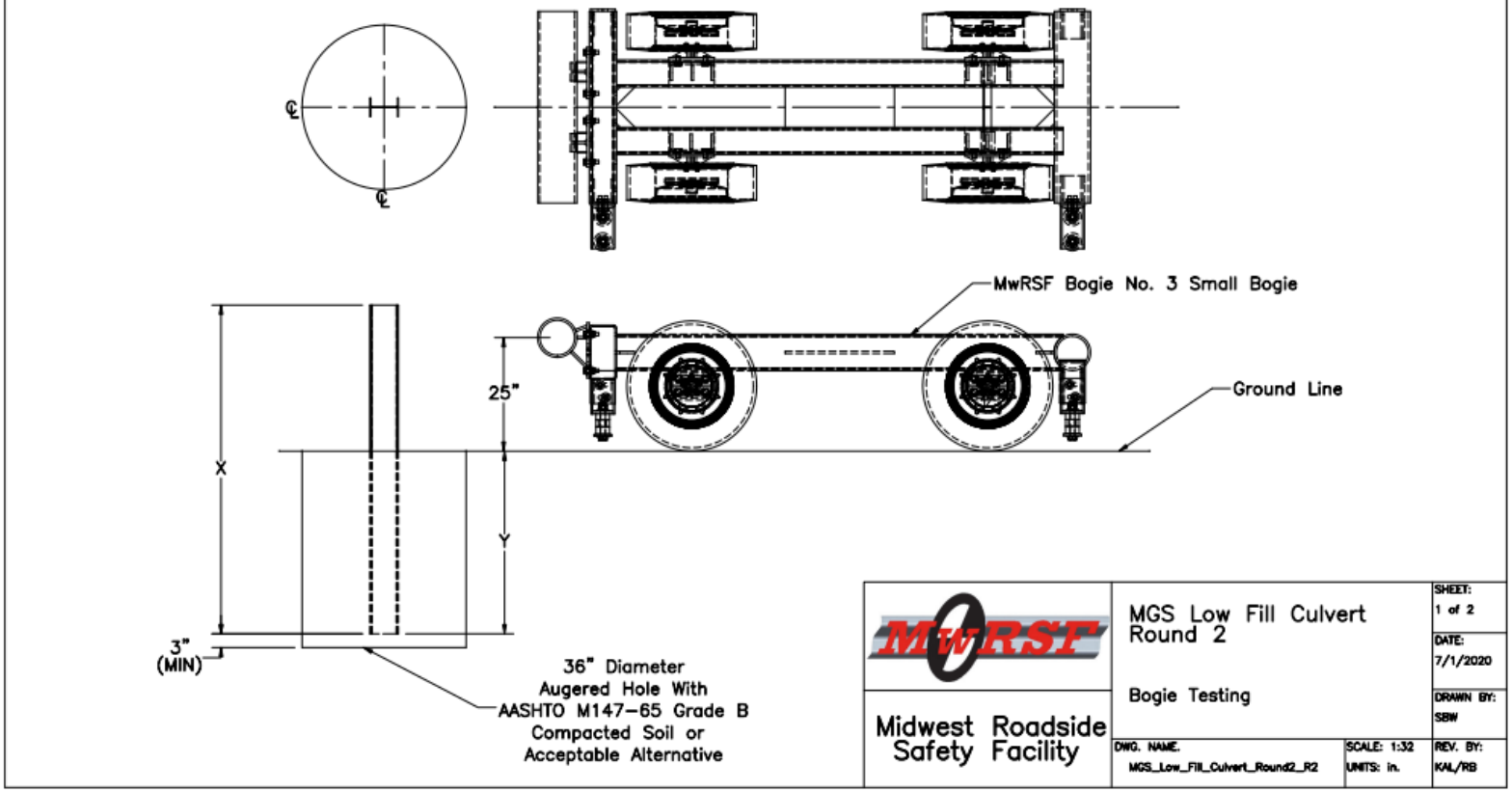

Figure 3. Bogie Testing Matrix and Setup, Test Nos. LFCB-7 through LFCB-9

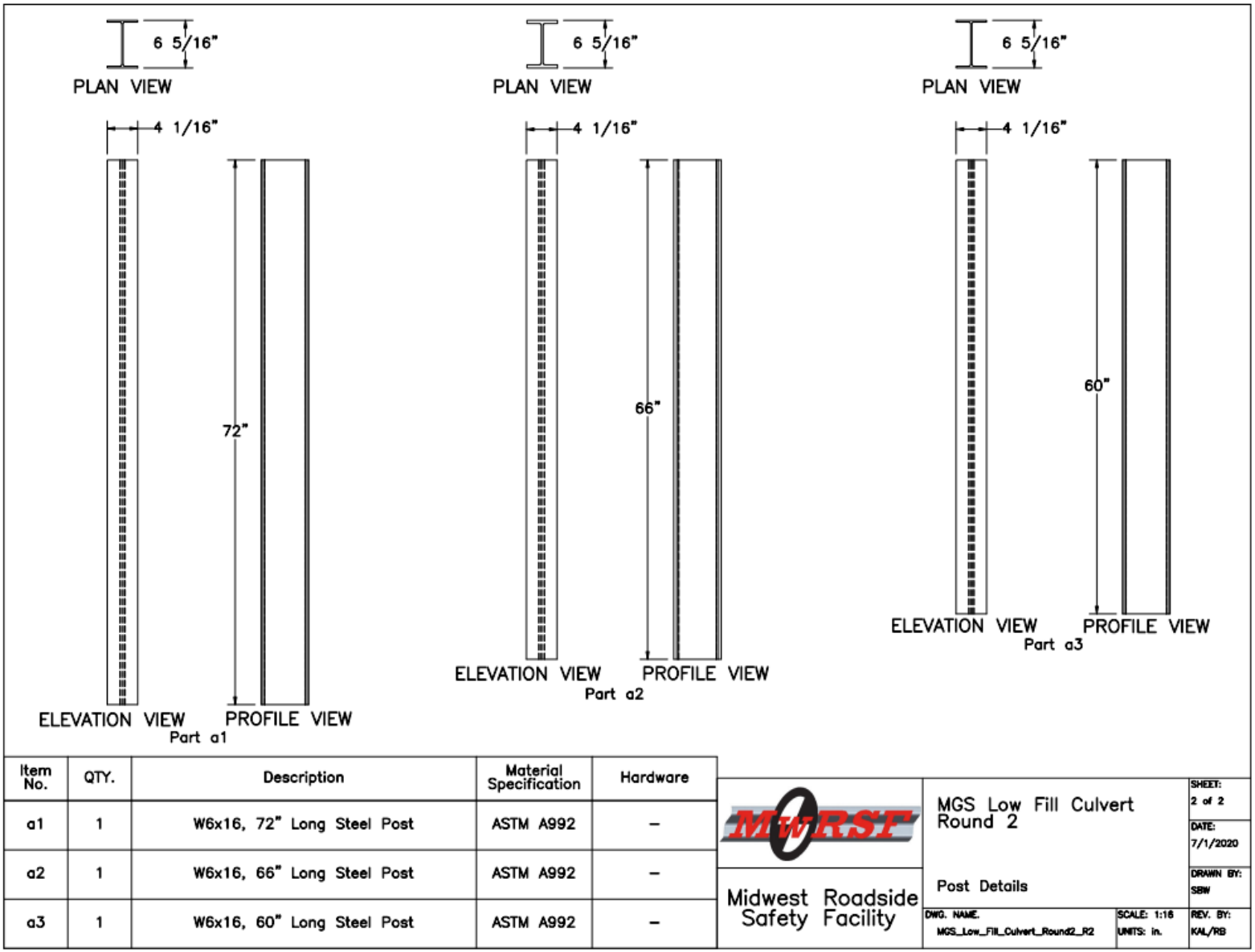

Item No.	QTY.	Description	Material Specification	Hardware
a1	1	W6x16, 72" Long Steel Post	ASTM A992	–
a2	1	W6x16, 66" Long Steel Post	ASTM A992	–
a3	1	W6x16, 60" Long Steel Post	ASTM A992	–

Midwest Roadside Safety Facility

MGS Low Fill Culvert Round 2

Post Details

SHEET: 2 of 2
DATE: 7/1/2020
DRAWN BY: SBW
REV. BY: KAL/RB
DWG. NAME. MGS_Low_Fill_Culvert_Round2_R2
SCALE: 1:16
UNITS: in.

Figure 4. W6x16 Steel Post Details, Test Nos. LFCB-7 through LFCB-9

Figure 5. Installation Photographs, Test Nos. LFCB-1 through LFCB-6

Figure 6. Installation Photographs, Test Nos. LFCB-7 through LFCB-9

2.3 Equipment and Instrumentation

Equipment and instrumentation utilized to collect and record data during the dynamic bogie tests included a bogie vehicle, onboard accelerometers, a retroreflective speed trap, high-speed and standard-speed digital video, and still cameras.

2.3.1 Bogie Vehicle

A rigid-frame bogie was used to impact the posts. The bogie head was constructed of 8-in. diameter, ½-in. thick standard steel pipe, with ¾-in. neoprene belting wrapped around the pipe to prevent local damage to the post from the impact. The impact head was bolted to the bogie vehicle, creating a rigid frame with an impact height of 24⅞ in. The mass of the bogie with the addition of the mountable impact head and accelerometers was 1,865 lb and 1,873 lb for test nos. LFCB-1 through LFCB-6 and test nos. LFCB-7 through LFCB-9, respectively.

A pickup truck with a reverse-cable tow system was used to propel the bogie to a target impact speed of 20 mph. When the bogie approached the end of the guidance system, it was released from the tow cable allowing it to be free rolling when it impacted the post. A radio-controlled brake system was installed on the bogie, allowing it to be brought safely to rest after the test.

2.3.2 Accelerometers

A SLICE 6DX accelerometer system was mounted on the bogie vehicle near its center of gravity (c.g.) to measure the acceleration in the longitudinal, lateral, and vertical directions. However, only the longitudinal acceleration was processed and reported.

A SLICE 6DX, was a modular data acquisition system manufactured by DTS of Seal Beach, California. The acceleration sensors were mounted inside the body of the custom-built SLICE 6DX event data recorder and recorded data at 10,000 Hz to the onboard microprocessor. The SLICE 6DX was configured with 7 GB of non-volatile flash memory, a range of ±500 g's, a sample rate of 10,000 Hz, and a 1,650 Hz (CFC 1000) anti-aliasing filter. The "SLICEWare" computer software programs and a customized Microsoft Excel worksheet were used to analyze and plot the accelerometer data.

2.3.3 Retroreflective Optic Speed Trap

A retroreflective optic speed trap was used to determine the speed of the bogie vehicle before impact. Four retroreflective targets, spaced at approximately 18-in. intervals, were applied to the side of the bogie vehicle. When the emitted beam of light was reflected by the targets and returned to the Emitter/Receiver, a signal was sent to the data acquisition computer, recording at 10,000 Hz, as well as the external LED box activating the LED flashes. The speed was then calculated using the spacing between the retroreflective targets and the time between the signals. LED lights and high-speed digital video analysis are used as a backup if vehicle speeds cannot be determined from the electronic data.

2.3.4 Digital Photography

One AOS high-speed digital video camera, one GoPro digital video camera, and one Panasonic digital camera were used to document each test. The AOS, GoPro, and Panasonic cameras had frame rates of 500, 120, and 120 frames per second, respectively. The cameras were placed laterally from the post, with a view perpendicular to the bogie's direction of travel. A digital still camera was used to document pre- and post-test conditions for all tests.

2.4 End of Test Determination

When the impact head initially contacts the test article, the force exerted by the bogie vehicle is directly perpendicular. However, as the post rotates, the bogie's orientation and path move away from perpendicular. This introduces two sources of error: (1) the contact force between the impact head and the post has a vertical component and (2) the impact head slides upward along the test article. Therefore, only the initial portion of the accelerometer trace should be used since variations in the data become significant as the system rotates and the bogie overrides the system. Additionally, guidelines were established to define the end of test time using the high-speed video of the impact. The first occurrence of either of the following events was used to determine the end of the test: (1) the test article fractured or (2) the bogie overrode or lost contact with the test article.

2.5 Data Processing

The electronic accelerometer data obtained in dynamic testing was filtered using the SAE Class 60 Butterworth filter conforming to the SAE J211/1 specification [17]. The pertinent acceleration signal was extracted from the bulk of the data signals. The processed acceleration data was then multiplied by the mass of the bogie to get the impact force using Newton's Second Law. Next, the acceleration trace was integrated to find the change in velocity versus time. Initial velocity of the bogie, calculated from the retroreflective optic speed trap data, was then used to determine the bogie's velocity and the calculated velocity trace was integrated to find the bogie's displacement. This displacement is also the displacement of the post. Combining the previous results, a force vs. displacement curve was plotted for each test. Finally, integration of the force vs. displacement curve provided the energy vs. displacement curve for each test.

The information desired from the bogie tests was the relation between the applied impact force and displacement of the post at the impact height. This data was then used to find the total energy, i.e., the area under the force versus deflection curve dissipated during each dynamic component test. The energy vs. displacement curve was utilized to compute the average force at a specific displacement. The average force at specific post deflection was computed by dividing the energy by displacement of post at the impact height.

Although the acceleration data was applied to the impact height, the data came from the c.g. of the bogie. Error was added to the data since the bogie was not perfectly rigid and sustained vibration. The bogie may have also rotated during impact, causing differences in accelerations between the bogie center of mass and the impact head. While these issues may affect the data, the data was valid. Filtering procedures were applied to the data to smooth out vibrations and rotation of the bogie during the test was minor. One useful aspect of using accelerometer data was that it includes influences of the post inertia on the resistive force. This was important as the mass of the post would affect barrier performance as well as test results.

3 COMPONENT TESTING RESULTS AND DISCUSSION

3.1 Results

A total of nine dynamic component tests were conducted with the bogie vehicle impacting posts at various embedment depths. Descriptions of each test, including sequential and post-test photographs, are contained in the following sections. The accelerometer data for each test was processed to obtain acceleration, velocity, and displacement curves, as well as force vs. displacement and energy vs. displacement curves. Although the individual transducers produced similar results, the values reported herein were calculated from the SLICE data curves in order to provide a common basis for comparing results from multiple tests. Test results for all transducers are provided in Appendix B.

3.1.1 Test No. LFCB-1

Test no. LFCB-1 was conducted with the bogie impacting the W6x8.5 steel post with a 36-in. embedment depth at a height of 24⅞ in. and an angle of 90 degrees (through the strong-axis of the post) at a speed of 20.6 mph. The impact caused the post to deflect backward as a plastic hinge formed in the post 8 in. below the ground, and the post twisted. The bogie ultimately overrode the post at a displacement of 31.7 in.

Force-displacement and energy-displacement curves were created from the DTS SLICE accelerometer data and are shown in Figure 7. A peak force of 14.8 kips occurred at a displacement of 3.1 in., and an average force of 10.9 kips occurred through 20 in. of displacement. The test article had absorbed 217.3 k-in. of energy through 20 in. of displacement, and 264.5 k-in. through 31.7 of displacement at the time the bogie overrode the post. Time sequential and post-impact photographs are shown in Figure 8.

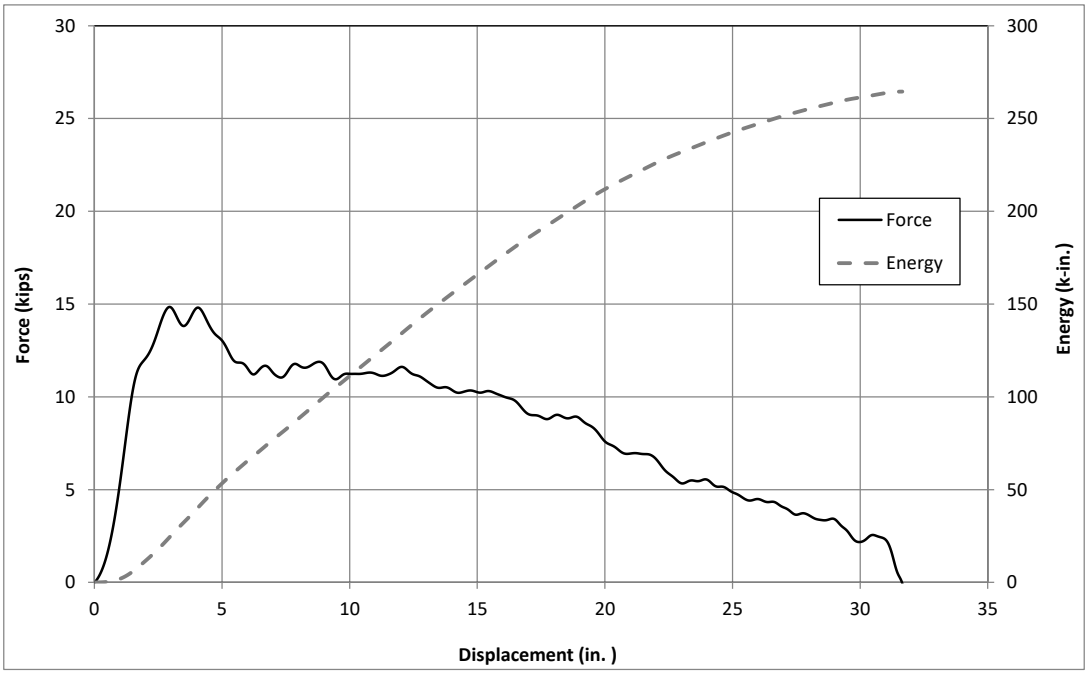

Figure 7. Force vs. Displacement and Energy vs. Displacement, Test No. LFCB-1

IMPACT

0.050 sec

0.100 sec

0.150 sec

0.200 sec

0.250 sec

Figure 8. Time-Sequential and Post-Impact Photographs, Test No. LFCB-1

3.1.2 Test No. LFCB-2

Test no. LFCB-2 was conducted with the bogie impacting the W6x8.5 steel post with a 36-in. embedment depth at a height of 24⅞ in. and an angle of 90 degrees at a speed of 22.3 mph. Similar to test no. LFCB-1, the impact caused the post to deflect backward as a plastic hinge formed in the post 8 in. below the ground and the post twisted. The bogie ultimately overrode the post at a displacement of 30.5 in.

Force-displacement and energy-displacement curves were created from the DTS SLICE accelerometer data and are shown in Figure 9. A peak force of 15.7 kips occurred at a displacement of 3.1 in., and an average force of 10.2 kips occurred through 20 in. of displacement. The test article had absorbed 203.4 k-in. of energy through 20 in. of displacement, and 225.3 k-in. through 30.5 of displacement at the time the bogie overrode the post. Time sequential and post-impact photographs are shown in Figure 10.

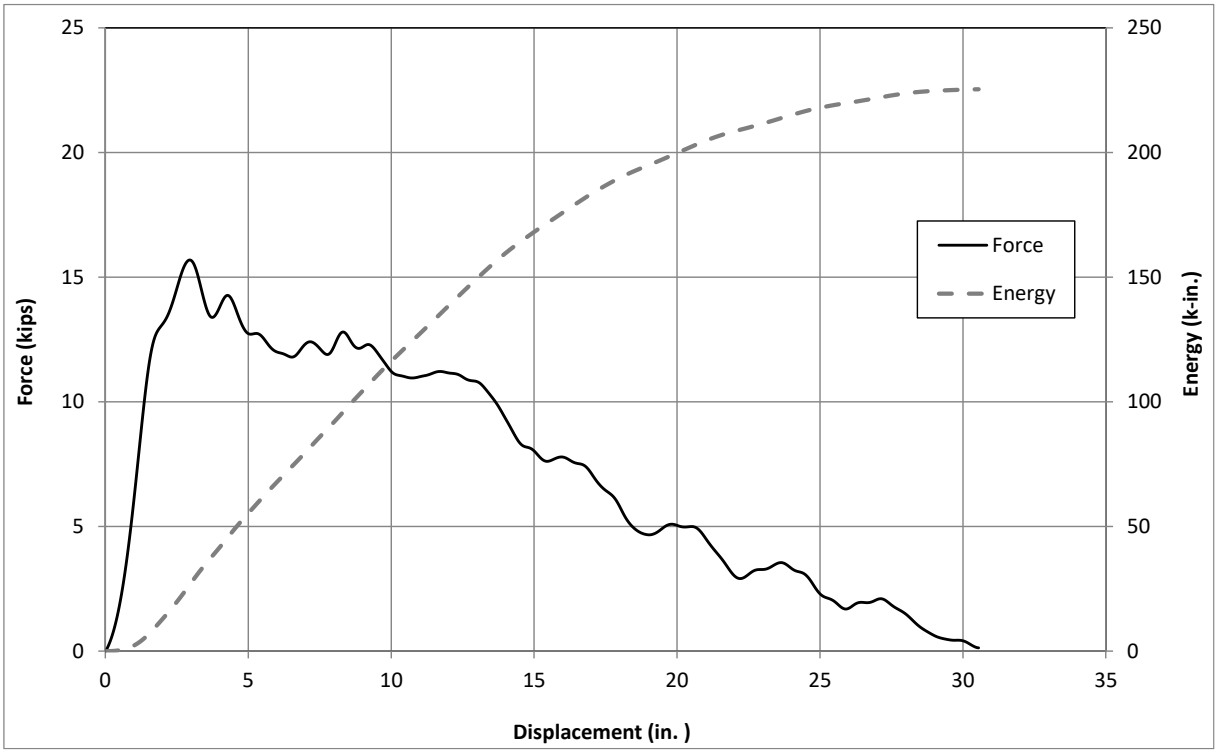

Figure 9. Force vs. Displacement and Energy vs. Displacement, Test No. LFCB-2

IMPACT

0.050 sec

0.100 sec

0.150 sec

0.200 sec

0.250 sec

Figure 10. Time-Sequential and Post-Impact Photographs, Test No. LFCB-2

3.1.3 Test No. LFCB-3

Test no. LFCB-3 was conducted with the bogie impacting the W6x8.5 steel post with a 32-in. embedment depth at a height of 24⅞ in. and an angle of 90 degrees at a speed of 20.4 mph. The impact caused the post to deflect backward as a plastic hinge formed in the post 4.5 in. below the ground and the post twisted. The bogie ultimately overrode the post at a displacement of 31.2 in.

Force-displacement and energy-displacement curves were created from the DTS SLICE accelerometer data and are shown in Figure 11. A peak force of 15.8 kips occurred at a displacement of 2.5 in., and an average force of 10.9 kips occurred through 20 in. of displacement. The test article had absorbed 217.9 k-in. of energy through 20 in. of displacement, and 265.7 k-in. through 31.2 of displacement at the time the bogie overrode the post. Time sequential and post-impact photographs are shown in Figure 12.

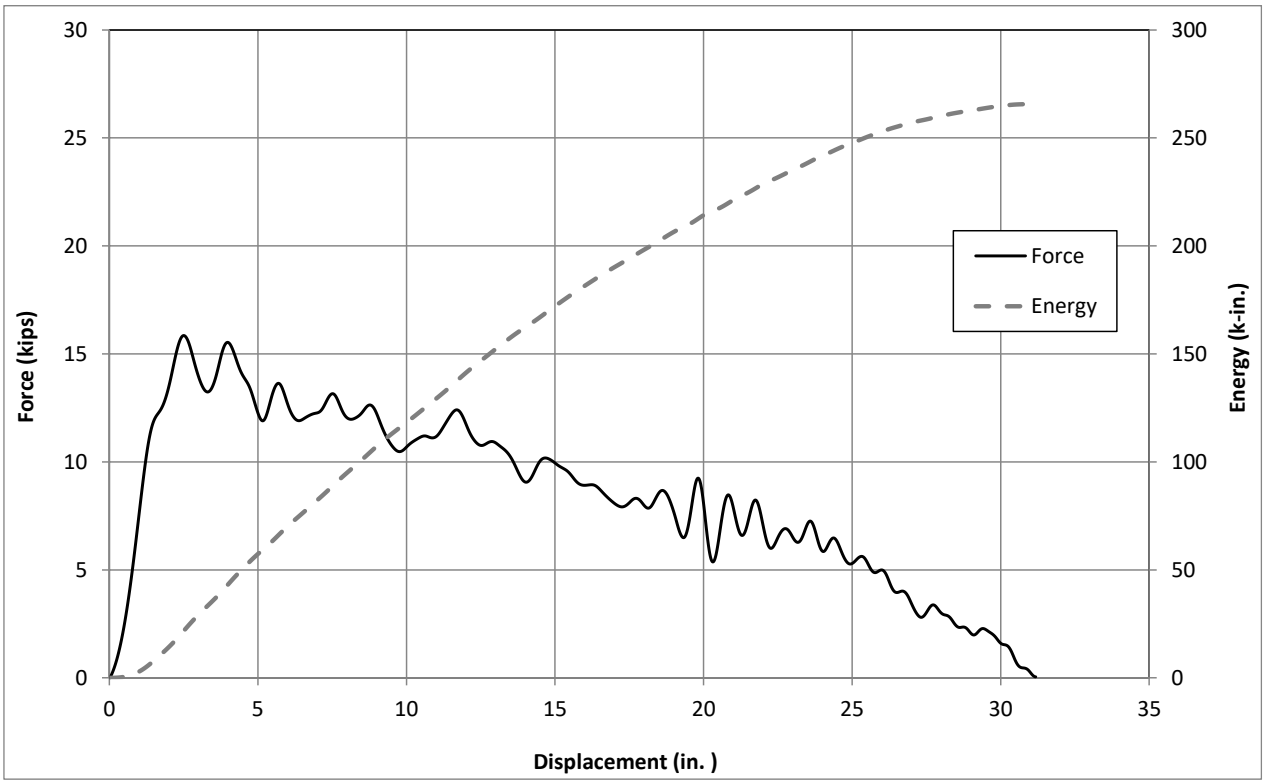

Figure 11. Force vs. Displacement and Energy vs. Displacement, Test No. LFCB-3

IMPACT

0.050 sec

0.100 sec

0.150 sec

0.200 sec

0.250 sec

Figure 12. Time-Sequential and Post-Impact Photographs, Test No. LFCB-3

3.1.4 Test No. LFCB-4

Test no. LFCB-4 was conducted with the bogie impacting the W6x8.5 steel post with a 32-in. embedment depth at a height of 24⅞ in. and an angle of 90 degrees at a speed of 20.3 mph. Similar to test no. LFCB-3, the impact caused the post to deflect backward as a plastic hinge formed in the post 8 in. below the ground and the post twisted. The bogie ultimately overrode the post at a displacement of 30.4 in.

Force-displacement and energy-displacement curves were created from the DTS SLICE accelerometer data and are shown in Figure 13. A peak force of 17.3 kips occurred at a displacement of 2.7 in., and an average force of 11.2 kips occurred through 20 in. of displacement. The test article had absorbed 223.8 k-in. of energy through 20 in. of displacement, and 258.1 k-in. through 30.4 of displacement at the time the bogie overrode the post. Time sequential and post-impact photographs are shown in Figure 14.

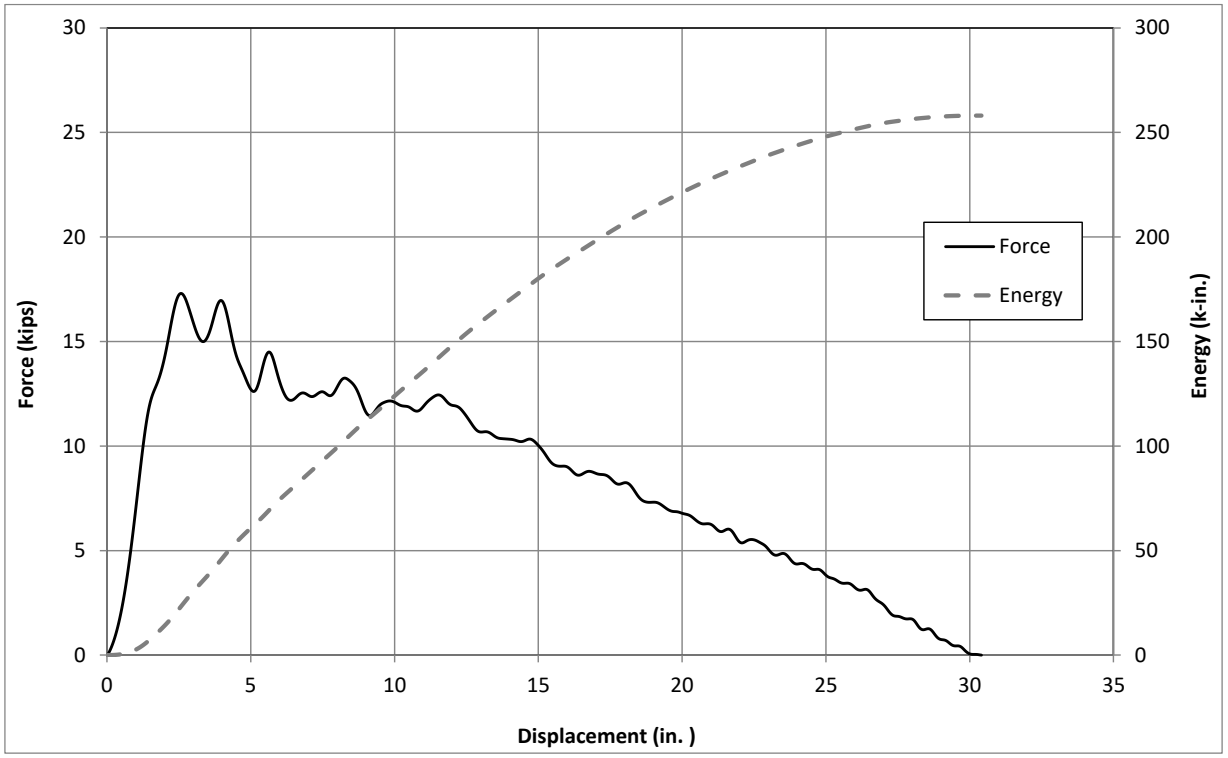

Figure 13. Force vs. Displacement and Energy vs. Displacement, Test No. LFCB-4

IMPACT

0.050 sec

0.100 sec

0.150 sec

0.200 sec

0.250 sec

Figure 14. Time-Sequential and Post-Impact Photographs, Test No. LFCB-4

3.1.5 Test No. LFCB-5

Test no. LFCB-5 was conducted with the bogie impacting the W6x8.5 steel post with a 28-in. embedment depth at a height of 24⅞ in. and an angle of 90 degrees ad at a speed of 22.7 mph. The impact caused the post to deflect backward and twist. The bogie ultimately overrode the post at a displacement of 32.9 in. The post had minor bending approximately 6 in. below the ground.

Force-displacement and energy-displacement curves were created from the DTS SLICE accelerometer data and are shown in Figure 15. A peak force of 17.6 kips occurred at a displacement of 3.5 in., and an average force of 10.6 kips occurred through 20 in. of displacement. The test article had absorbed 212.8 k-in. of energy through 20 in. of displacement, and 237.7 k-in. through 32.9 of displacement at the time the bogie overrode the post. Time sequential and post-impact photographs are shown in Figure 16.

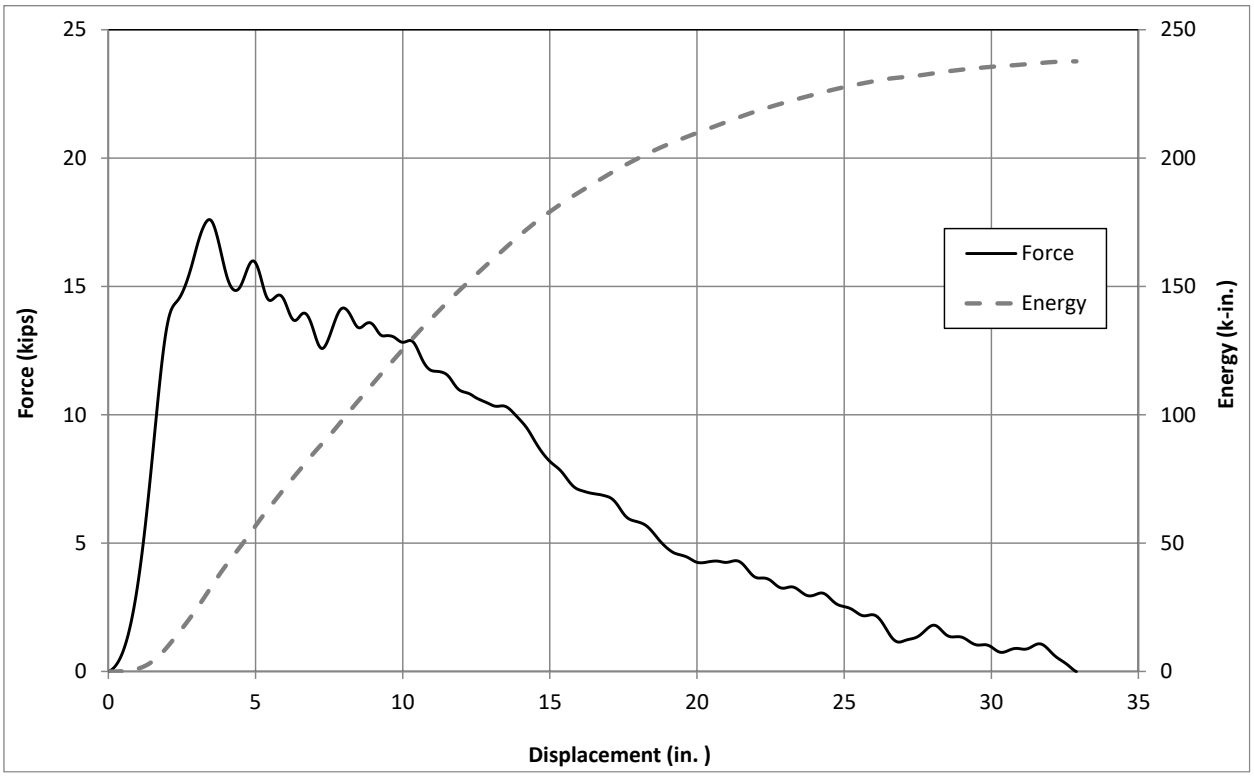

Figure 15. Force vs. Displacement and Energy vs. Displacement, Test No. LFCB-5

IMPACT

0.050 sec

0.100 sec

0.150 sec

0.200 sec

0.250 sec

Figure 16. Time-Sequential and Post-Impact Photographs, Test No. LFCB-5

3.1.6 Test No. LFCB-6

Test no. LFCB-6 was conducted with the bogie impacting the W6x8.5 steel post with a 28-in. embedment depth at a height of 24⅞ in. and an angle of 90 degrees at a speed of 20.8 mph. The impact caused the post to deflect backward and twist. The bogie ultimately overrode the post at a displacement of 34.5 in. The post was undamaged.

Force-displacement and energy-displacement curves were created from the DTS SLICE accelerometer data and are shown in Figure 17. A peak force of 11.4 kips occurred at a displacement of 4.3 in., and an average force of 7.3 kips occurred through 20 in. of displacement. The test article had absorbed 145.7 k-in. of energy through 20 in. of displacement, and 162.1 k-in. through 34.5 of displacement at the time the bogie overrode the post. Time sequential and post impact photographs are shown in Figure 18.

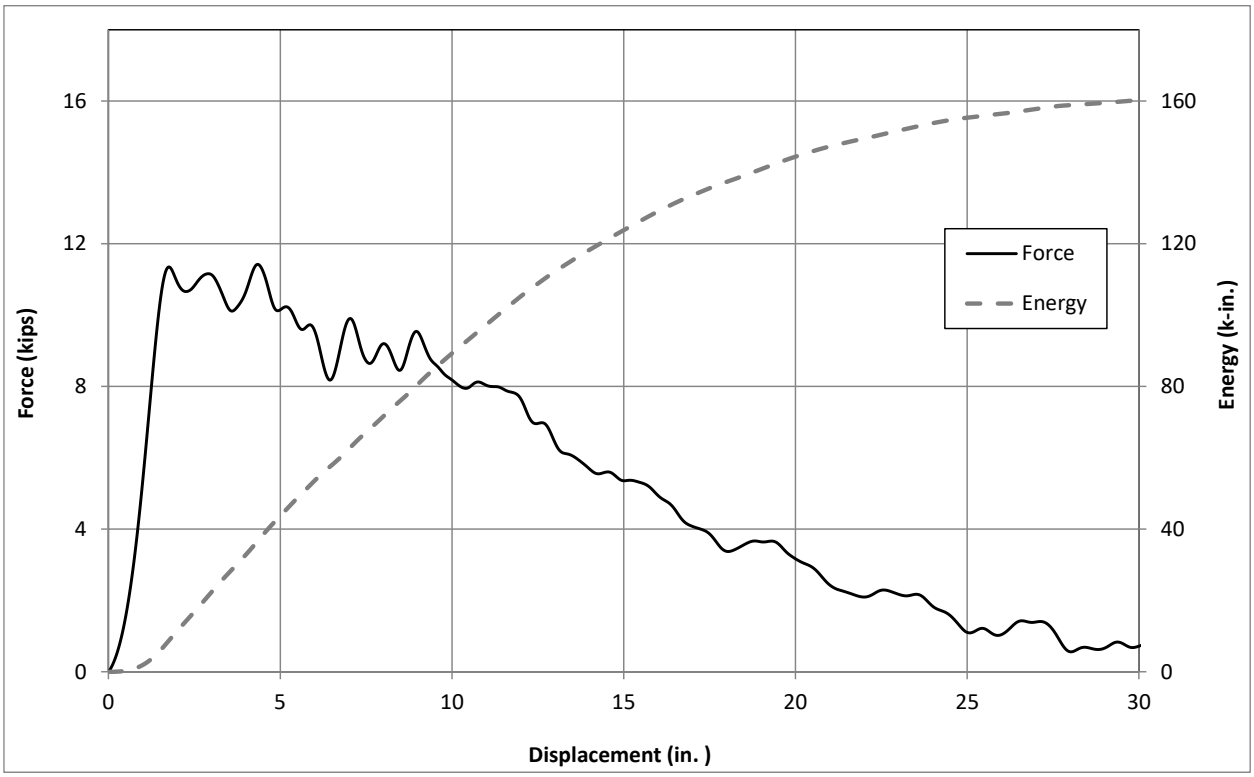

Figure 17. Force vs. Displacement and Energy vs. Displacement, Test No. LFCB-6

IMPACT

0.050 sec

0.100 sec

0.150 sec

0.200 sec

0.250 sec

Figure 18. Time-Sequential and Post-Impact Photographs, Test No. LFCB-6

3.1.7 Test No. LFCB-7

Test no. LFCB-7 was conducted with the bogie impacting the W6x16 steel post with a 40-in. embedment depth at a height of 24⅞ in. and an angle of 90 degrees at a speed of 20.2 mph. The impact caused the post to deflect backward. The bogie ultimately overrode the post at a displacement of 28.5 in. The post was undamaged.

Force-displacement and energy-displacement curves were created from the DTS SLICE accelerometer data and are shown in Figure 19. A peak force of 23.4 kips occurred at a displacement of 2.8 in., and an average force of 13.5 kips occurred through 20 in. of displacement. The test article had absorbed 270.2 k-in. of energy through 20 in. of displacement, and 303.3 k-in. through 28.5 of displacement at the time the bogie overrode the post. Time sequential and post impact photographs are shown in Figure 20.

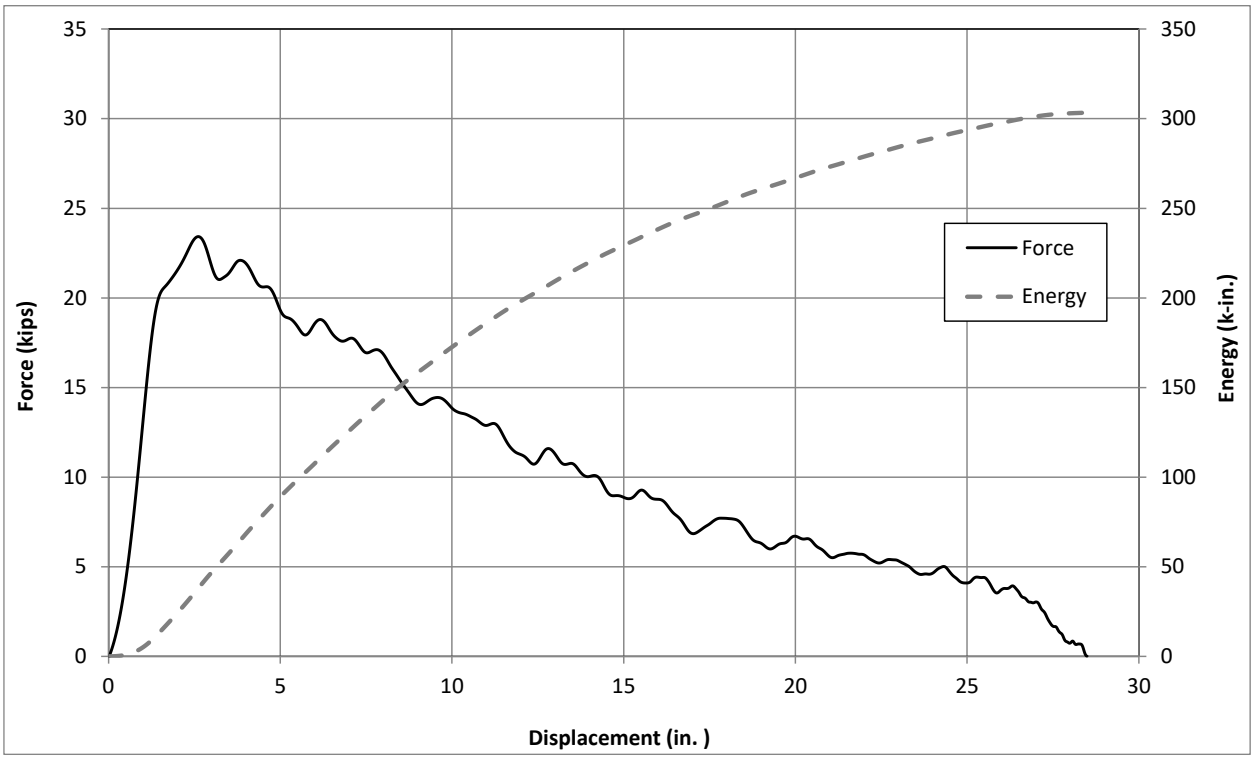

Figure 19. Force vs. Displacement and Energy vs. Displacement, Test No. LFCB-7

IMPACT

0.050 sec

0.100 sec

0.150 sec

0.200 sec

0.250 sec

Figure 20. Time-Sequential and Post-Impact Photographs, Test No. LFCB-7

3.1.8 Test No. LFCB-8

Test no. LFCB-8 was conducted with the bogie impacting the W6x16 steel post with a 34-in. embedment depth at a height of 24⅞ in. and an angle of 90 degrees at a speed of 21.0 mph. The impact caused the post to deflect backward. The bogie ultimately overrode the post at a displacement of 33.1 in. The post was undamaged.

Force-displacement and energy-displacement curves were created from the DTS SLICE accelerometer data and are shown in Figure 21. A peak force of 18.5 kips occurred at a displacement of 1.8 in., and an average force of 11.8 kips occurred through 20 in. of displacement. The test article had absorbed 236.6 k-in. of energy through 20 in. of displacement, and 277.2 k-in. through 33.1 of displacement at the time the bogie overrode the post. Time sequential and post impact photographs are shown in Figure 22.

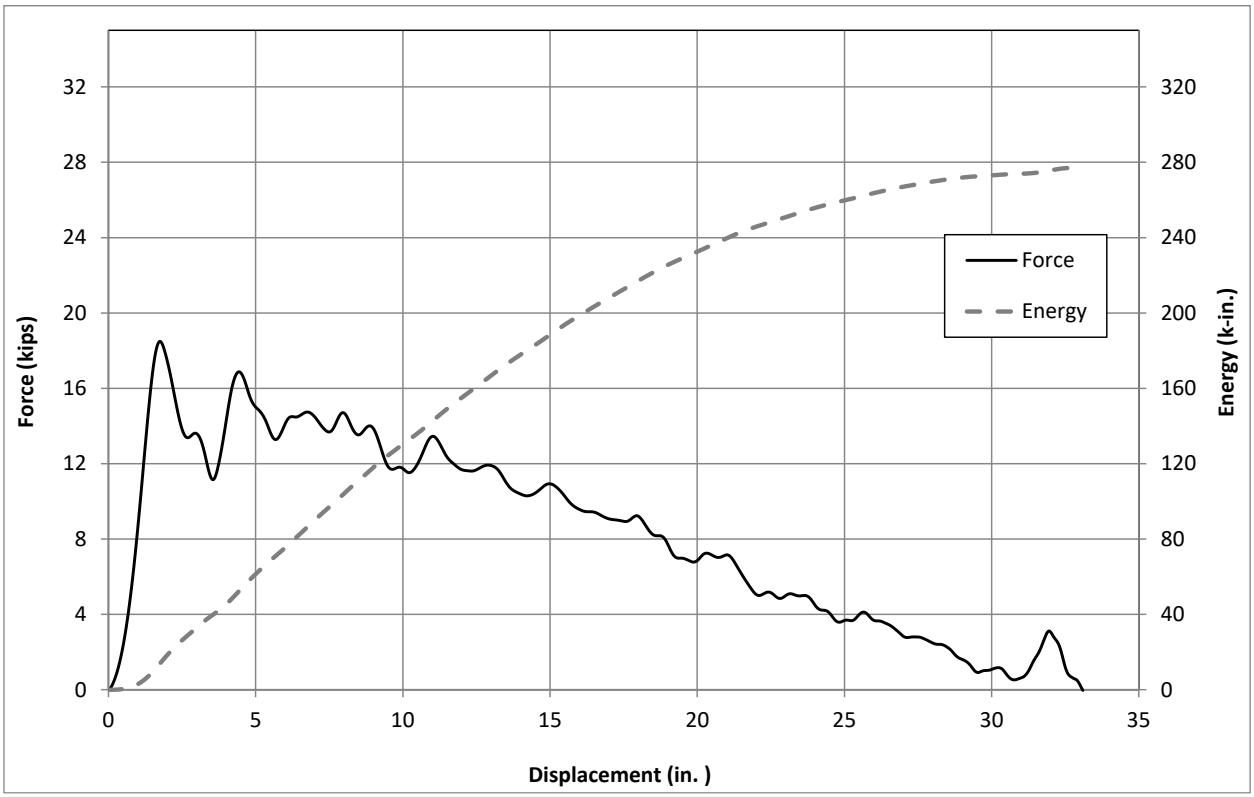

Figure 21. Force vs. Displacement and Energy vs. Displacement, Test No. LFCB-8

IMPACT

0.050 sec

0.100 sec

0.150 sec

0.200 sec

0.250 sec

Figure 22. Time-Sequential and Post-Impact Photographs, Test No. LFCB-8

3.1.9 Test No. LFCB-9

Test no. LFCB-9 was conducted with the bogie impacting the W6x16 steel post with a 28-in. embedment depth at a height of 24⅞ in. and an angle of 90 degrees at a speed of 21.0 mph. The impact caused the post to deflect backward. The bogie ultimately overrode the post at a displacement of 34.2 in. The post was undamaged.

Force-displacement and energy-displacement curves were created from the DTS SLICE accelerometer data and are shown in Figure 23. A peak force of 15.7 kips occurred at a displacement of 1.8 in., and an average force of 7.9 kips occurred through 20 in. of displacement. The test article had absorbed 158.7 k-in. of energy through 20 in. of displacement, and 181.4 k-in. through 34.2 of displacement at the time the bogie overrode the post. Time sequential and post impact photographs are shown in Figure 24.

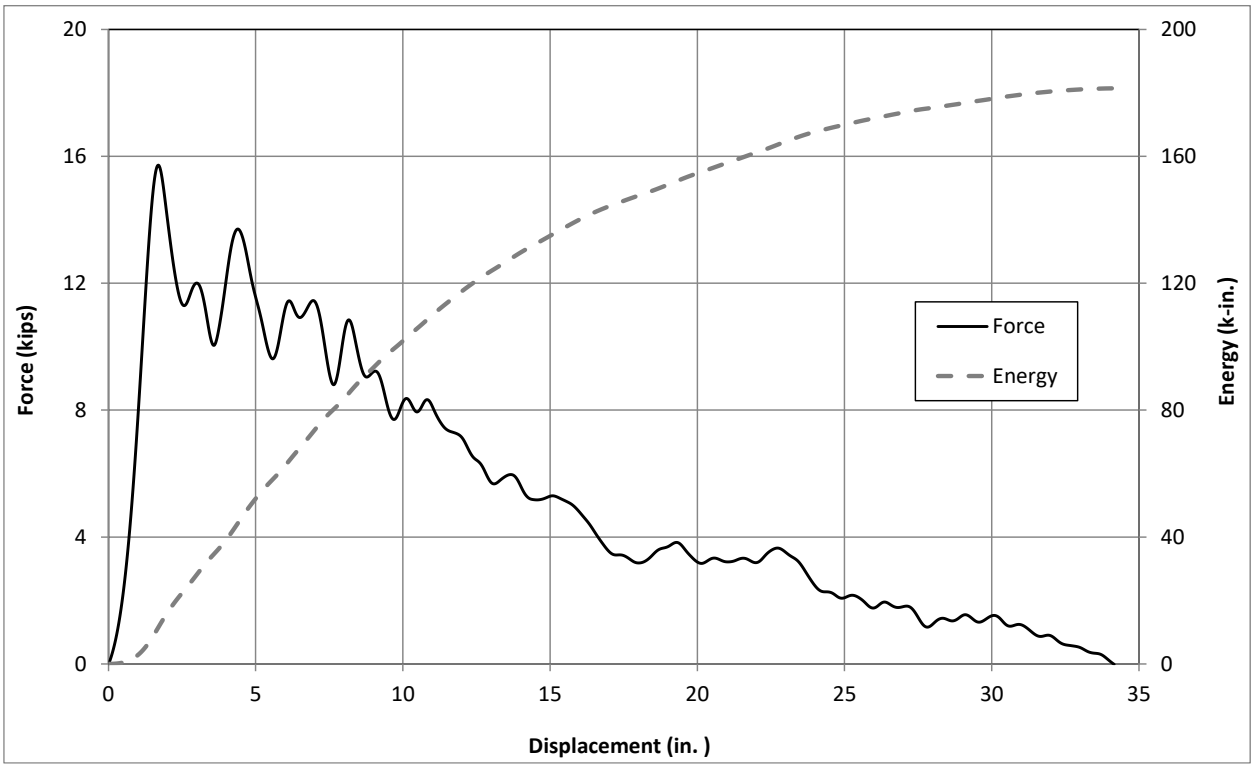

Figure 23. Force vs. Displacement and Energy vs. Displacement, Test No. LFCB-9

IMPACT

0.050 sec

0.100 sec

0.150 sec

0.200 sec

0.250 sec

Figure 24. Time-Sequential and Post-Impact Photographs, Test No. LFCB-9

3.2 Summary of Dynamic Bogie Testing

Nine tests were conducted on W6x8.5 and W6x16 steel posts at different embedment depths to establish the post-soil force vs. displacement and energy vs. displacement characteristics. The results are summarized in Table 2. The impact speeds remained consistent throughout all tests. All bogie tests on the W6x8.5 post resulted in plastic bending of the posts below the ground except test nos. LFCB-5 and LFCB-6, which were at a 28-in. embedment depth. In all bogie tests on the W6x16 post (test nos. LFCB-7 through LFCB-9), the post was undamaged. The force vs. displacement and energy vs. displacement curves for the lateral impacts are shown in Figures 25 through 28.

Test nos. LFCB-1 and LFCB-2, conducted on W6x8.5 steel posts with a 36-in. embedment depth, provided similar force and energy vs. displacement characteristics, as shown in Figures 29 and 30. A plastic hinge was formed in the post below the ground line. The average forces for these two tests were 10.8, 11.2, 10.9, and 9.9 kips, respectively, through 5, 10, 15, and 20 in. of post displacement at the impact height. The average energy was 244.9 kips-in. through the maximum displacement of 31.1 in.

Test nos. LFCB-3 and LFCB-4, conducted on W6x8.5 steel posts with a 32-in. embedment depth, provided similar force vs. displacement and energy vs. displacement characteristics, as shown in Figures 31 and 32. A plastic hinge was formed in the post below the ground line. The average forces for these two tests were 11.9, 12.2, 11.9 and 11.1 kips, respectively, through 5, 10, 15, and 20 in. of post displacement at the impact height. The average energy was 261.9 kips-in. through the maximum displacement of 30.8 in.

Test nos. LFCB-5 and LFCB-6 were conducted on the W6x8.5 steel posts with a 28-in. embedment depth. The impact response of these post-soil systems was primarily governed by the soil failure rather than post yielding. Test no. LFCB-5 resulted in average forces of 11.4, 12.5, 11.9, and 10.5 kips at 5, 10, 15, and 20 in. of post displacement at the impact height, respectively. The total energy was 237.7 kips-in. through the maximum post displacement of 32.9 in. Test no. LFCB-6 resulted in average forces of 8.7, 8.9, 8.3, and 7.2 kips at 5, 10, 15, and 20 in. of post displacement, respectively. The total energy was 162.1 kips-in. through the maximum displacement of 34.5 in.

Test nos. LFCB-7 and LFCB-8 were conducted on W6x16 steel posts with 34-in. and 40-in. embedment depths, respectively. Force vs. displacement and energy vs. displacement curves from test nos. LFCB-7 and LFCB-8 are shown in Figures 37 and 38. Test no. LFCB-7 resulted in average forces of 17.8, 17.3, 15.3, and 13.4 kips at 5, 10, 15, and 20 in. of post displacement, respectively. The energy was 303.3 kips-in. through the maximum displacement of 28.5 in. Test no. LFCB-8 resulted in average forces of 12.3, 13.0, 12.6, and 11.6 kips at 5, 10, 15, and 20 of post displacement, respectively. The energy was 277.2 kips-in. through the maximum displacement of 33.1 in. Test no. LFCB-9 was conducted on the W6x16 steel post with 28-in. embedment depth. Test no. LFCB-9 resulted in average forces of 10.4, 10.2, 9.0, and 7.7 kips at 5, 10, 15 in., and 20 in. of post displacement at the impact height, respectively. The total energy absorbed by the post-soil system was 181.4 kips-in. through the maximum displacement of 34.2 in.

Test nos. LFCB-6 and LFCB-9 showed similar force vs. displacement and energy vs. displacement curves, while test no. LFCB-5 deviated from these two tests, as shown in Figures 33

through 36. In test nos. LFCB-6 and LFCB-9, the post did not yield, as expected, while in test no. LFCCB-5, a plastic hinge was formed and the post yielded. The reason for this deviation could be due to the discrepancy in soil compaction, grain-size distribution, moisture content, and the contact forces between the particles. Thus, test no. LFCB-5 was considered an outlier.

Table 2. Dynamic Bogie Testing Results

Test No.	Post Type	Peak Force (kips)	Average Force (kips)				Max Displacement (in.)	Total Energy (k-in.)	Failure Type
			5 (in.)	10 (in.)	15 (in.)	20 (in.)			
36-in. Embedment Depth									
LFCB-1	W6x8.5	14.8	10.5	10.8	10.6	9.8	31.7	264.5	Rotation in Soil and Yielding
LFCB-2	W6x8.5	15.7	11.1	11.6	11.2	10.0	30.5	225.3	Rotation in Soil and Yielding
Average		15.3	10.8	11.2	10.9	9.9	31.1	244.9	
32-in. Embedment Depth									
LFCB-3	W6x8.5	15.8	11.6	12.0	11.7	11.0	31.2	265.7	Rotation in Soil and Yielding
LFCB-4	W6x8.5	17.3	12.2	12.4	12.0	11.1	30.4	258.1	Rotation in Soil and Yielding
Average		16.6	11.9	12.2	11.9	11.1	30.8	261.9	
28-in. Embedment Depth									
LFCB-5	W6x8.5	17.6	11.4	12.5	11.9	10.5	32.9	237.7	Rotation in Soil and Yielding (Outlier)
LFCB-6	W6x8.5	11.4	8.7	8.9	8.3	7.2	34.5	162.1	Rotation in Soil
40-in. Embedment Depth									
LFCB-7	W6x16	23.4	17.8	17.3	15.3	13.4	28.5	303.3	Rotation in Soil
34-in. Embedment Depth									
LFCB-8	W6x16	18.5	12.3	13.0	12.6	11.6	33.1	277.2	Rotation in Soil
28-in. Embedment Depth									
LFCB-9	W6x16	15.7	10.4	10.2	9.0	7.7	34.2	181.4	Rotation in Soil

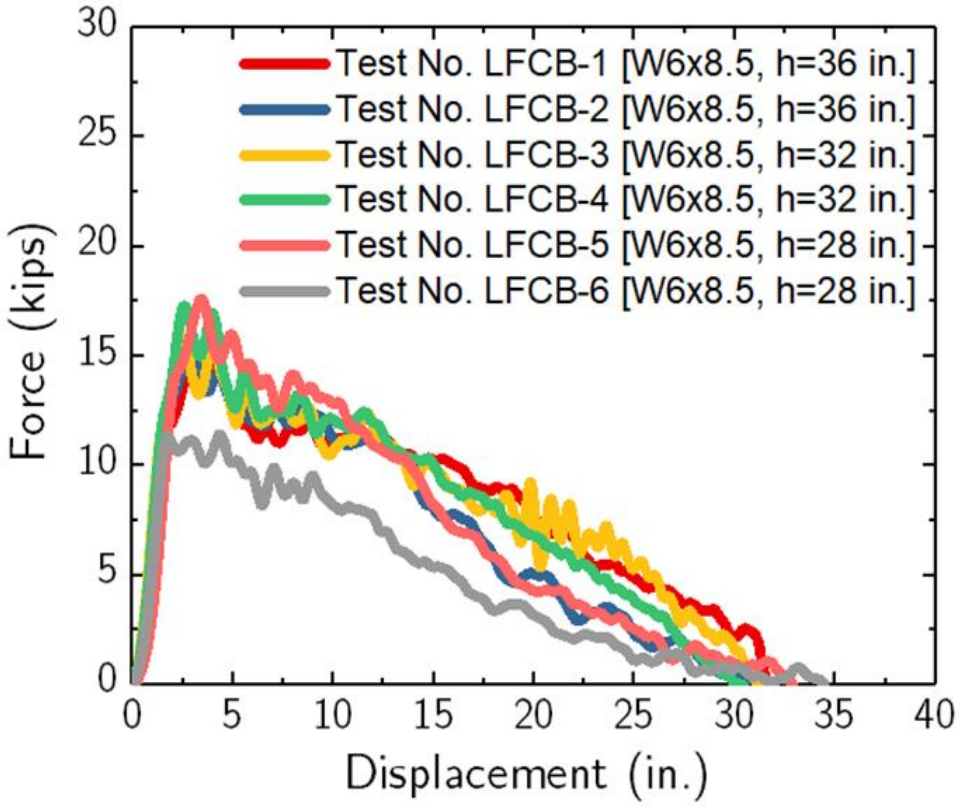

Figure 25. Force vs. Displacement Curves, Test Nos. LFCB-1 through LFCB-6

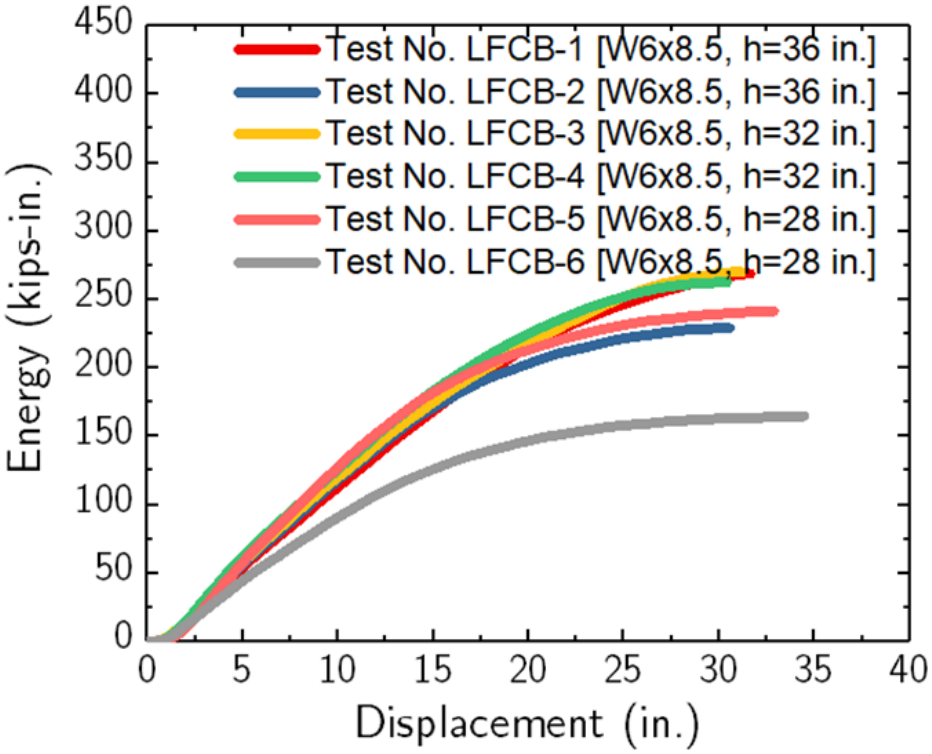

Figure 26. Energy vs. Displacement Curves, Test Nos. LFCB-1 through LFCB-6

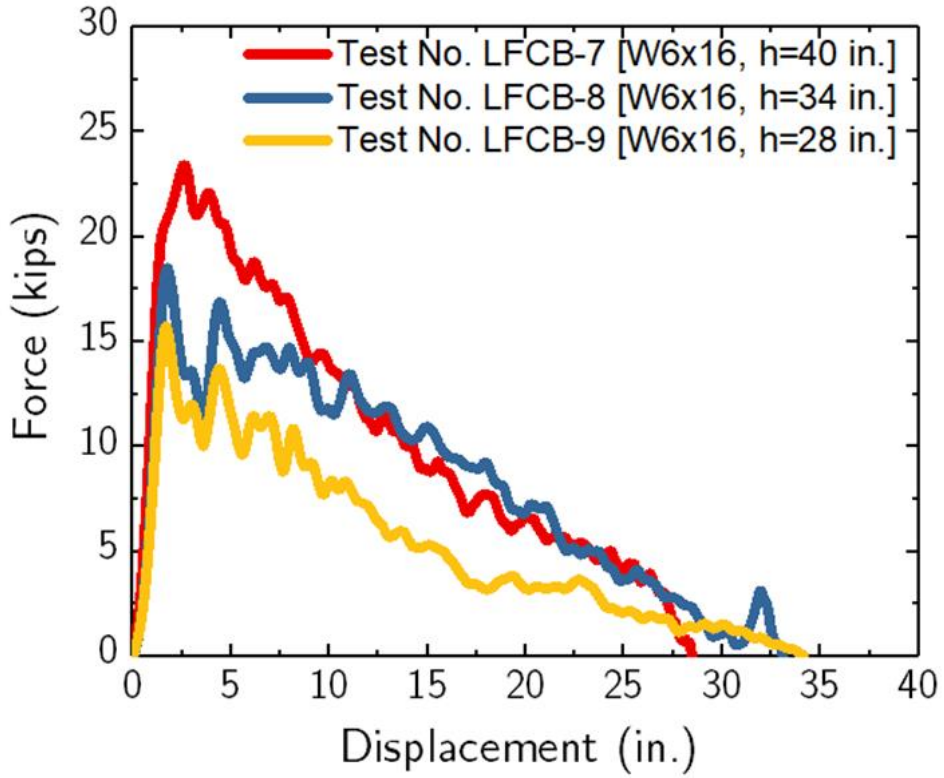

Figure 27. Force vs. Displacement Curves, Test Nos. LFCB-7 through LFCB-9

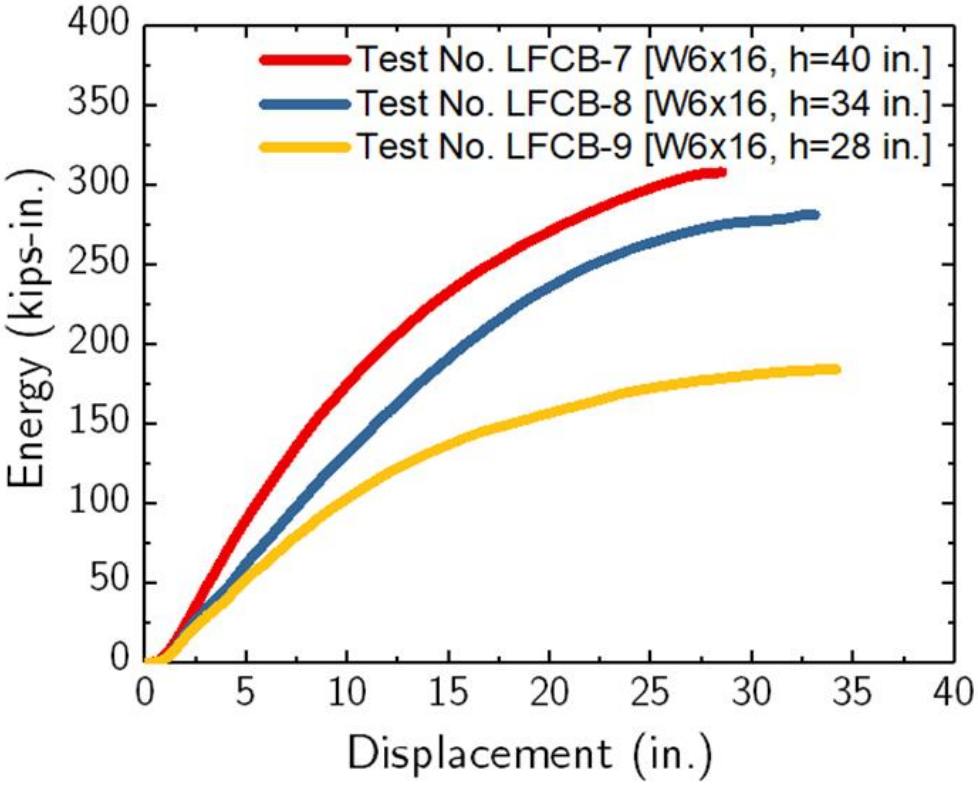

Figure 28. Energy vs. Displacement Curves, Test Nos. LFCB-7 through LFCB-9

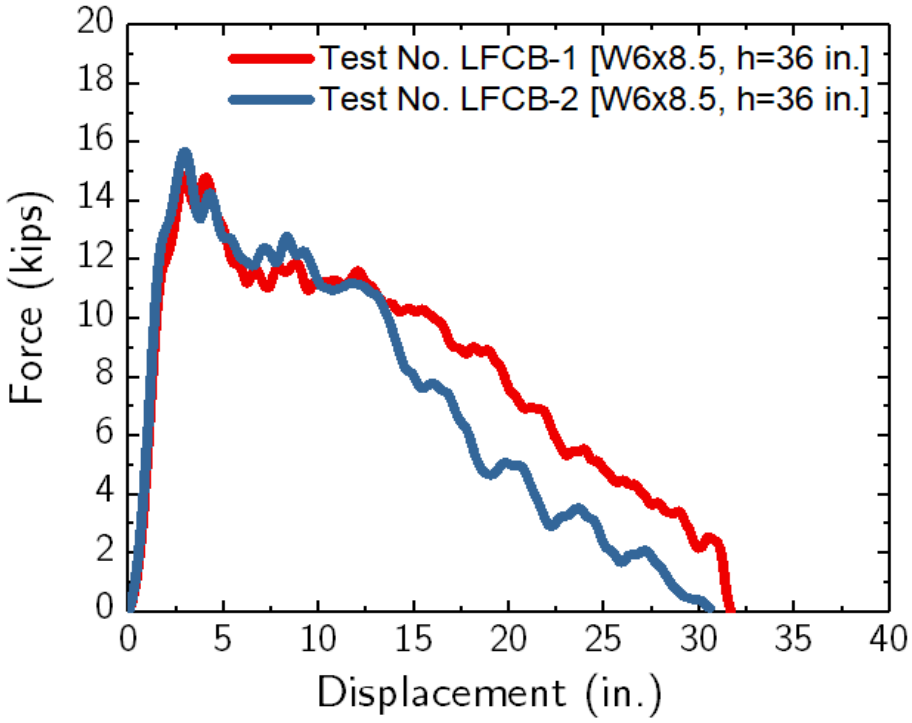

Figure 29. Force vs. Displacement Curves, Test Nos. LFCB-1 and LFCB-2

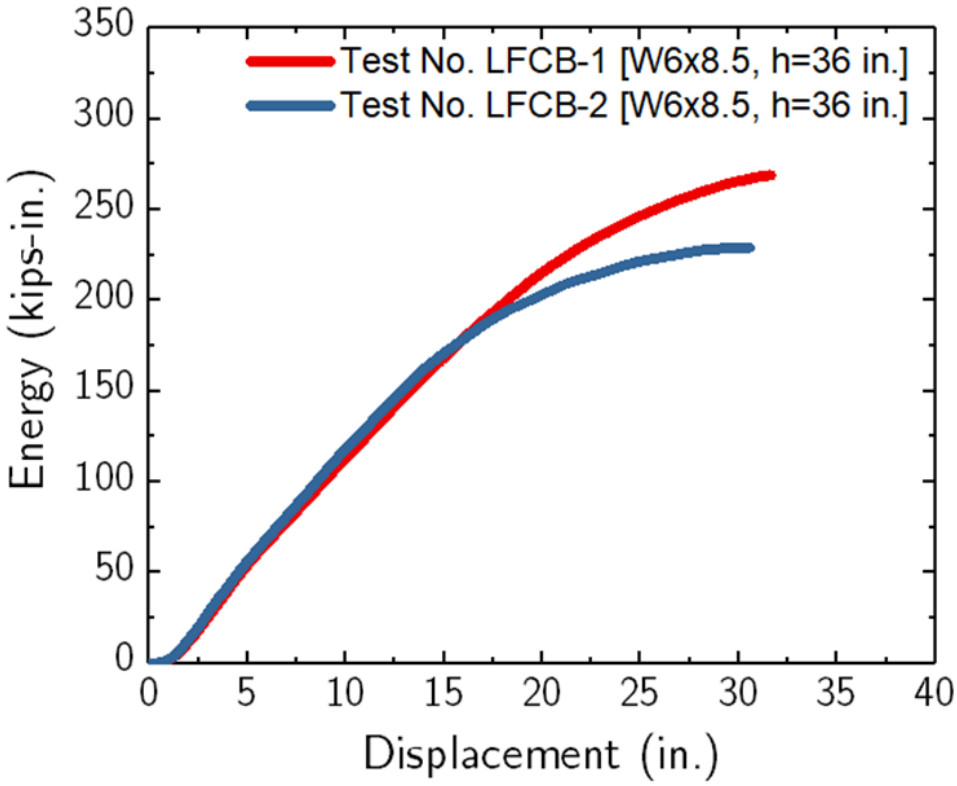

Figure 30. Energy vs. Displacement Curves, Test Nos. LFCB-1 and LFCB-2

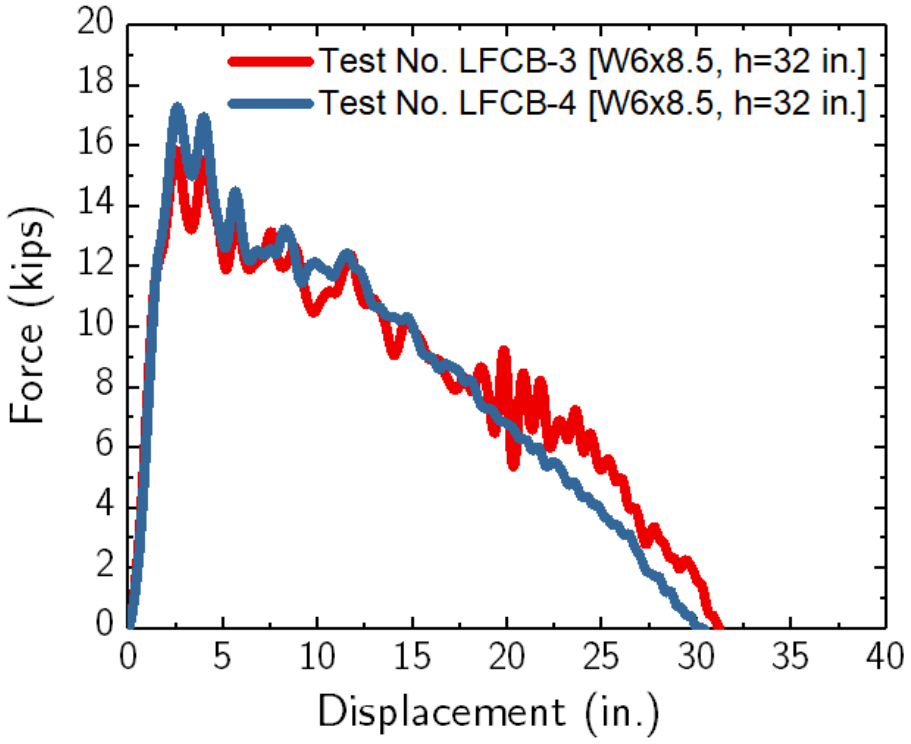

Figure 31. Force vs. Displacement Curves, Test Nos. LFCB-3 and LFCB-4

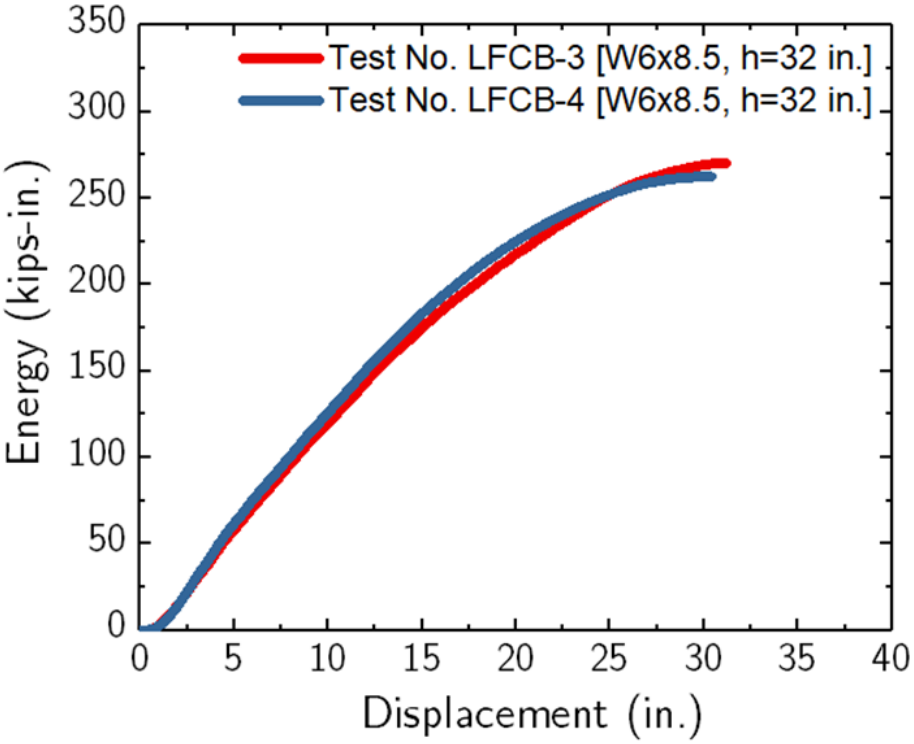

Figure 32. Energy vs. Displacement Curves, Test Nos. LFCB-3 and LFCB-4

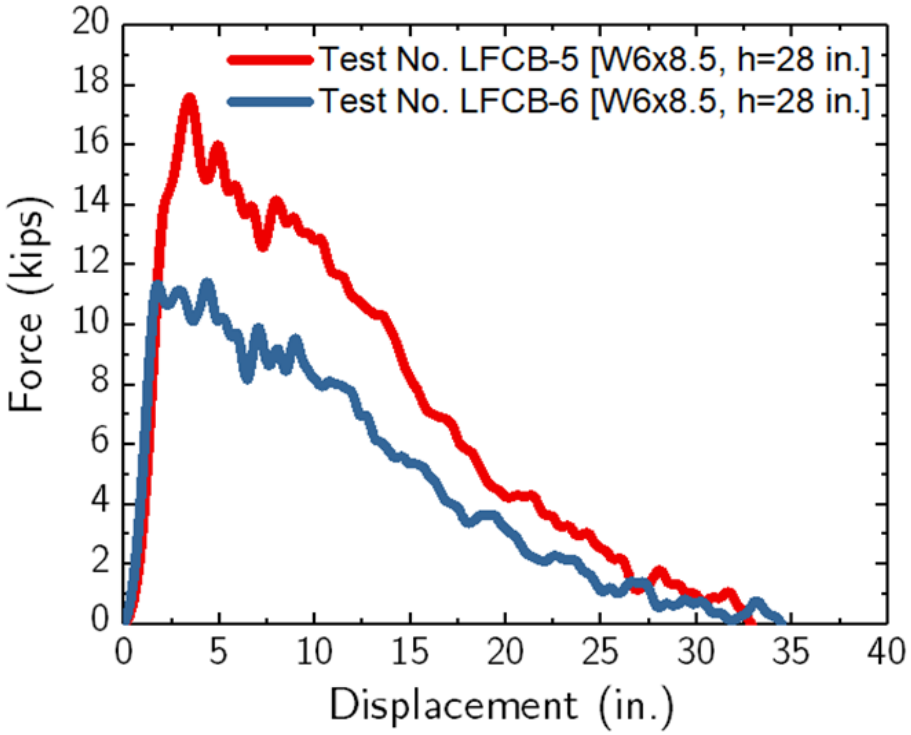

Figure 33. Force vs. Displacement Curves, Test Nos. LFCB-5 and LFCB-6

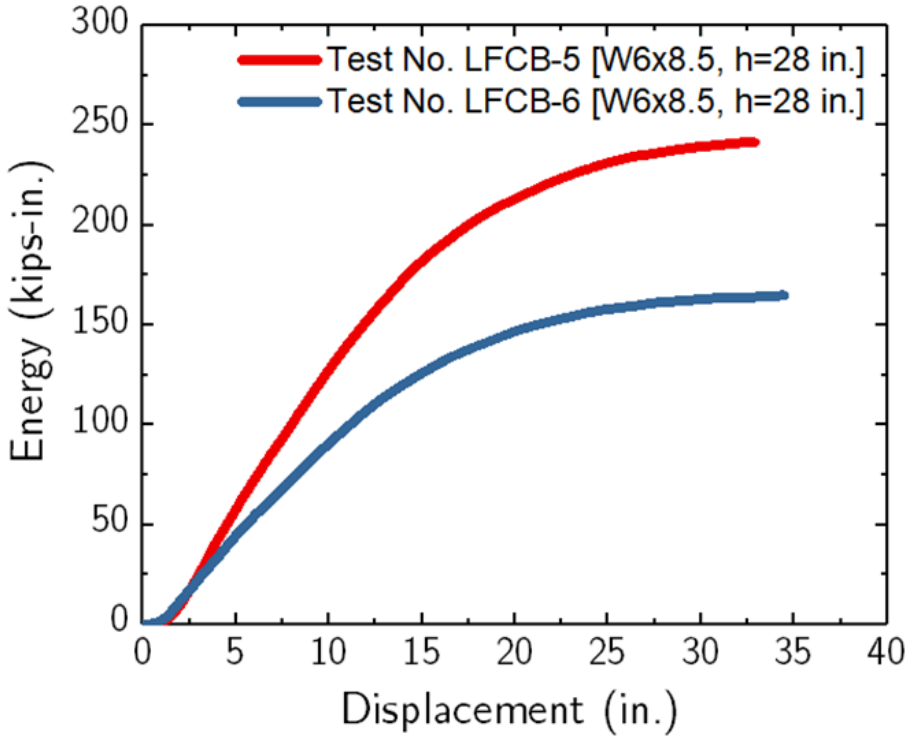

Figure 34. Energy vs. Displacement Curves, Test Nos. LFCB-5 and LFCB-6

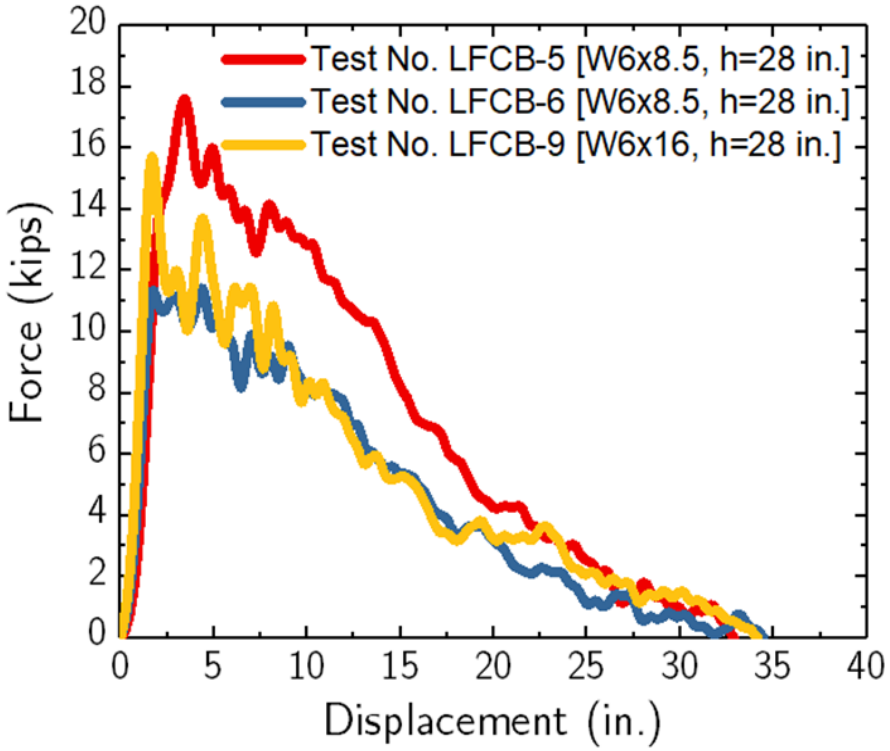

Figure 35. Force vs. Displacement Curves, Test Nos. LFCB-5, LFCB-6, and LFCB-9

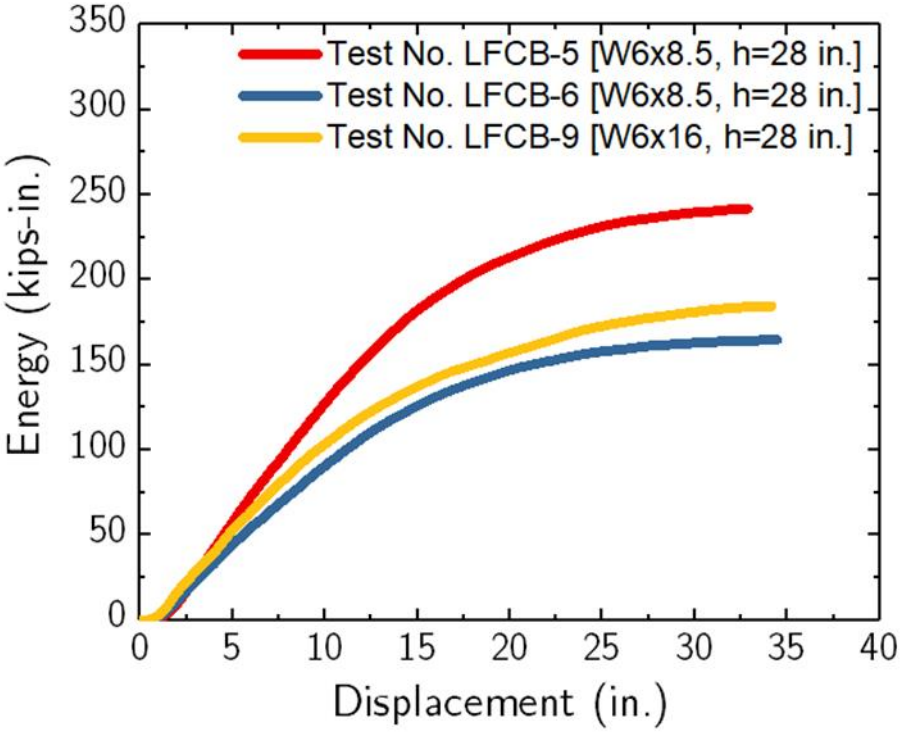

Figure 36. Energy vs. Displacement Curves, Test Nos. LFCB-5, LFCB-6, and LFCB-9

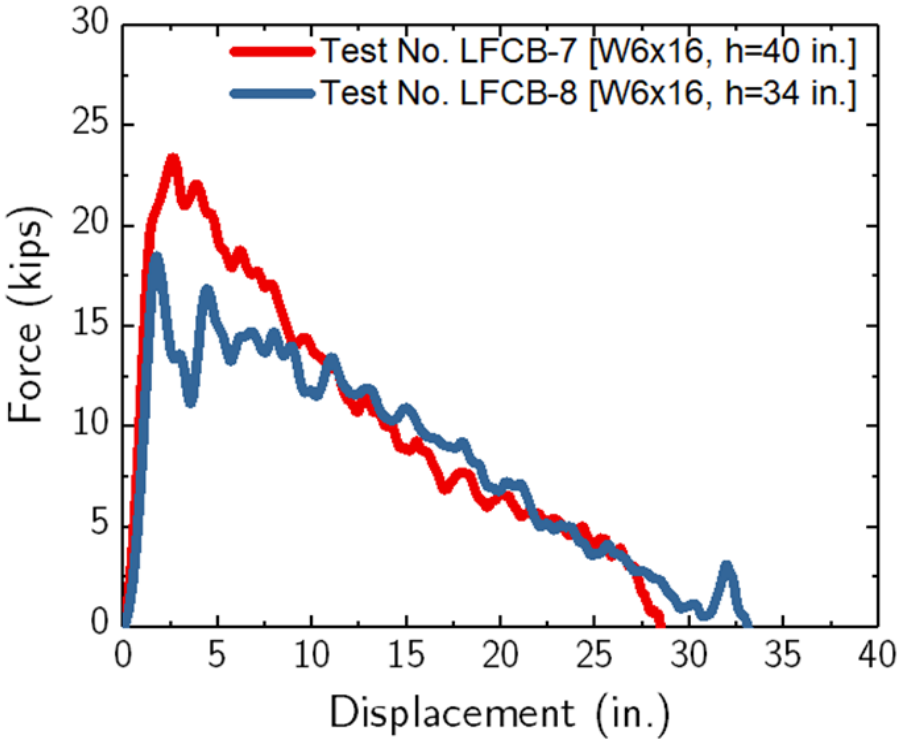

Figure 37. Force vs. Displacement Curves, Test Nos. LFCB-7 and LFCB-8

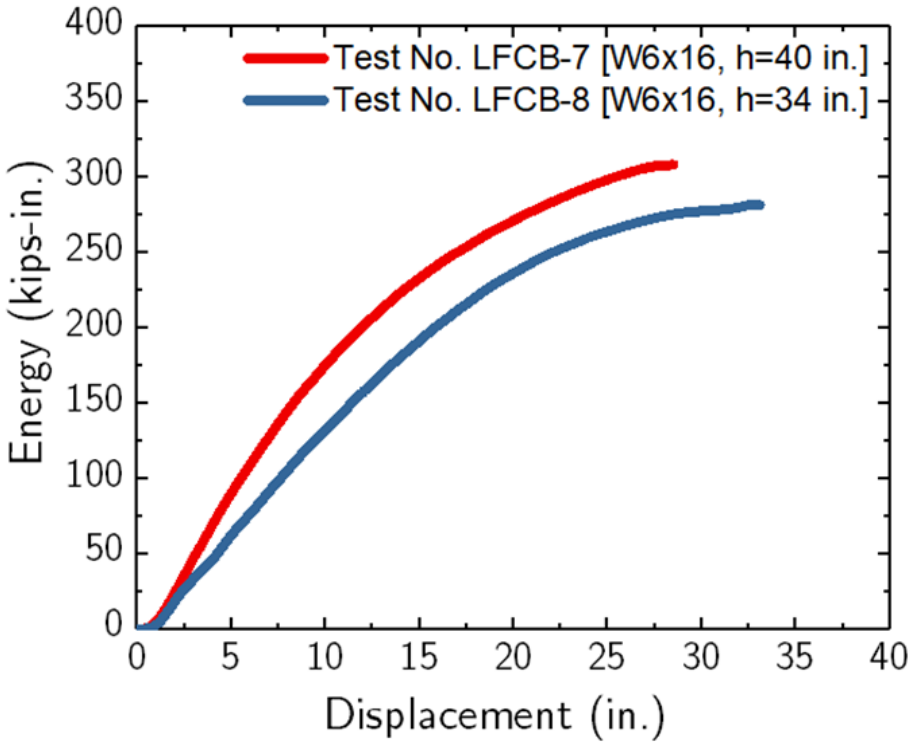

Figure 38. Energy vs. Displacement Curves, Test Nos. LFCB-7 and LFCB-8

4 COMPONENT MODELING AND SIMULATION

4.1 Soil-Spring Model Development

A series of finite element analyses were conducted using the LS-DYNA program [18] to evaluate the soil-embedded posts at different embedment depths under impact loading. LS-DYNA has an extensive library of material models and element formulations and has been widely used to solve non-linear, complex dynamic problems such as vehicle impacts. In a direct approach, a volume of soil needs to be modeled as a discretized block using solid elements. This approach might be relatively robust but is computationally inefficient. In addition, it has been difficult to select a proper constitutive model to reasonably replicate soil behavior under impact loads. Other shortcomings of this approach include its large dependency on the input parameters for material as well as induced hourglass energies (i.e., non-physical and zero-energy modes caused by large deformations).

The researchers at MwRSF have developed a simplified practice-oriented soil-spring model to predict the performance of a 40-in. deep soil-embedded post under vehicle impact [19]. Basically, soil springs in the model represent the soil resistance along the post. In order to develop the soil-spring model, bogie testing was conducted on a steel W6x16 post. The W6x16 was selected because it was desired the post not plastically deform, ensuring that only the soil would fail. Using the bogie test results, the force-deflection curve associated with the soil springs was determined and incorporated into the full LS-DYNA MGS model. Previously, the simplified soil-spring model was validated for 40-in. embedded posts in the full MGS model impacted by a pickup truck. This MGS model consisted of in-line W6x9 steel posts. Two soil springs were utilized in both the lateral and longitudinal directions attached to the top of a soil tube approximately 6 in. below the ground line to model the soil resistance, as shown in Figure 39a. The past full-scale crash tests revealed that post tend to rotate around two-thirds of the post embedment depth. In order to replicate this rotation point in a simplified soil model, the soil tubes were rigid and constrained from movement, except that they could rotate backward about their centroid, or at two-thirds of the post embedment depth. In order to simulate the bogie tests, a previously developed bogie model was utilized, as shown in Figure 39b. The bogie model had an initial velocity and weight of 20 mph and 1,876 lb, respectively, to match the actual bogie vehicle. A *CONTACT_ AUTOMATIC_GENERAL command was used for the contact between the bogie head and the fracturing bolt post. The simulation results were compared to a previously conducted full-scale crash test. The proposed soil-spring model indicated promising results to replicate post deformation in a guardrail-vehicle impact.

In that study, the soil force vs. deflection curve was developed for a 40-in. deep post and was based on one bogie test. The current research aims to study the applicability of this simplified method for shallower depths, in particular, embedment depths between 28 in. and 40 in.

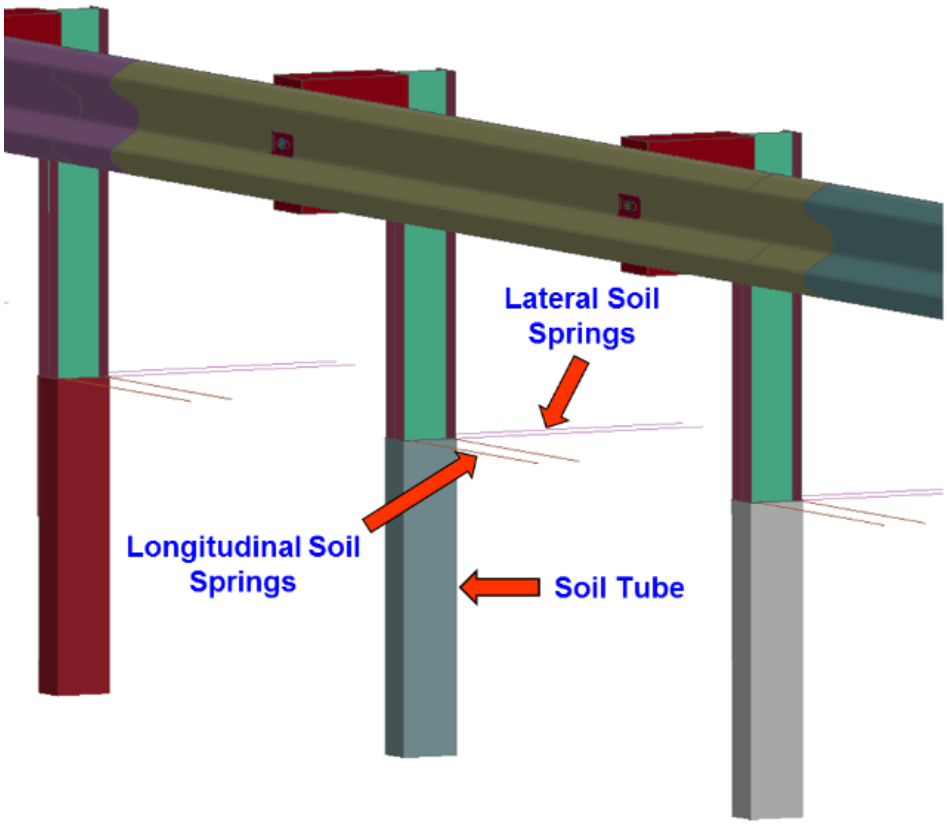

(a)

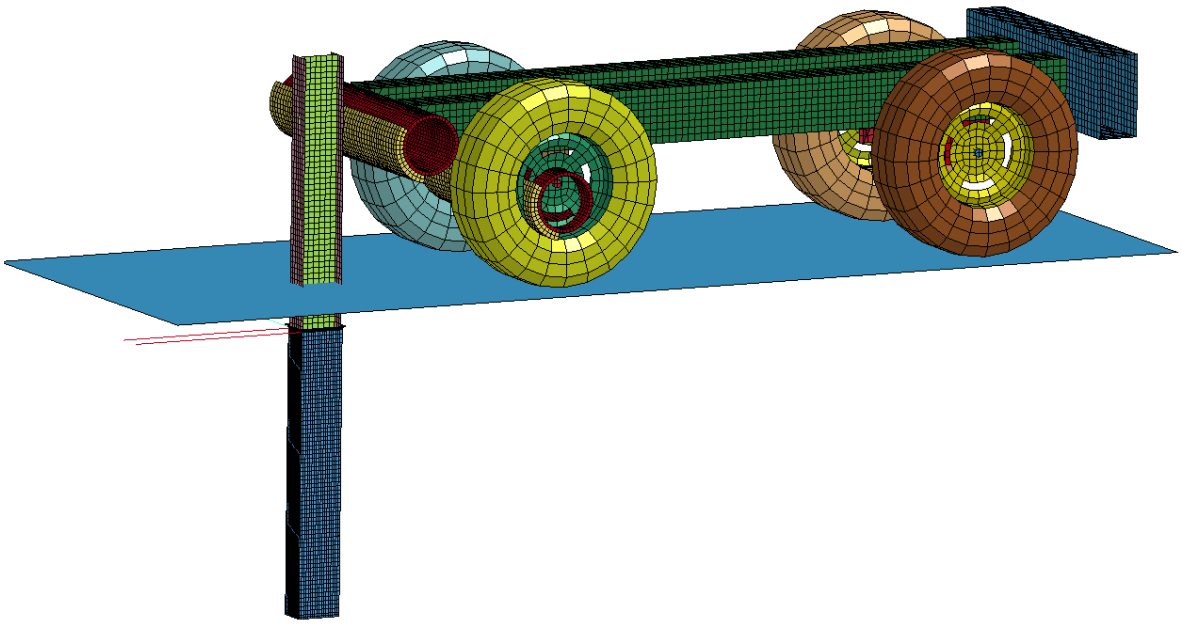

(b)

Figure 39. (a) W6x9 Steel Post and Soil Spring Model, and (b) Post and Bogie Model

In the current study, a series of bogie tests were conducted on W6x8.5 and W6x16 steel posts. As explained in Section 2.2, the first round of bogie tests, test nos. LFCB-1 through LFCB-5, with W6x8.5 steel posts did not provide desired data for shallower post embedment depths due to the post yielding. In the next round of bogie tests, test nos. LFCB-7 through LFCB 9, as well as in test no. LFCB-6, the post did not yield and only rotated, which isolated the soil resistance from the post resistance in the impact events. Thus, the data from test nos. LFCB-7 through LFCB-9 and test no. LFCB-6 was used to establish the soil spring curve. The analysis approach for one test, using test no. LFCB-7 as an example, is as follows. The same approach was repeated for the analysis of other bogie tests.

- Force vs. displacement curve was obtained from test no. LFCB-7 and a simplified curve was approximated, as shown in Figure 40.

- Using the side-splitter theorem for similar triangles, the soil resistance force was calculated from the force applied at the impact level, as shown in Figure 41. For the development of the soil spring model, the rotation point was assumed to be two-thirds of the embedment depth below ground. There is not one definite rotation point, as it can vary slightly between tests and with soil properties and compaction levels.

- The soil resistance is a continuous resistive force applied to the entire depth of the embedded post. However, this force was simplified to a one soil resistance force, F_{soil}, located at 6 in. below the ground line. The applied force, F_{impact}, was located at a height of 24.875 in.

- Sum of the moments about the rotation point, M_o, are equal to zero, the soil resistance force can be solved by using the following equations.

$$\sum M_0 = F_{soil}(26.67\ in. - 6\ in.) - F_{impact}(26.67\ in. + 24.875) = 0$$

$$F_{soil} = 2.493F_{impact}$$

  Thus, the simplified applied force vs. displacement curve in Figure 40 was multiplied by 2.493 to obtain a soil resistance curve.

- The force and displacement were converted into units of kN and mm, respectively, to be incorporated into the LS-DYNA model.

- Additionally, since two soil springs were attached to the soil tubes in each of the lateral and longitudinal directions, the soil resistance curve for one spring was found by dividing the curve by two, as shown in Figure 42.

- These steps were repeated for all three W6x16 post bogie tests (i.e., test nos. LFCB-7 through LFCB-9).

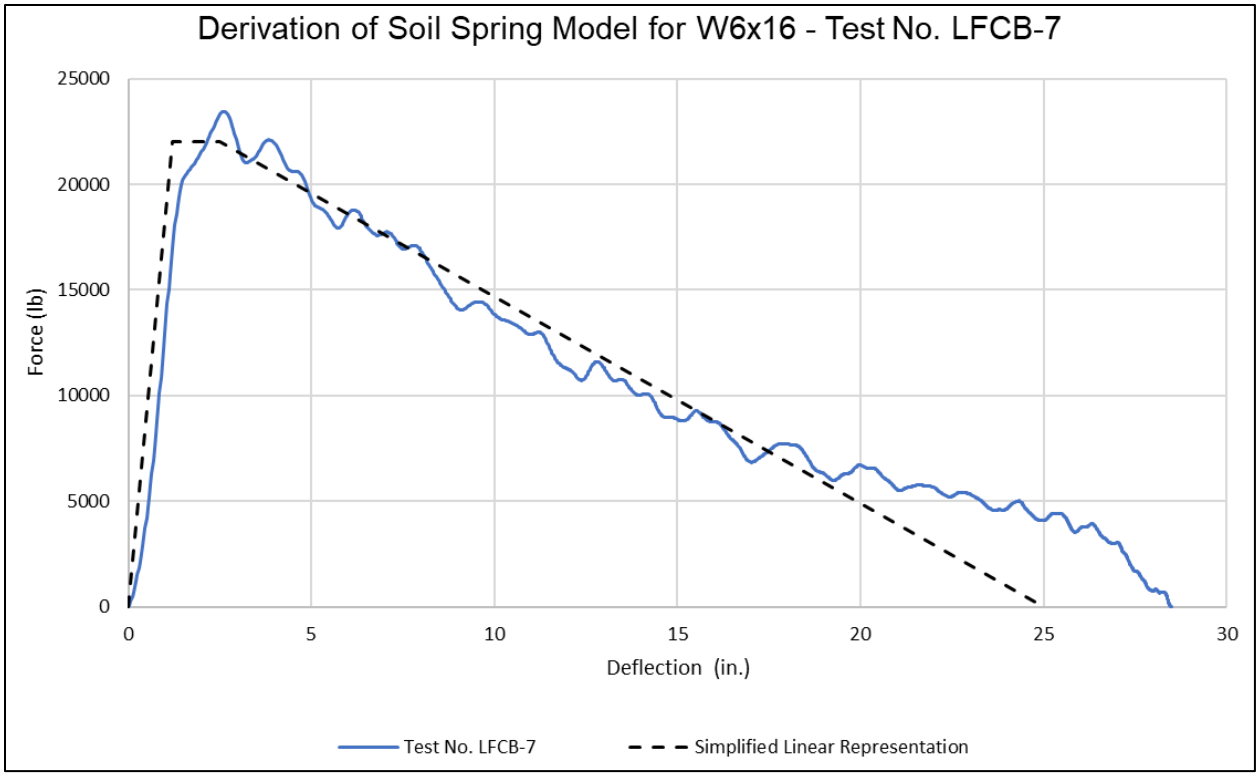

Figure 40. Force vs. Displacement at Impact Height, Test No. LFCB-7

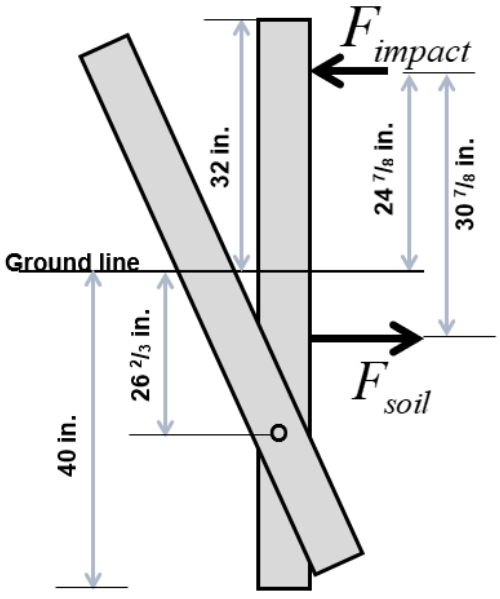

Figure 41. Free-Body Diagram of Bogie, Post, and Soil – Test No. LFCB-7 with Post Embedment Depth of 40 in.

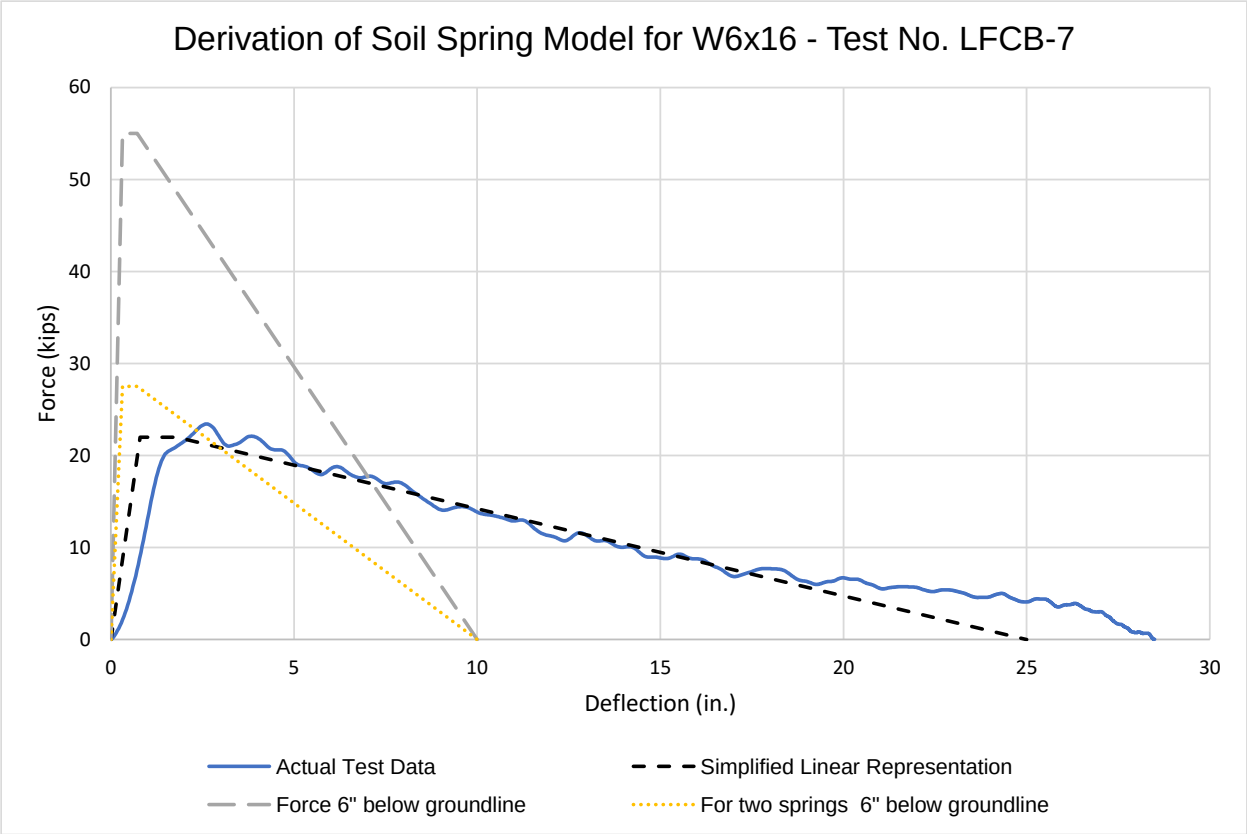

Figure 42. Force vs. Displacement Curve for Soil Springs at 6-in. below Ground, Test No. LFCB-7

4.2 Initial Model Results

Test nos. LFCB-7 through LFCB-9, using a W6x16 post, were simulated incorporating the soil-spring model. Using the approximation method, explained in the previous section, the soil force vs. displacement curves were obtained for 40, 34, and 28-in. embedment depths. Simulated average force and energy over 5, 10, 15, and 20 in. of displacement were compared with the measured forces and energy in the associated bogie tests (i.e., test nos. LFCB-7 through LFCB-9). The approach was repeated until a reasonable match was achieved between the simulated and measured average force and energy, as shown in Figures 43 and 44. It was challenging to find the perfect match for all displacements, in particular in the first 5 in. of displacement. The goal was to achieve the overall best possible match in all displacements as well as energies.

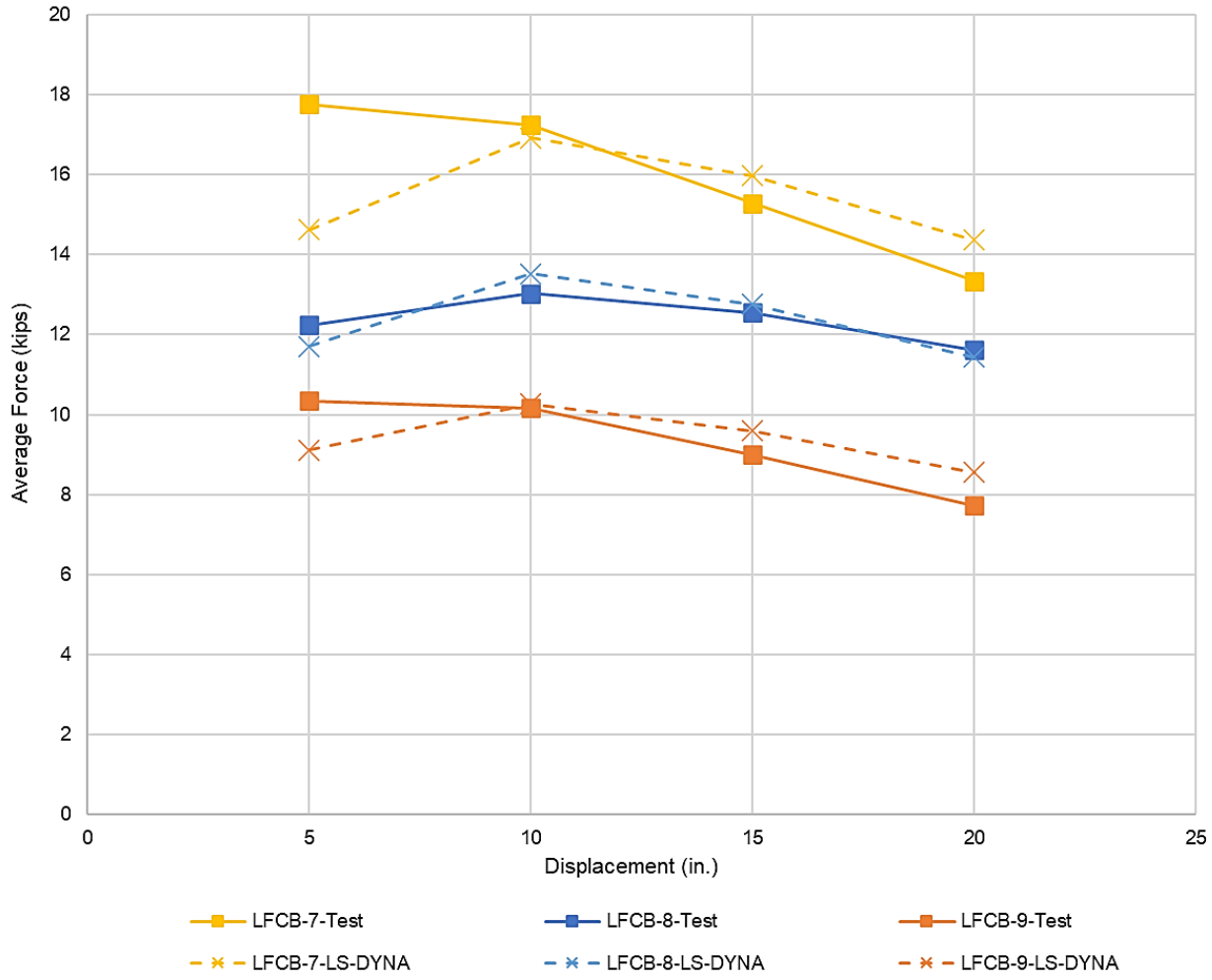

Figure 43. Average Force vs. Displacement, Test Nos. LFCB-7 through LFCB-9

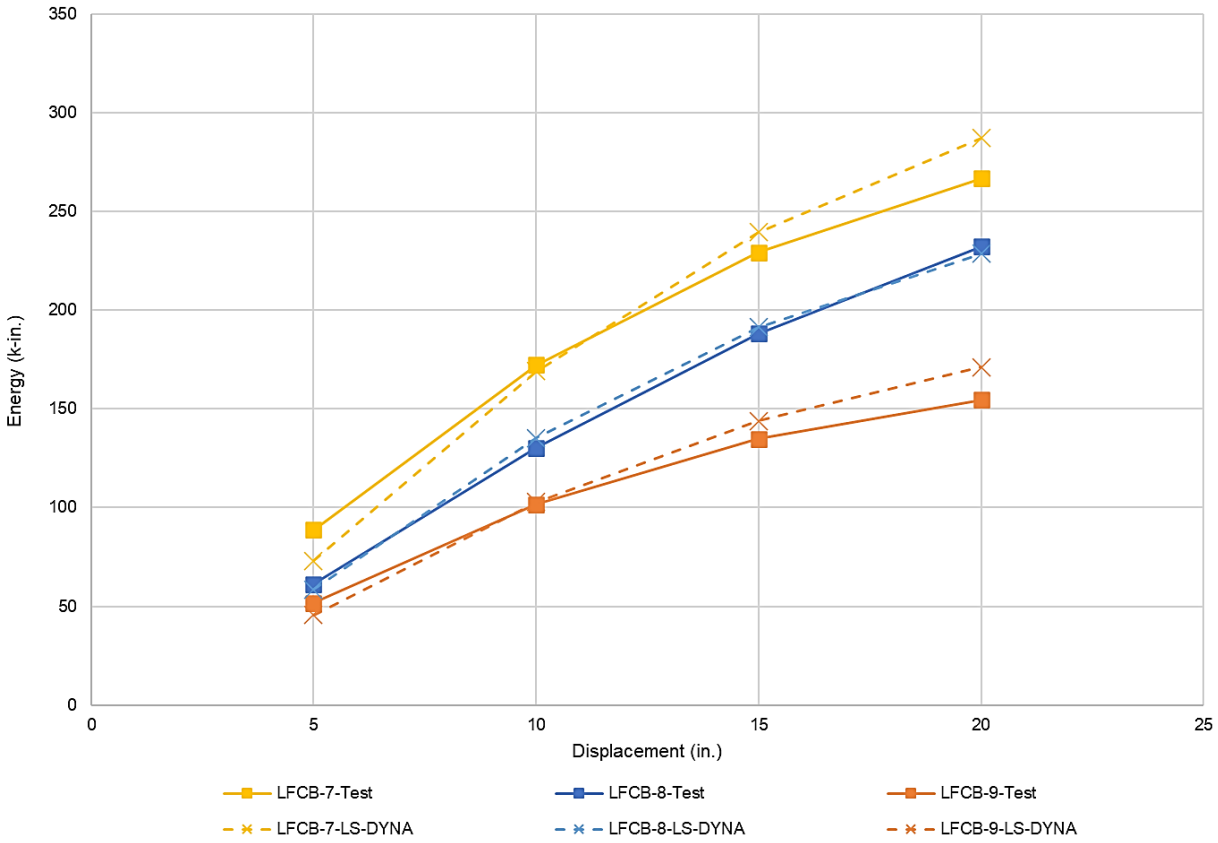

Figure 44. Energy vs. Displacement, Test Nos. LFCB-7 through LFCB-9

The soil force vs. displacement that led to the reasonable match for test nos. LFCB-7 through LFCB- 9 were adopted to continue the simulation of bogie tests with a W6x8.5 post (i.e., test nos. LFCB-1 through 6, except the outlier test, test no. LFCB-5). Note that this force vs. displacement relates to soil springs at spring level, not at the impact height level.

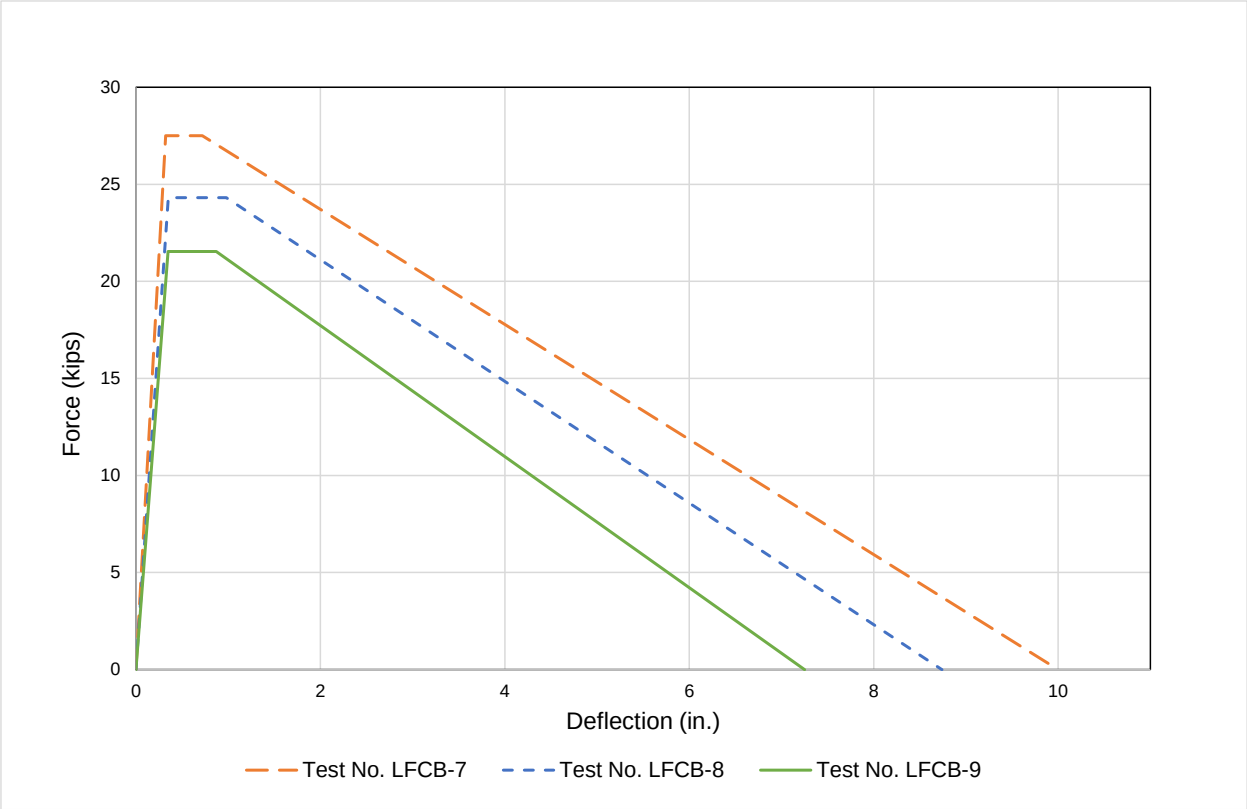

Figure 45. Soil Spring Force vs. Displacement, Test Nos. LFCB-7 through LFCB-9

4.3 Improved Soil Tube Development

Next, the obtained soil spring curves were incorporated in the LS-DYNA simulations of test nos. LFCB-1 through LFCB-4 and LFCB-6, which used a W6x8.5 post. The simulated force at the impact height was compared to the actual force in the bogie test. It was realized that the simulated force dropped significantly right after the post yielded, while in the bogie tests with a W6x8.5 post, the post could carry force over a longer displacement. This observation was believed to relate to the sharp edges of the soil tube that was artificially used in the simulation. In the bogie tests, the surrounding soil allows the post to gradually deform and buckle at the ground line where the hinge develops. Thus, the post would carry a larger amount of force after hinge deformation in the post at the ground line. A comparison of the simulated and measured force in test nos. LFCB-1 and LFCB-2 are shown in Figure 46.

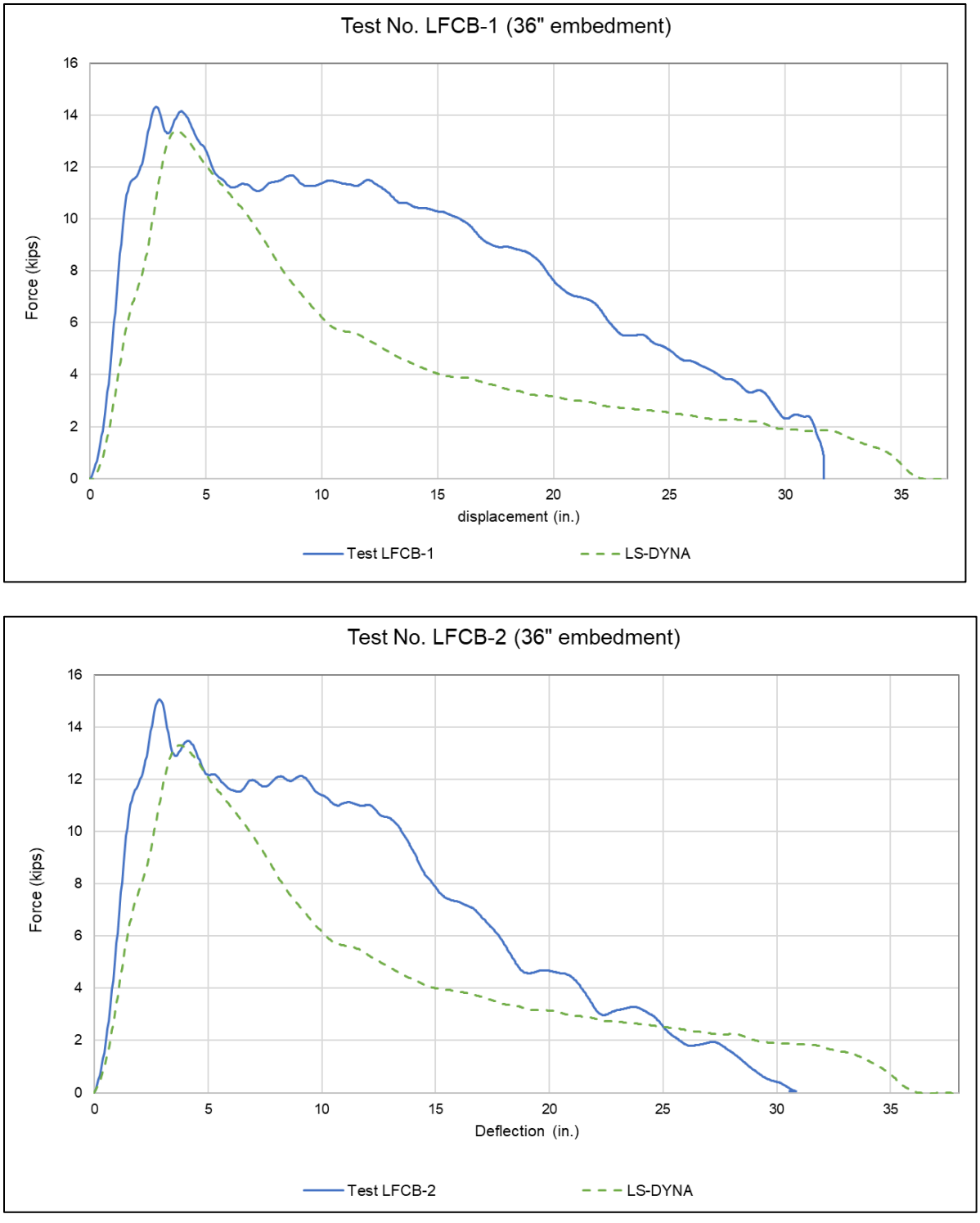

Figure 46. Simulated and Measured Force vs. Displacement at Impact Height, Test Nos. LFCB-1 and LFCB-2

The simulation efforts continued to revise the soil tube configuration for a better prediction of post deformation at the ground line. A number of soil tubes with various straight and curved flares with different heights were explored, as shown in Tables 4 and 5. The simulation with a soil

tube configuration of a 6-in. height and 5-degree flare led to the best results in terms of predicting post deformation and force and energy vs. displacement, as shown in Figures 47 through 49. Comparing the simulation results confirmed that the 4C-5deg soil tube model provided the best overall response.

Table 3. Soil Tube Configurations for Improved Soil-Spring Model Investigation

Steel Tube Concepts			
2 in. Height Straight Flare	**6 in. Height Straight Flare**	**2 in. Height Straight + Curve Flare**	**6 in. Height Straight + Curve Flare**
5-deg. flare	5-deg. flare	5-deg. flare	5-deg. flare
15-deg. flare	15-deg. flare	15-deg. flare	15-deg. flare
15-deg. flare	15-deg. flare	15-deg. flare	15-deg. flare
20-deg. flare	20-deg. flare	20-deg. flare	20-deg. flare
25-deg. flare	25-deg. flare	25-deg. flare	25-deg. flare
30-deg. flare	30-deg. flare	30-deg. flare	30-deg. flare

Table 4. Soil Tube Configurations for Improved Soil-Spring Model Investigation – Straight Flare

2-in. Height + Straight Flare

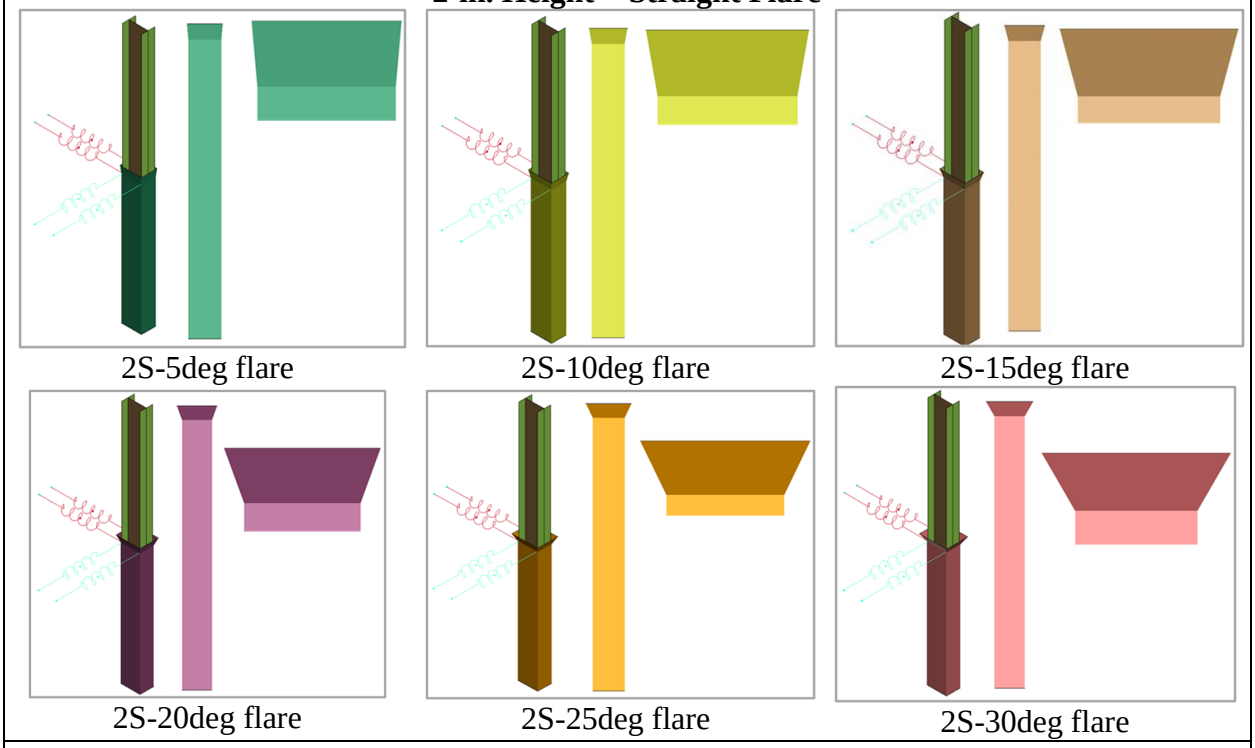

2S-5deg flare | 2S-10deg flare | 2S-15deg flare

2S-20deg flare | 2S-25deg flare | 2S-30deg flare

6-in. Height + Straight Flare

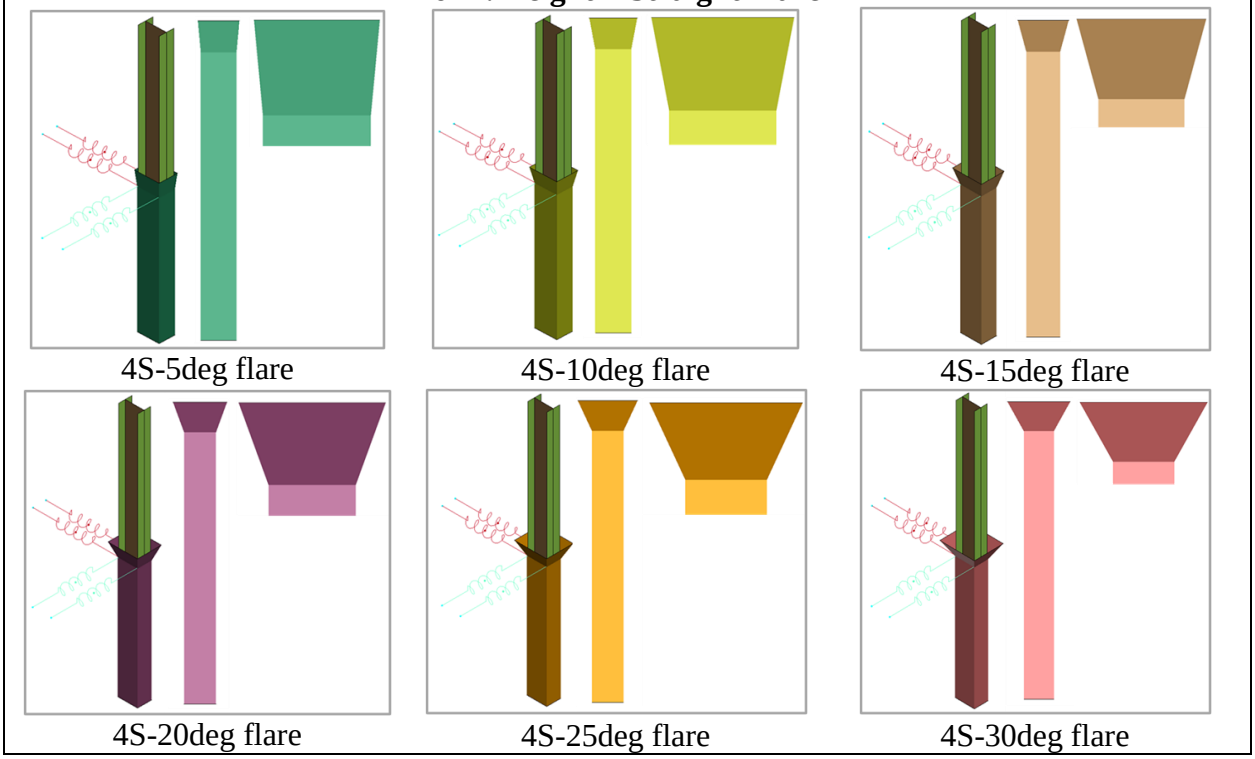

4S-5deg flare | 4S-10deg flare | 4S-15deg flare

4S-20deg flare | 4S-25deg flare | 4S-30deg flare

Table 5. Soil Tube Configurations for Improved Soil-Spring Model Investigation – Curved Flare

2-in. Height + Curved Flare

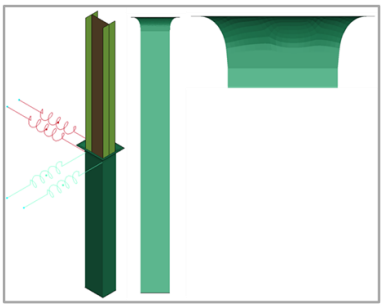

2C-5deg flare

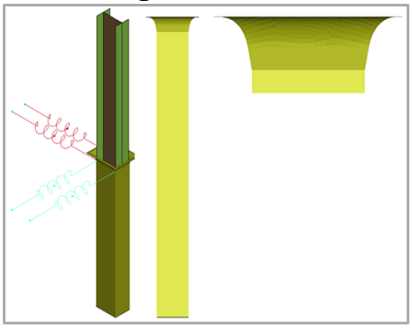

2C-10deg flare

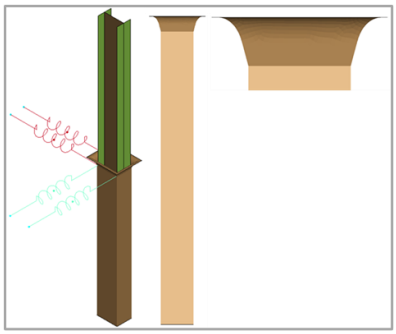

2C-15deg flare

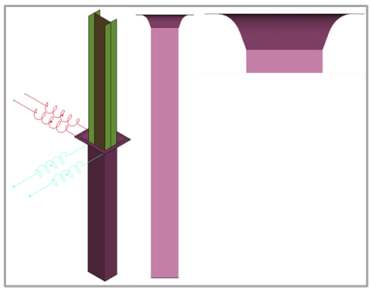

2C-20deg flare

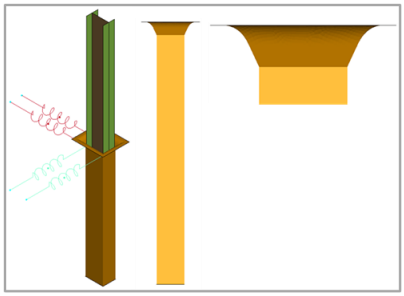

2C-25deg flare

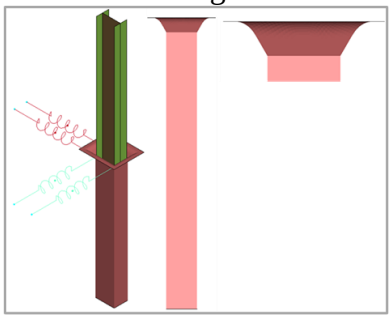

2C-30deg flare

6-in. Height + Curved Flare

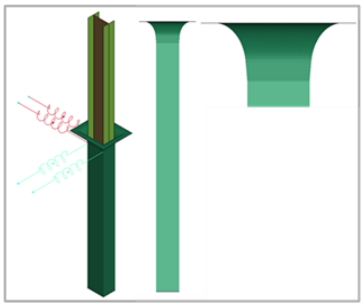

4C-5deg flare

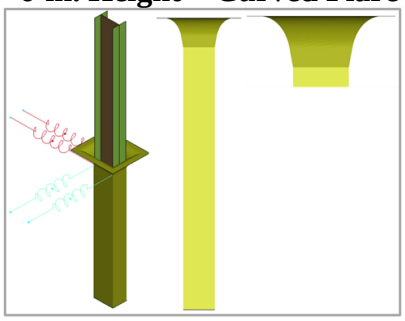

4C-10deg flare

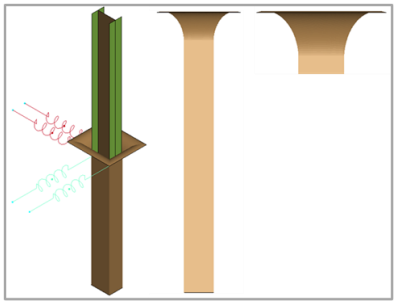

4C-15deg flare

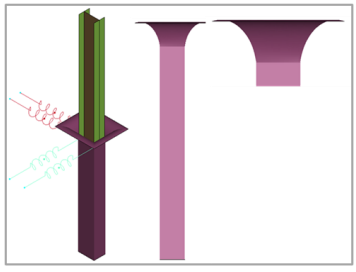

4C-20deg flare

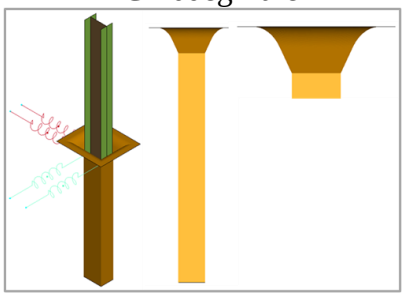

4C-25deg flare

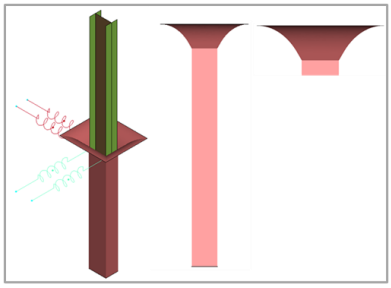

4C-30deg flare

Test Nos. LFCB-1 and LFCB-2

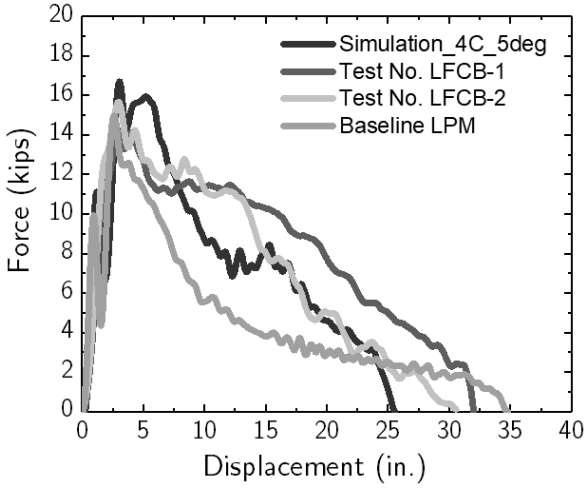

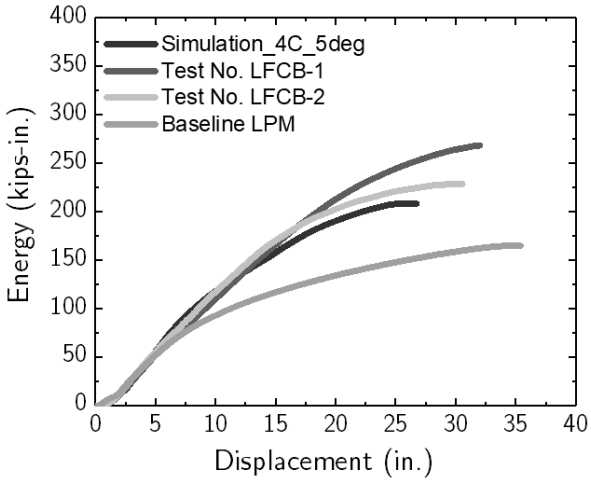

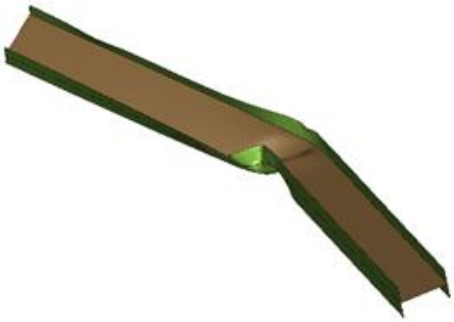

Simulation

Test No. LFCB-1

Test No. LFCB-2

Figure 47. Simulation Results with 4C-5deg Soil Tube, Test Nos. LFCB-1 and LFCB-2

Test Nos. LFCB-3 and LFCB-4

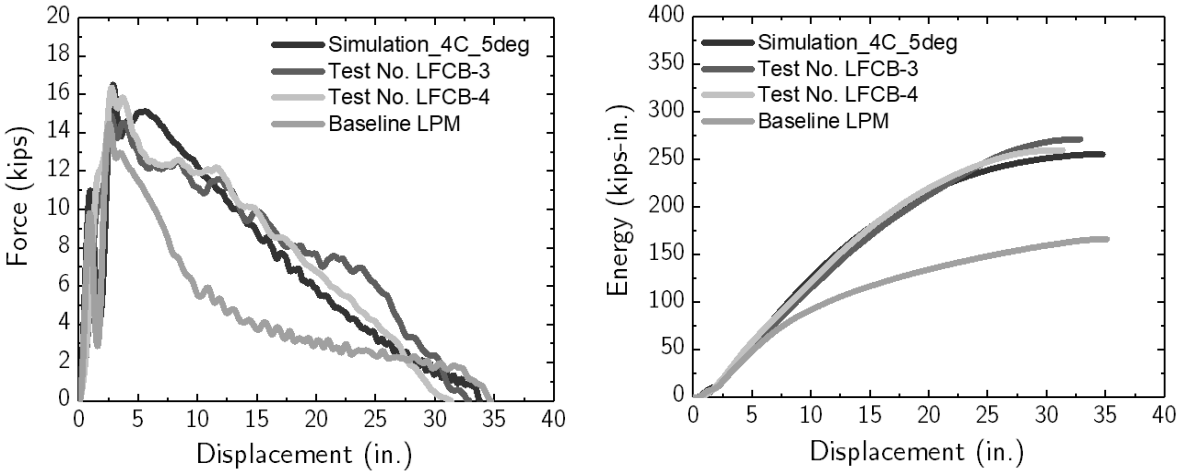

Simulation | Test No. LFCB-3 | Test No. LFCB-4

Figure 48. Simulation Results with 4C-5deg Soil Tube Configuration, Test Nos. LFCB-3 and LFCB-4

Test No. LFCB-6

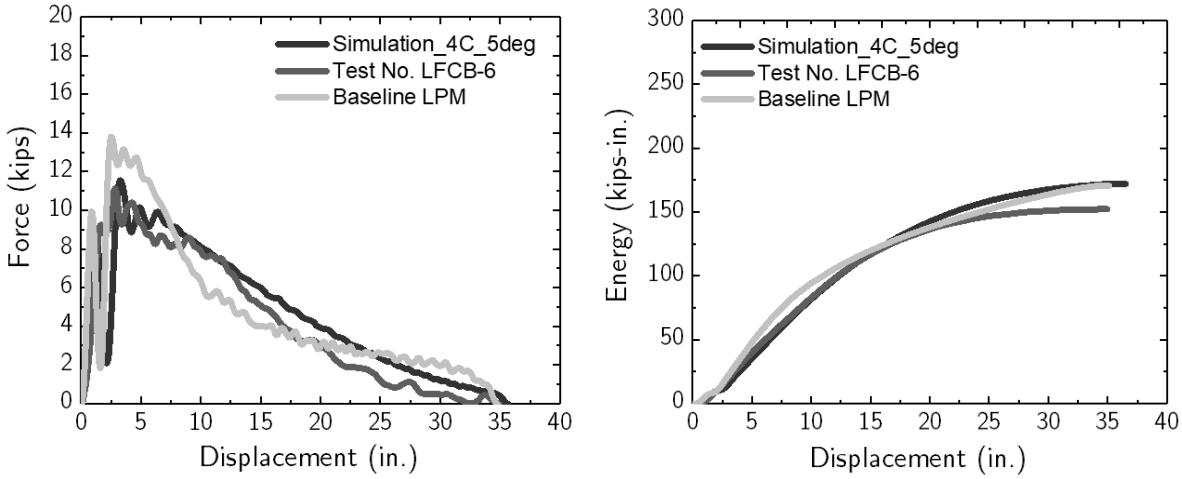

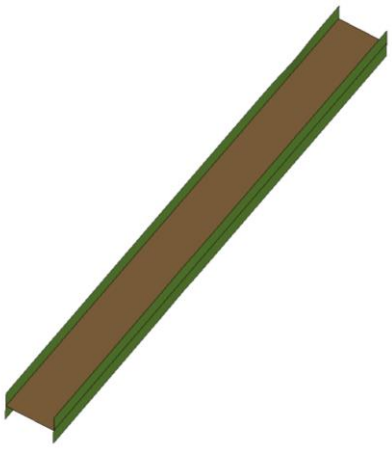

Simulation

Test No. LFCB-6

Figure 49. Simulation Results with 4C-5deg Soil Tube Configuration, Test No. LFCB-6

4.4 Selected Soil-Spring Model

Comparing the simulation results confirmed that the model with the soil tube configuration of a 6-in. height and 5-degree flare provided best overall response. A comparison of the error (i.e., difference between actual measured force and simulated force) for various soil tube configurations is shown in Table 6. The least error was found for the 4C-5deg soil tube model. Thus, this soil tube model was selected for further modeling.

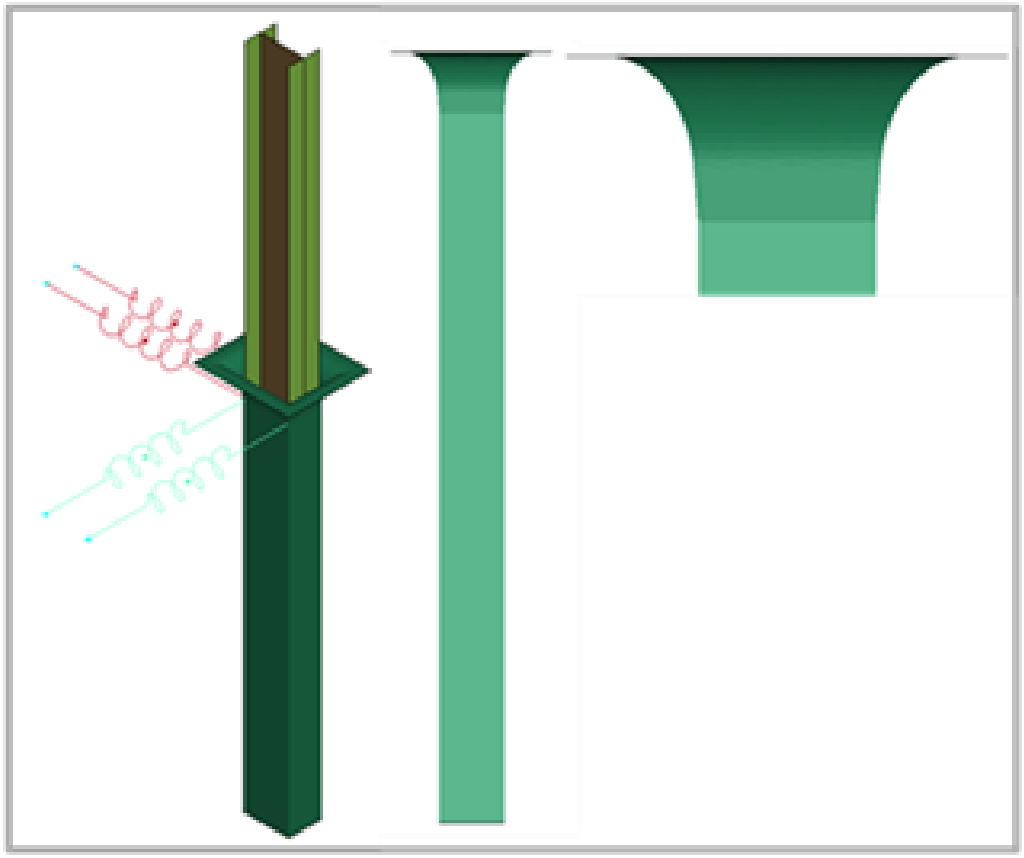

Figure 50. Selected 4C-5deg Soil Tube Configuration

Additionally, a numerical simulation technique based on the adaptive coupling of Finite Element Method (FEM) and Smoothed-particle hydrodynamics (SPH) methods was employed for modeling the impact dynamics of posts embedded in stiffer MASH strong soil, test nos. LFCB-1 through LFCB-4, which is detailed in Appendix C. An important aspect in evaluating the predictive capability of the adaptive FEM-SPH method was the accuracy of numerical simulation results in determining the force vs. displacement and energy vs. displacement responses of the post-soil system. Comparisons of results from simulation and physical impact tests were discussed. It was believed that the adoption of this soil modeling method for that project would improve the analysis of design for this research project and provide insight into future soil modeling efforts. Since this effort was out of the scope of the project and this advanced method would significantly increase the computational time for a full MGS model, this method was not pursued and the simplified soil spring model was adopted for full MGS simulations under TL-2 and TL-3 impact conditions, as reported in the following chapter.

Table 6. Calculated Errors in Prediction of Average Force for Various Soil Tube Configurations

Item	**Average Force (kN) [%Error]**			
	@ 5 in.	**@10 in.**	**@ 15 in.**	**@ 20 in.**
Simulation: 4S_5 deg. flare	50.72 [-6.31%]	53.40 [6.54%]	44.71 [9.24%]	39.62 [11.11%]
Simulation: 4C_5 deg. flare	49.48 [-3.71%]	51.89 [-3.53%]	46.18 [6.25%]	41.77 [6.28%]
Simulation: 4C_25 deg. flare	46.47 [2.60%]	45.35 [9.52%]	43.10 [12.51%]	40.92 [8.19%]
Simulation: 4C_30 deg. flare	46.04 [3.50%]	44.41[11.39%]	41.97 [14.80%]	38.66 [13.26%]
Test No. LFCB-1	46.17	48.50	48.66	46.71
Test No. LFCB-2	49.24	51.73	49.86	44.43
Test Average	47.71	50.12	49.26	44.57

Item	**Average Force (kN) [%Error]**			
	@ 5 in.	**@10 in.**	**@ 15 in.**	**@ 20 in.**
Simulation: 4S_5 deg. flare	50.85 [-3.23%]	59.43 [-14.35%]	56.50 [-11.05%]	50.97 [-7.46%]
Simulation: 4C_5 deg. flare	48.27 [2.01%]	55.05 [-5.93%]	52.26 [-2.71%]	47.29 [0.30%]
Simulation: 4C_25 deg. flare	46.33 [5.95%]	51.27 [1.35%]	48.36 [4.95%]	43.64 [7.99%]
Simulation: 4C_30 deg. flare	45.91 [6.80%]	50.27 [3.27%]	47.29 [7.06%]	42.65 [10.08%]
Test No. LFCB-3	47.14	50.59	49.60	46.62
Test No. LFCB-4	51.38	53.35	52.16	48.23
Test Average	49.26	51.97	50.88	47.43

Item	**Average Force (kN) [%Error]**			
	@ 5 in.	@10 in.	@ 15 in.	@ 20 in.
Simulation: 4S_5 deg. flare	34.82 [-2.16%]	39.51 [-8.13%]	37.29 [-9.13%]	33.42 [-11.70%]
Simulation: 4C_5 deg. flare	31.55 [-11.35%]	36.03 [1.40%]	34.45 [-0.82%]	31.30 [-4.61%]
Simulation: 4C_25 deg. flare	29.71 [16.52%]	34.10 [6.68%]	32.81 [3.98%]	30.01 [-0.30%]
Simulation: 4C_30 deg. flare	29.20 [17.95%]	33.56 [8.16%]	32.34 [5.36%]	29.65 [0.90%]
Test No. LFCB-6	35.59	36.54	34.17	29.92

5 SIMULATION OF BASELINE MGS MODEL WITH DODGE RAM VEHICLE

5.1 Introduction

In this study, a finite element model of the MGS was utilized and altered to evaluate the potential for systems with reduced post embedment and reduced post spacing to effectively and adequately contain pickup trucks. Note that the small car simulations were deemed unnecessary due to lower impact loads and thus lower dynamic deflection as compared to the pickup impacts.

Previously, all MGS simulations used the 2007 Chevrolet Silverado vehicle model. During this project, researchers obtained a vehicle model of a 2018 Ram Pickup truck. It was believed that the 2018 Ram vehicle model would provide a better correlation between the simulations and the full-scale test as compared to the 2007 Silverado vehicle model since it was more geometrically similar to the Ram full-scale crash test vehicle. This chapter describes the MGS simulations at TL-2 and TL-3 impact conditions and comparison with the associated crash tests, if available.

5.2 Baseline MGS Model

An improved, updated generation of the MGS LS-DYNA model was developed by researchers at MwRSF [20]. The model was updated to (1) refine the system mesh for improved barrier deflection performance; (2) improve end anchorage design to better match full-scale system construction and results; and (3) improve vehicle-to-barrier interaction and results. Simulation models of the 175-ft long, 31-in. high MGS were successfully calibrated and validated against full-scale crash testing [20-22] using the Roadside Safety Verification and Validation Program (RSVVP) [21]. The calibrated and validated MGS model has been used in many LS-DYNA simulations at MwRSF [23-24]. The MGS is 21.3 in. wide from the front of the W-beam to the back of the posts. The MGS model has evolved to its current version, shown in Figure 51, based on the validation of different components through testing. A comparison of the physical barrier system and the finite element model of the simulated overall barrier system and end anchorage system, as well as the MGS post-rail-soil model, is shown in Figures 51 through 53.

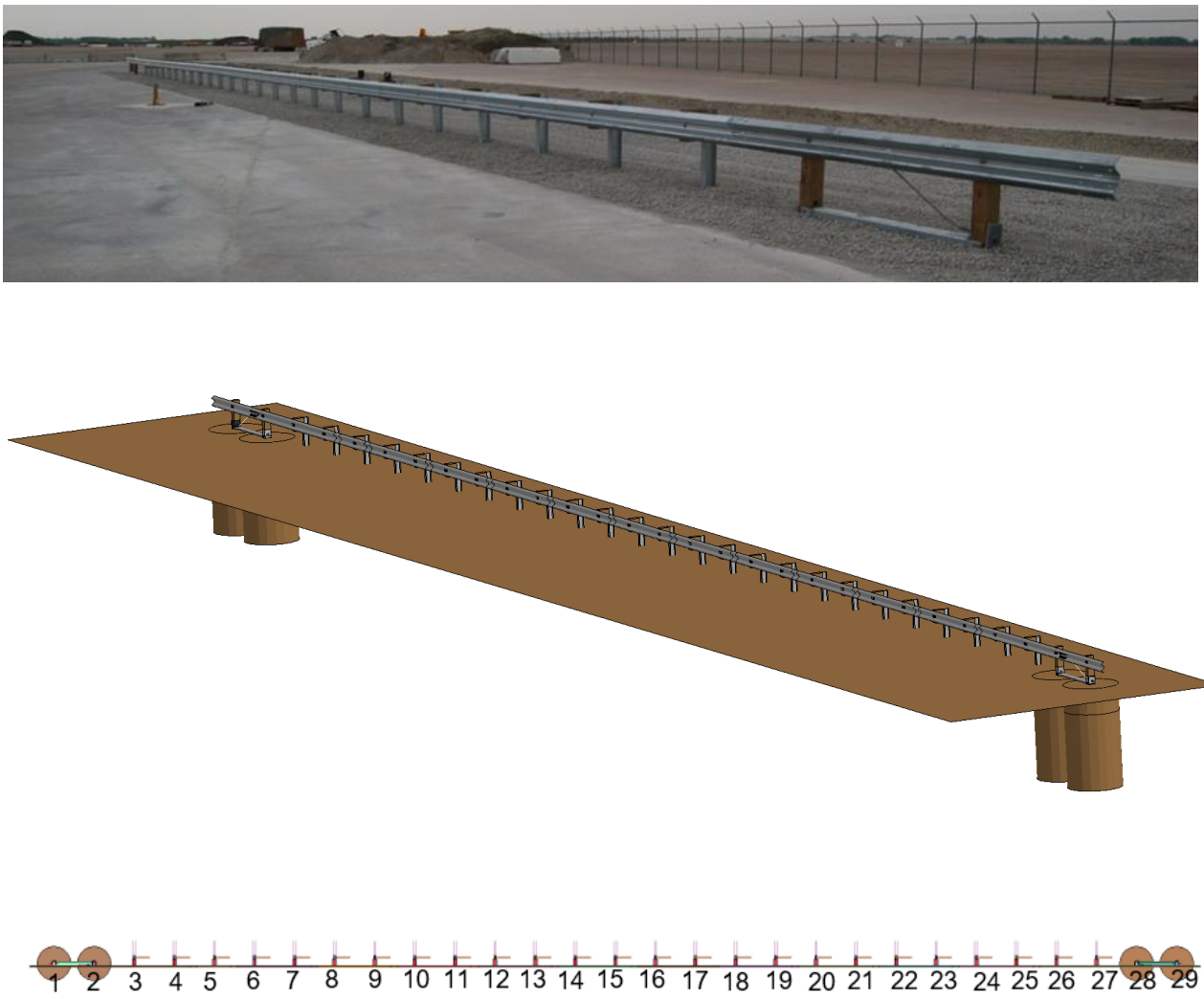

Figure 51. MGS System and 175-ft Long MGS Model

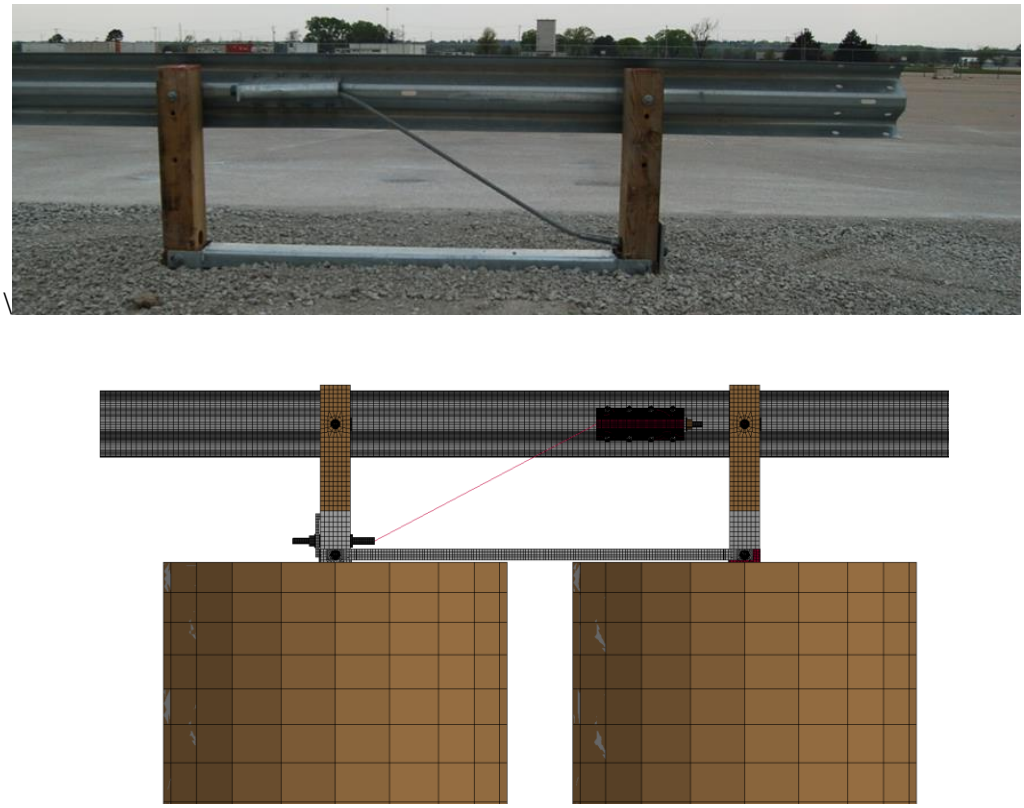

Figure 52. MGS End Anchorage and LS-DYNA Simulation Model

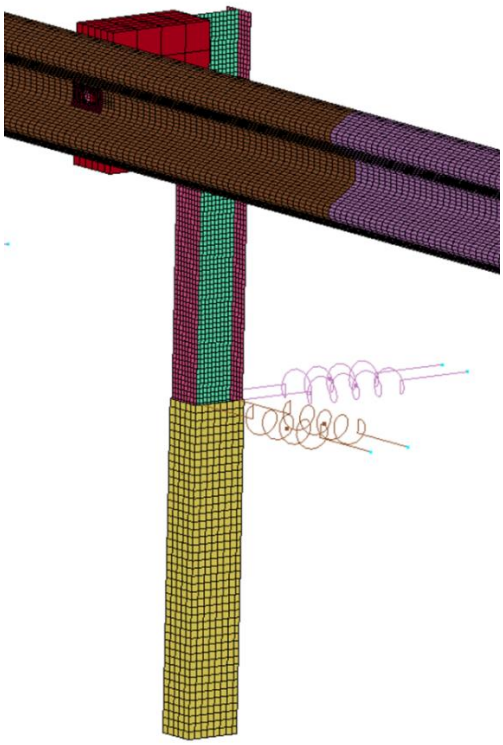

Figure 53. MGS Model – Post, Rail, and Soil

5.2.1 Post Model

The 72-in. long posts are ASTM A36 steel W6x9 sections spaced at 6 ft – 3 in. The post material model is *MAT_PIECEWISE_LINEAR_ PLASTICITY (*MAT_024). True stress versus effective plastic strain is defined as a series of eight points for this material model. The first point defined is the yield strength. The seventh point corresponds to ultimate strength converted to true stress. The eighth point corresponds to the failure of the material. However, failure criteria were not activated in the material model, so the posts cannot tear or rupture. The mechanical properties of the ASTM A36 baseline post material are average, nominal values obtained from past tensile tests. The ASTM A36 baseline post material true stress versus effective plastic strain curve is shown in Figure 54.

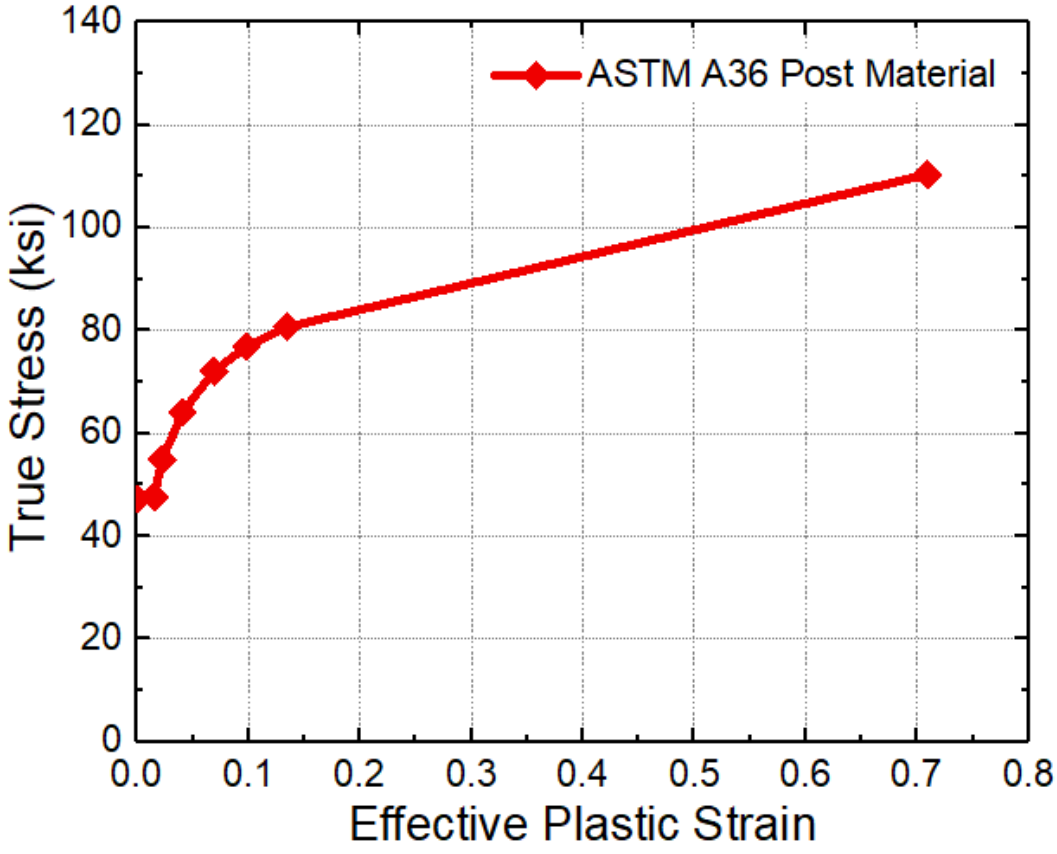

Figure 54. True Stress vs. Effective Plastic Strain – ASTM A36 Post Material

5.2.2 Rail Model

The MGS rails are AASHTO M180 steel standard MGS 12-gauge W-beam. The rail sections are 12 ft – 6 in. long and spliced at the midspan between posts. The actual bolted splice connection is not modeled. The rail material model is *MAT_PIECEWISE_ LINEAR_PLASTICITY (*MAT_024). True stress versus effective plastic strain is defined as a series of eight points. The first point defined is the yield strength. The seventh point corresponds to the ultimate strength converted to true stress. However, failure criteria were not activated in the

material model, so the rail cannot tear or rupture. The mechanical properties of the AASHTO M180 baseline rail material are average, nominal values obtained from past tensile tests. The AASHTO M180 baseline rail material true stress versus effective plastic strain curve is shown in Figure 55.

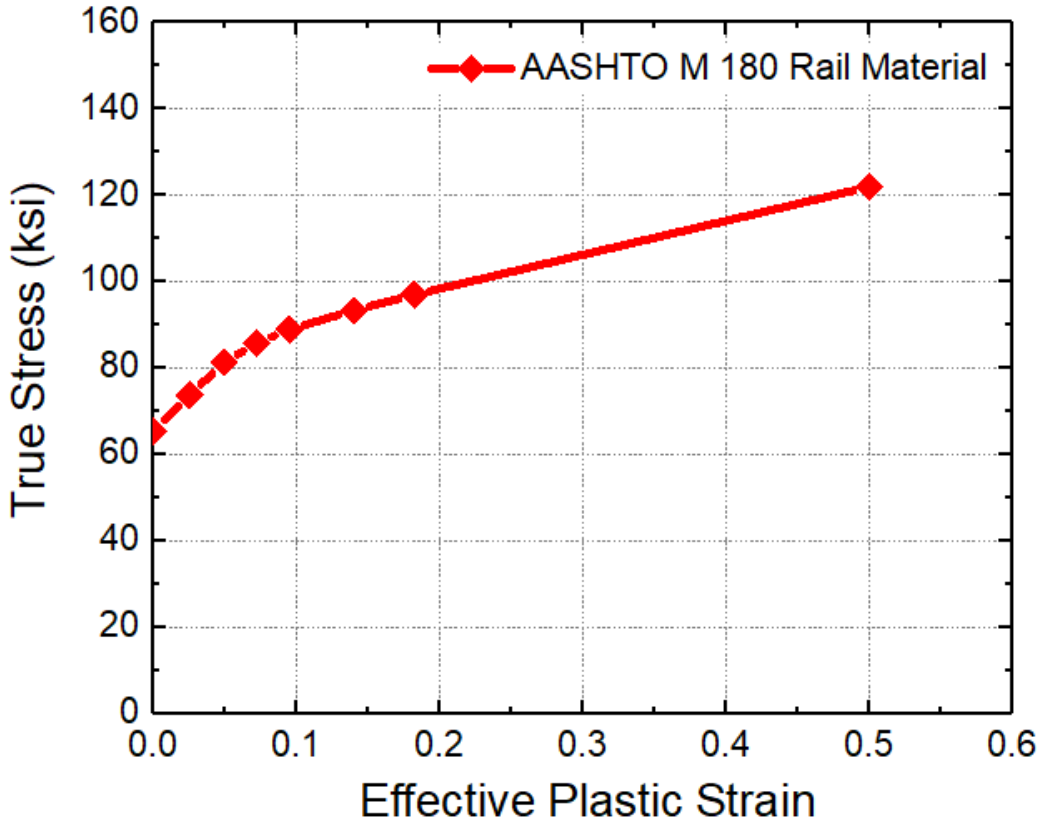

Figure 55. True Stress vs. Effective Plastic Strain – AASHTO M180 Rail Material

5.2.3 Soil Model

The soil for post nos. 3 through 27 were modeled with a rigid soil tube around the base of each post with a pair of soil springs attached to the top of the soil tube in the lateral and longitudinal directions, as shown in Figure 56. The soil tubes were pinned at their center of gravity, which allowed rotation. The soil springs simulated the reaction of the soil on the post and were used for improved computational efficiency over solid elements.

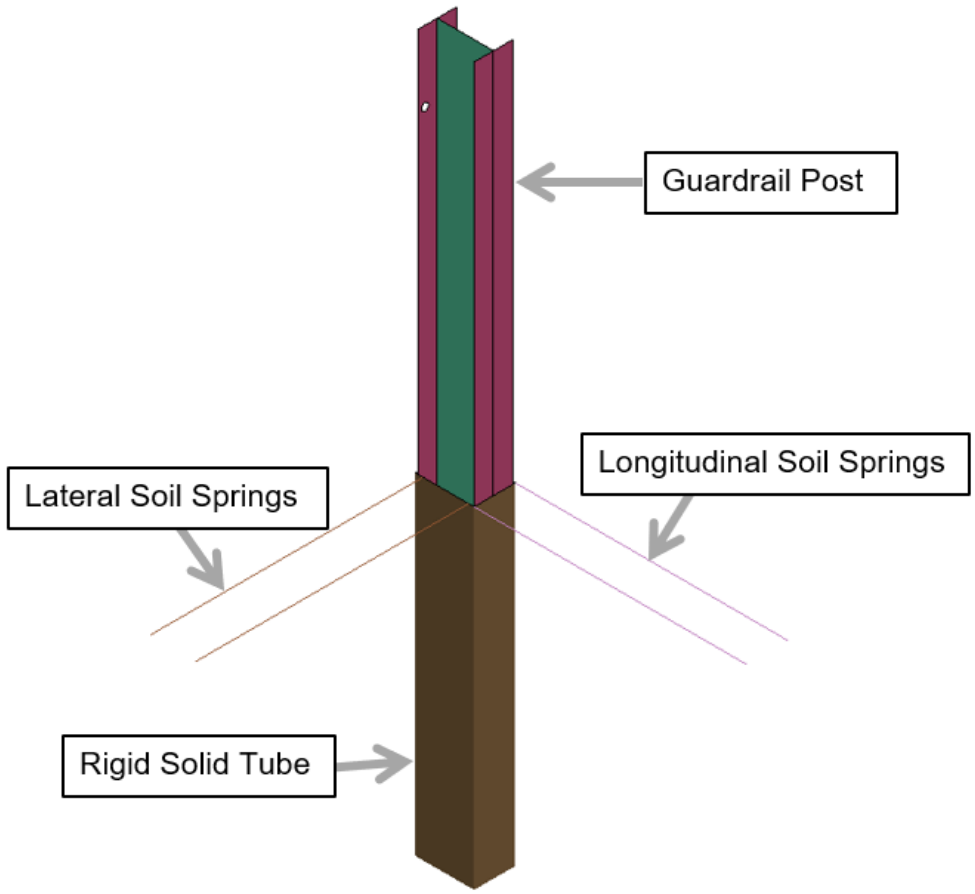

Figure 56. Guardrail Post with Soil Tube and Soil Springs

The soil spring material was *MAT_SPRING_GENERAL_NONLINEAR (*MAT_S06). The soil springs were assigned a loading curve that modeled the resistance of soil used on full-scale crash tests conducted at MwRSF. The force versus displacement curve determined through dynamic bogie testing a W6x16 post embedded in MASH strong soil simulates a standard soil representative of the soil strength requirement provided in MASH. The force vs. displacement curve is shown in Figure 57. Post nos. 1 and 2 and post nos. 28 and 29 were embedded into solid Drucker-Prager soil elements, which offered a more accurate representation of soil deformation.

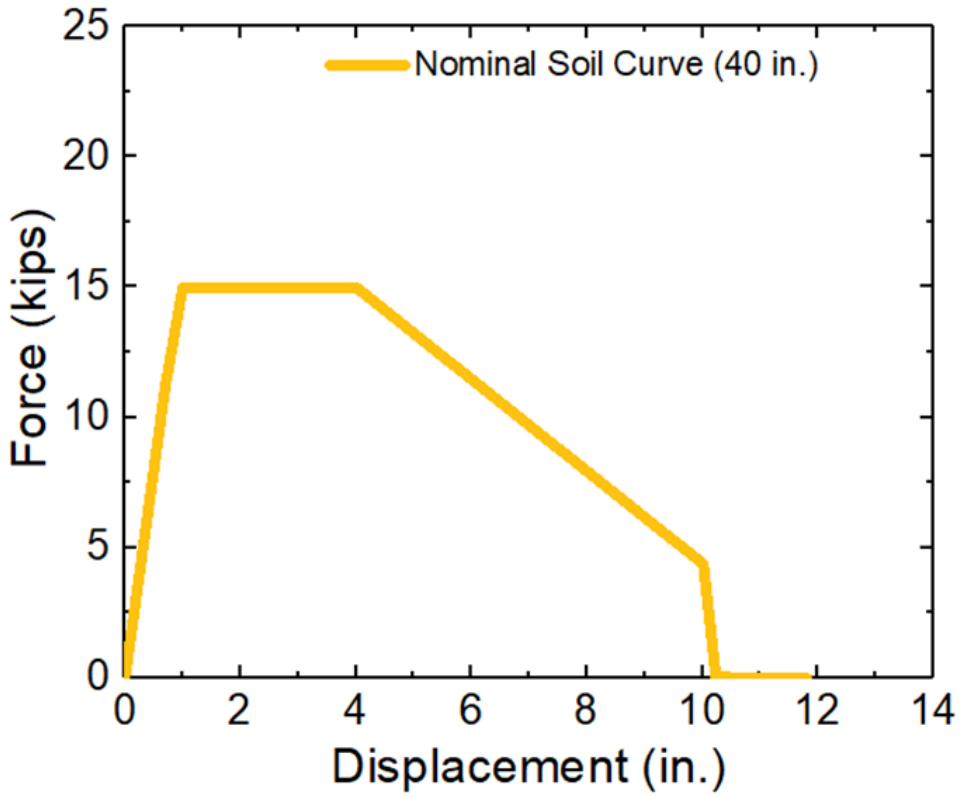

Figure 57. Force vs. Displacement Curve for Soil Springs

5.2.4 Upstream and Downstream Anchorages Model

As noted previously, the upstream and downstream end of the MGS was modeled after the actual MGS upstream and downstream anchorages [25-27]. The anchorages consisted of two timber breakaway cable terminal (BCT) posts embedded in solid Drucker-Prager soil elements, a groundline strut spanning post nos. 1 and 2 and post nos. 28 and 29, a cable anchor bracket attached to the backside of the W-beam rail, a cable anchor spanning from the cable anchor bracket through the ground line hole in post nos. 1 and 29, and an anchor bearing plate. The calibration of the material parameters for the anchorage components, including the failure of the BCT posts and resistance of the anchorage system, was based on a series of dynamic component tests performed at MwRSF [25]. The upstream and downstream anchorage assemblies are shown in Figure 58. Each of the anchorage components was composed of multiple systems, including the bolted connections between parts.

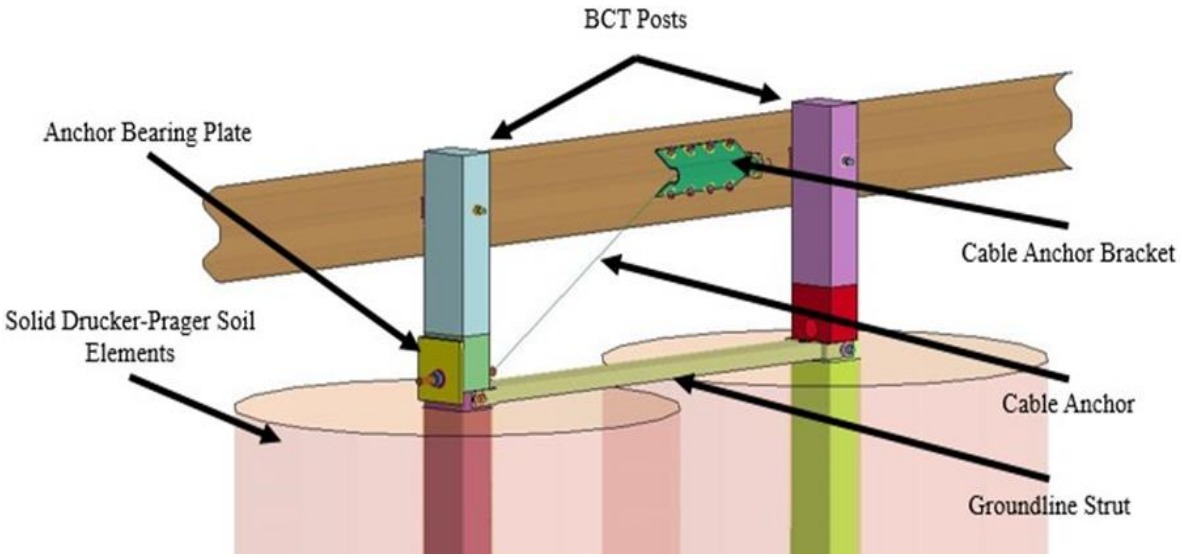

Figure 58. MGS Upstream and Downstream Anchorages Model

The timber BCT posts were modeled with type 2 (fully integrated S/R) solid elements given a *MAT_PLASTIC_KINEMATIC material formulation. As shown in Figure 59, the region near the groundline of BCT post nos. 1 and 2 and post nos. 28 and 29 was modeled as a separate part. These regions of the BCT posts near the ground line had a plastic failure strain defined and were modeled with type 3 (fully integrated quadratic 8-node element with nodal rotations) solid elements given a *MAT_ISOTROPIC_ELASTIC_FAILURE material formulation. An abbreviated list of MGS model parts and the associated LS-DYNA modeling parameters is shown in Table 7.

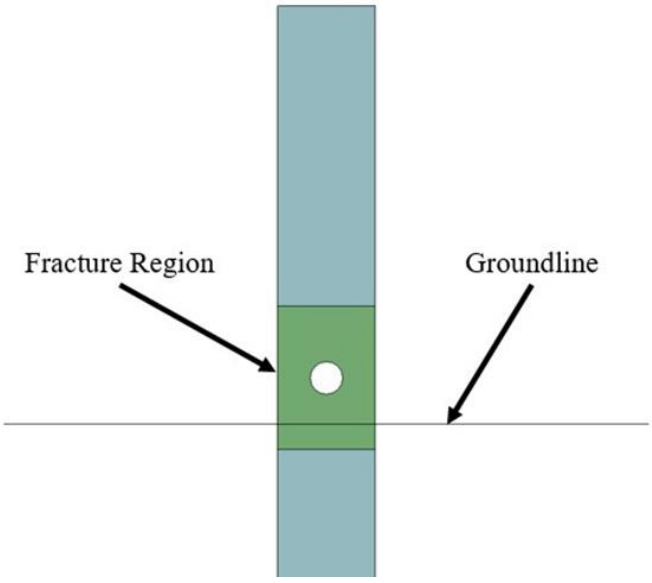

Figure 59. BCT Post Nos. 1 and 2 and Post Nos. 28 and 29

Table 7. Summary of MGS Model Part Properties

Part Name	Element Type	Element Formulation	Material Type	Material Formulation
Anchor Cable	Beam	Belytschko-Schwer, Resultant Beam	6x19 3/4" Wire Rope	Moment, Curvature Beam
Anchor Post Bolt	Solid	Constant Stress Solid Element	ASTM A36	Rigid
Anchor Post Bolt Heads	Shell	Belytschko-Tsay	ASTM A36	Rigid
Anchor Post Washers	Solid	Constant Stress Solid Element	ASTM A36	Rigid
BCT Anchor Post	Solid	Fully Integrated, S/R	Wood	Plastic Kinematic
Bearing Plate	Solid	Constant Stress Solid Element	ASTM A36	Rigid
Blockout	Solid	Fully Integrated, S/R	Wood	Elastic
Blockout Bolts	Shell	Belytschko-Tsay	ASTM A36	Rigid
Bolt Springs	Discrete	DRO=Translational Spring/Damper	ASTM A36	Spring, Non-Linear Elastic
Ground-Line Strut	Shell	Belytschko-Tsay	ASTM A36	Piecewise, Linear Plastic
Post Soil Tubes	Shell	Belytschko-Tsay	Equivalent Soil	Rigid
Soil Springs	Discrete	DRO=Translational Spring/Damper	Equivalent Soil	Spring, General Non-Linear
W-beam Guardrail Section	Shell	Fully Integrated, Shell Element	AASHTO M 180 Rail Material	Piecewise, Linear Plastic
W6x9 Post	Shell	Fully Integrated, Shell Element	ASTM A36	Piecewise, Linear Plastic

5.2.5 Dodge Ram Vehicle Model

During this project, researchers obtained a vehicle model of a 2018 Dodge Ram pickup truck. The 2018 Ram vehicle model was originally developed by the Center for Collision Safety and Analysis at George Mason University [28] and was modified by MwRSF researchers for use in roadside safety applications. It was believed that the 2018 Ram vehicle model would provide a much better correlation between the simulations and the full-scale test than the 2007 Silverado vehicle model since it was more geometrically similar to the Ram full-scale crash test vehicle. Therefore, this study utilized a 2018 Ram pickup truck vehicle model for all simulations. The 2018 Ram vehicle model is shown in Figure 60.

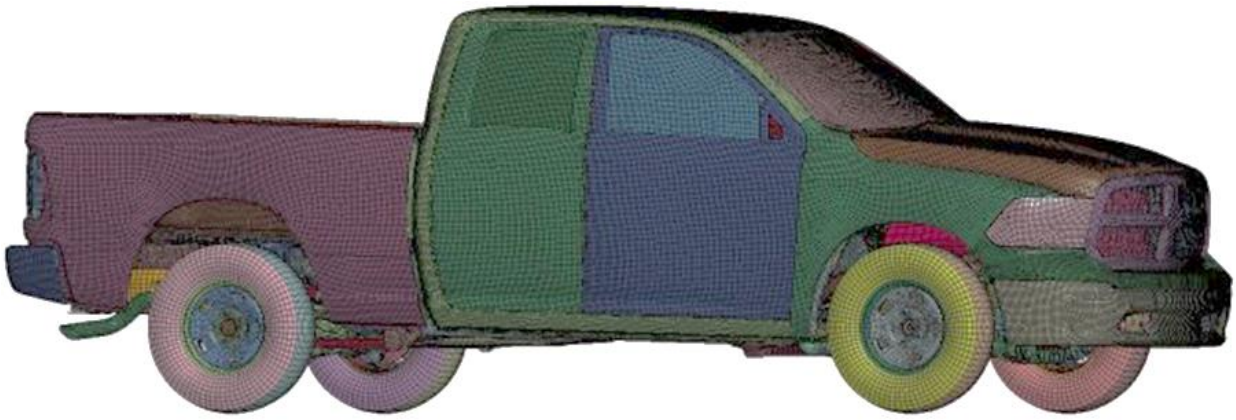

Figure 60. 2018 Ram Finite Element Model

5.3 Baseline MGS-RAM Simulation at TL-3 Impact Conditions

The baseline model of the MGS was calibrated with the results from test nos. 2214MG-2 and ILT-1 and consisted of a 2018 Dodge Ram pickup truck impacting the MGS installed in standard MASH strong soil. Impact conditions were consistent with MASH TL-3. The simulated impact conditions were based on the actual impact speed and angle determined from test results. As noted previously, the MGS model consisted of calibrated end anchorages, refined meshes in critical rail locations, and improved vehicle-to-barrier contacts.

5.3.1 Vehicle Stability and Barrier Deflections

In test nos. 2214MG-2 and ILT-1, the pickup truck was stable during and after redirection with minimal pitch or roll motion. The simulation model reasonably predicted rotations, as shown in Figure 61. Results from the MGS-Ram simulation and full-scale crash test nos. 2214MG-2 and ILT-1 are summarized in Table 8. The dynamic deflection of the pickup truck during test nos. 2214MG-2 and ILT-1 was comparable to simulation model prediction. The simulated maximum dynamic deflection was within 5 percent of the maximum dynamic deflections of the tests, as shown in Table 8.

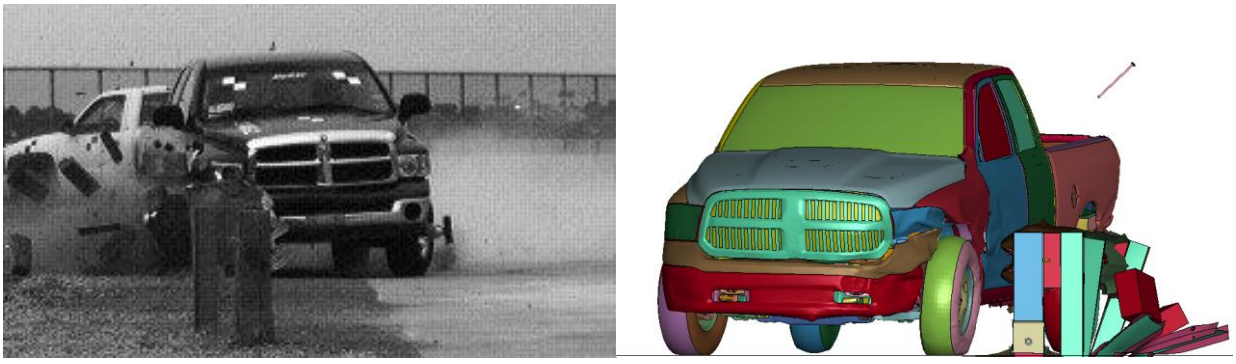

Figure 61. Vehicle Behavior Comparison Between Test No. 2214MG-2 and Simulation

Table 8. Summary of Results for Test No. 2214MG-2 and ILT-1 and MGS-Ram Simulation

Evaluation Criteria		Test No. 2214 MG-2	Test No. ILT-1	Simulation	MASH 2016 Limits
OIV ft/s (m/s)	Longitudinal	15.32 (4.67)	-15.42 (-4.70)	-16.63 (-5.07)	±40 (12.20)
	Lateral	15.62 (4.76)	14.11 (-4.30)	-15.97 (-4.88)	±40 (12.20)
ORA g's	Longitudinal	8.23	-14.70	-5.64	±20.49
	Lateral	6.93	-7.80	-7.07	±20.49
Maximum Angular Displacement deg.	Roll	3.00	-3.00	-1.97	±75
	Pitch	1.80	-5.40	1.89	±75
	Yaw	-43.00	-33.60	-37.75	Not Required
THIV ft/s (m/s)		N/A	N/A	N/A	Not Required
PHD g's		N/A	N/A	N/A	Not Required
ASI		N/A	N/A	N/A	Not Required
Dynamic Deflection in. (mm)		43.0 (1,114)	44.1 (1,120)	43.5 (1,090)	Not Required

Vehicle yaw, roll, and pitch behaviors indicate the vehicle stability and redirection capability of the system after the vehicle impacts the barrier system, as well as possible vehicle wheel snagging behavior during the test. As shown in Table 8, angular displacement values obtained from the simulation correlated well with the full-scale crash tests. Additionally, the simulation exhibited similar lateral and longitudinal occupant ridedown accelerations (ORA) and occupant impact velocity (OIV) values compared to test no. 2214MG-2 and test no. ILT-1 results. As shown in Figures 62 through 64, the vehicle was smoothly redirected with no instabilities.

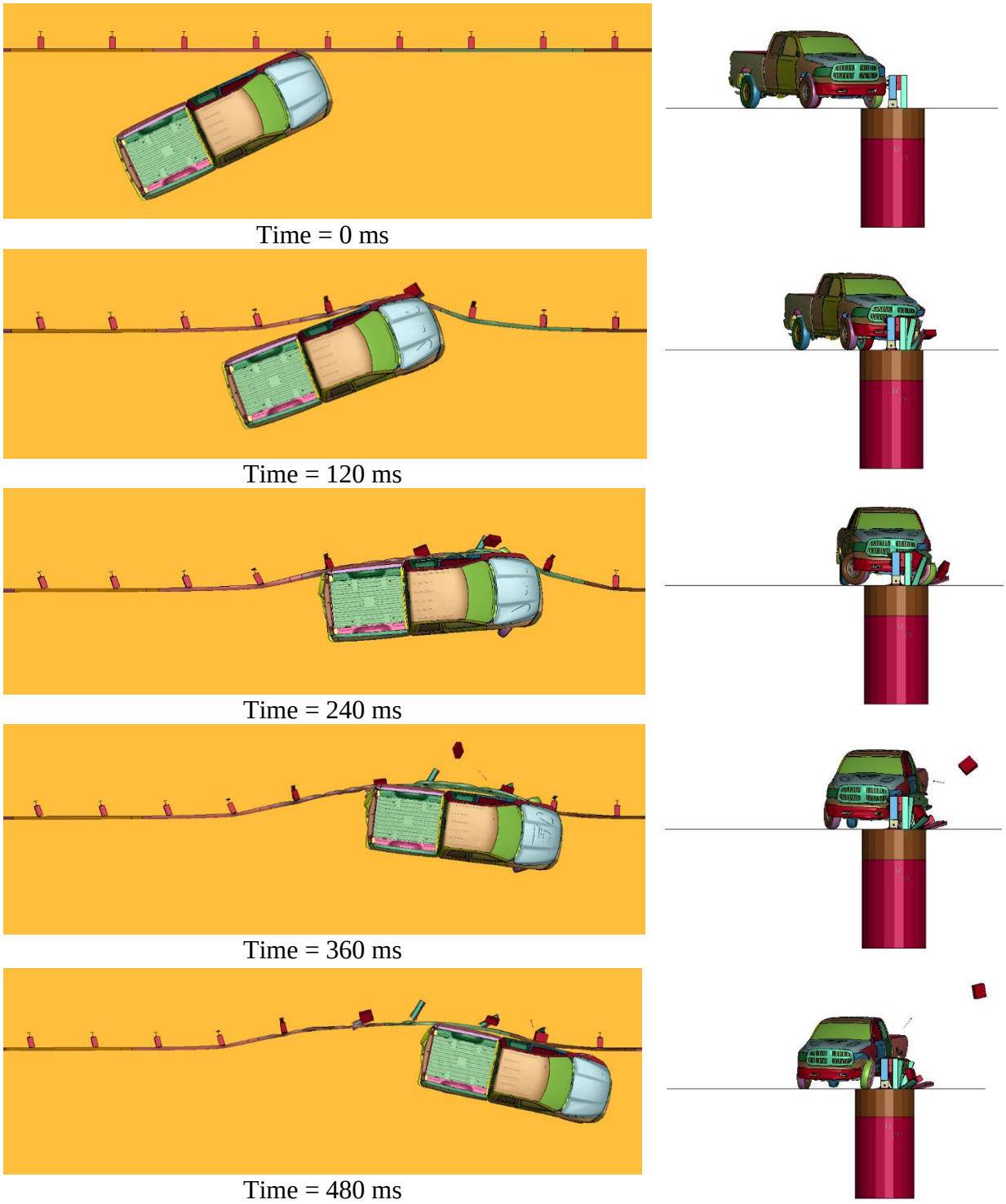

Figure 62. Sequential Images, Baseline MGS-Ram Simulation under TL-3 Impact Conditions

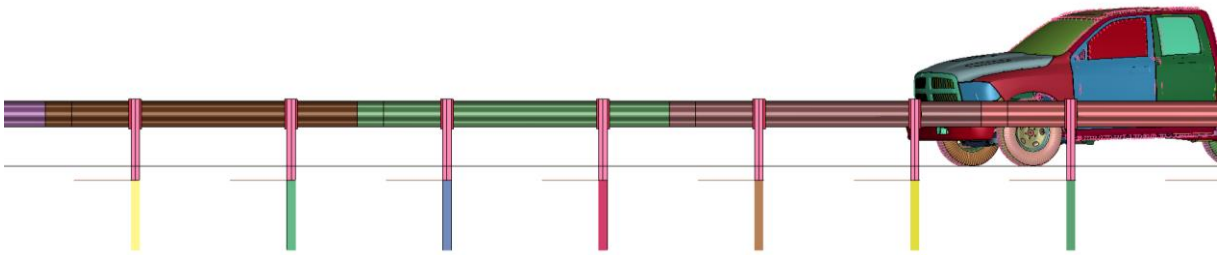

Time = 0 ms

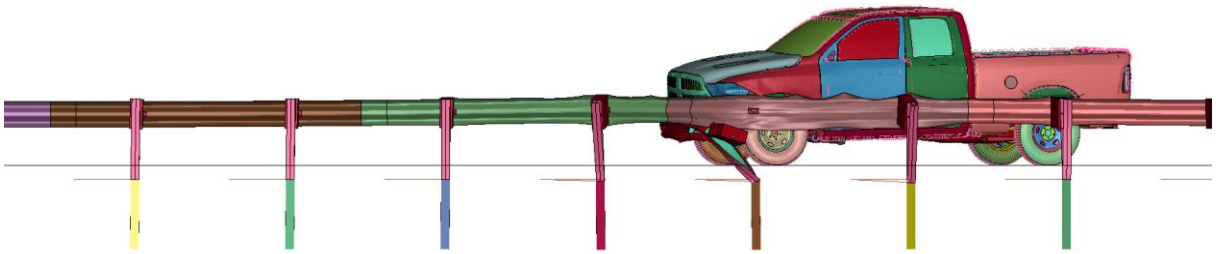

Time = 120 ms

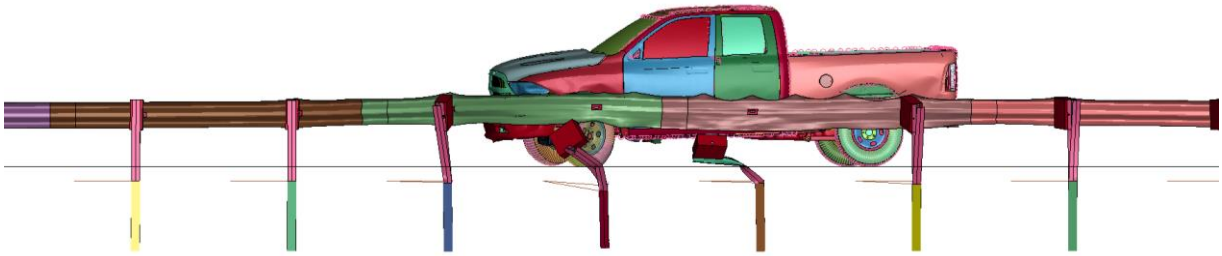

Time = 240 ms

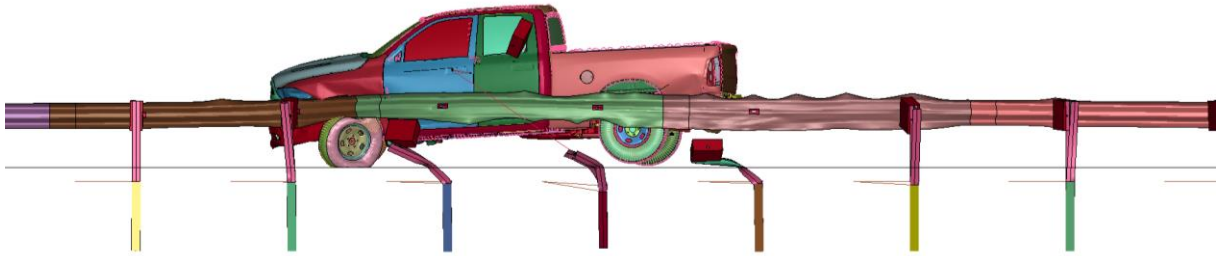

Time = 360 ms

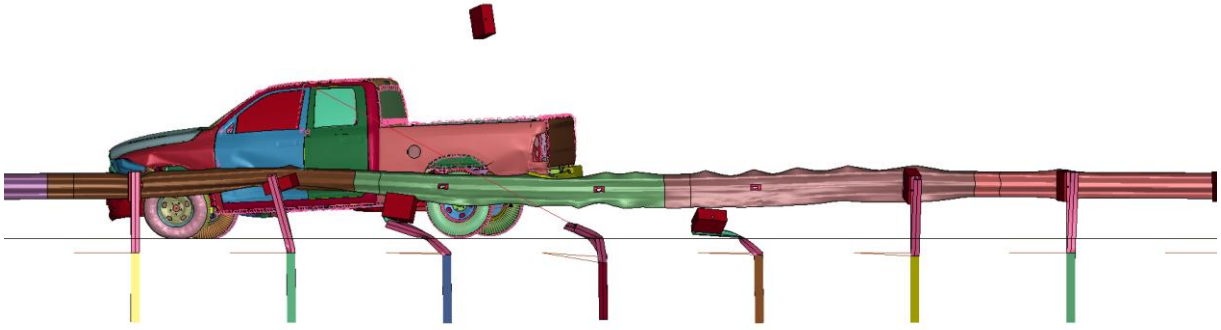

Time = 480 ms

Figure 63. Sequential Images, Baseline MGS-Ram Simulation under TL-3 Impact Conditions

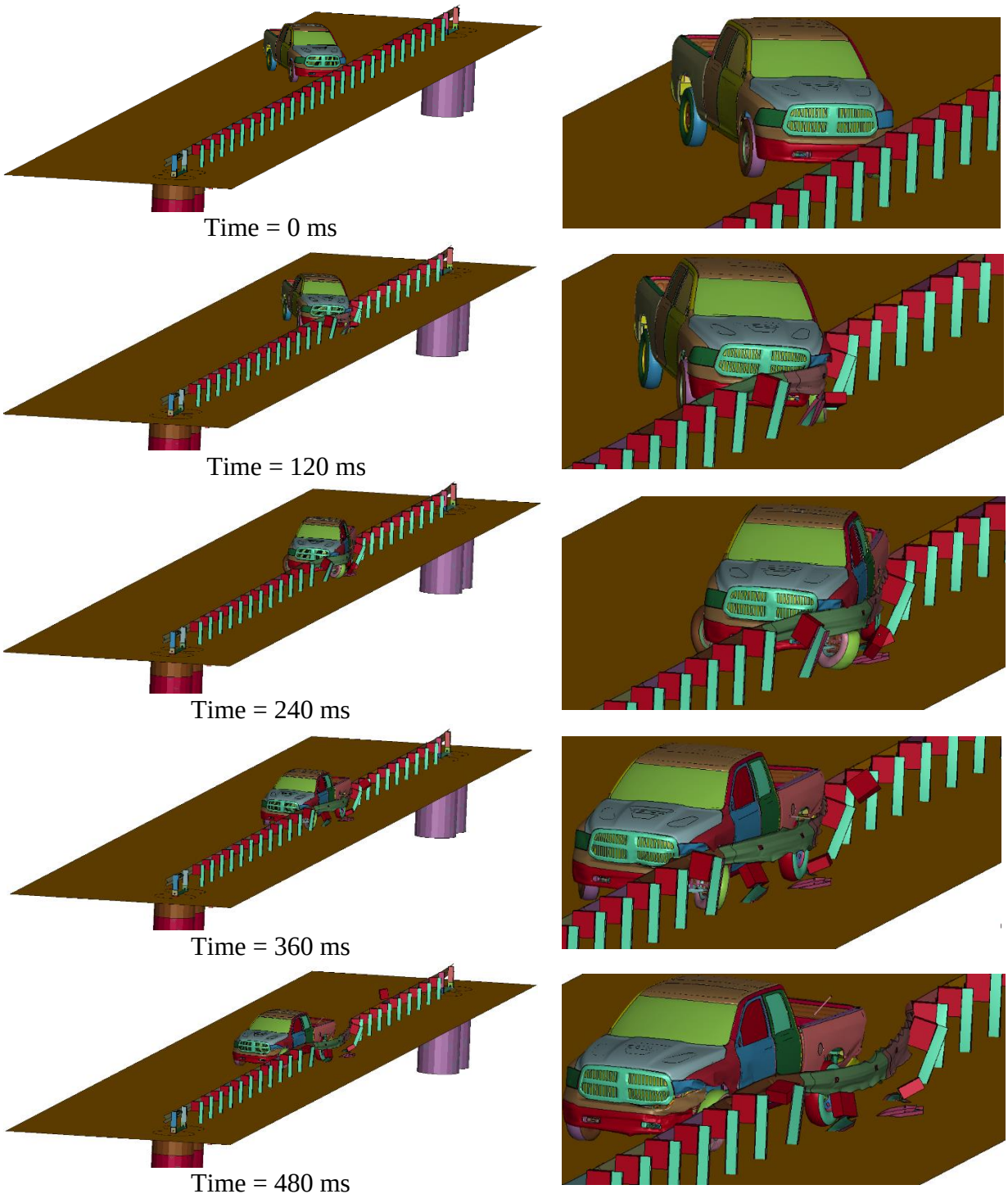

Figure 64. Sequential Images, Baseline MGS-Ram Simulation under TL-3 Impact Conditions

5.3.2 Velocity Profile

Accelerations, velocities, and displacements were found at the center of gravity of the 2018 Ram model at every 0.01 ms and filtered using a customized Excel spreadsheet used for filtering full-scale crash test data. A comparison of the changes in longitudinal velocity for the tests and simulation is shown in Figure 65. As shown in Figure 65, the change in longitudinal velocity obtained from the Ram-MGS simulation model correlated well with the full-scale crash test results.

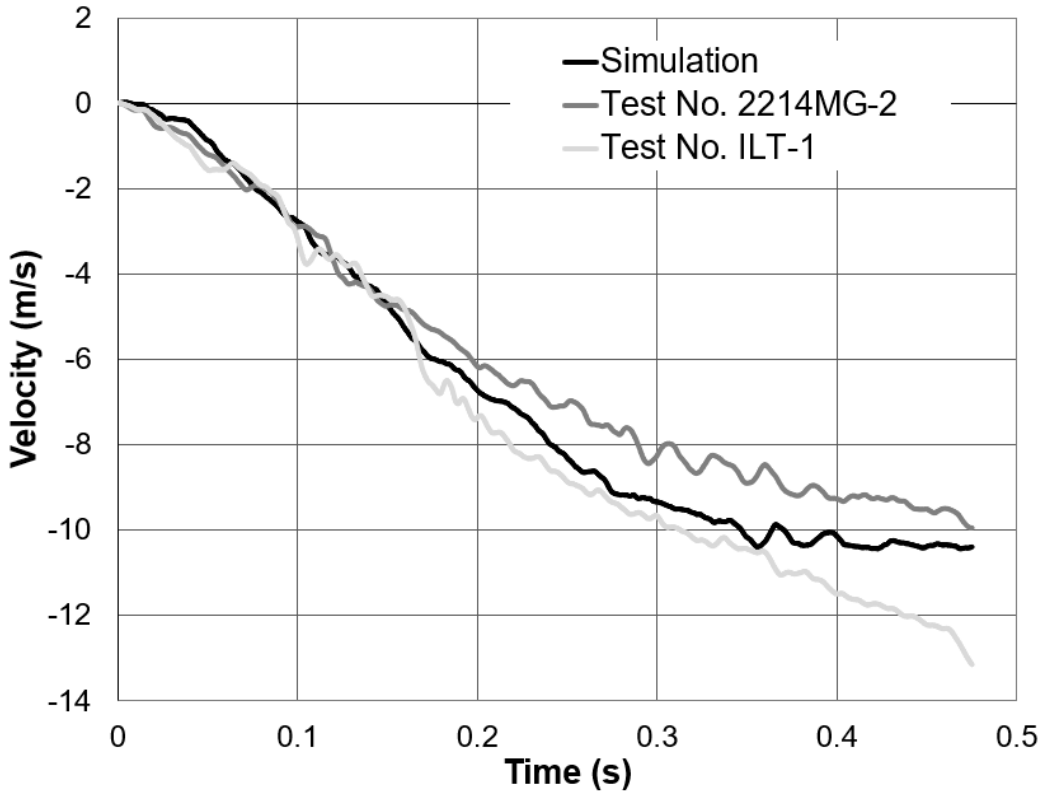

Figure 65. Longitudinal Velocity Profile, Simulation and Test Nos. 2214MG-2 and ILT-1

The changes in lateral velocity for the tests and simulation are shown in Figure 66. The tests and the simulation change in lateral velocity results were processed using a similar procedure. As shown in Figure 66, the change in lateral velocity obtained from the Ram-MGS simulation model correlated reasonably well with the test results.

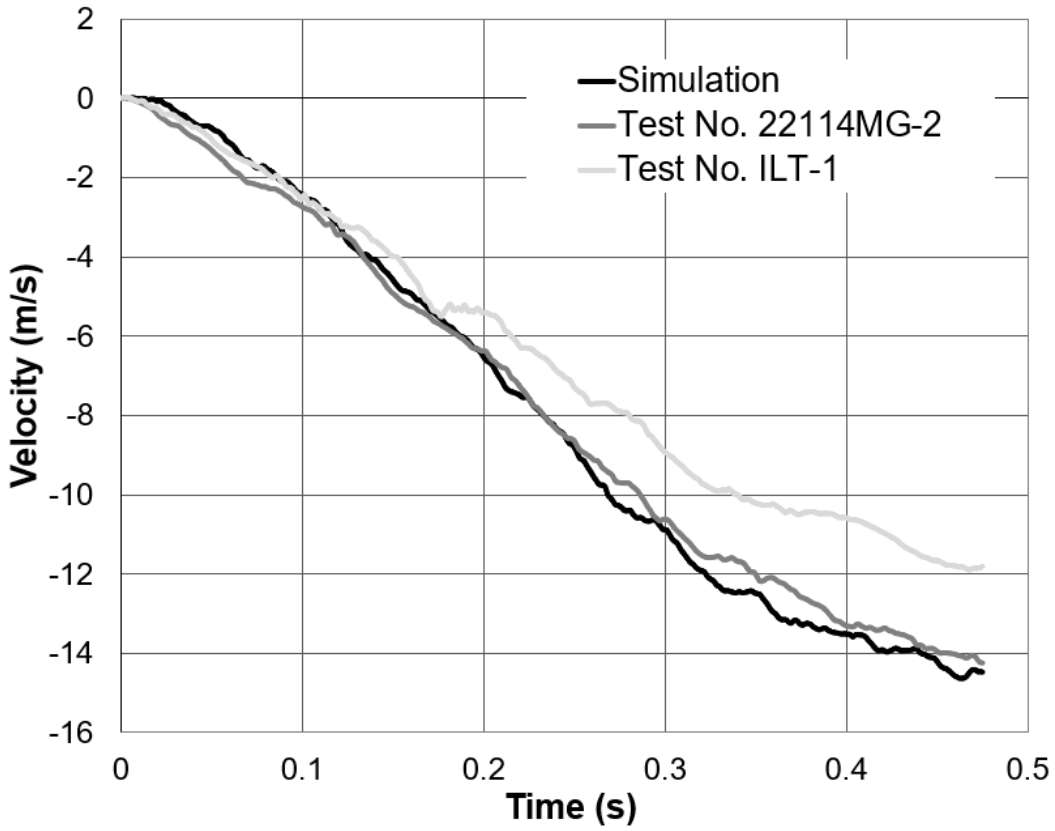

Figure 66. Lateral Velocity, Simulation and Test Nos. 2214MG-2 and ILT-1

5.4 Baseline MGS-RAM Simulation at TL-2 Impact Conditions

The baseline simulation of the Dodge Ram pickup truck impacting a tangent 175-ft long MGS in standard (nominal) soil was modified to simulate impact at speed of 44 mph. This lower impact speed corresponds to impacts with the MGS at TL-2 impact conditions. This simulation was conducted to establish baseline values, such as maximum barrier dynamic deflections for standard MGS at TL-2 impacts.

5.4.1 Vehicle Stability and Barrier Deflections

The vehicle was stable during and after redirection, with minimal pitch or roll motion. Results from the MGS-Ram TL-2 simulation are summarized in Table 9. The maximum dynamic deflection decreased as impact speed decreased. The barrier deflection decreased by more than 50 percent in the TL-2 simulation compared to the simulation at TL-3 impact conditions.

Table 9. Summary of Results for MGS-Ram MASH TL-2 Simulation

Evaluation Criteria		Standard Embedment (40 in.) MGS	MASH 2016 Limits
OIV ft/s (m/s)	Longitudinal	-14.52 (4.43)	±40 (12.2)
	Lateral	-13.69 (4.17)	±40 (12.2)
ORA g's	Longitudinal	-4.08	±20.49
	Lateral	-4.67	±20.49
Maximum Angular Displacement deg.	Roll	2.56	±75
	Pitch	1.55	±75
	Yaw	-39.99	not required
THIV ft/s (m/s)		N/A	not required
PHD g's		N/A	not required
ASI		N/A	not required
Max. Dynamic deflection in. (mm)		25.40 (645)	N/A

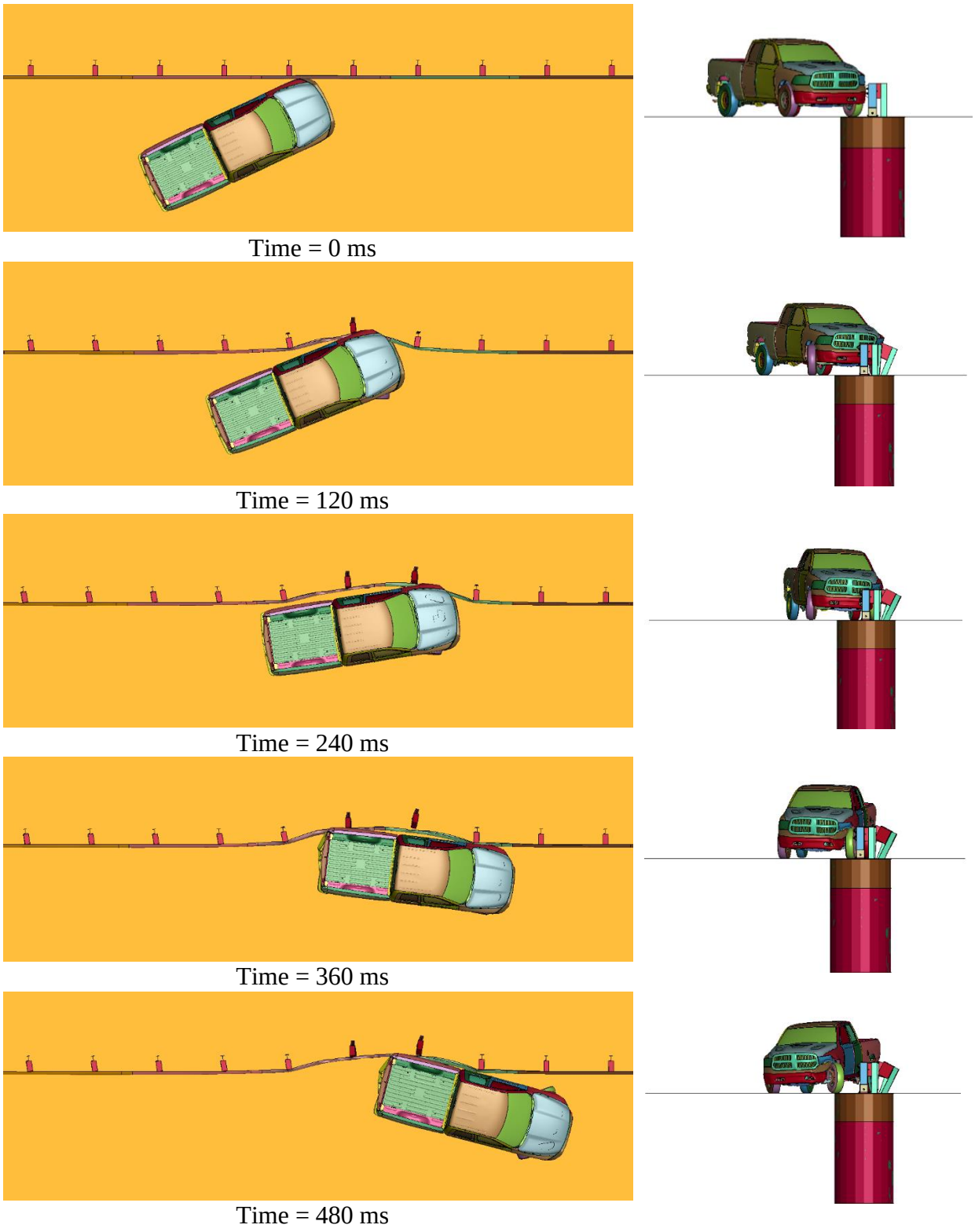

Figure 67. Sequential Images, Baseline Ram-MGS Simulations at TL-2 Impact Conditions

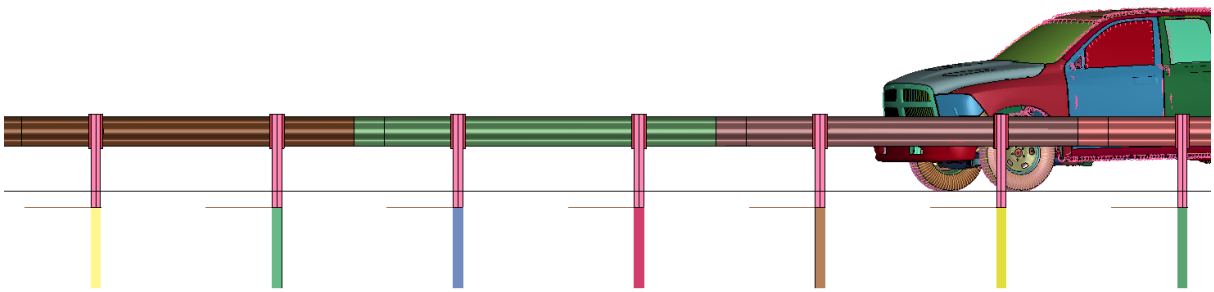

Time = 0 ms

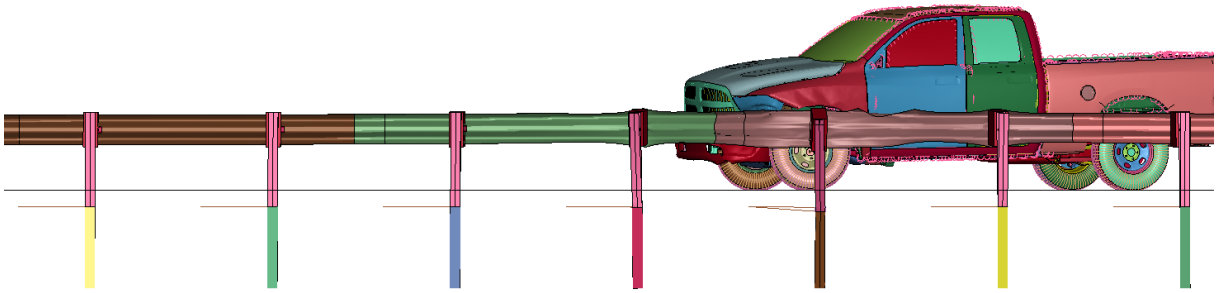

Time = 120 ms

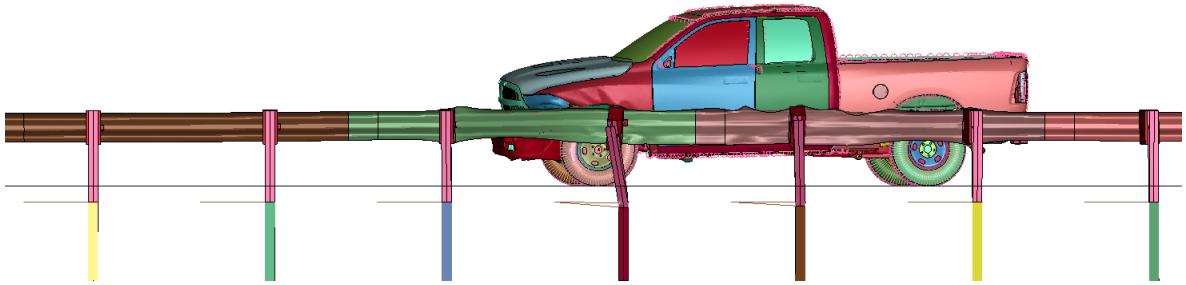

Time = 240 ms

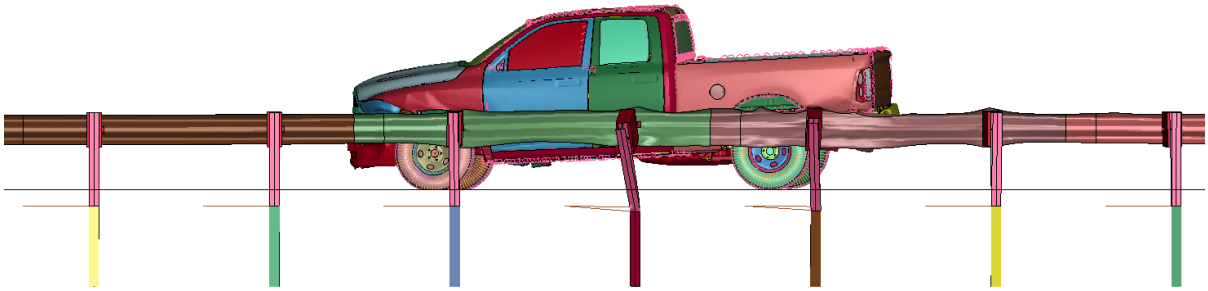

Time = 360 ms

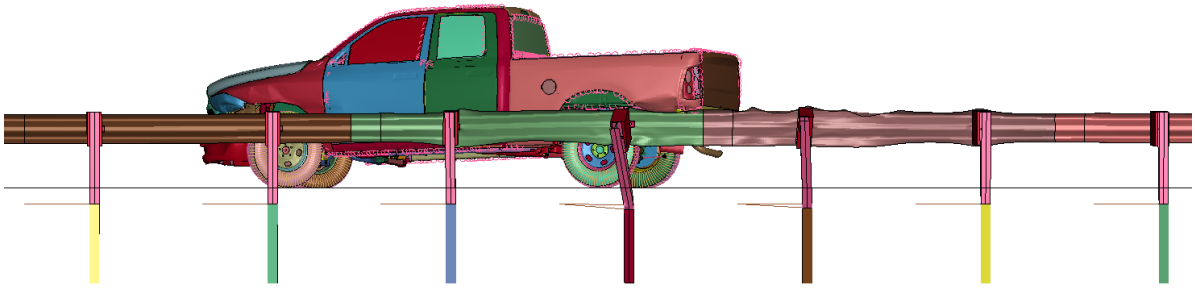

Time = 480 ms

Figure 68. Sequential Images, Baseline Ram-MGS Simulations at TL-2 Impact Conditions

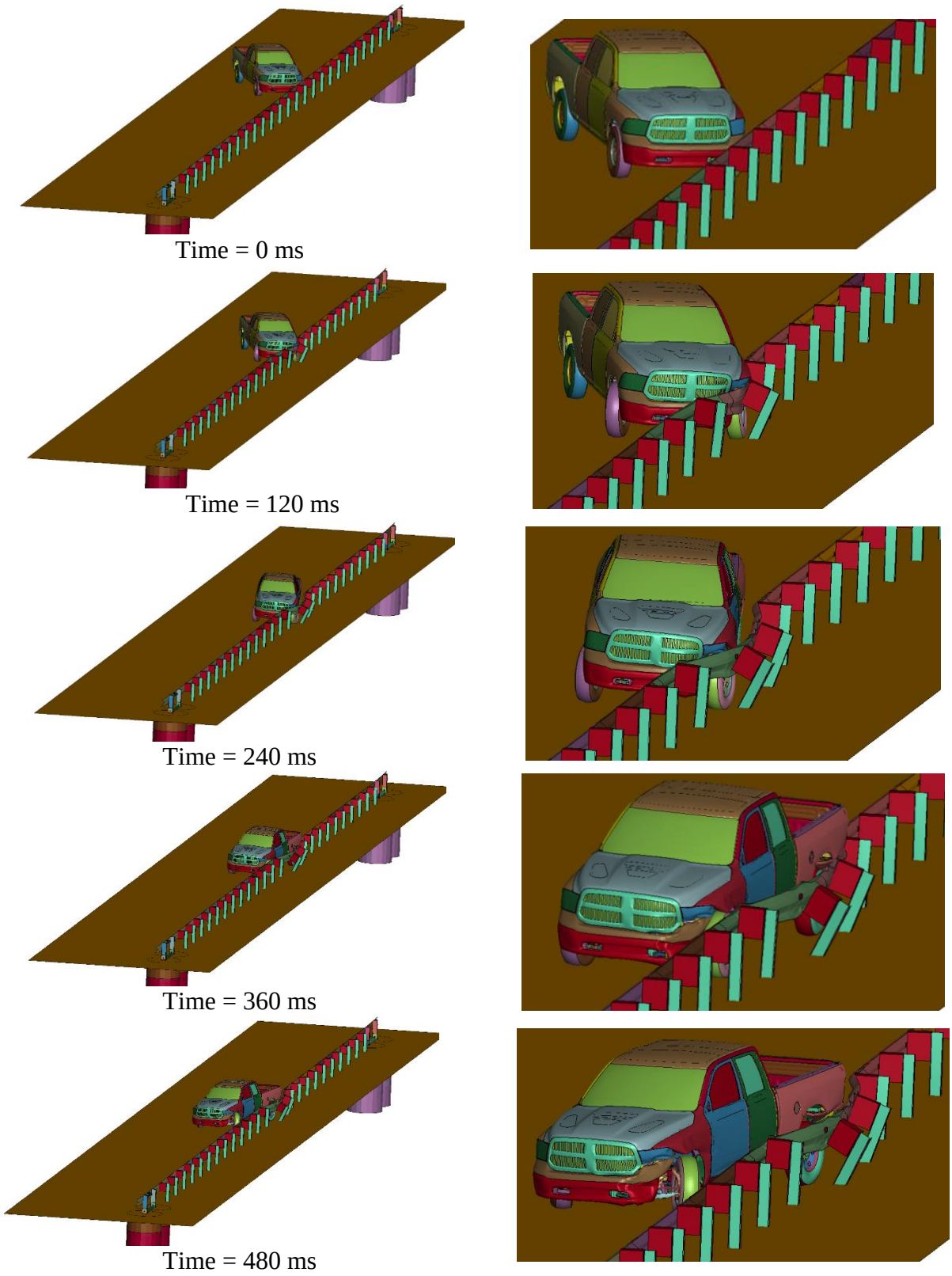

Figure 69. Sequential Images, Baseline MGS at TL-2 Impact Conditions

5.5 Discussion

Several metrics, including visual analysis and comparisons between velocity profiles, barrier deflections, and occupant risk values, were used to evaluate the baseline Ram-MGS model simulations against test nos. 2214MG-2 and ILT-1. The baseline simulation produced results that were comparable with the full-scale crash tests. The velocity profiles predicted by the simulations were relatively close to the velocity profiles produced during the full-scale crash tests, i.e., test nos. 2214MG-2 and ILT-1. Similarly, the maximum dynamic deflection obtained from the baseline simulation closely matches the deflection observed in the full-scale crash tests.

The Ram-MGS model accurately represented the system response and vehicle behavior observed in full-scale crash testing based on the evaluated metrics. Therefore, the baseline Ram-MGS model can be utilized to develop the reduced-post embedment and reduced-post spacing design and draw a reasonable conclusion about the performance of reduced embedment and reduced post spacing MGS for low-fill culverts and other applications at TL-2 and TL-3 impact conditions.

6 LS-DYNA ANALYSIS OF REDUCED POST EMBEDMENT AND REDUCED POST SPACING MGS INSTALLATIONS

6.1 Introduction

A finite element model of the standard MGS was modified to represent the MGS with reduced post embedment and reduced post spacing. The MGS models with the shallowest embedment depth of 28 in. with full-post (75 in.), half-post (37.5 in.), and quarter-post (18.75 in.) spacings were developed using the updated soil spring models described in Chapter 4 and are shown in Figures 70 through 72.

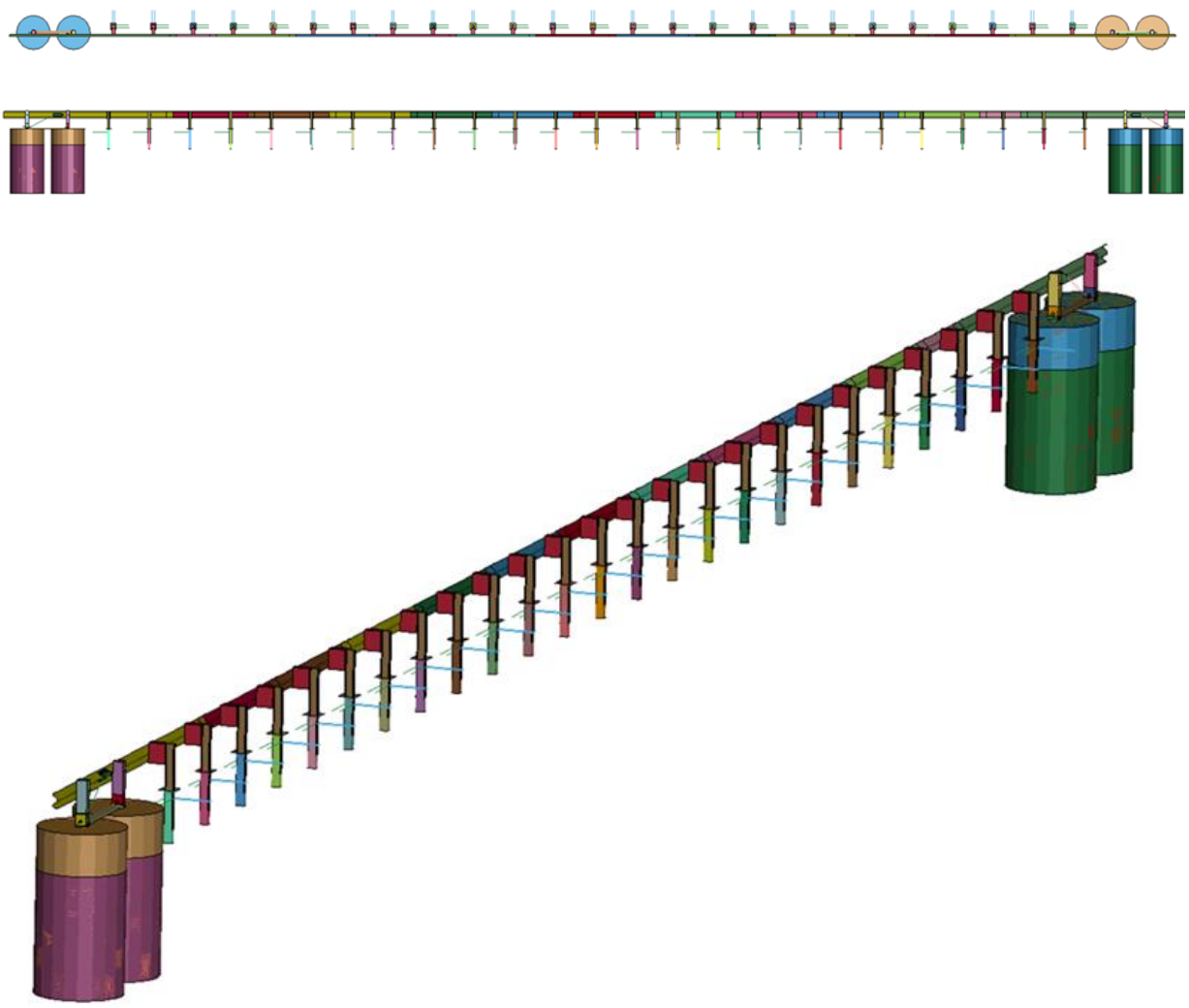

Figure 70. MGS Model with Shallow Post Embedment of 28 in. and Full-Post Spacing

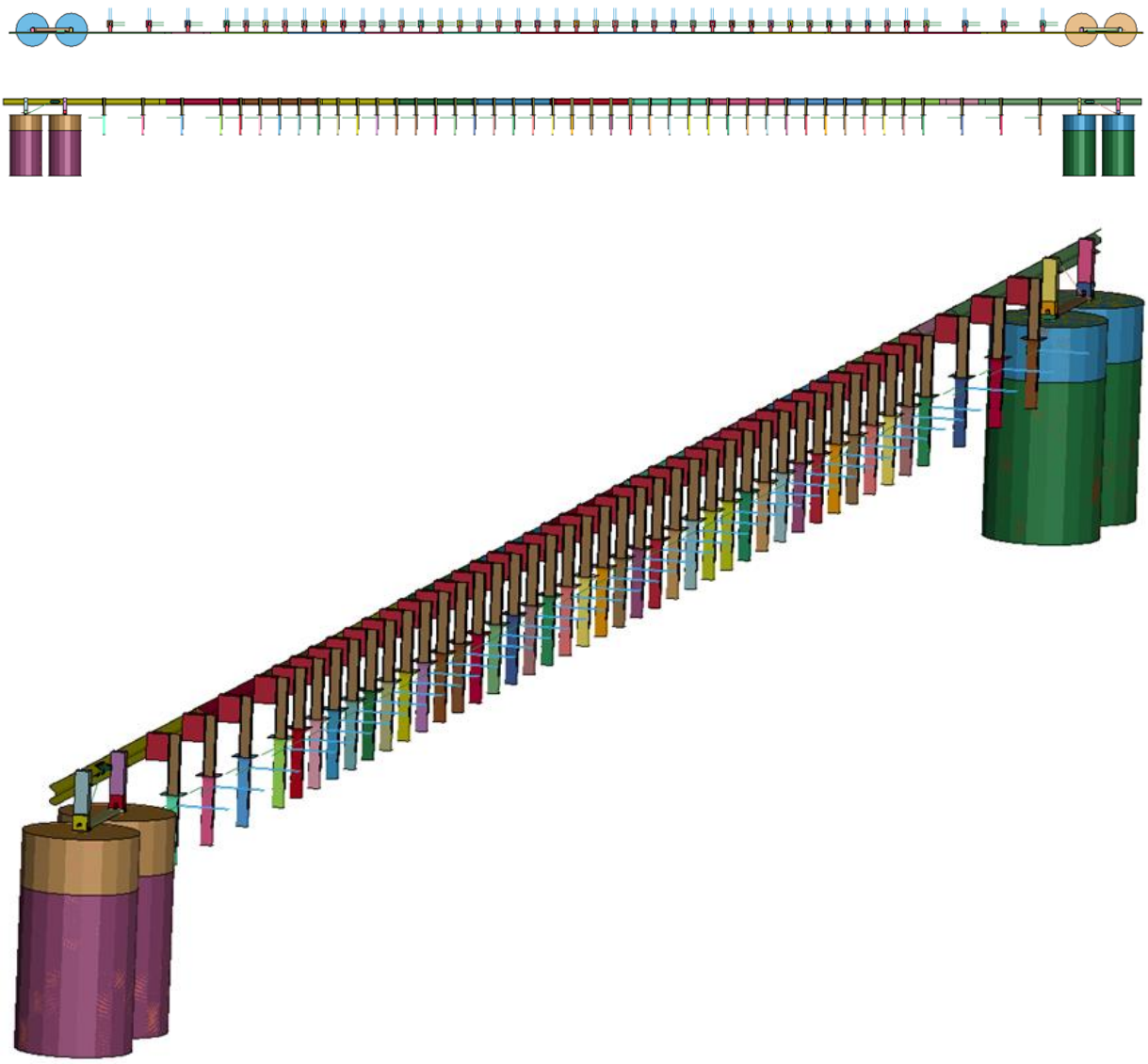

Figure 71. MGS Model with Shallow Post Embedment of 28 in. and Half-Post Spacing

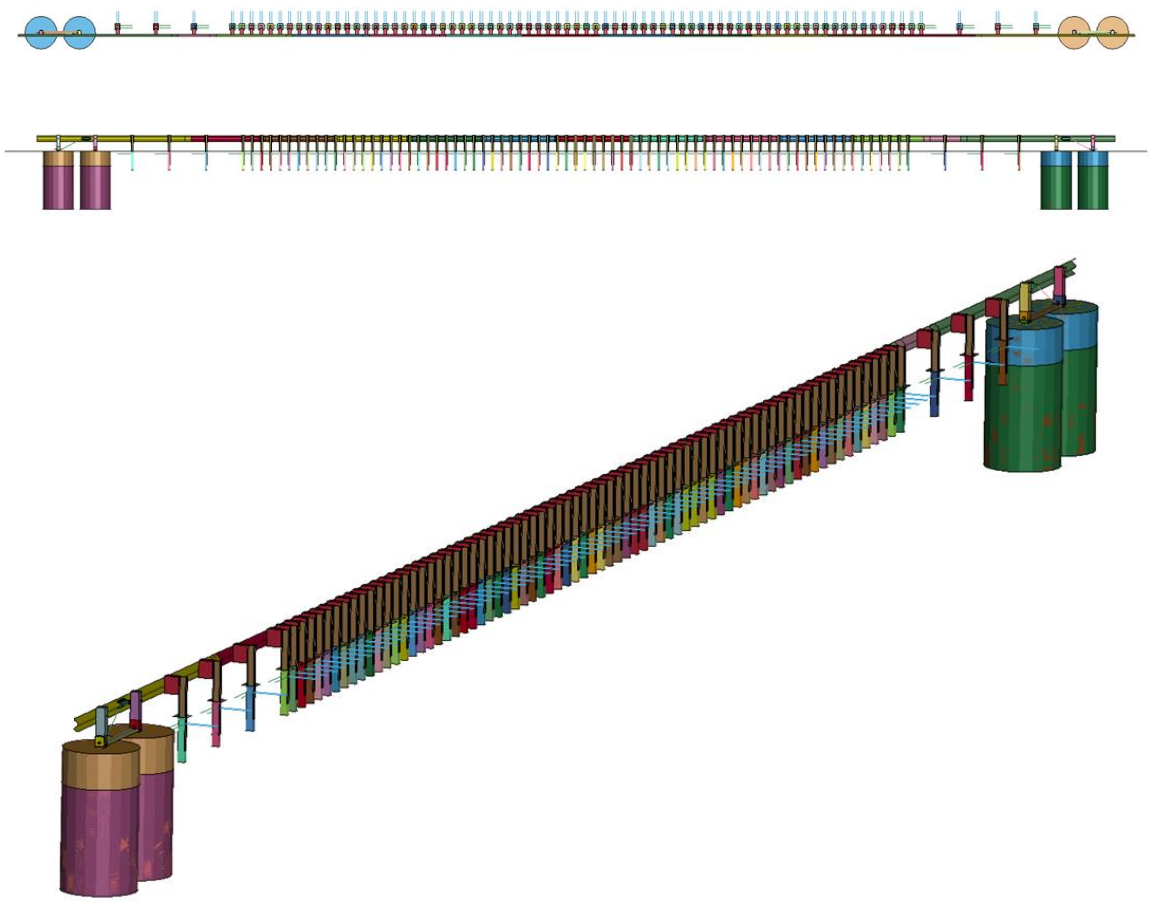

Figure 72. MGS Model with Shallow Post Embedment of 28 in. and Quarter-Post Spacing

Soil conditions vary widely from state to state, and even within a state. It is impossible to accurately predict MGS behavior, in particular dynamic deflection and working width, without knowing the type, strength, moisture content, and cohesiveness of the soil. Other complicating factors, such as asphalt overlays or posts embedded in soil tubes, can affect vehicle-to-barrier impact dynamics. In order to account for the soil strength variabilities, lower and upper bounds were considered for soil strength in the analysis of reduced post embedment and/or reduced post spacing, as shown in Figure 73. As such, the upper-bound soil strength was set associated with the relatively strong and stiff soil used in the LFCB test series, while the lower-bound soil was set based on the MASH soil limit curve (minimum acceptable strength curve). The soil curve that was used in the MGS model representing past crash tests (i.e., test nos. 2214MG-2 and ILT-1) was called "nominal" soil. Note that the nominal soil does not represent the average or ideal. As shown Figure 73, the upper-bound soil curves for 40-in. and 28-in. embedment depths were derived from test nos. LFCB-7 and LFCB-9, respectively. The nominal soil curve for a 40-in. embedment depth was associated with the soil used in the MGS model representing past crash tests. The lower-bound soil curve for a 40-in. embedment depth was the MASH soil limit curve [1]. The lower-bound soil curve for a 40-in. embedment depth was scaled down to represent the case of 28-in. embedment depth using the same proportion observed in test nos. LFCB-7 (for 40-in. depth) and LFCB-9 (for 28-in. depth). A scaling factor of 1.5 was used to derive the lower-bound soil curve for MGS with a 28-in. embedment depth.

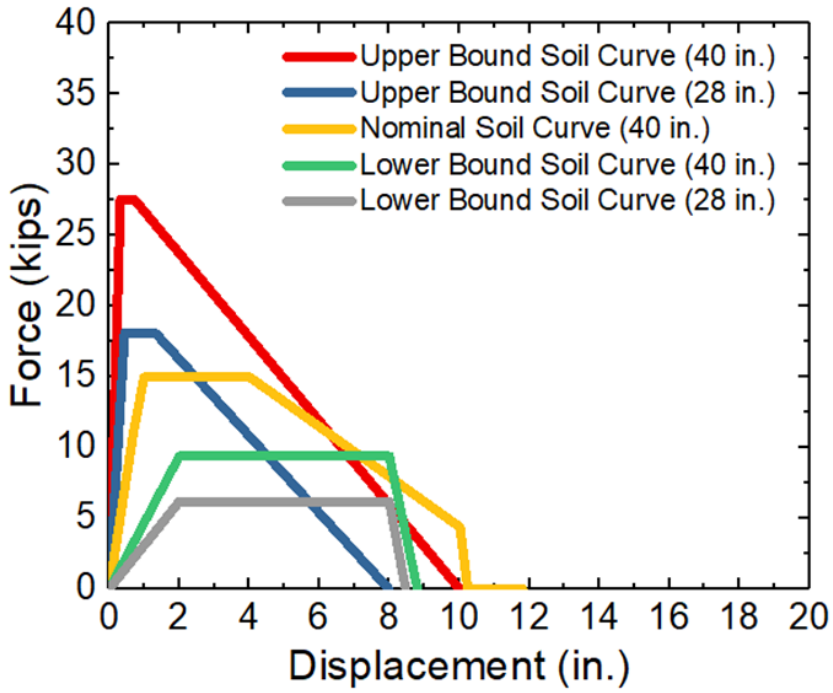

Figure 73. Force vs. Displacement Curves – LS-DYNA Soil Spring Input Curves

The MGS with 28-in. and 40-in. embedment depths at full-, half-, and quarter-post spacing posts with upper-bound and lower-bound soil strengths was simulated and analyzed at TL-2 and TL-3 impact conditions. For each simulation, the dynamic deflection and working width were collected and compared. The working width is the maximum dynamic lateral position of any major part of the system or vehicle measured from the original position of the front of the rail. The MGS system is 21.3 in. wide. Thus, when a post was a working width indicator, the maximum working width would be the sum of 21.3 in. and the maximum dynamic post deflections.

6.2 MASH TL-2 Simulations with Lower-Bound Soil Strength

Analysis of the MGS with lower-bound soil strength began with TL-2 impact conditions (i.e., speed of 44 mph and angle of 25 degrees), using the impact points determined per MASH 2016 [1]. A total of four cases were investigated, with two embedment depths of standard embedment (i.e., 40 in.) and shallow embedment (i.e., 28 in.) and three post spacings (i.e., full-, half-, and quarter-post spacing).

6.2.1 MGS with Standard Post Embedment and Full-Post Spacing

The 5,000-lb Dodge Ram model impacted the MGS with standard post embedment and full-post spacing 10 in. downstream from post no. 12 at a speed of 44 mph and an angle of 25 degrees, as shown in Figure 74. The vehicle was redirected with only a minor tire snag on the posts. Four steel posts displaced without noticeable plastic deformation during the impact event. Overall, the vehicle behavior during redirection was acceptable, and there was no indication of potential vehicle instabilities. Sequential photographs of the simulations are shown in Figures 75 through 77.

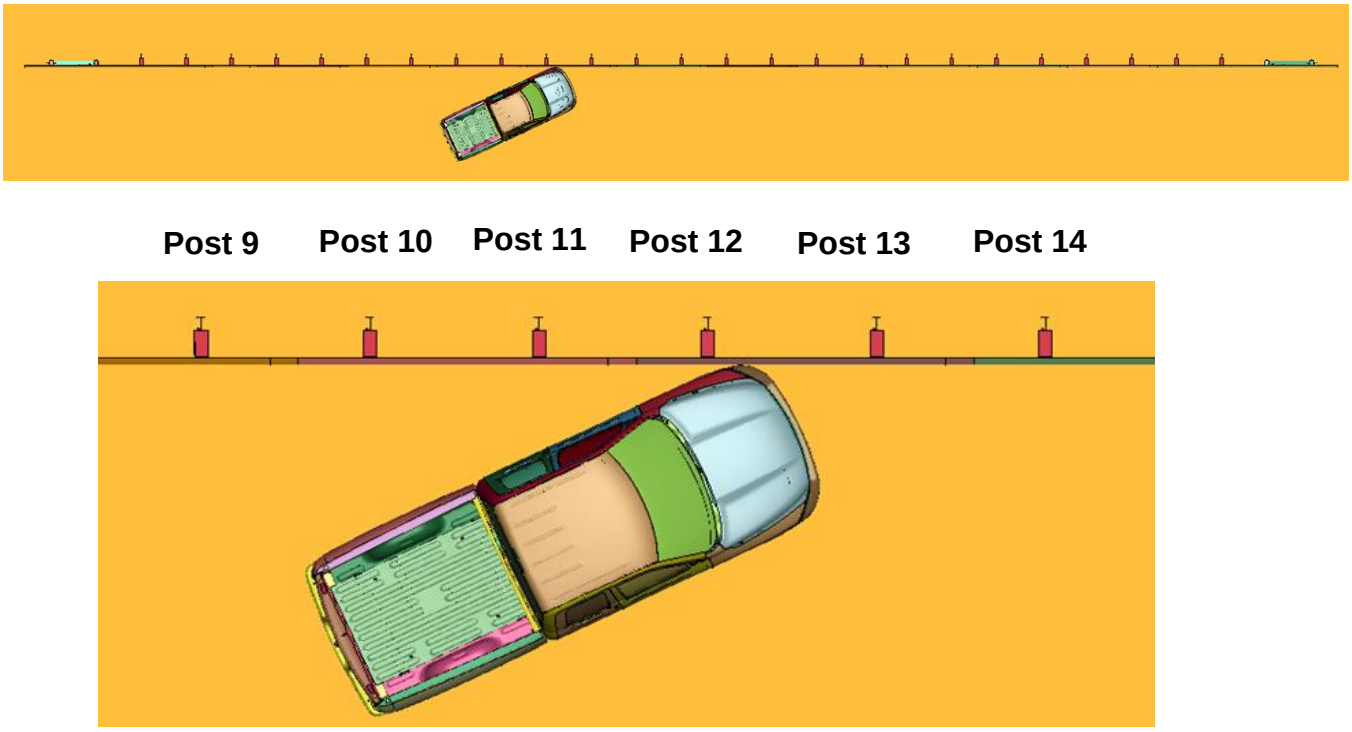

Figure 74. Dodge Ram Vehicle Model Impacting MGS with Standard Post Embedment, Full-Post Spacing, and Lower-Bound Soil Strength

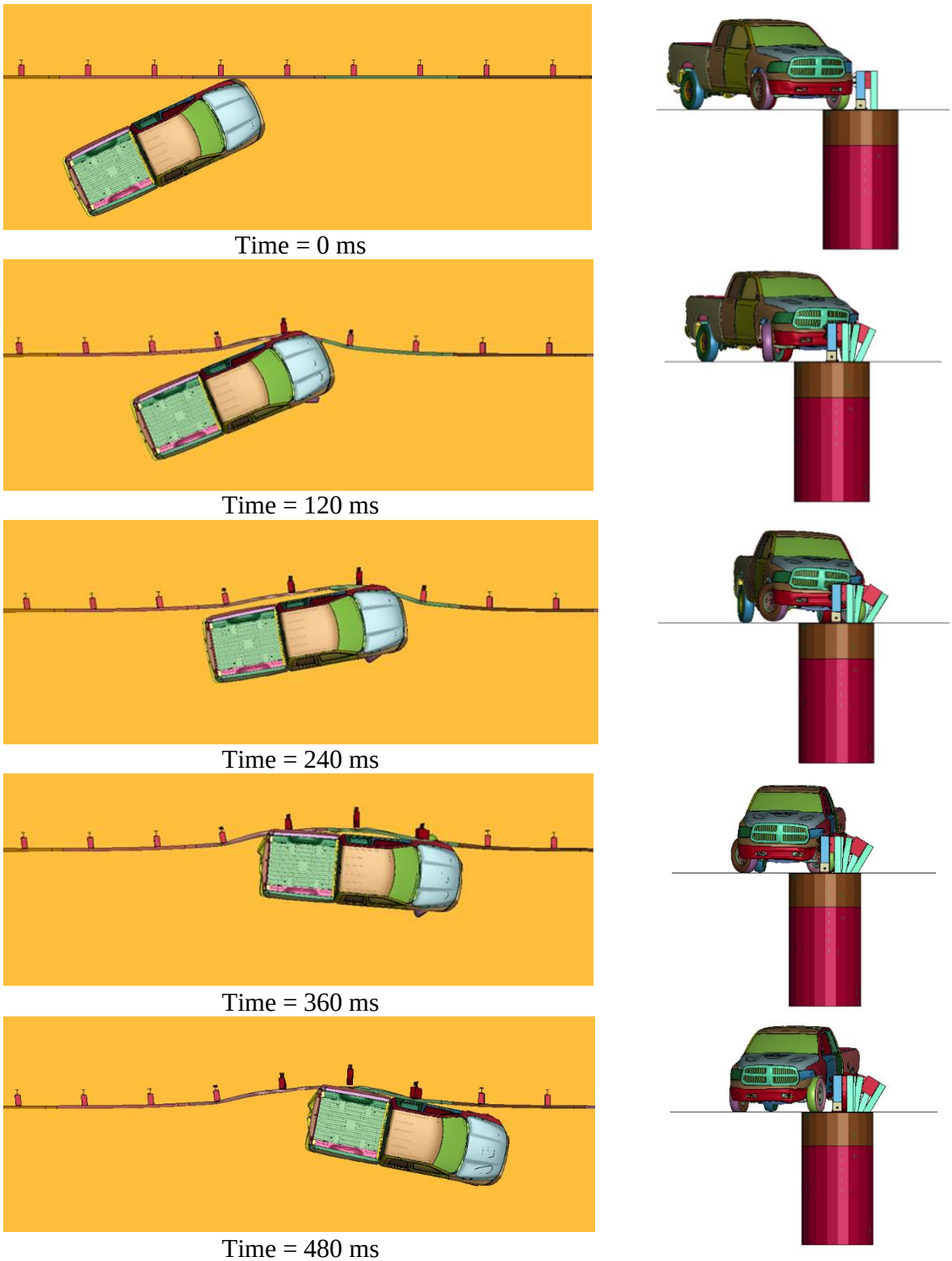

Figure 75. Sequential Images, MGS with Standard Post Embedment, Full-Post Spacing, and Lower-Bound Soil Strength at TL-2 Impact Conditions

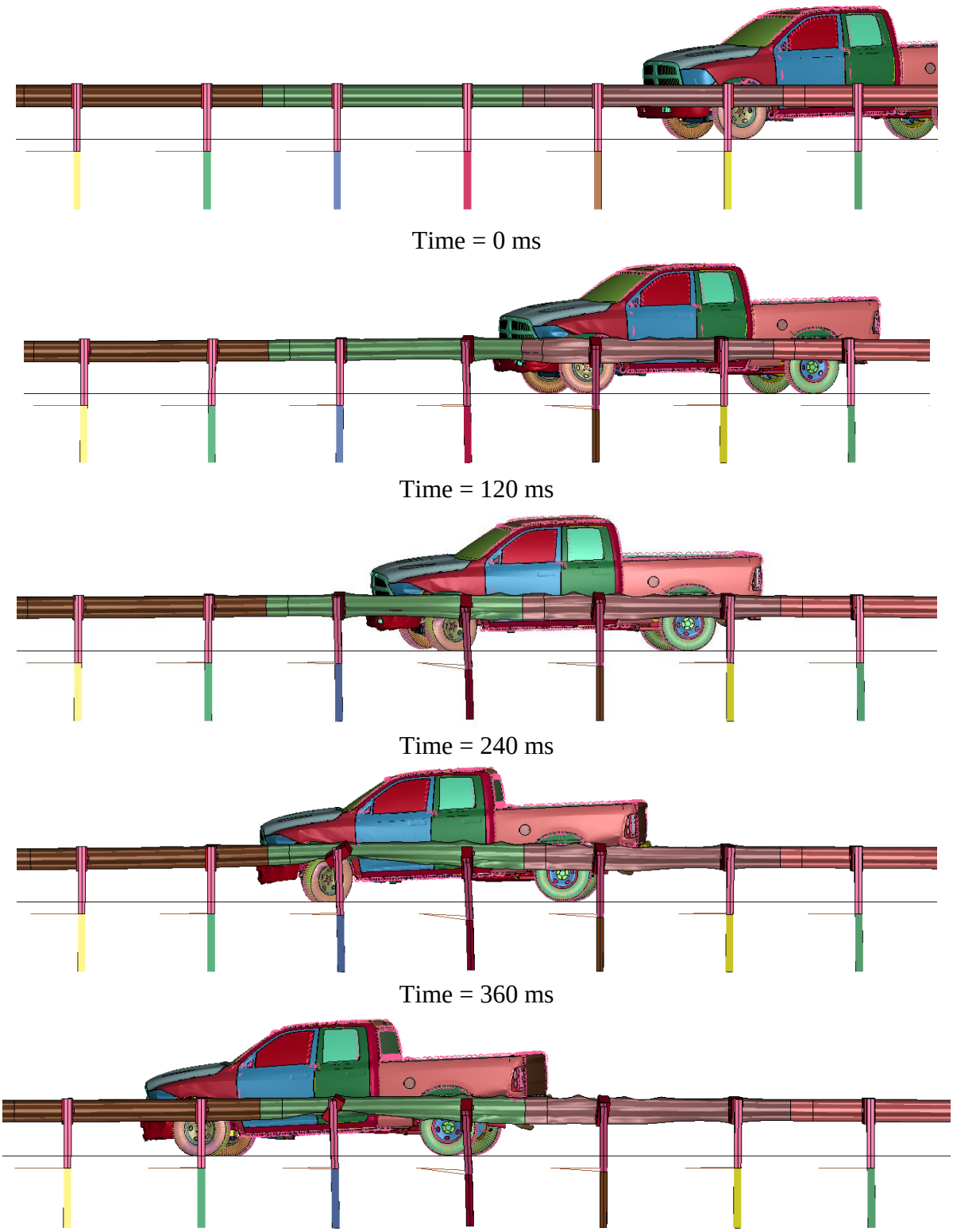

Figure 76. Sequential Images, MGS with Standard Post Embedment, Full-Post Spacing, and Lower-Bound Soil Strength at TL-2 Impact Conditions

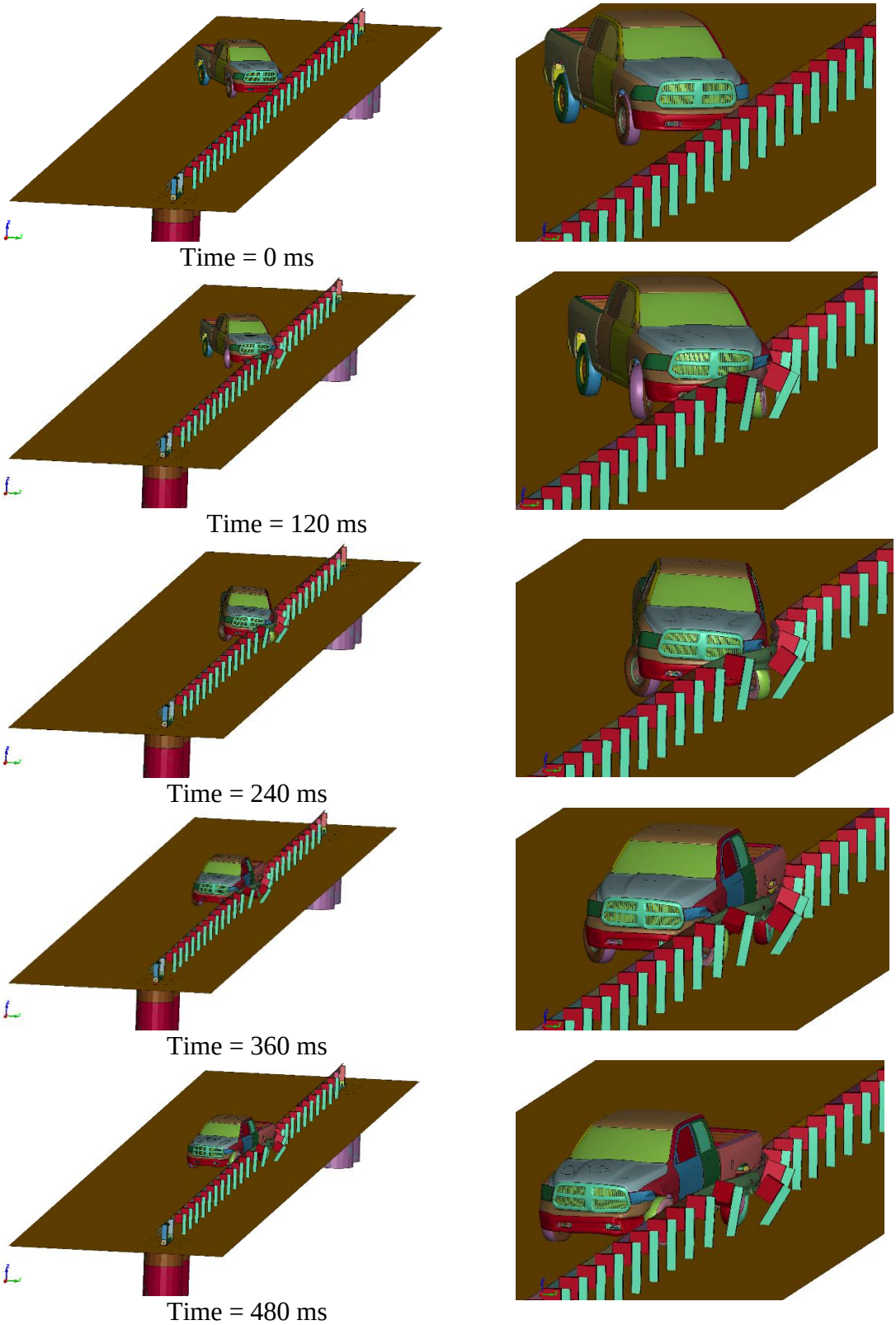

Figure 77. Sequential Images, Sequential Images, MGS with Standard Post Embedment, Full-Post Spacing, and Lower-Bound Soil Strength at TL-2 Impact Conditions (Isometric View)

A summary of the TL-2 simulation results, including dynamic deflection and working width, for the MGS with standard post embedment, full-post spacing, and lower-bound soil strength is shown in Table 10. The Euler angles and occupant risk values were well within the limit set in MASH.

Table 10. TL-2 Simulation of MGS with Standard Post Embedment, Full-Post Spacing, and Lower-Bound Soil Strength

Evaluation Criteria		Standard Embedment: 40 in.	MASH 2016 Limits
OIV ft/s (m/s)	Longitudinal	-12.50 (-3.81)	±40 (12.2)
	Lateral	-13.20 (4.20)	±40 (12.2)
ORA g's	Longitudinal	-4.47	±20.49
	Lateral	-3.91	±20.49
Maximum Angular Displacement deg.	Roll	-2.89	±75
	Pitch	1.56	±75
	Yaw	-36.39	not required
THIV ft/s (m/s)		N/A	not required
PHD g's		N/A	not required
ASI		N/A	not required
Max. Dynamic Deflection in. (mm)		31.16 (791)	N/A
Working Width in. (mm)		51.86 (1,317)	N/A

6.2.2 MGS with Shallow Post Embedment and Full-Post Spacing

The Dodge Ram model impacted the MGS with shallow post embedment of 28 in. and full-post spacing 10 in. upstream from post no. 13 at a speed of 44 mph and an angle of 25 degrees, as shown in Figure 78. The vehicle was redirected with only a minor tire snag on the posts. Seven steel posts displaced during the impact, and three steel posts bent and sustained plastic deformation. Overall, the vehicle behavior during redirection was acceptable, and there was no indication of potential vehicle instabilities. Sequential photographs from the simulations are shown in Figures 79 through 81.

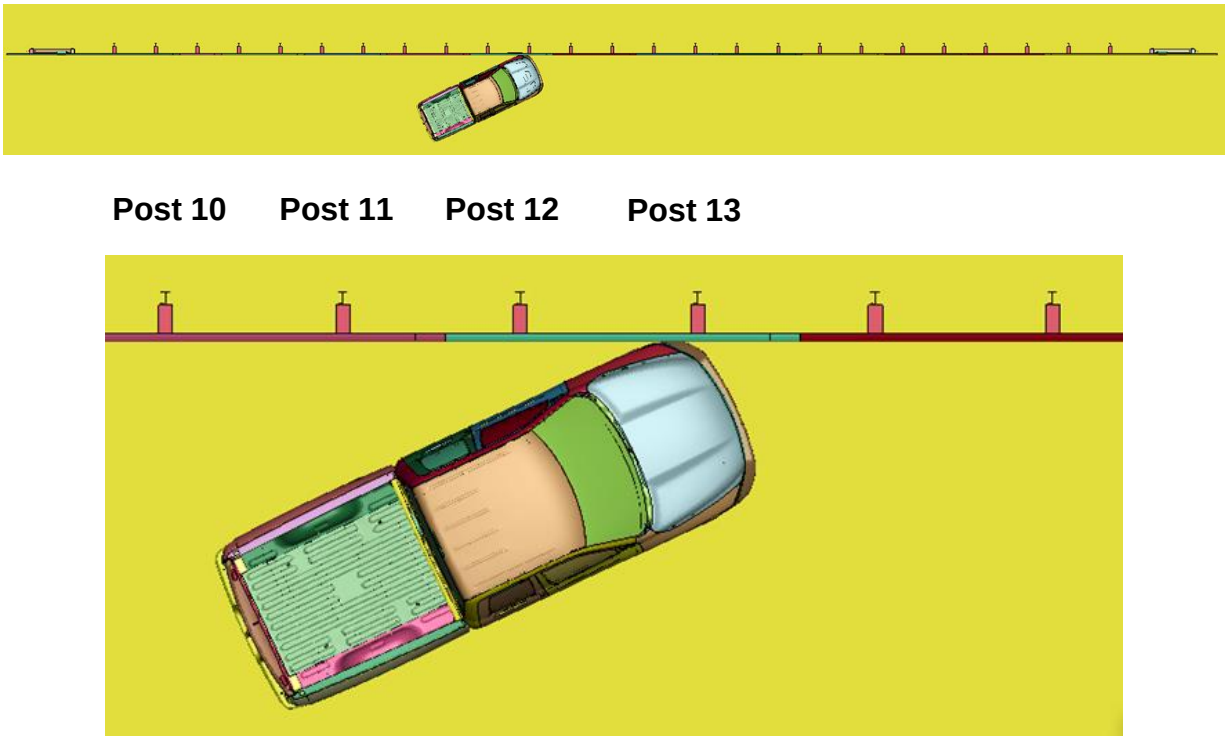

Figure 78. Dodge Ram Model Impacting MGS with Shallow Post Embedment, Full-Post Spacing, and Lower-Bound Soil Strength

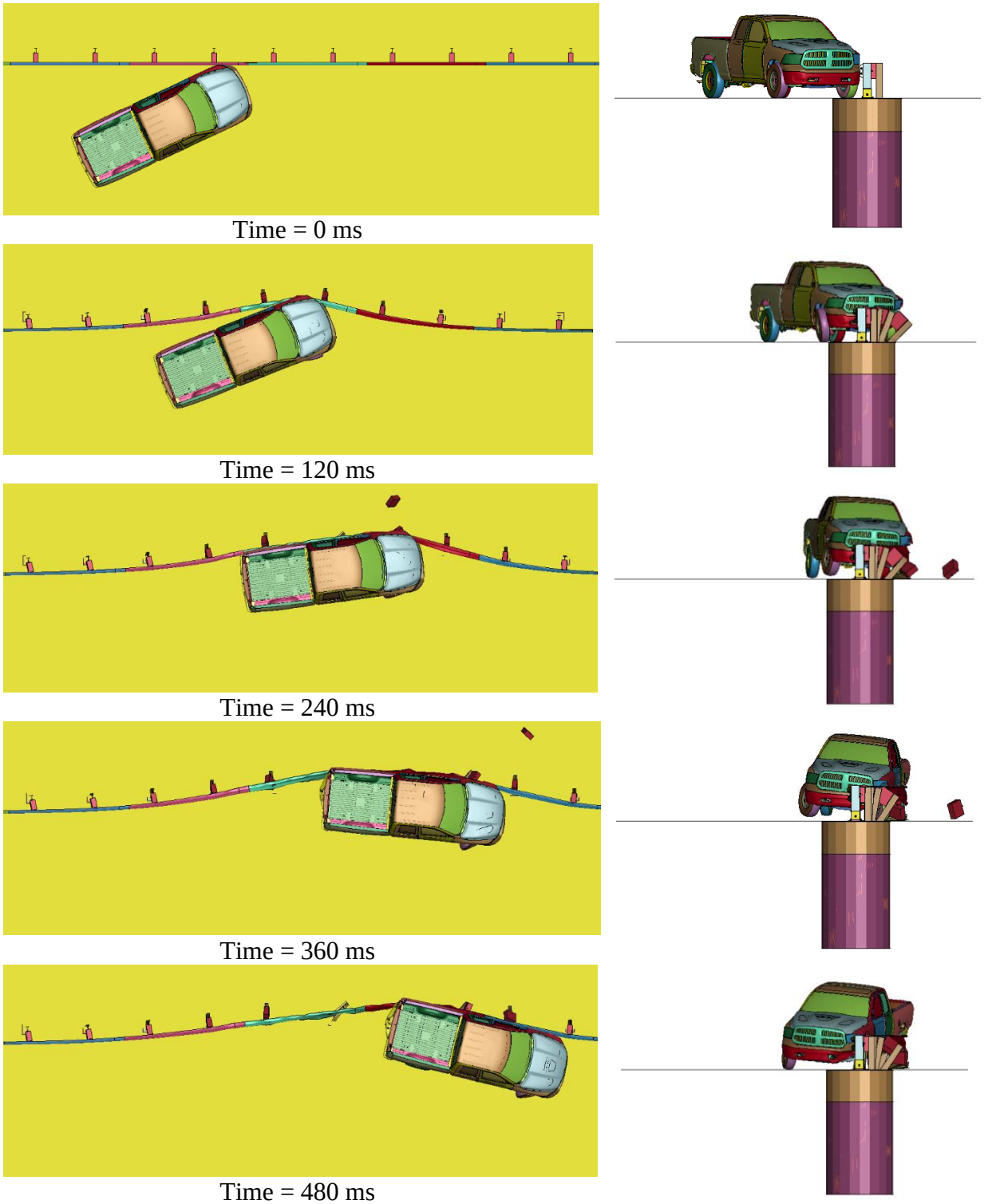

Figure 79. Sequential Images, MGS with Shallow Post Embedment of 28 in., Full-Post Spacing, and Lower-Bound Soil Strength at TL-2 Impact Conditions

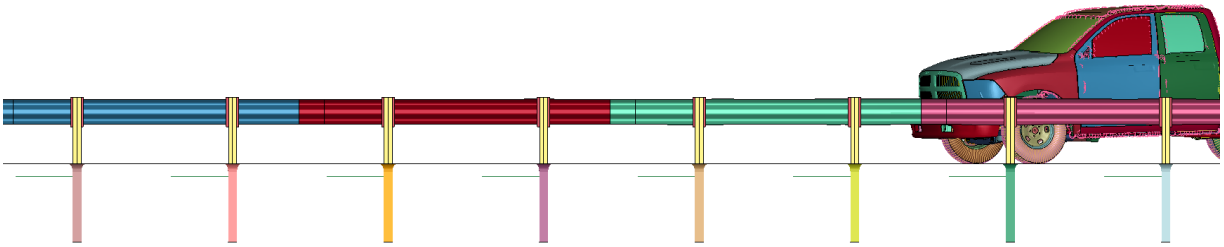

Time = 0 ms

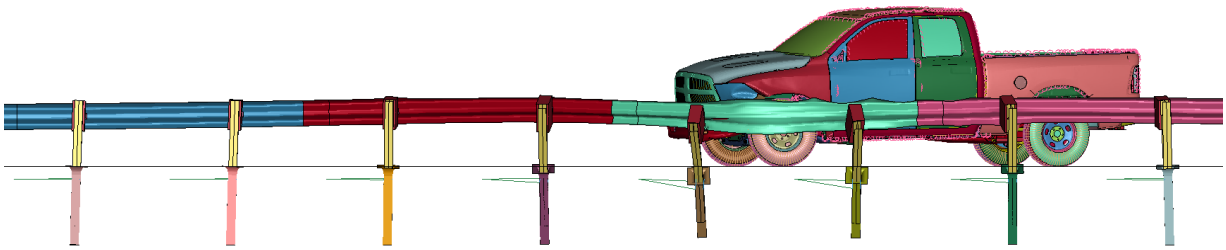

Time = 120 ms

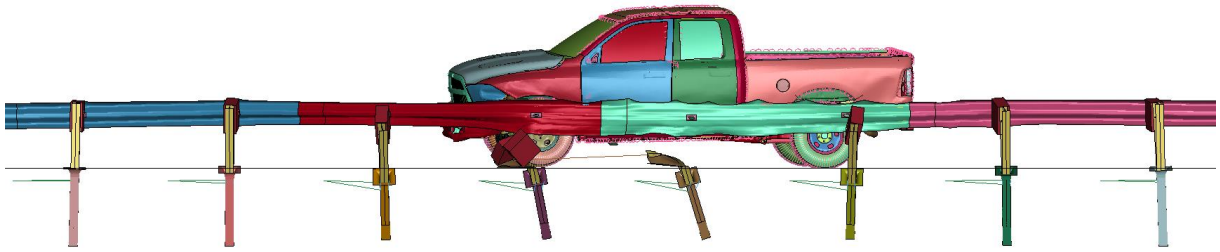

Time = 240 ms

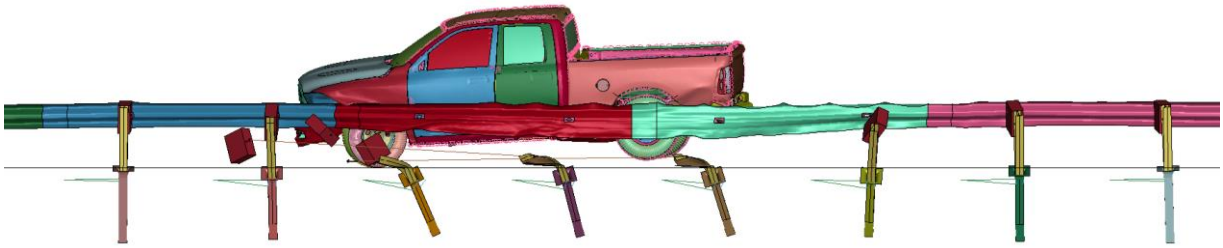

Time = 360 ms

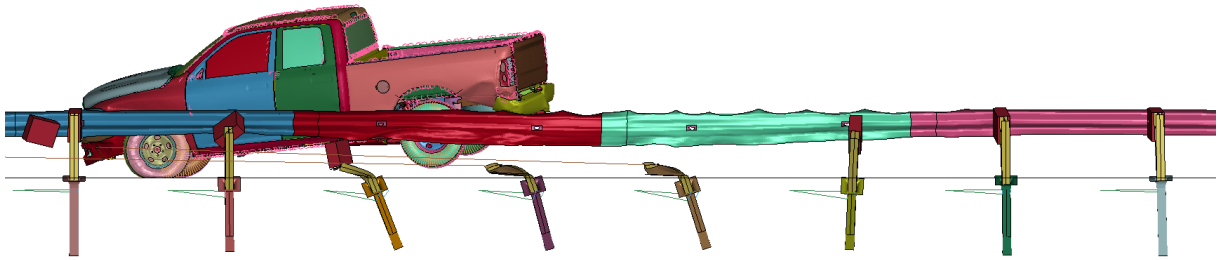

Time = 480 ms

Figure 80. Sequential Images, MGS with Shallow Post Embedment of 28 in., Full-Post Spacing, and Lower-Bound Soil Strength at TL-2 Impact Conditions

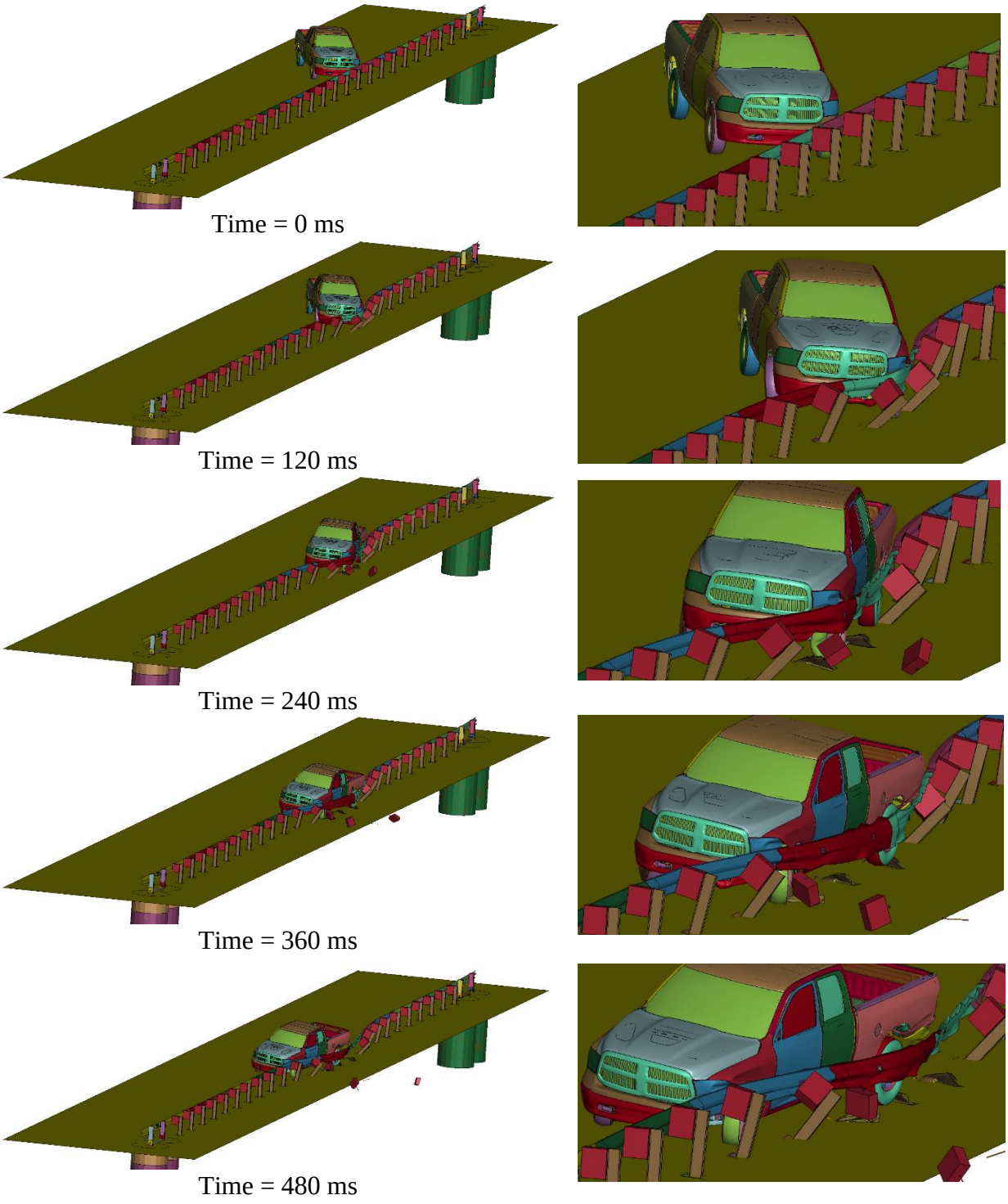

Figure 81. Sequential Images, MGS with Shallow Post Embedment of 28 in., Full-Post Spacing, and Lower-Bound Soil Strength at TL-2 Impact Conditions (Isometric View)

A summary of TL-2 simulation results, including dynamic deflection and working width, for the MGS with shallow embedment, standard post-spacing, and lower-bound soil strength is shown in Table 11. The Euler angles and occupant risk values were well within the limit set in MASH.

Table 11. TL-2 Simulation of MGS with Shallow Post Embedment of 28 in., Full-Post Spacing, and Lower-Bound Soil Strength

Evaluation Criteria		Shallow Embedment: 28 in.	MASH 2016 Limits
OIV ft/s (m/s)	Longitudinal	-10.07	±40 (12.2)
	Lateral	-12.14	±40 (12.2)
ORA g's	Longitudinal	-5.06	±20.49
	Lateral	-4.45	±20.49
Maximum Angular Displacement deg.	Roll	-3.02	±75
	Pitch	-0.91	±75
	Yaw	-35.93	not required
THIV ft/s (m/s)		N/A	not required
PHD g's		N/A	not required
ASI		N/A	not required
Max. Dynamic Deflection in. (mm)		36.38 (924)	N/A
Working Width in. (mm)		55.15 (1,400)	N/A

6.2.3 MGS with Shallow Post Embedment and Half-Post Spacing

The MGS post spacing was altered from 75 to 37.5 in., which stiffened the system. The Dodge Ram model impacted the MGS with shallow post embedment and half-post spacing, 13 in. upstream from post no. 19 at a speed of 44 mph and an angle of 25 degrees, as shown in Figure 82. The vehicle was redirected with only a minor tire snag on the posts. Eight steel posts displaced without noticeable plastic deformation during the impact event. Overall, the vehicle behavior during redirection was acceptable, and there was no indication of potential vehicle instabilities. Sequential photographs of the simulations are shown in Figures 83 through 85.

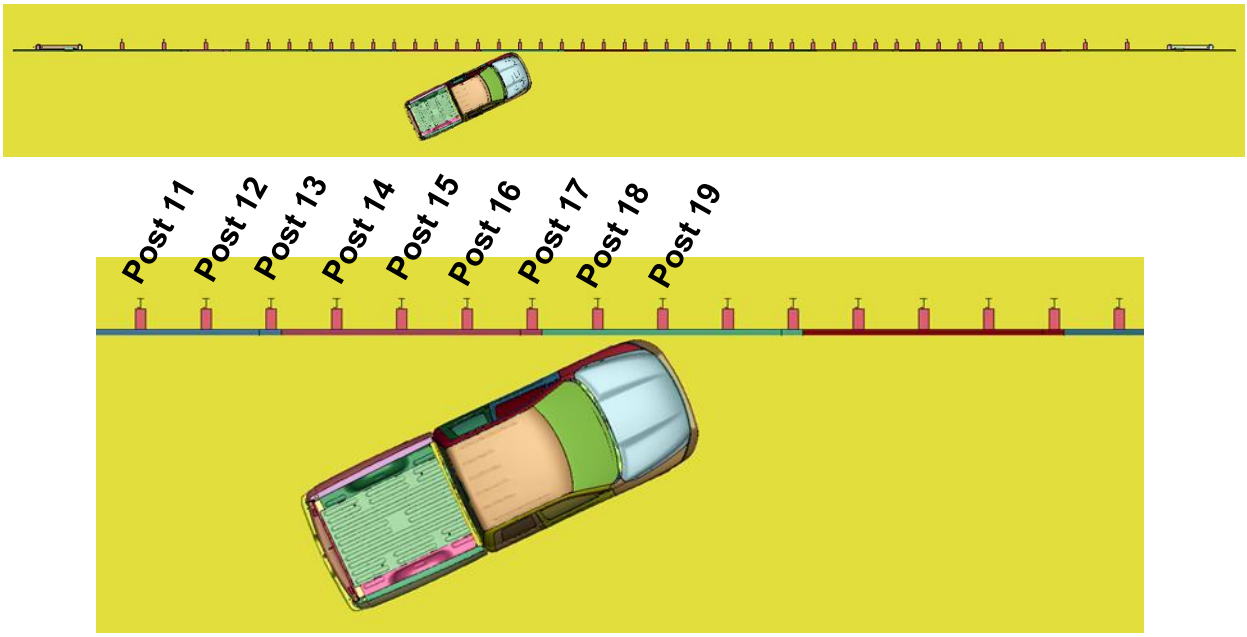

Figure 82. Dodge Ram Vehicle Model Impacting MGS with Shallow Post Embedment, Half-Post Spacing, and Lower-Bound Soil Strength

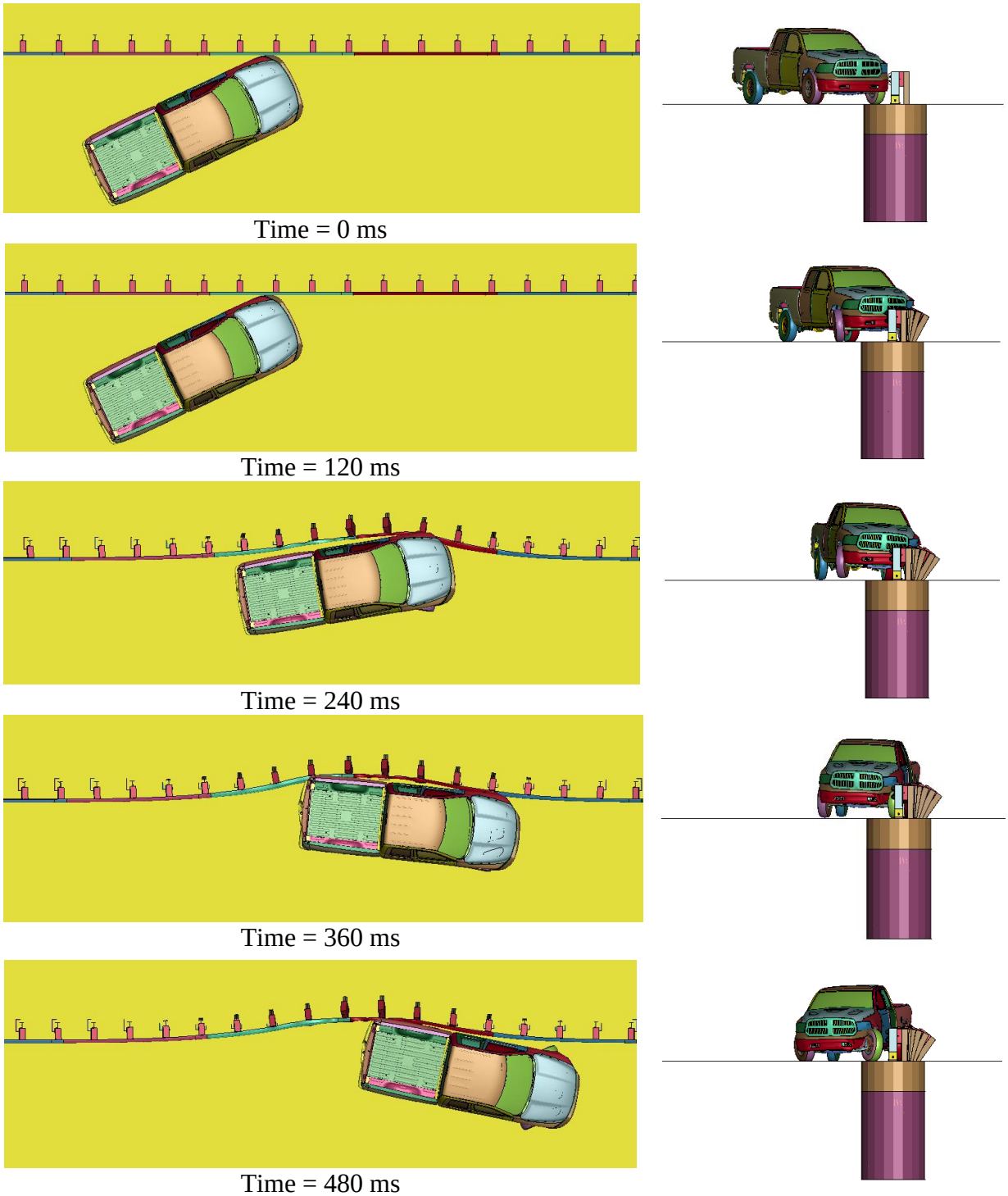

Figure 83. Sequential Images, MGS with Shallow Post Embedment of 28 in. and Half-Post Spacing, and Lower-Bound Soil Strength at TL-2 Impact Conditions

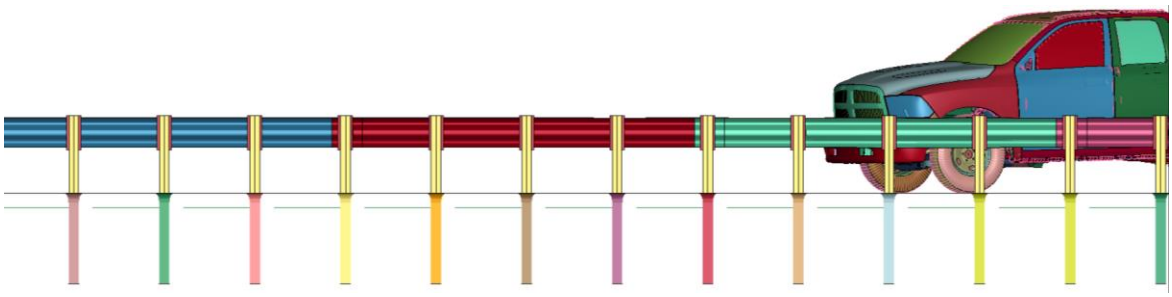

Time = 0 ms

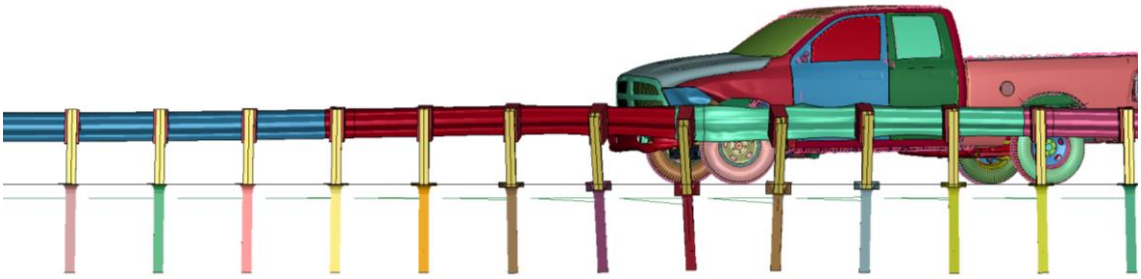

Time = 120 ms

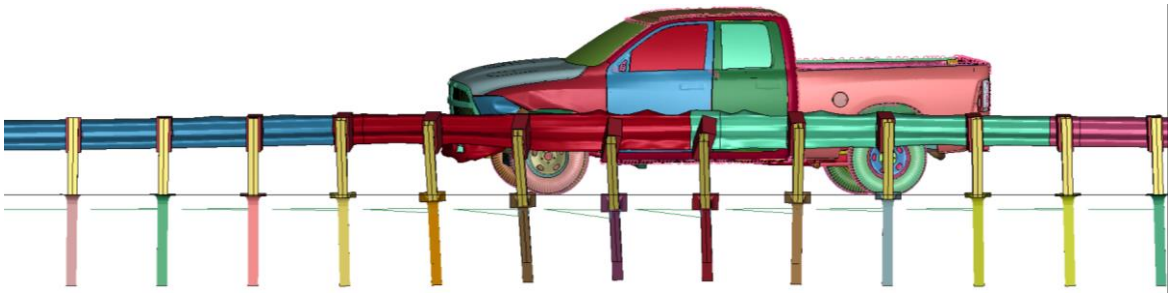

Time = 240 ms

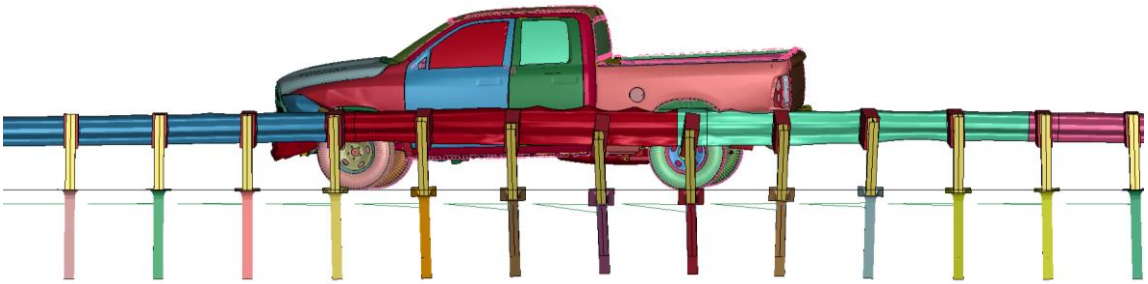

Time = 360 ms

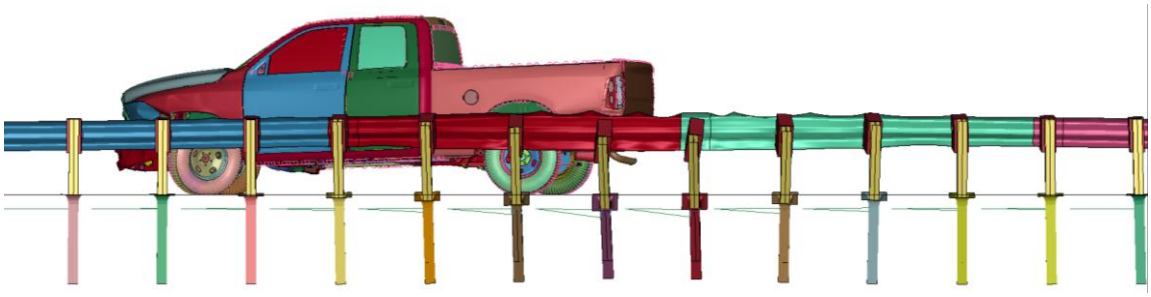

Time = 480 ms

Figure 84. Sequential Images, MGS with Shallow Post Embedment of 28 in., Half-Post Spacing, and Lower-Bound Soil Strength at TL-2 Impact Conditions

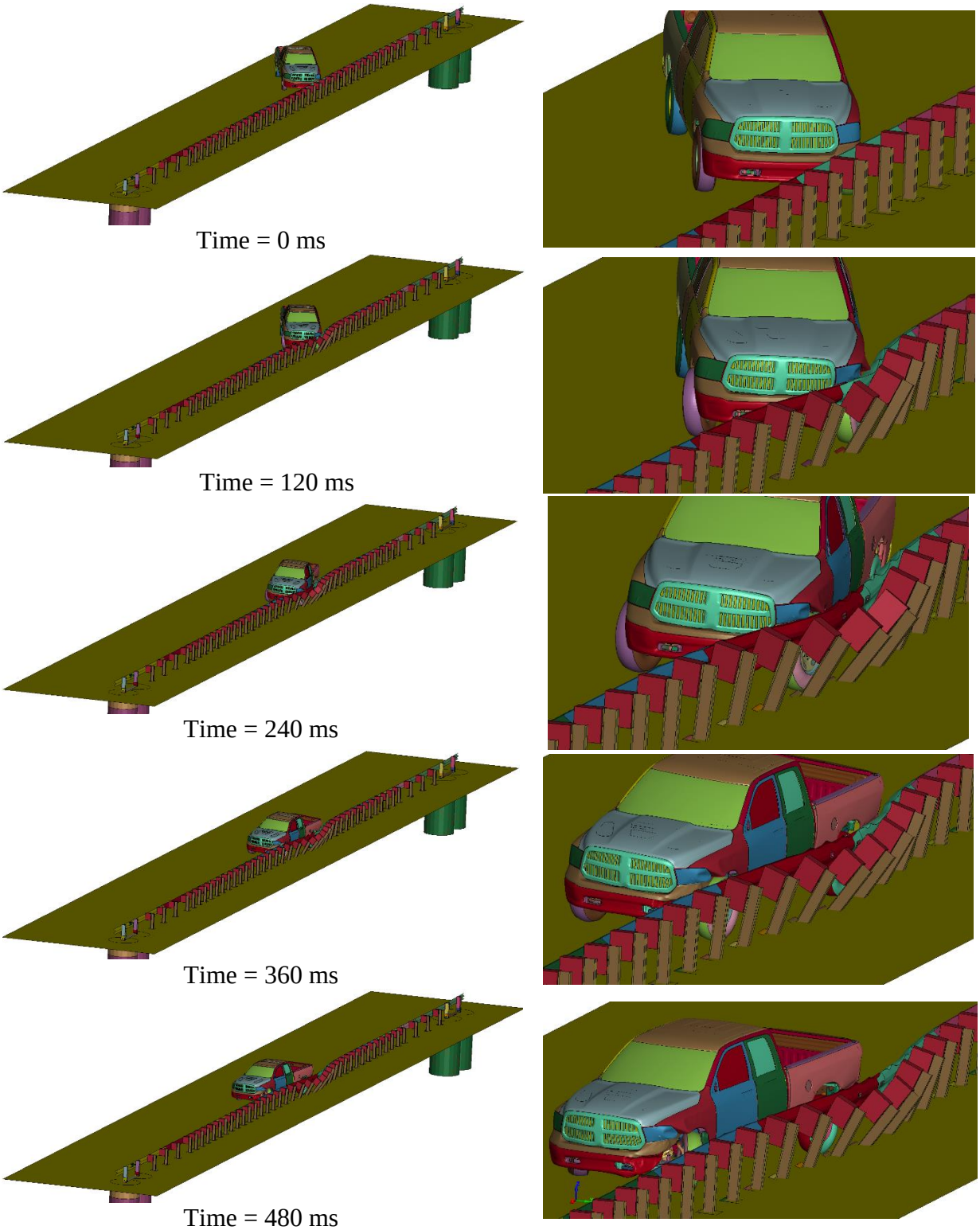

Figure 85. Sequential Images, MGS with Shallow Post Embedment of 28 in., Half-Post Spacing, and Lower-Bound Soil Strength at TL-2 Impact Conditions (Isometric View)

A summary of TL-2 simulation results, including dynamic deflection and working width, for the MGS with shallow embedment, half-post spacing, and lower-bound soil strength is shown in Table 12. The Euler angles and occupant risk values were well within the limit set in MASH.

Table 12. TL-2 Simulation of MGS with Shallow Post Embedment of 28 in., Half-Post Spacing, and Lower-Bound Soil Strength

Evaluation Criteria		Shallow Embedment: 28 in.	MASH 2016 Limits
OIV ft/s (m/s)	Longitudinal	-11.72 (-3.57)	±40 (12.20)
	Lateral	-13.47 (-4.11)	±40 (12.20)
ORA g's	Longitudinal	-4.77	±20.49
	Lateral	-4.64	±20.49
Maximum Angular Displacement deg.	Roll	-2.84	±75
	Pitch	-1.30	±75
	Yaw	-36.83	not required
THIV ft/s (m/s)		N/A	not required
PHD g's		N/A	not required
ASI		N/A	not required
Max. Dynamic Deflection in. (mm)		28.30 (719)	N/A
Working Width in. (mm)		50.18 (1,275)	N/A

6.2.4 MGS with Shallow Post Embedment and Quarter-Post Spacing

The MGS post spacing was altered from 37.5 to 18.75 in., which further stiffened the system. The Dodge Ram model impacted the MGS with shallow post embedment and quarter-post spacing 3 in. downstream from post no. 32 at a speed of 44 mph and an angle of 25 degrees, as shown in Figure 86. The vehicle was redirected with only a minor tire snag on the posts. Sixteen steel posts displaced without noticeable plastic deformation during the impact event. Overall, the vehicle behavior during redirection was acceptable, and there was no indication of potential vehicle instabilities. Sequential photographs of the simulations are shown in Figures 87 through 89.

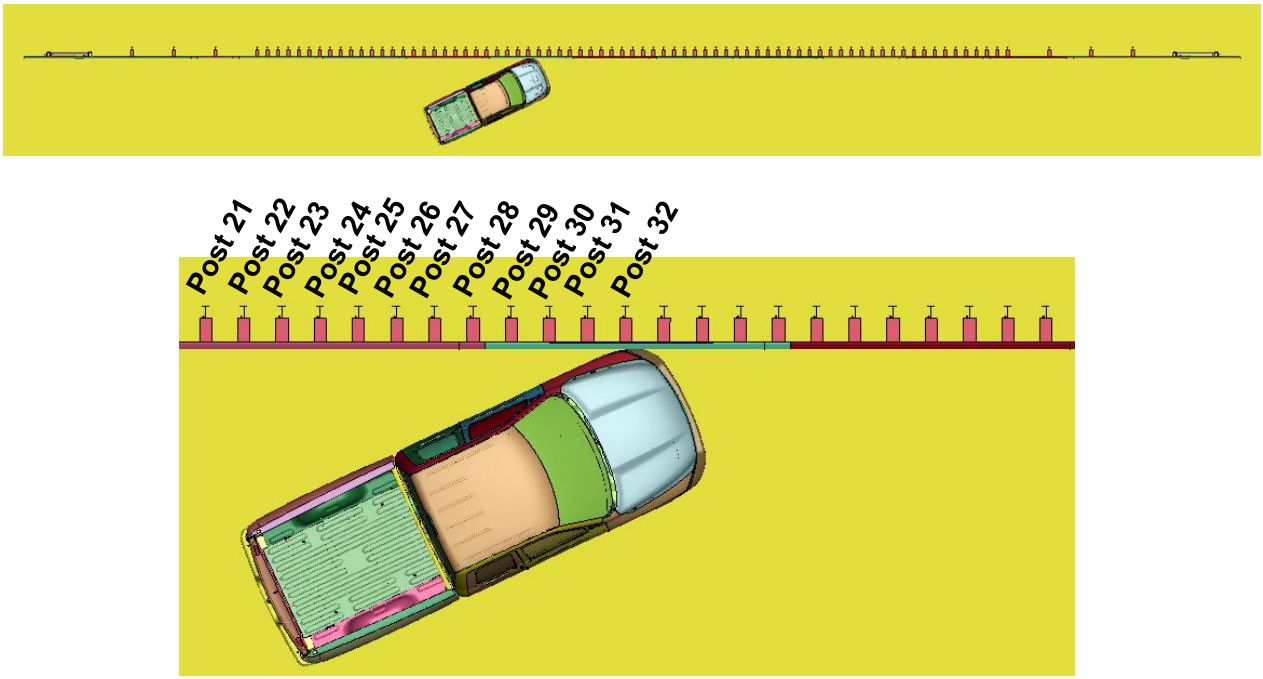

Figure 86. Dodge Ram Vehicle Model Impacting MGS with Shallow Post Embedment, Quarter-Post Spacing, and Lower-Bound Soil Strength

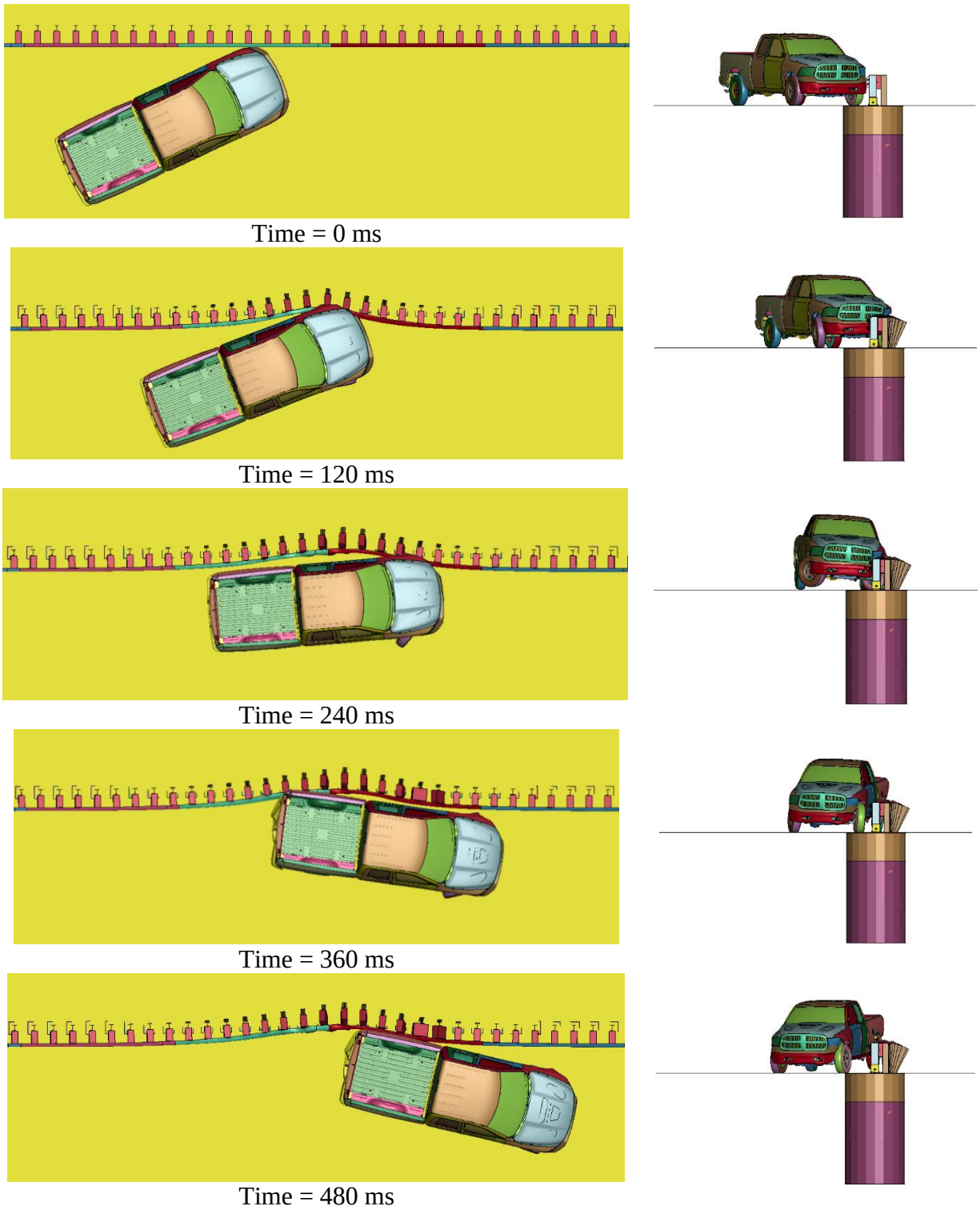

Figure 87. Sequential Images, MGS with Shallow Post Embedment of 28 in., Quarter-Post Spacing, and Lower-Bound Soil Strength at TL-2 Impact Conditions

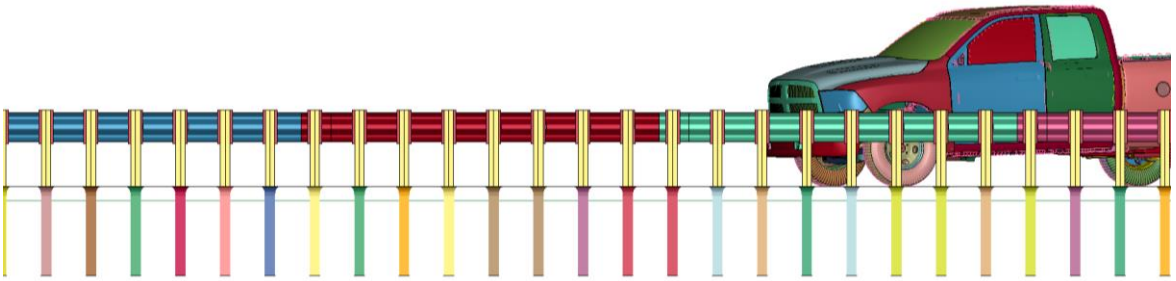

Time = 0 ms

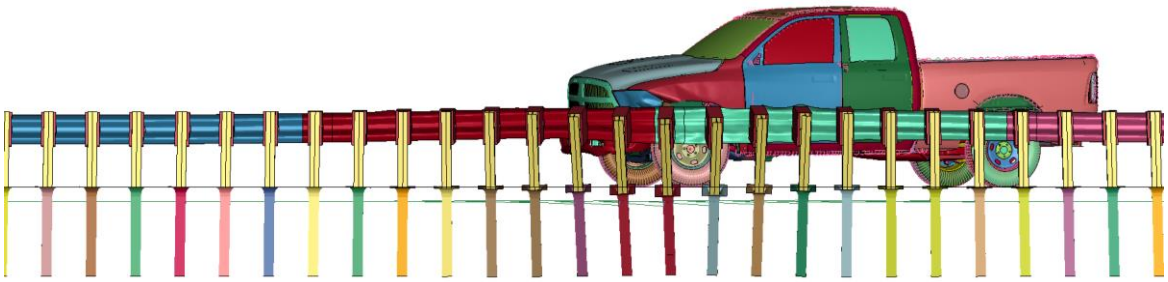

Time = 120 ms

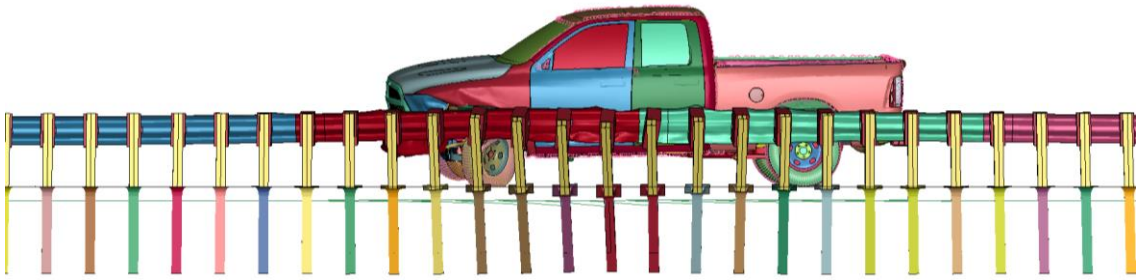

Time = 240 ms

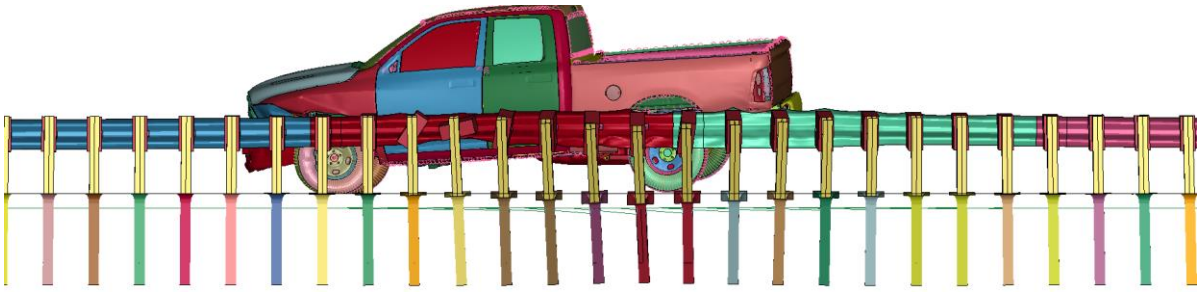

Time = 360 ms

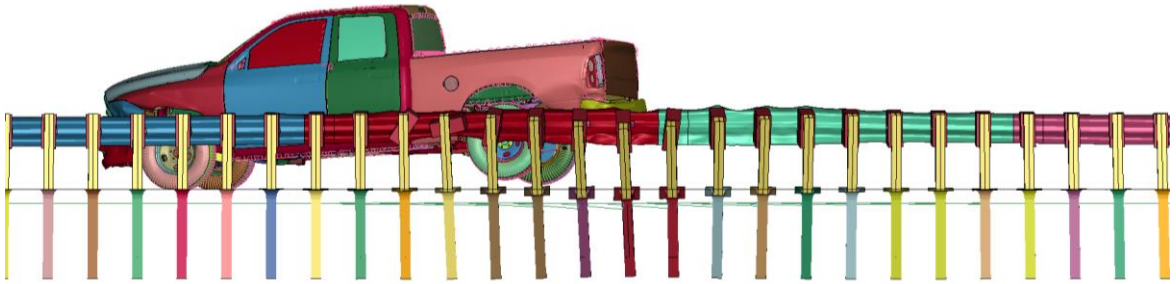

Time = 480 ms

Figure 88. Sequential Images, MGS with Shallow Post Embedment of 28 in., Half-Post Spacing, and Lower-Bound Soil Strength at TL-2 Impact Conditions

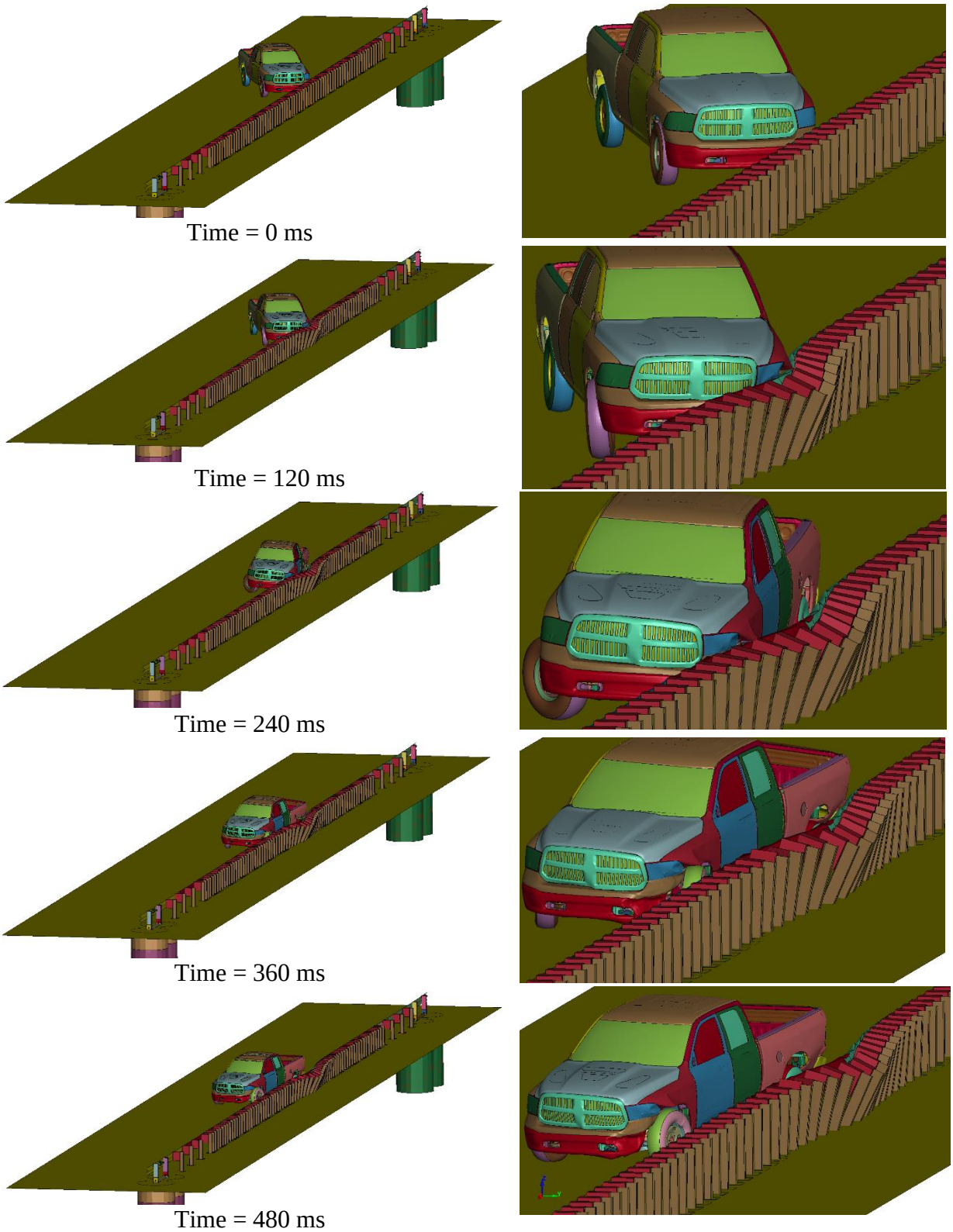

Figure 89. Sequential Images, MGS with Shallow Post Embedment of 28 in., Quarter-Post Spacing, and Lower-Bound Soil Strength at TL-2 Impact Conditions (Isometric View)

A summary of TL-2 simulation results, including dynamic deflection and working width, for MGS with shallow embedment, quarter-post spacing, and lower-bound soil strength is shown in Table 13. The Euler angles and occupant risk values were well within the limit set in MASH.

Table 13. TL-2 Simulation of Shallow Post Embedment of 28 in., Quarter-Post Spacing, and Lower-Bound Soil Strength

Evaluation Criteria		Shallow Embedment: 28 in.	MASH 2016 Limits
OIV ft/s (m/s)	Longitudinal	-13.56 (-4.13)	±40 (12.20)
	Lateral	-15.37 (-4.68)	±40 (12.20)
ORA g's	Longitudinal	-4.68	±20.49
	Lateral	-5.37	±20.49
Maximum Angular Displacement deg.	Roll	-4.38	±75
	Pitch	2.93	±75
	Yaw	-38.53	not required
THIV ft/s (m/s)		N/A	not required
PHD g's		N/A	not required
ASI		N/A	not required
Max. Dynamic Deflection in. (mm)		21.40 (544)	N/A
Working Width in. (mm)		44.71 (1,136)	N/A

6.2.5 Discussion

The simulated dynamic deflection and working width for MGS with reduced post embedment and reduced post spacing with lower-bound soil strength at TL-2 impact conditions are summarized in Table 14. The shallow post embedment and full-post spacing MGS showed the highest dynamic deflection of 36.38 in., as expected. The dynamic deflection and working width of the shallow post embedment and half-post spacing MGS were comparable with the standard post embedment and full-post spacing MGS (i.e., baseline MGS model).

The dynamic deflection for the MGS with a 40-in. embedment depth and lower-bound soil strength was 31.16 in. The lowest dynamic deflection of 21.40 in. was obtained for the MGS with shallower post embedment and quarter-post spacing. As previously noted, the post-soil forces for lower-bound soil strength represented the soil that met the minimum soil strength specified in MASH. Therefore, the dynamic deflection and working width for MGS with lower-bound soil strength simulations were believed to be conservative.

Table 14. MASH TL-2 Simulation Results for MGS with Lower-Bound Soil Strength

Evaluation Criteria	Standard Post Embedment & Full-Post Spacing	Shallow Post Embedment of 28 in.			MASH 2016 Limits
		Full-Post Spacing	Half-Post Spacing	Quarter-Post Spacing	
Max. Dynamic Deflection in. (mm)	31.16 (791)	36.38 (924)	28.30 (719)	21.40 (544)	N/A
Working Width in. (mm)	51.86 (1,317)	55.15 (1,400)	50.18 (1,275)	44.71 (1,136)	N/A

6.3 MASH TL-2 Simulations with Upper-Bound Soil

Analysis of the MGS continued with upper-bound soil at TL-2 impact conditions. A total of four cases were investigated, with two embedment depths (i.e., standard embedment of 40 in. and shallow embedment of 28 in.) and three post spacings (i.e., full-, half-, and quarter-post spacing).

6.3.1 MGS with Standard Post Embedment and Full-Post Spacing

The Dodge Ram model impacted the standard post embedment and full-post spacing MGS 10 in. downstream from post no. 12 at a speed of 44 mph and an angle of 25 degrees, as shown in Figure 90. The vehicle was redirected with only a minor tire snag on the posts. Four steel posts displaced during the impact, and three steel posts bent and sustained plastic deformation. Overall, the vehicle behavior during redirection was acceptable, and there was no indication of potential vehicle instabilities. Sequential photographs of the simulations are shown in Figures 91 through 93.

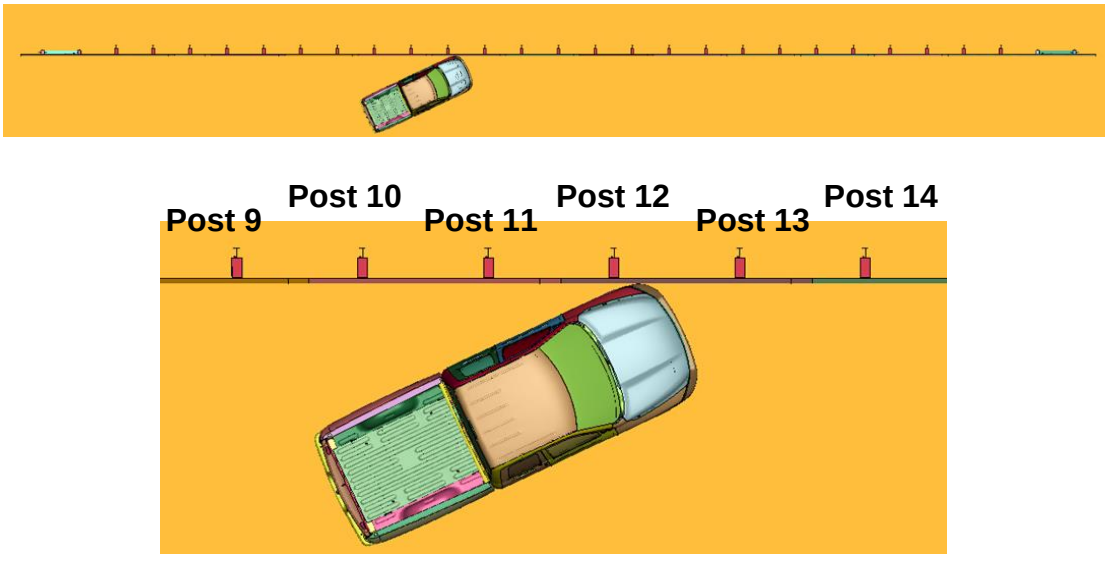

Figure 90. Dodge Ram Vehicle Model Impacting MGS with Standard Post Embedment, Full-Post Spacing, and Upper-Bound Soil

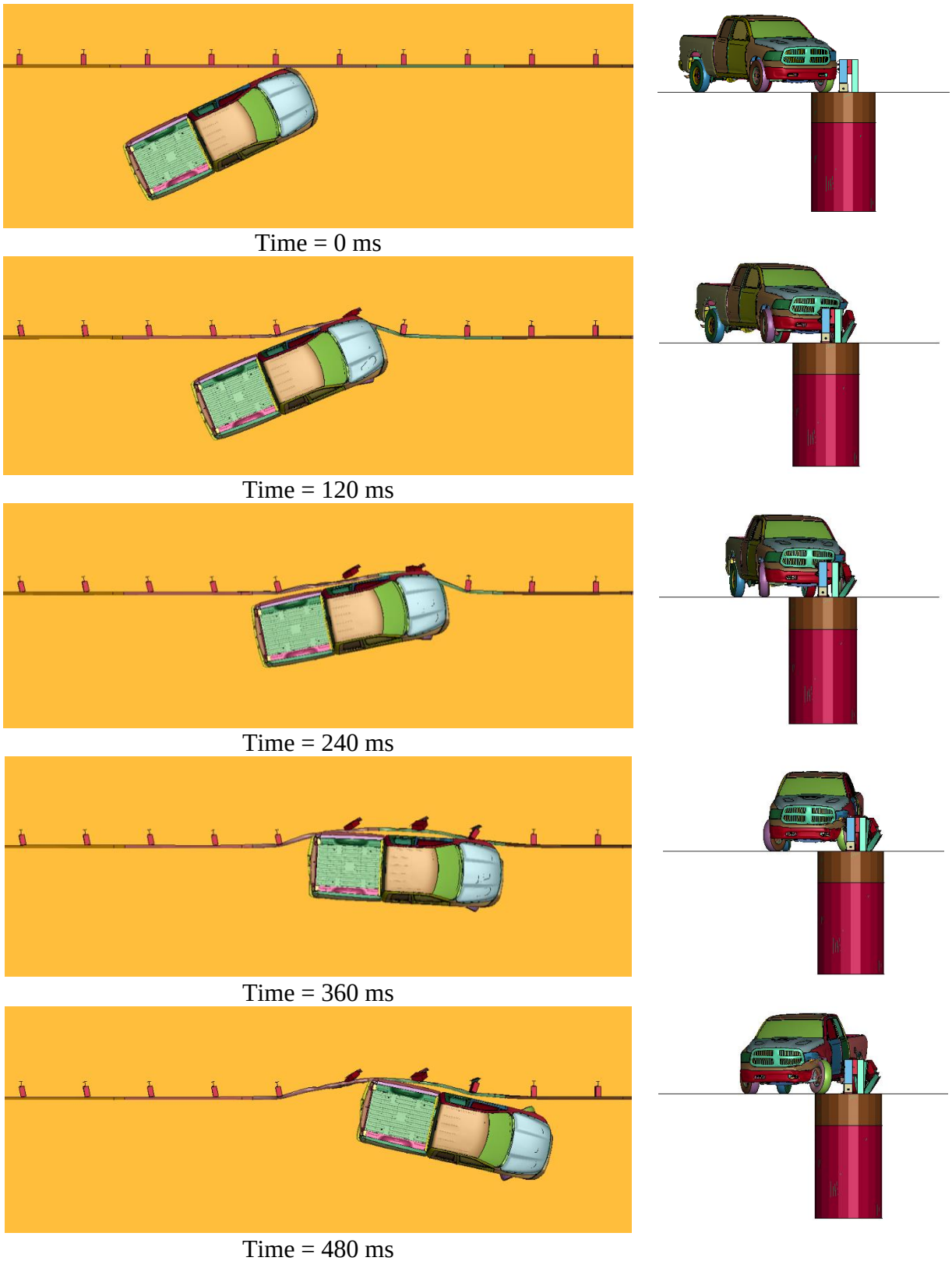

Figure 91. Sequential Images, MGS with Standard Post Embedment, Full-Post Spacing, Upper-Bound Soil at TL-2 Impact Conditions

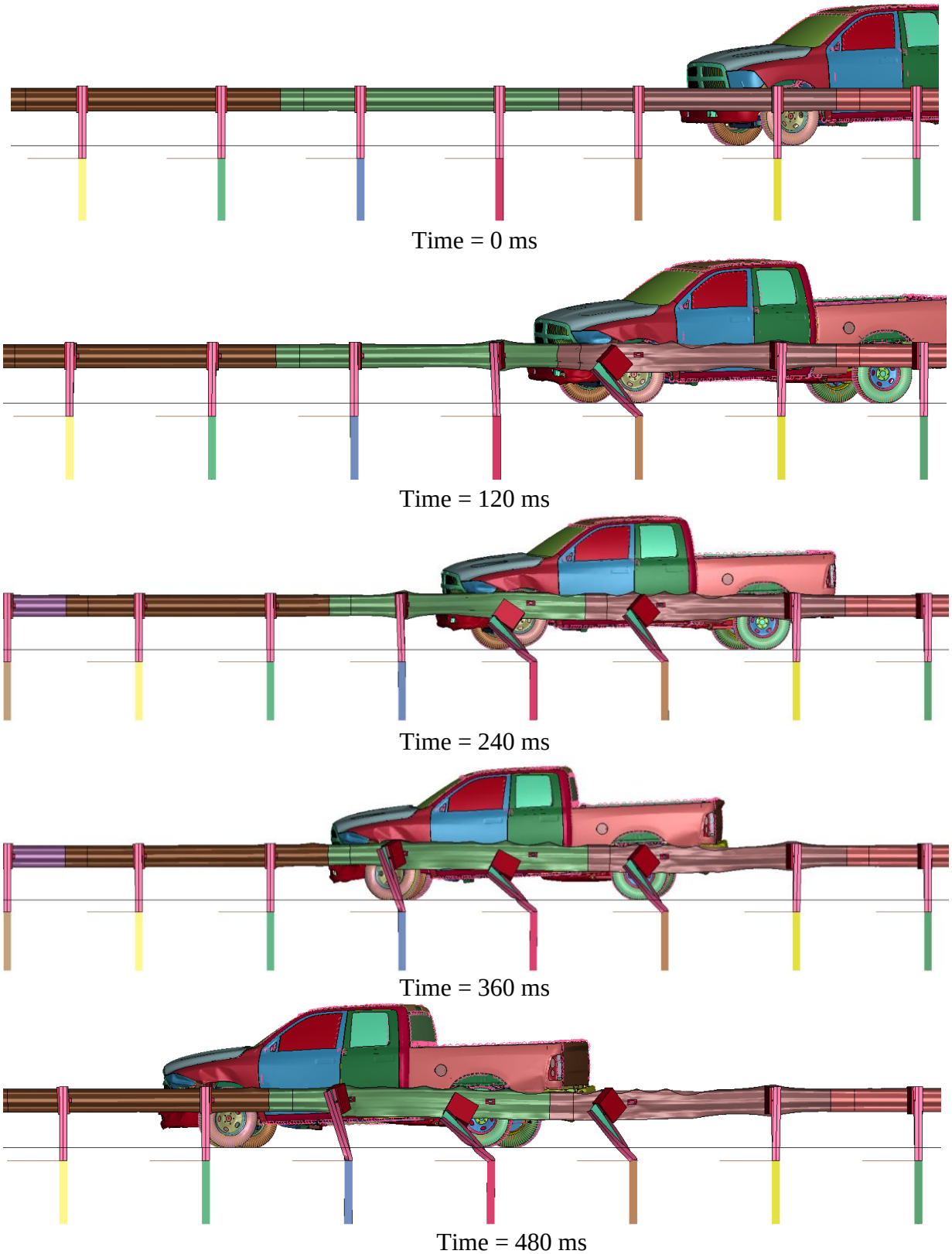

Figure 92. Sequential Images, MGS with Standard Post Embedment, Full-Post Spacing, Upper-Bound Soil at TL-2 Impact Conditions

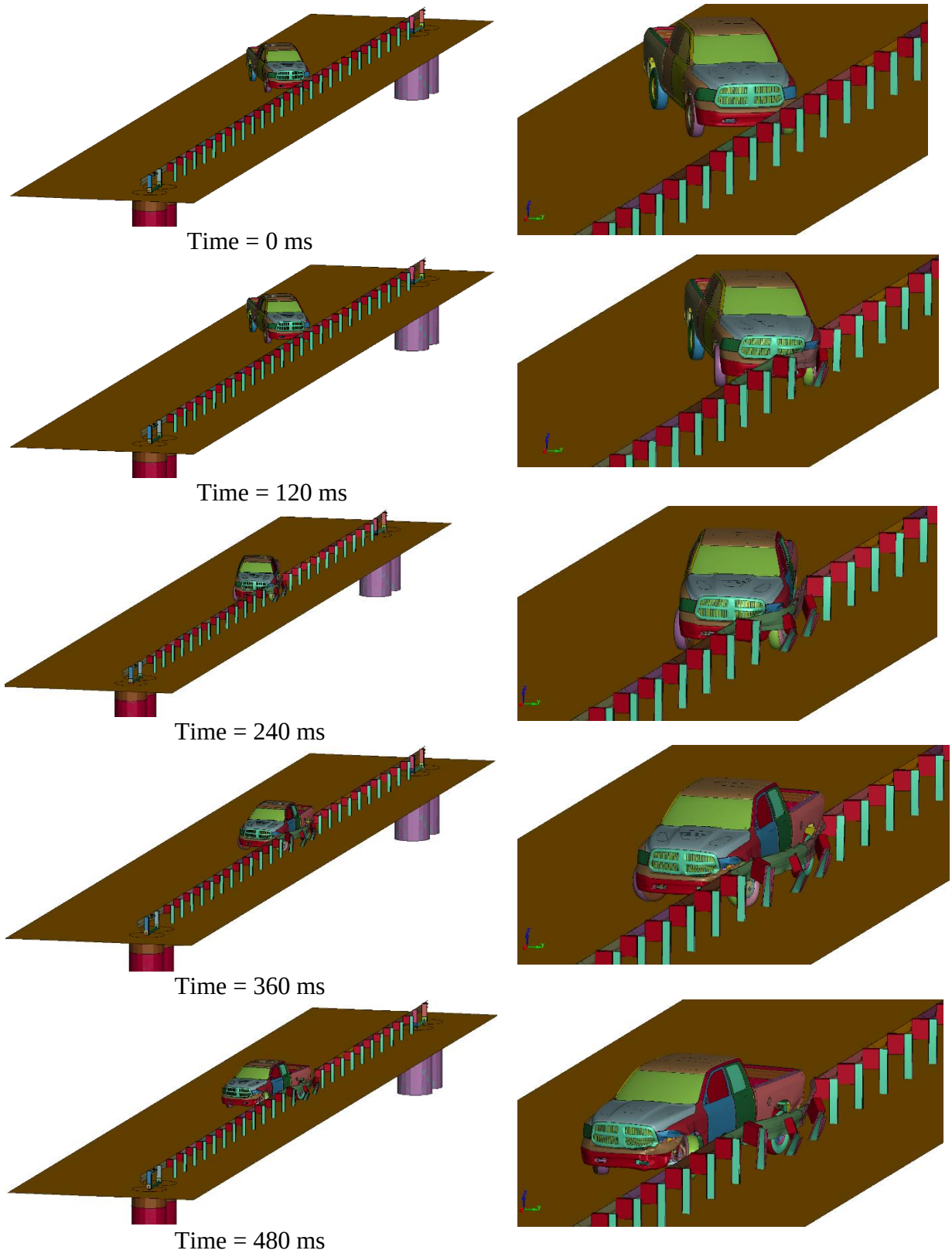

Figure 93. Sequential Images, MGS with Standard Post Embedment, Full-Post Spacing, Upper-Bound Soil at TL-2 Impact Conditions (Isometric View)

A summary of TL-2 simulation results, including dynamic deflection and working width, for the MGS with shallow embedment, full-post spacing, and upper-bound soil is shown in Table 15. The Euler angles and occupant risk values were well within the limit set in MASH.

Table 15. TL-2 Simulation of MGS with Standard Post Embedment of 40 in., Full-Post Spacing, and Upper-Bound Soil

Evaluation Criteria		Standard Embedment of 40 in.	MASH 2016 Limits
OIV ft/s (m/s)	Longitudinal	-14.39 (4.39)	±40 (12.2)
	Lateral	-13.09 (3.99)	±40 (12.2)
ORA g's	Longitudinal	-4.04	±20.49
	Lateral	-5.07	±20.49
Maximum Angular Displacement deg.	Roll	-2.13	±75
	Pitch	1.00	±75
	Yaw	-38.15	not required
THIV ft/s (m/s)		N/A	not required
PHD g's		N/A	not required
ASI		N/A	not required
Max. Dynamic Deflection in. (mm)		25.00 (635)	N/A
Working Width in. (mm)		36.14 (918)	N/A

6.3.2 MGS with Shallow Post Embedment and Full-Post Spacing

The Dodge Ram model impacted the MGS with shallow post embedment of 28 in. and full-post spacing, 10 in. upstream from post no. 13 at a speed of 44 mph and an angle of 25 degrees, as shown in Figure 94. The vehicle was redirected out of the system with only minor tire snag on the posts. Three steel posts displaced during the impact, and two steel posts bent and sustained plastic deformation. Overall, the vehicle behavior during redirection was acceptable, and there was no indication of potential vehicle instabilities. Sequential photographs of the simulations are shown in Figures 95 through 97.

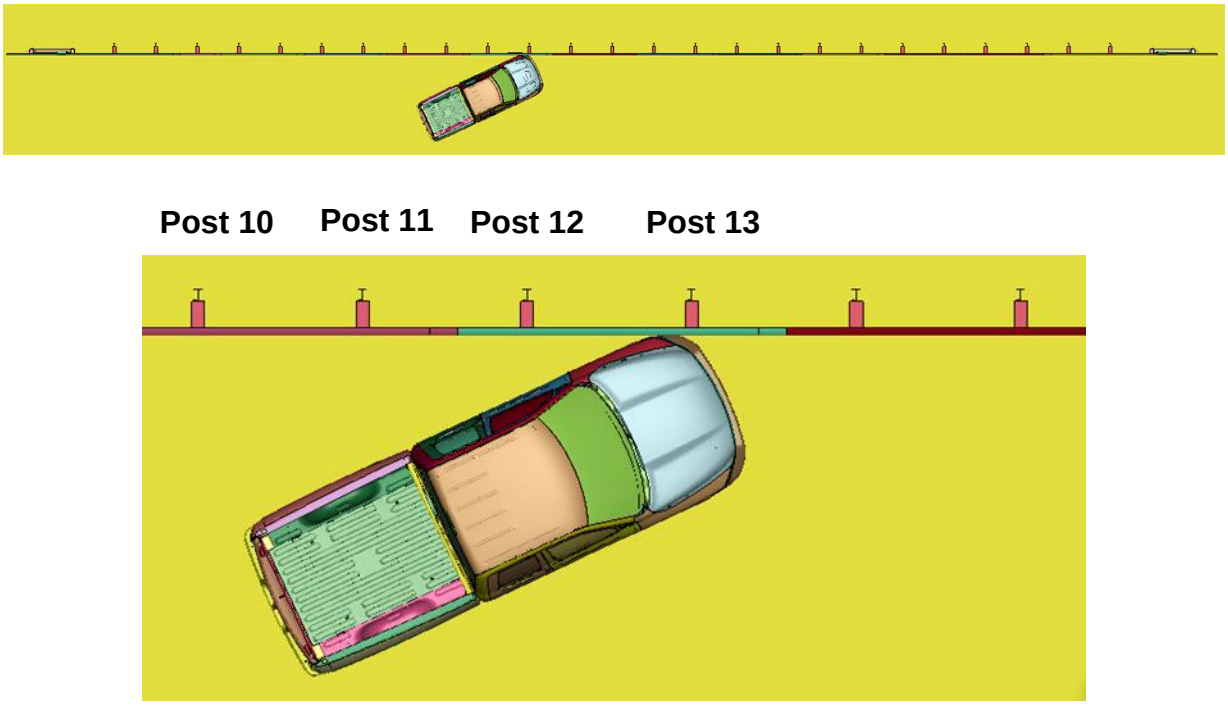

Figure 94. Dodge Ram Vehicle Model Impacting MGS with Shallow Post Embedment, Full-Post Spacing, and Upper-Bound Soil Strength

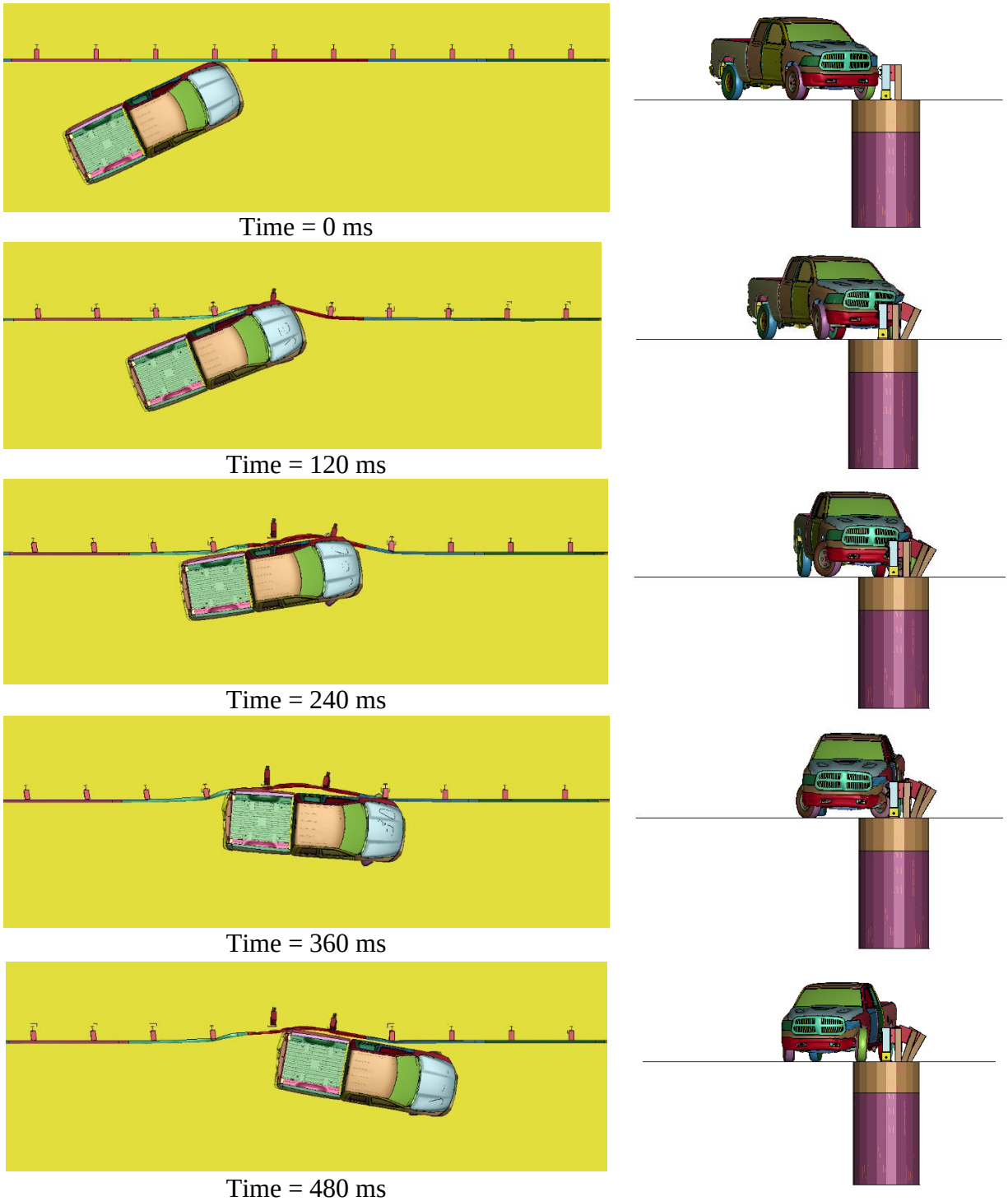

Figure 95. Sequential Images, MGS with Shallow Post Embedment of 28 in., Full-Post Spacing, and Upper-Bound Soil at TL-2 Impact Conditions

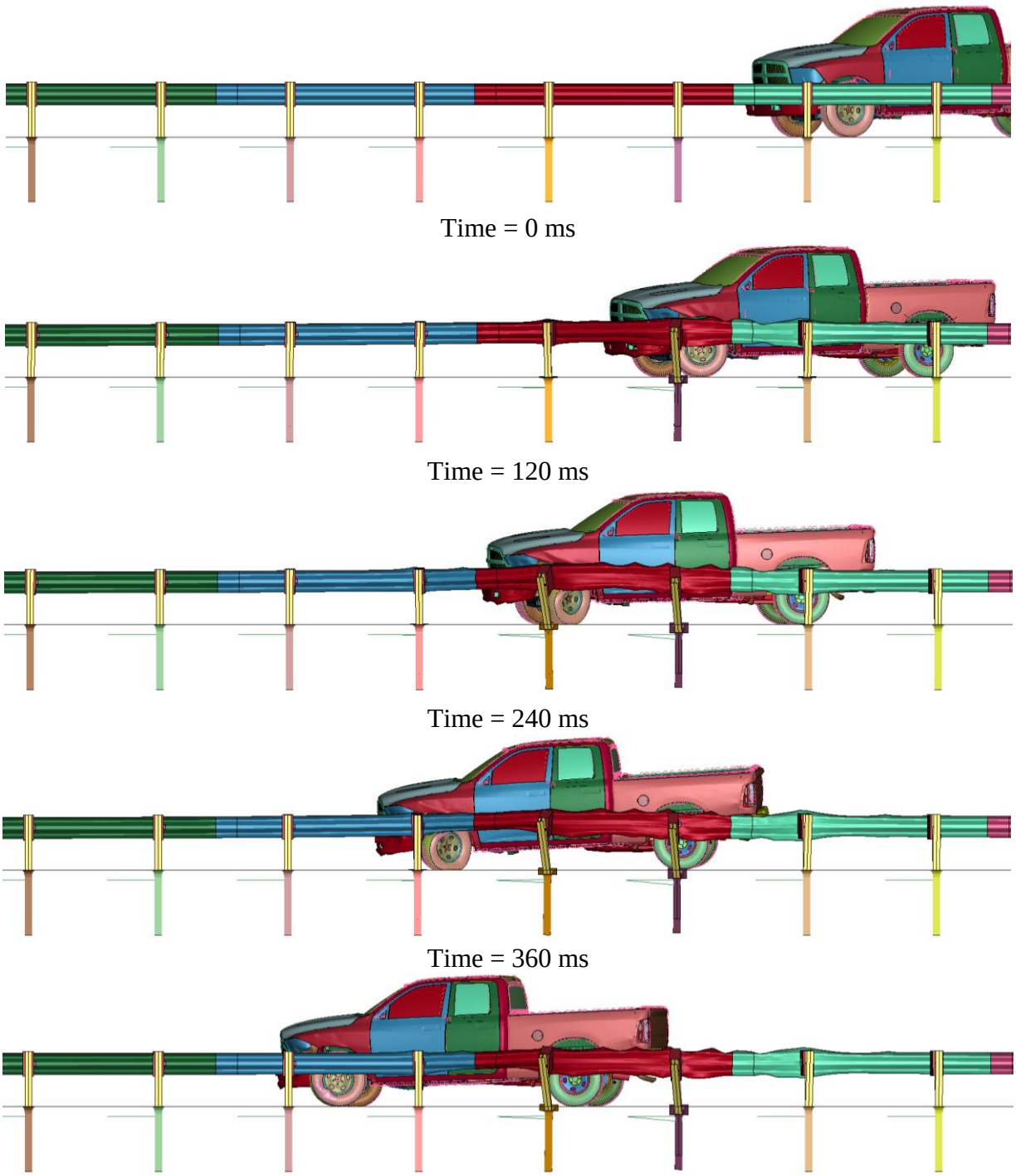

Figure 96. Sequential Images, MGS with Shallow Post Embedment of 28 in., Full-Post Spacing, and Upper-Bound Soil at TL-2 Impact Conditions

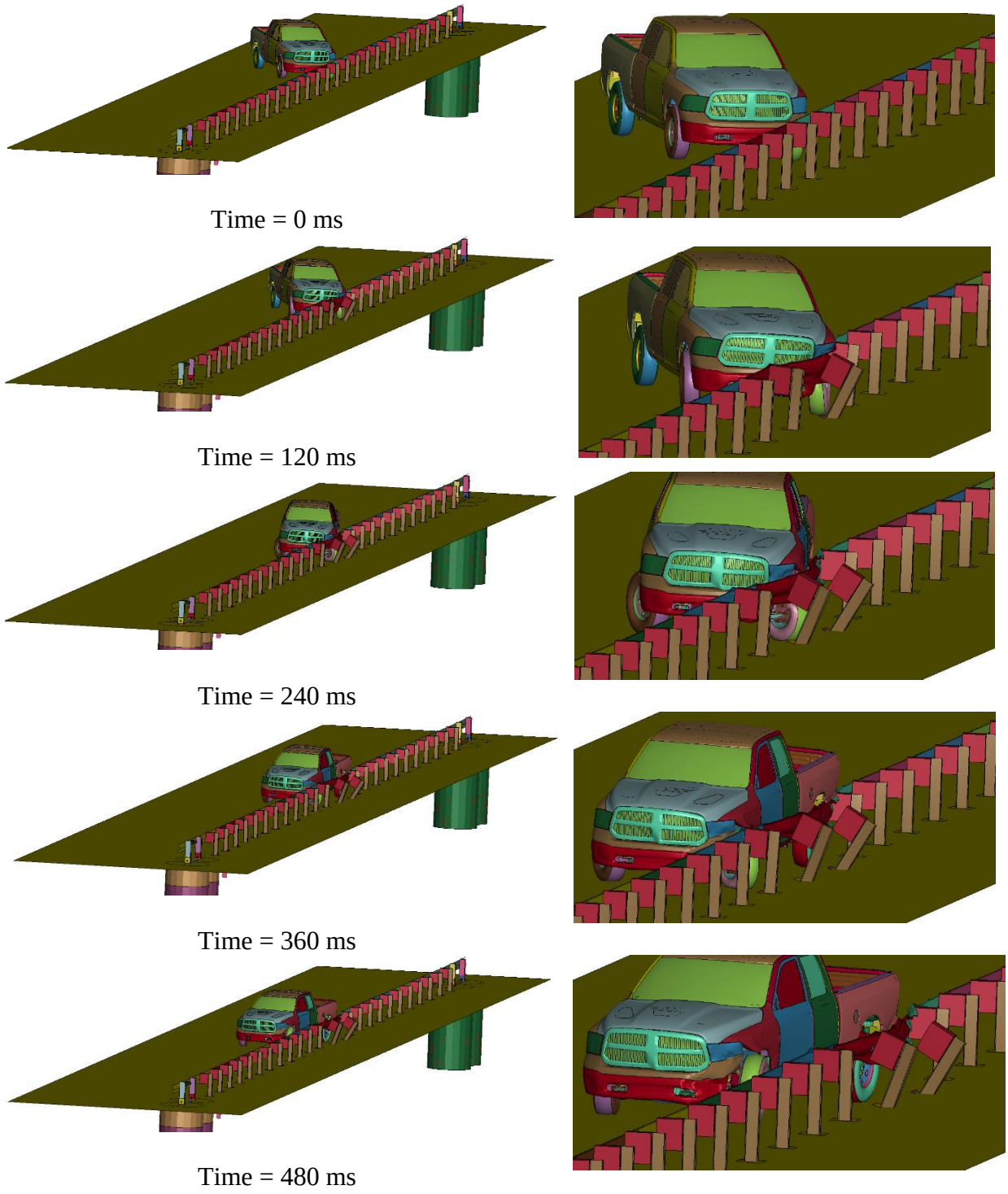

Figure 97. Sequential Images, MGS with Shallow Post Embedment of 28 in., Full-Post Spacing, and Upper-Bound Soil at TL-2 Impact Conditions (Isometric View)

A summary of TL-2 simulation results, including dynamic deflection and working width, for the MGS with shallow embedment, standard post-spacing, and upper-bound soil is shown in Table 16. The Euler angles and occupant risk values were well within the limit set in MASH.

Table 16. TL-2 Simulation of MGS with Shallow Post Embedment of 28 in., Full-Post Spacing, and Upper-Bound Soil

Evaluation Criteria		Shallow Embedment: 28 in.	MASH 2016 Limits
OIV ft/s (m/s)	Longitudinal	-14.42 (-4.40)	±40 (12.2)
	Lateral	-13.70 (-4.18)	±40 (12.2)
ORA g's	Longitudinal	-4.64	±20.49
	Lateral	-6.43	±20.49
Maximum Angular Displacement deg.	Roll	-1.89	±75
	Pitch	1.82	±75
	Yaw	-35.26	not required
THIV ft/s (m/s)		N/A	not required
PHD g's		N/A	not required
ASI		N/A	not required
Max. Dynamic Deflection in. (mm)		24.17 (614)	N/A
Working Width in. (mm)		45.82 (1,164)	N/A

6.3.3 MGS with Shallow Post Embedment and Half-Post Spacing

The Dodge Ram model impacted the MGS with shallow post embedment and half-post spacing 13 in. upstream from post no. 19 at a speed of 44 mph and an angle of 25 degrees, as shown in Figure 98. The vehicle was redirected with only minor tire snag on the posts. Four steel posts displaced during the impact, and two steel posts bent and sustained plastic deformation. Overall, the vehicle behavior during redirection was acceptable, and there was no indication of potential vehicle instabilities. Sequential photographs of the simulations are shown in Figures 99 through 101.

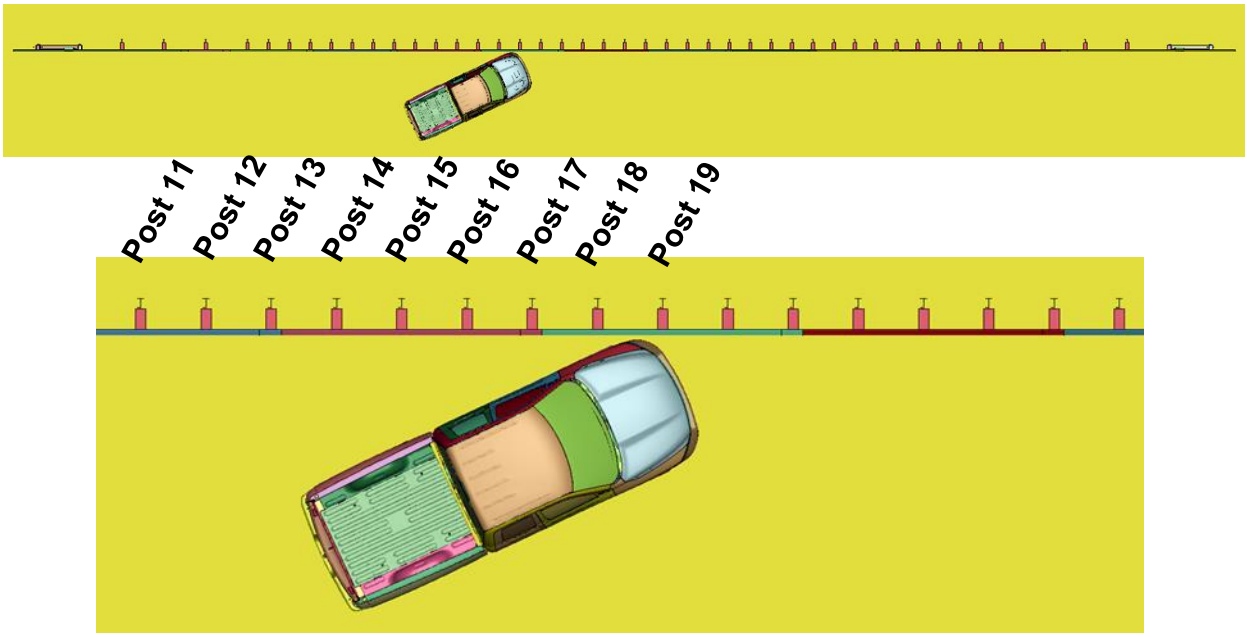

Figure 98. Dodge Ram Vehicle Model Impacting MGS with Shallow Post Embedment, Half-Post Spacing, and Upper-Bound Soil Strength

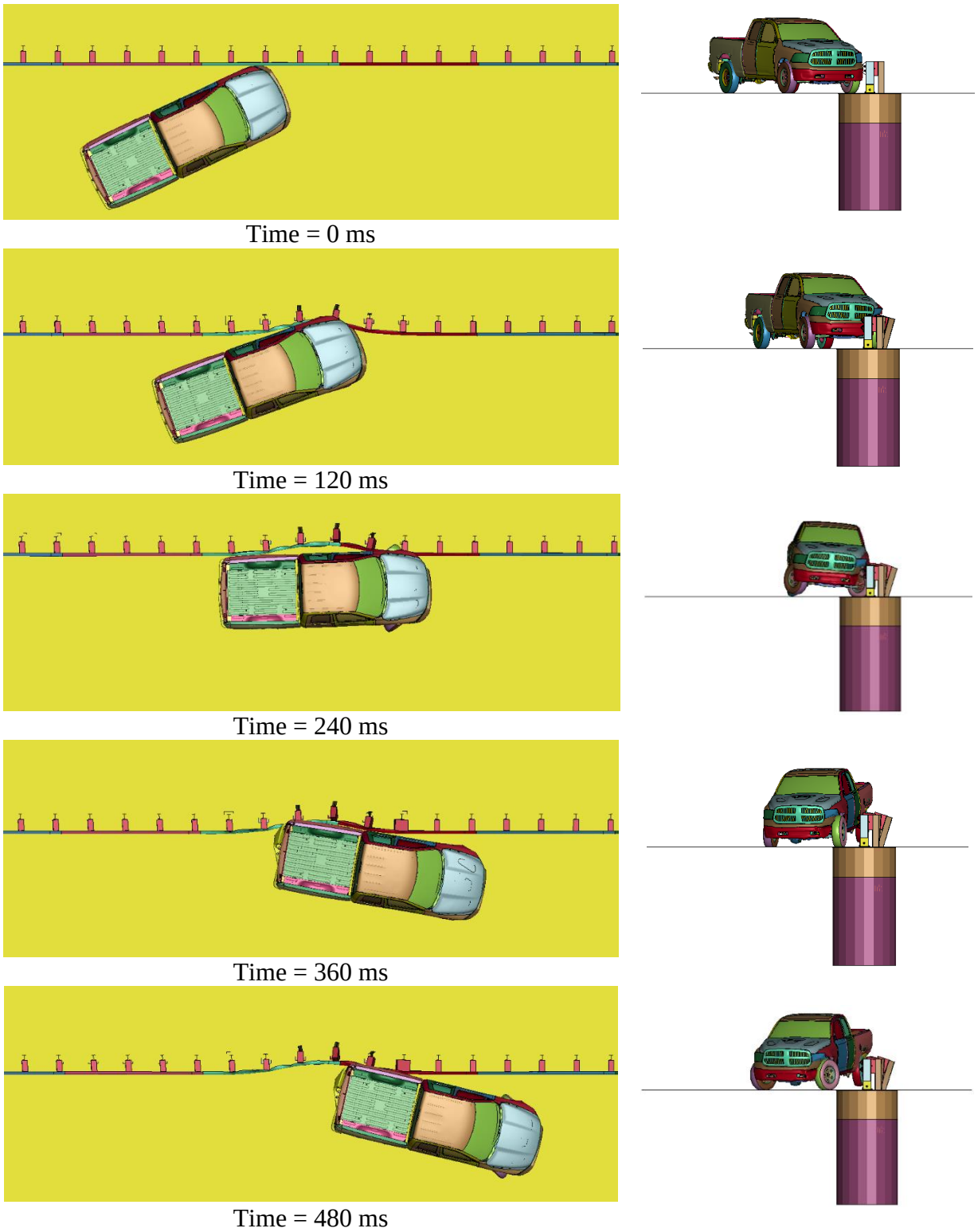

Figure 99. Sequential Images, MGS with Shallow Post Embedment of 28 in., Half-Post Spacing, and Upper-Bound Soil at TL-2 Impact Conditions

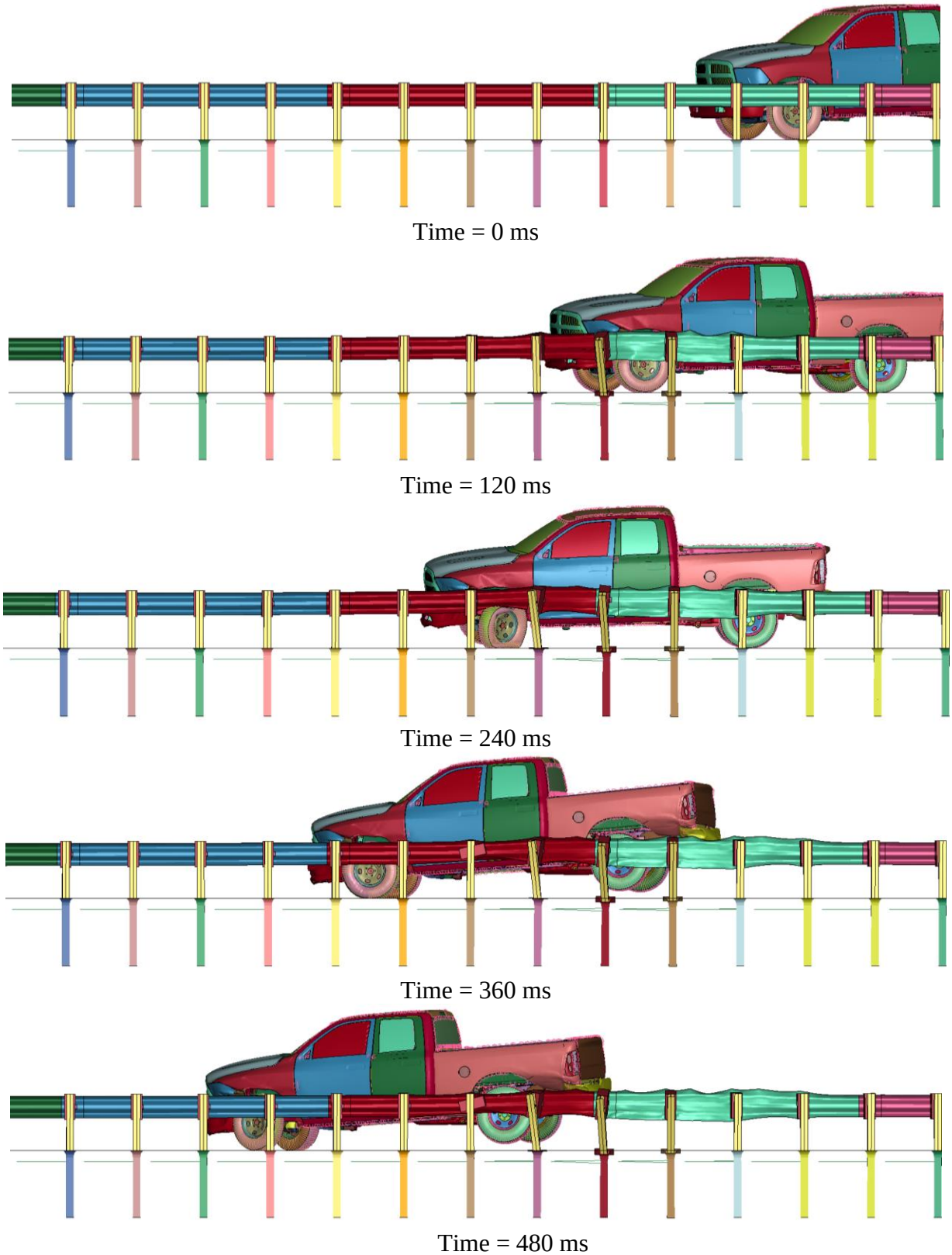

Figure 100. Sequential Images, MGS with Shallow Post Embedment of 28 in., Half-Post Spacing, and Upper-Bound Soil at TL-2 Impact Conditions

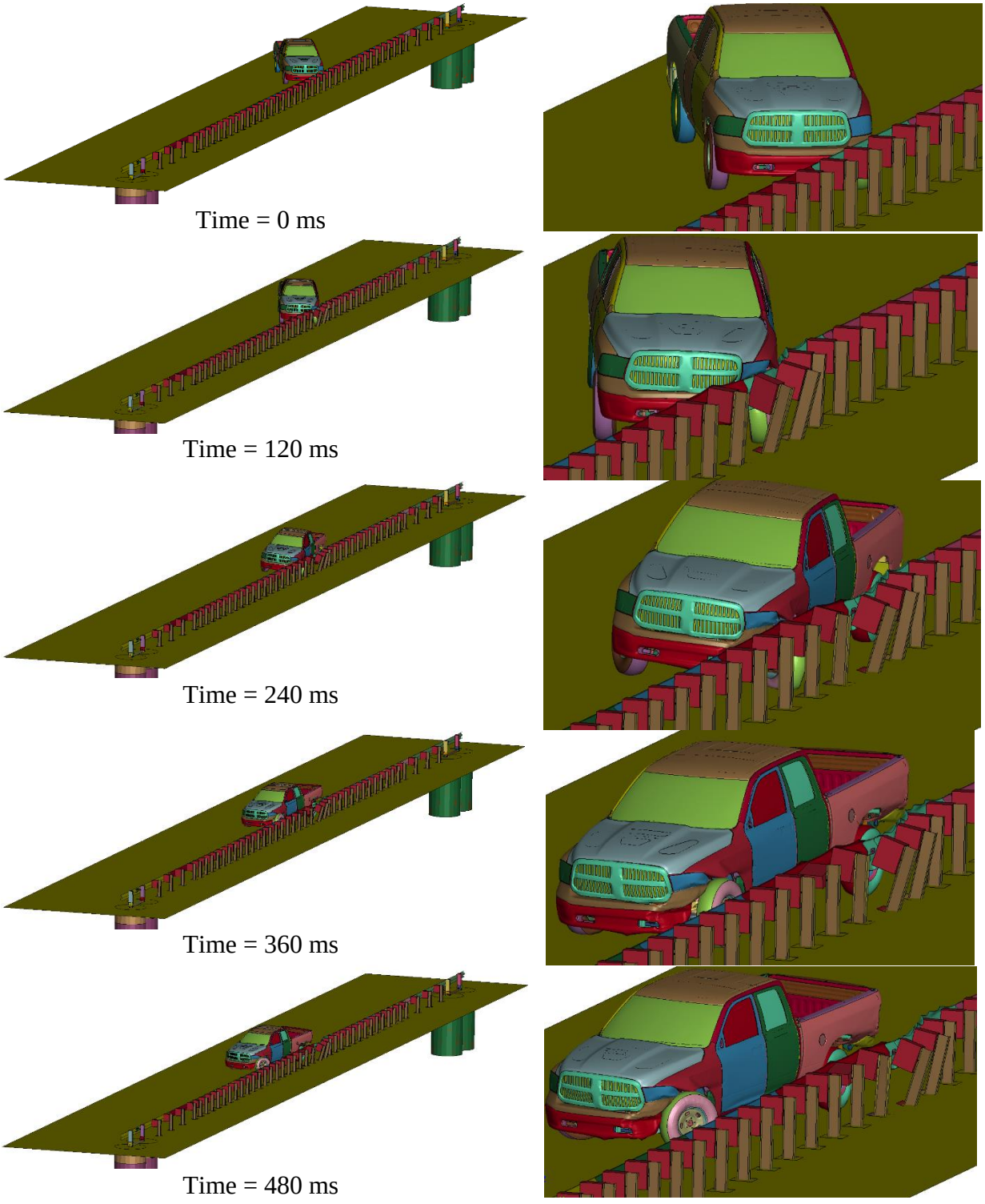

Figure 101. Sequential Images, MGS with Shallow Post Embedment of 28 in., Half-Post Spacing, and Upper-Bound Soil at TL-2 Impact Conditions

A summary of TL-2 simulation results, including dynamic deflection and working width, for the MGS with shallow embedment, half-post spacing, and upper-bound soil is shown in Table 17. The Euler angles and occupant risk values were well within the limit set in MASH.

Table 17. TL-2 Simulation of MGS with Shallow Post Embedment of 28 in., Half-Post Spacing, and Upper-Bound Soil

Evaluation Criteria		Shallow Embedment of 28 in.	MASH 2016 Limits
OIV ft/s (m/s)	Longitudinal	-15.29 (4.66)	±40 (12.20)
	Lateral	-16.31 (-4.97)	±40 (12.20)
ORA g's	Longitudinal	-4.74	±20.49
	Lateral	-4.55	±20.49
Maximum Angular Displacement deg.	Roll	-4.49	±75
	Pitch	1.50	±75
	Yaw	-38.80	not required
THIV ft/s (m/s)		N/A	not required
PHD g's		N/A	not required
ASI		N/A	not required
Max. Dynamic Deflection in. (mm)		15.20 (386)	N/A
Working Width in. (mm)		37.32 (948)	N/A

6.3.4 MGS with Shallow Post Embedment and Quarter-Post Spacing

The Dodge Ram model impacted the MGS with shallow post embedment and quarter-post spacing 3 in. downstream from post no. 32 at a speed of 44 mph and an angle of 25 degrees, as shown in Figure 102. The vehicle was redirected out of the system with only minor tire snag on the posts. Four steel posts displaced without noticeable plastic deformation during the impact event. Overall, the vehicle behavior during redirection was acceptable, and there was no indication of potential vehicle instabilities. Sequential photographs of the simulation are shown in Figures 103 through 105.

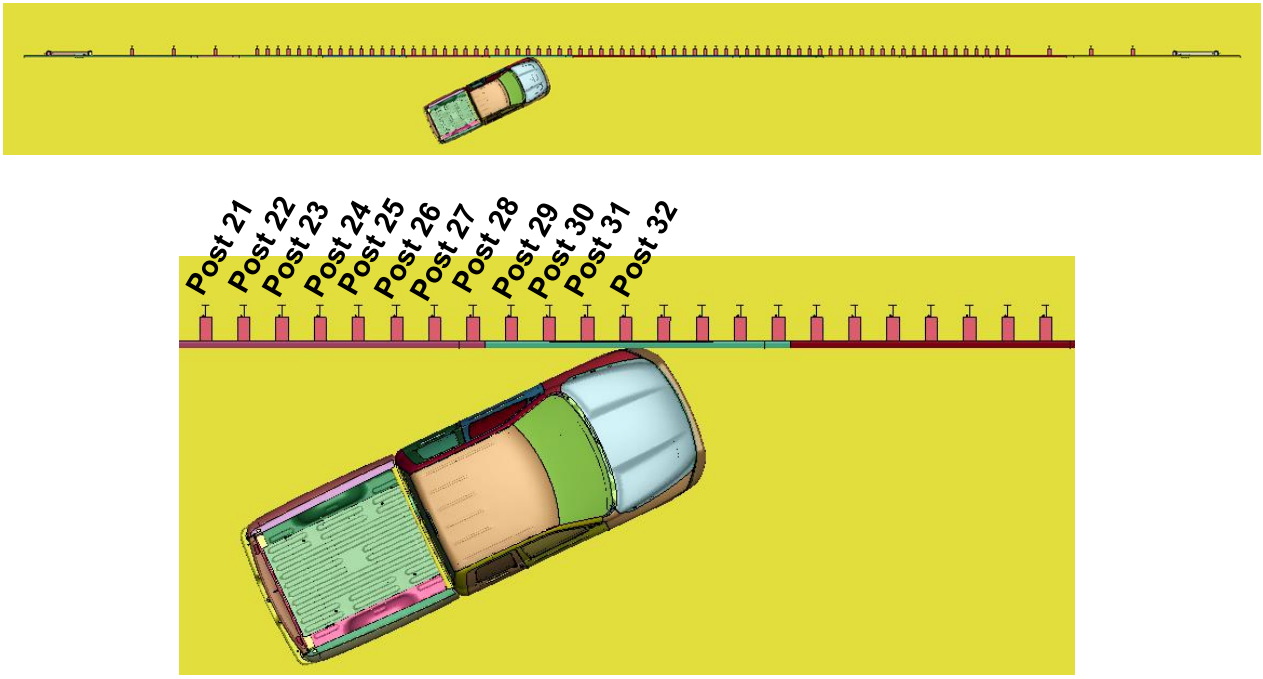

Figure 102. Dodge Ram Vehicle Model Impacting MGS with Shallow Post Embedment, Quarter-Post Spacing, and Upper-Bound Soil

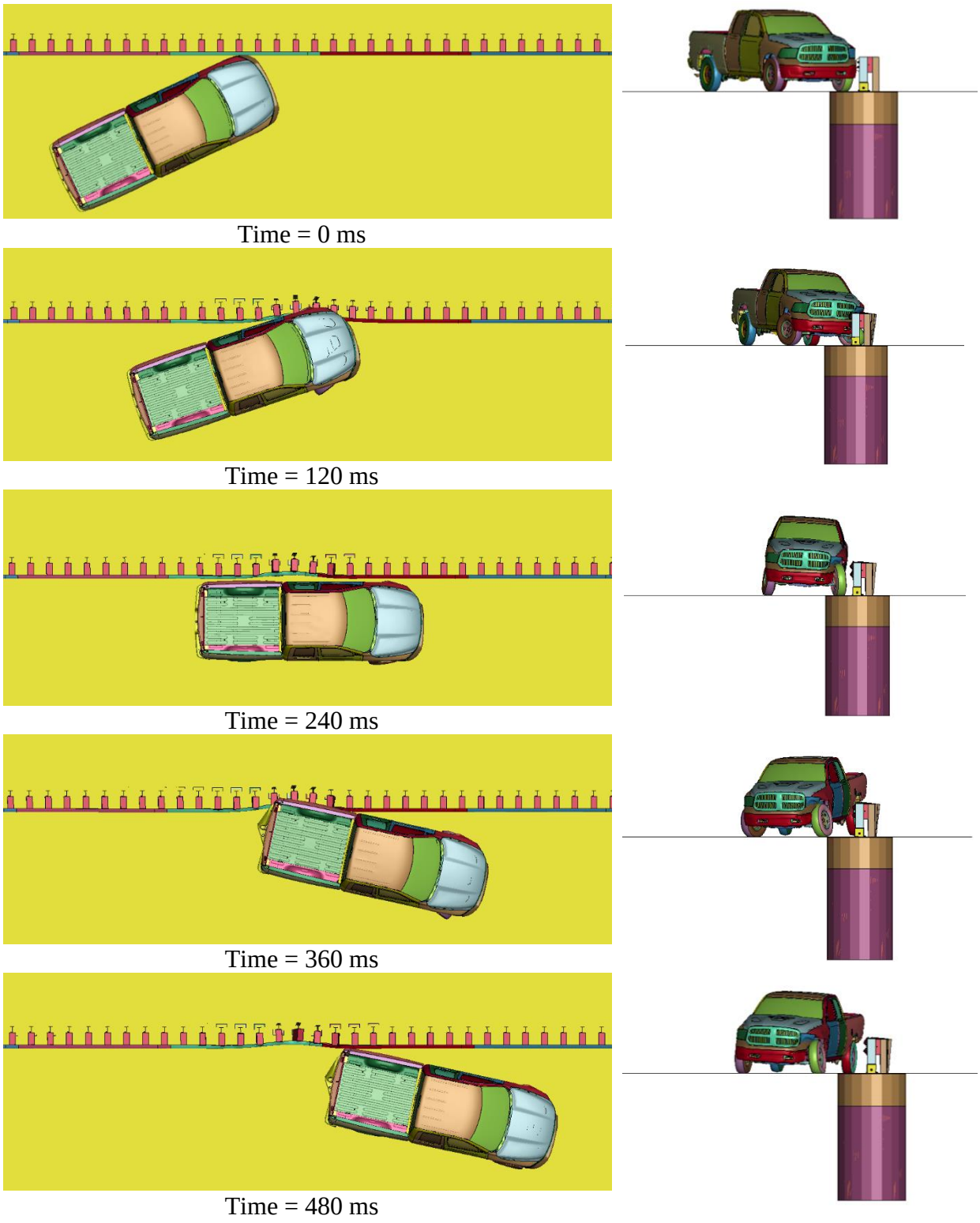

Figure 103. Sequential Images, Shallow Post Embedment of 28 in., Quarter-Post Spacing, and Upper-Bound Soil at TL-2 Impact Conditions

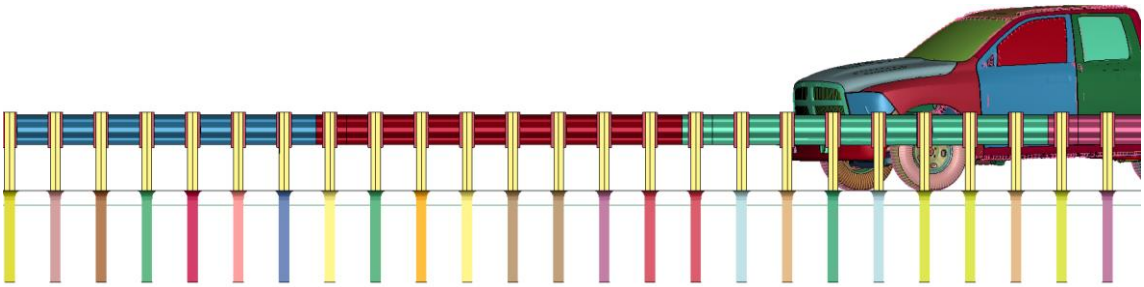

Time = 0 ms

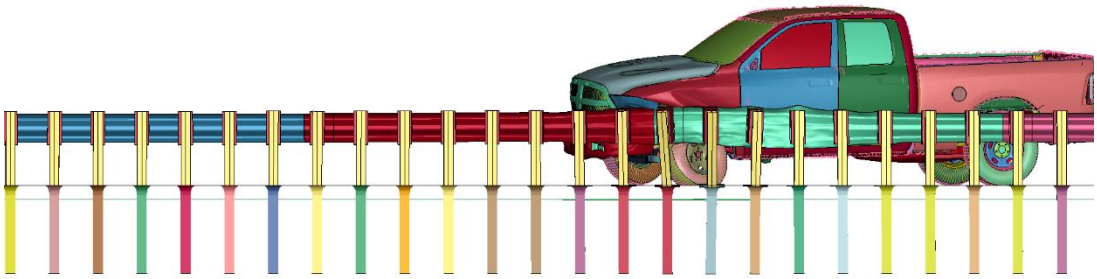

Time = 120 ms

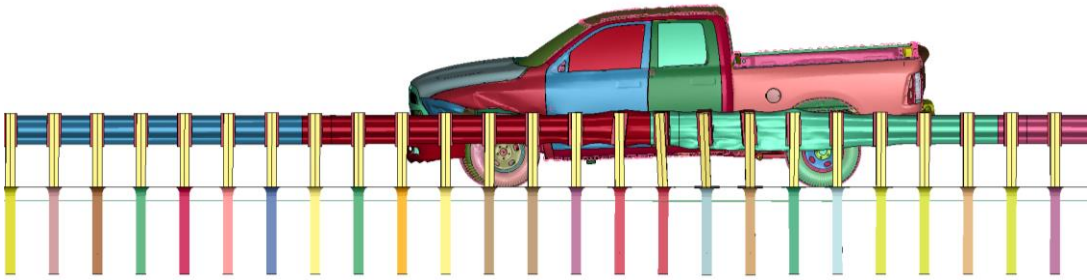

Time = 240 ms

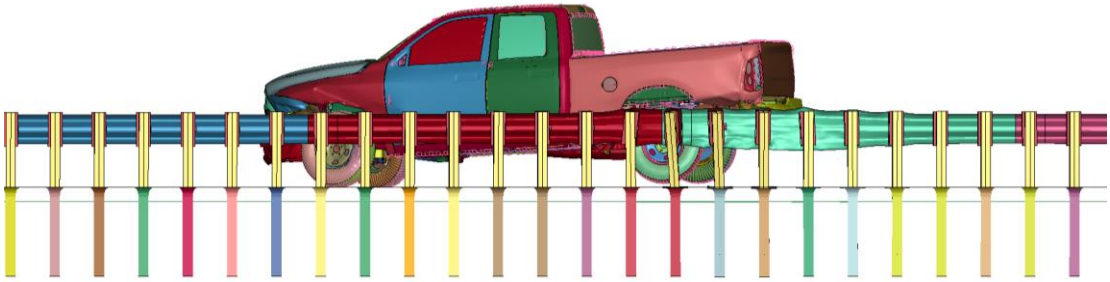

Time = 360 ms

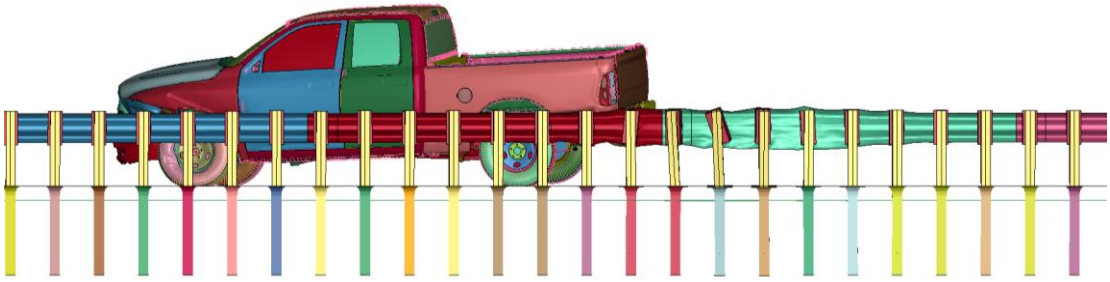

Time = 480 ms

Figure 104. Sequential Images, Shallow Post Embedment of 28 in., Quarter-Post Spacing, and Upper-Bound Soil at TL-2 Impact Conditions

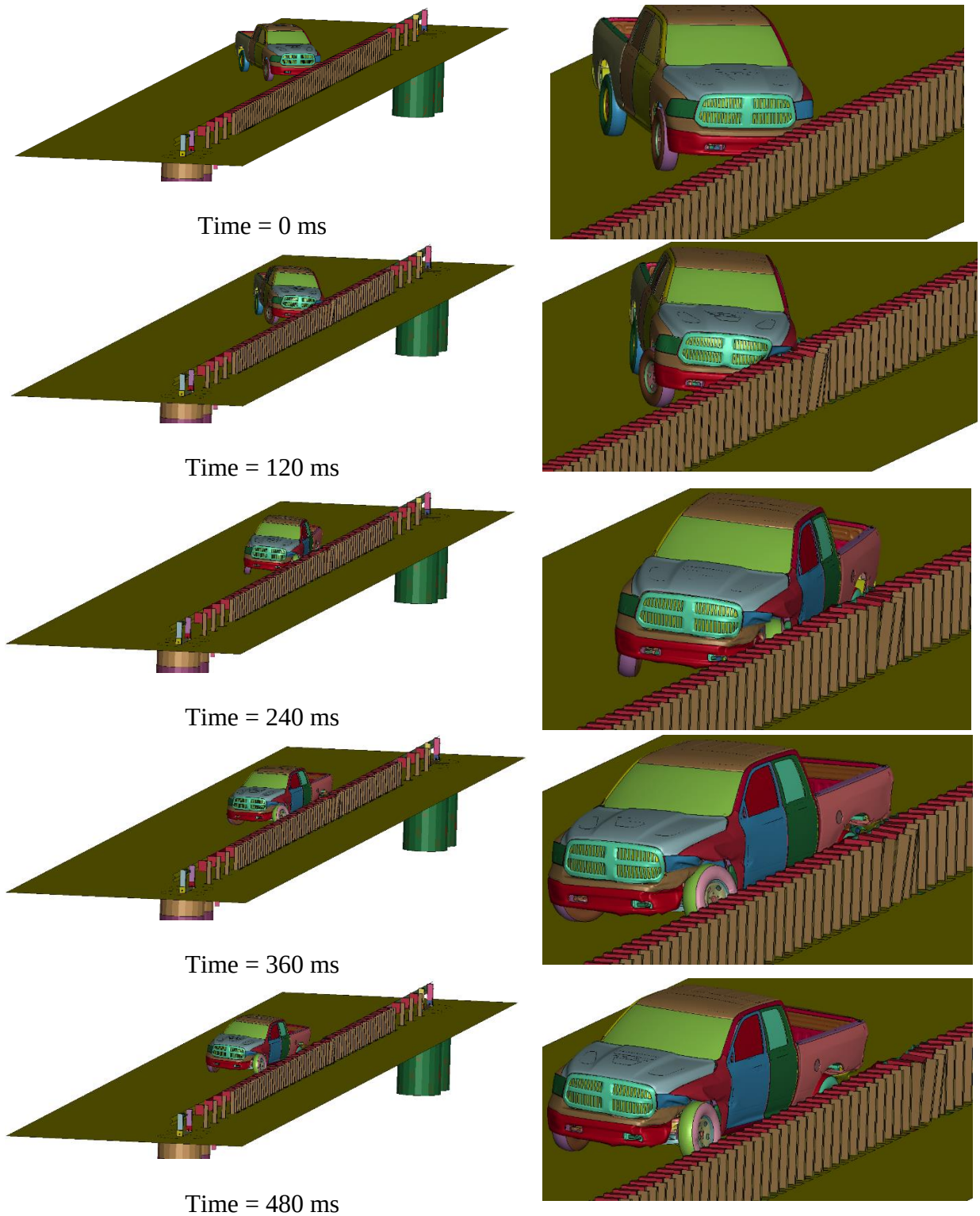

Figure 105. Sequential Images, Shallow Post Embedment of 28 in., Quarter-Post Spacing, and Upper-Bound Soil at TL-2 Impact Conditions (Isometric View)

A summary of TL-2 simulation results, including dynamic deflection and working width, for the MGS with shallow embedment, quarter-post spacing, and upper-bound soil is shown in Table 18. The Euler angles and occupant risk values were well within the limit set in MASH.

Table 18. TL-2 Simulation of MGS with Shallow Post Embedment of 28 in., Quarter-Post Spacing, and with Upper-Bound Soil

Evaluation Criteria		Shallow Embedment of 28 in.	MASH 2016 Limits
OIV ft/s (m/s)	Longitudinal	-17.29 (-5.27)	±40 (12.20)
	Lateral	-18.01 (5.49)	±40 (12.20)
ORA g's	Longitudinal	-4.42	±20.49
	Lateral	-5.43	±20.49
Maximum Angular Displacement deg.	Roll	-5.21	±75
	Pitch	1.84	±75
	Yaw	-38.06	not required
THIV ft/s (m/s)		N/A	not required
PHD g's		N/A	not required
ASI		N/A	not required
Max. Dynamic Deflection in. (mm)		7.44 (189)	N/A
Working Width in. (mm)		28.81 (732)	N/A

6.3.5 Discussion

The simulated dynamic deflections and working widths for the MGS with reduced post embedment and reduced post spacing with upper-bound soil at TL-2 impact conditions are summarized in Table 19. The MGS with shallow post embedment and full-post spacing exhibited the highest dynamic deflection of 24.17 in., while the shallow post embedment and quarter post-spacing MGS exhibited the lowest dynamic deflection. The working width of the shallow post embedment and half-post spacing MGS were comparable with the standard post embedment and full-post spacing MGS (i.e., baseline MGS model).

The MGS with shallower post embedment and full-post spacing deflected similarly to the MGS with standard post embedment and full-post spacing in upper-bound soil at TL-2 impact conditions, although deformation and yielding of posts had some differences in the simulation. In the MGS simulation with a standard embedment and full post spacing, three posts sustained severe plastic deformation and twisting, while two posts sustained plastic deformation with minor twisting in the MGS with shallow embedment and full-post spacing, as shown in Figure 106.

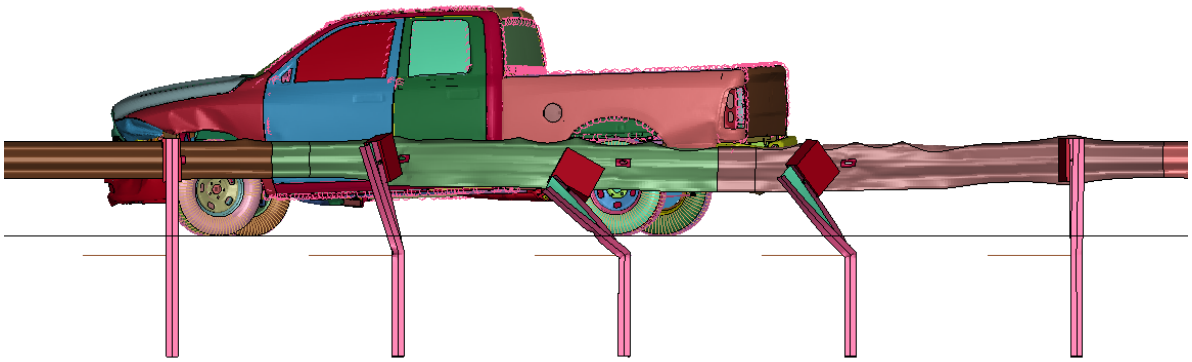

(a) Standard Post Embedment and Full-Post Spacing MGS (Time = 480 ms)

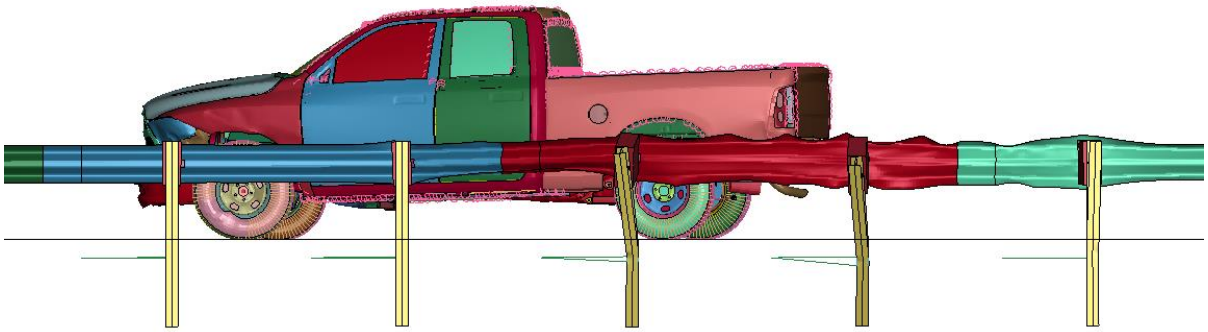

(b) Shallow Post Embedment (28 in.) and Full-Post Spacing MGS (Time = 480 ms)

Figure 106. Behavior of Steel Posts: (a) MGS with Standard Post Embedment and Full-Post Spacing, and (b) MGS with Shallow Post Embedment and Full-Post Spacing at TL-2 Impact Conditions

The maximum dynamic deflection for the baseline MGS model with upper-bound soil strength was 25 in. The post-soil forces for upper-bound soil strength represented load and deflection characteristics of posts embedded in stiffer and stronger soils. The MGS with shallower post embedment, quarter-post spacing, and upper-bound soil exhibited a dynamic deflection of 7.44 in. There was a significant difference between the highest and lowest maximum dynamic deflections due to the system dependency on post spacing (system stiffness) and post embedment depth (i.e., 28 in. vs. 40 in.).

Table 19. MASH TL-2 Simulation Results for MGS with Upper-Bound Soil

Evaluation Criteria	Standard Post Embedment & Full-Post Spacing	Shallow Post Embedment			MASH 2016 Limits
		Full-Post Spacing	Half-Post Spacing	Quarter-Post Spacing	
Max. Dynamic Deflection in. (mm)	25.00 (635)	24.17 (614)	15.20 (386)	7.44 (189)	N/A
Working Width in. (mm)	36.14 (918)	45.82 (1,164)	37.32 (948)	28.81 (732)	N/A

6.4 MASH TL-3 Simulations with Lower-Bound Soil Strength

The MGS with lower-bound soil strength was analyzed at TL-3 impact conditions (speed of 62 mph and angle of 25 degrees) using the impact points determined per MASH 2016 [1]. A total of four cases were investigated, with two embedment depths (i.e., standard embedment of 40 in. and shallow embedment of 28 in.) and three post spacings (i.e., full-, half-, and quarter-post spacing).

6.4.1 MGS with Standard Post Embedment and Full-Post Spacing

The Dodge Ram model impacted the standard post embedment and full-post spacing MGS 4 in. upstream from post no. 12 at a speed of 62 mph and an angle of 25 degrees, as shown in Figure 107. The vehicle was redirected with only minor tire snag on the posts. Five steel posts displaced during the impact, and three steel posts bent and sustained plastic deformation. Overall, the vehicle behavior during redirection was acceptable, and there was no indication of potential vehicle instabilities. Sequential photographs of the simulations are shown in Figures 108 through 110.

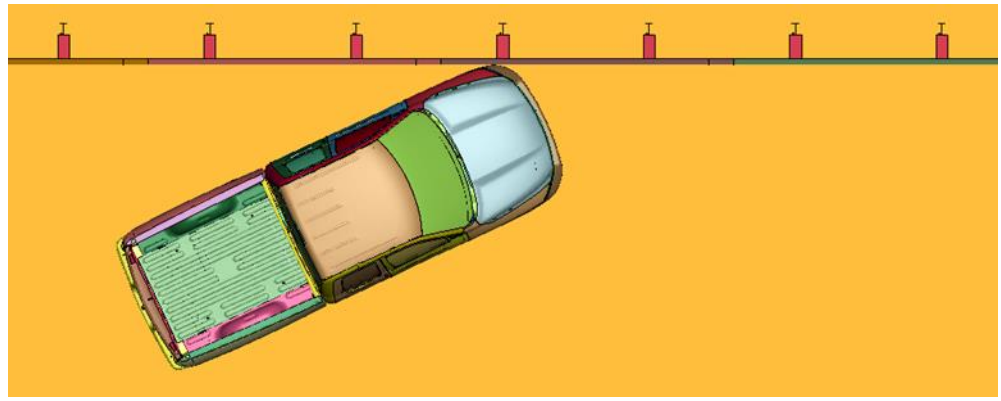

Figure 107. Dodge Ram Vehicle Model Impacting MGS with Standard Post Embedment, Full-Post Spacing, and Lower-Bound Soil Strength at TL-3 Impact Conditions

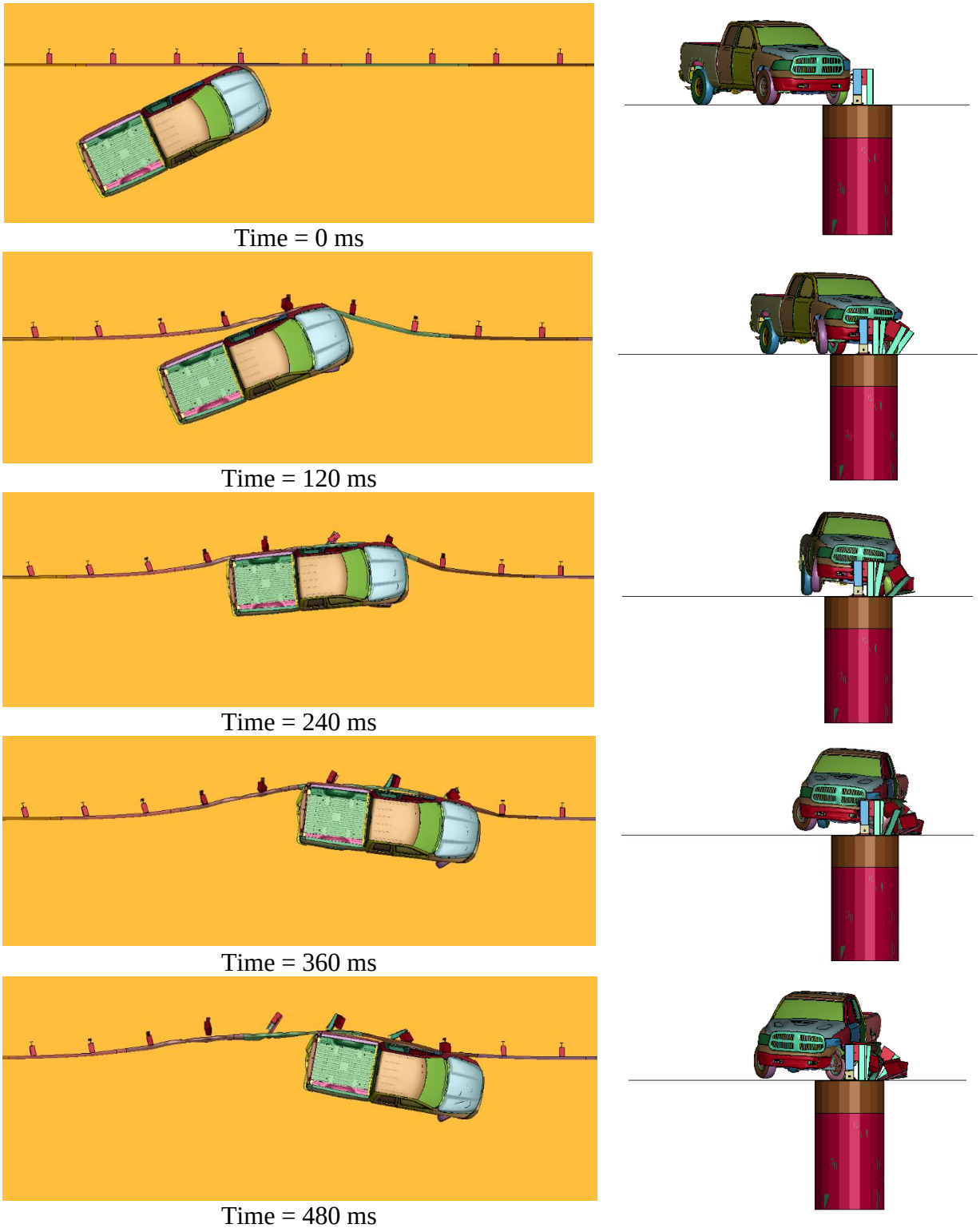

Figure 108. Sequential Images, MGS with Standard Post Embedment of 40 in., Full-Post Spacing, and Lower-Bound Soil Strength at TL-3 Impact Conditions

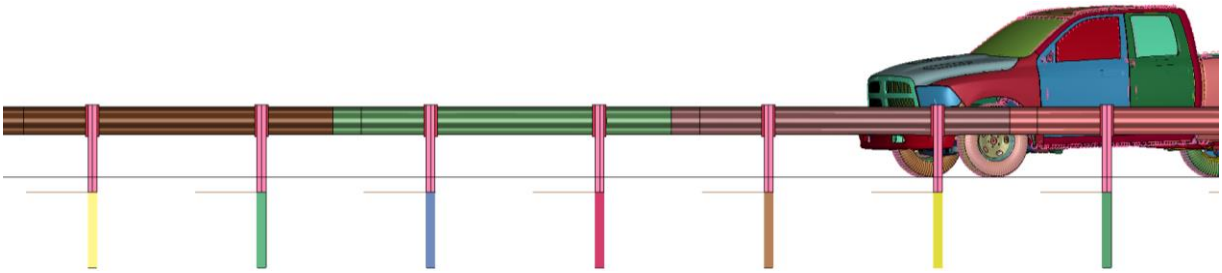

Time = 0 ms

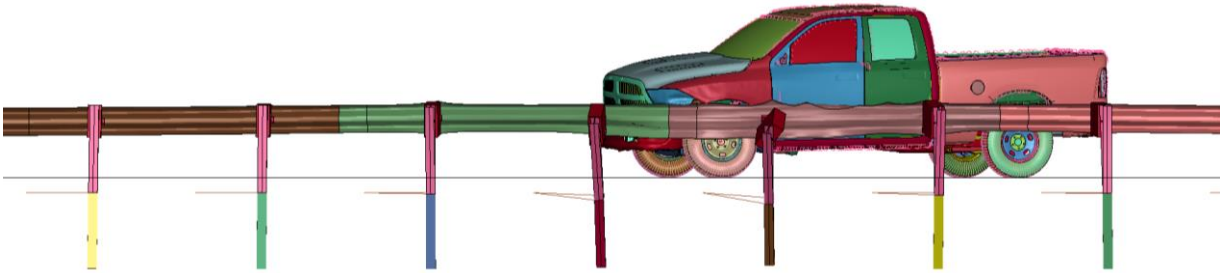

Time = 120 ms

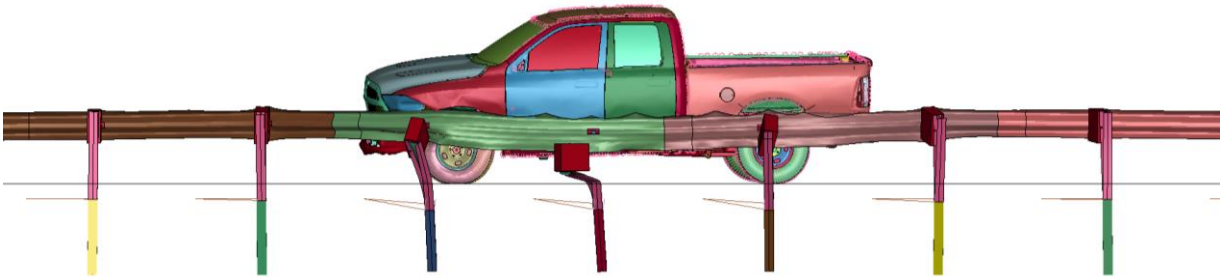

Time = 240 ms

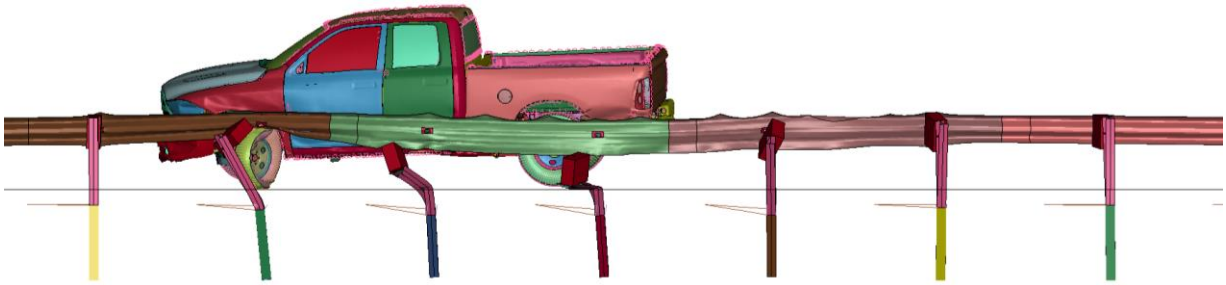

Time = 360 ms

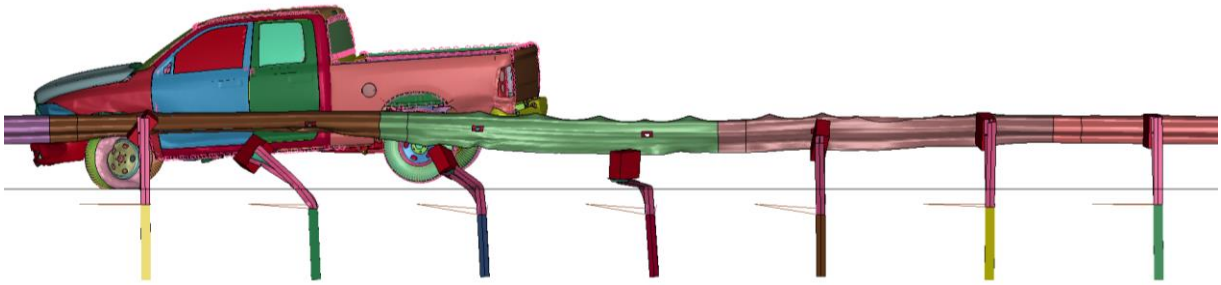

Time = 480 ms

Figure 109. Sequential Images, MGS with Standard Post Embedment of 40 in., Full-Post Spacing, and Lower-Bound Soil Strength at TL-3 Impact Conditions

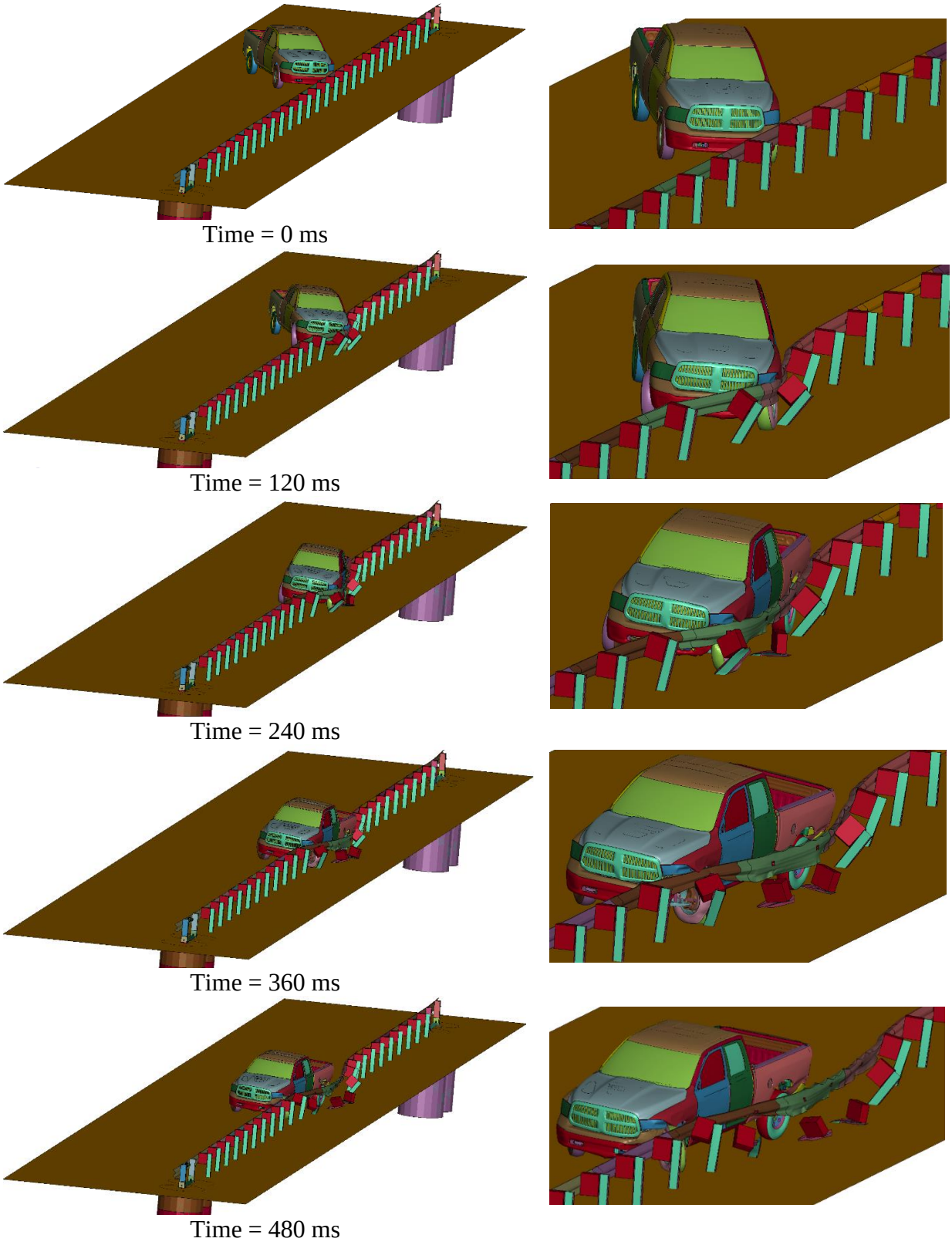

Figure 110. Sequential Images, MGS with Standard Post Embedment of 40 in., Full-Post Spacing, and Lower-Bound Soil Strength at TL-3 Impact Conditions

A summary of TL-3 simulation results, including dynamic deflection and working width, for the MGS with standard post embedment, standard post spacing, and lower-bound soil strength is shown in Table 20. The Euler angles and occupant risk values were well within the limit set in MASH.

Table 20. TL-3 Simulation of MGS with Standard Post Embedment of 40 in., Full-Post Spacing, and Lower-Bound Soil Strength

Evaluation Criteria		Standard Embedment of 40 in.	MASH 2016 Limits
OIV ft/s (m/s)	Longitudinal	-16.01 (-4.88)	±40 (12.20)
	Lateral	-16.08 (-4.90)	±40 (12.20)
ORA g's	Longitudinal	-8.76	±20.49
	Lateral	-7.51	±20.49
Maximum Angular Displacement deg.	Roll	-5.42	±75
	Pitch	2.43	±75
	Yaw	-35.57	not required
THIV ft/s (m/s)		N/A	not required
PHD g's		N/A	not required
ASI		N/A	not required
Max. Dynamic Deflection in. (mm)		47.33 (1,202)	N/A
Working Width in. (mm)		65.93 (1,675)	N/A

6.4.2 MGS with Shallow Post Embedment and Full-Post Spacing

The Dodge Ram model impacted the MGs with shallow post embedment of 28 in. and full-post spacing 9 in. downstream from post no. 11 at a speed of 62 mph and an angle of 25 degrees, as shown in Figure 111. The vehicle was redirected with minor tire snag on the posts. Seven steel posts displaced during the impact, and three steel posts bent and sustained plastic deformation. Overall, the vehicle behavior during redirection was acceptable, and there was no indication of potential vehicle instabilities. Sequential photographs of the simulations are shown in Figures 112 through 114.

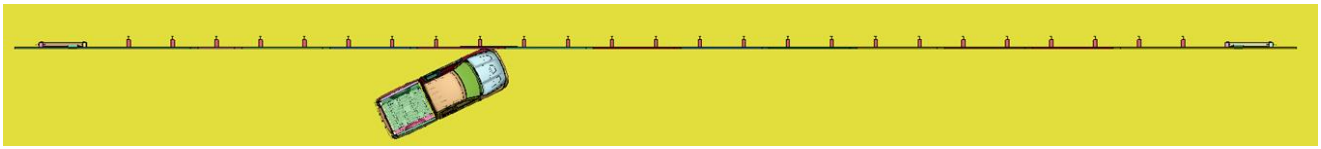

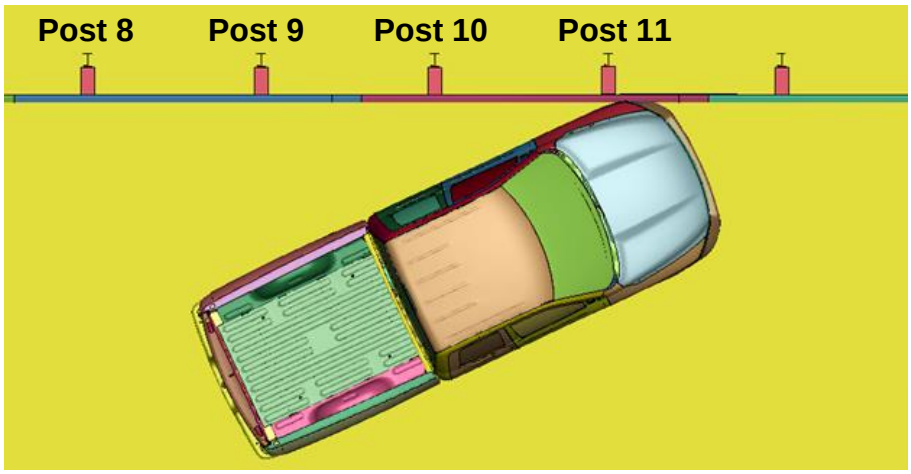

Figure 111. Dodge Ram Vehicle Model Impacting MGS with Shallow Post Embedment, Full-Post Spacing, and Lower-Bound Soil Strength at TL-3 Impact Conditions

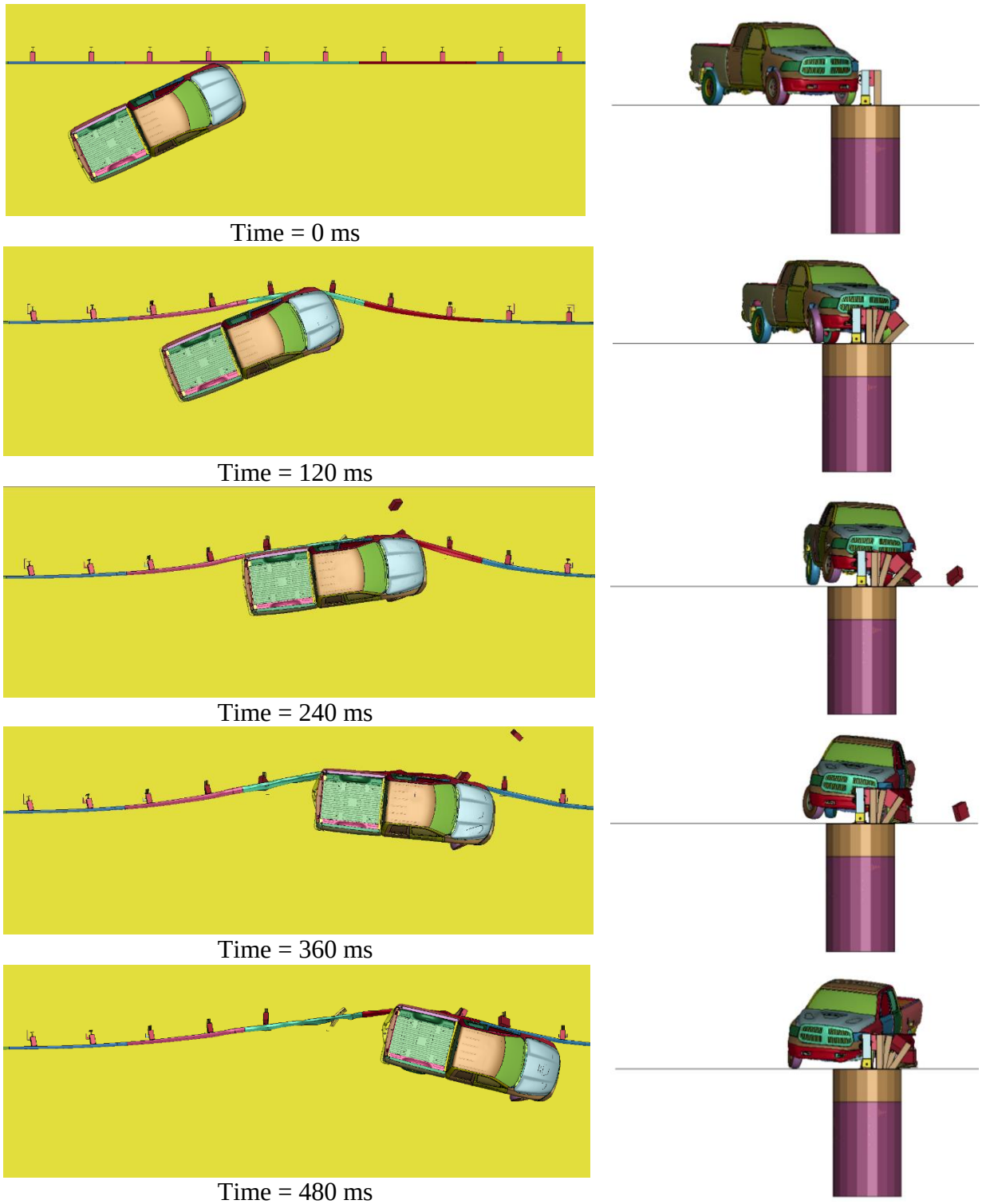

Figure 112. Sequential Images, MGS with Shallow Post Embedment of 28 in., Full-Post Spacing, and Lower-Bound Soil Strength at TL-3 Impact Conditions

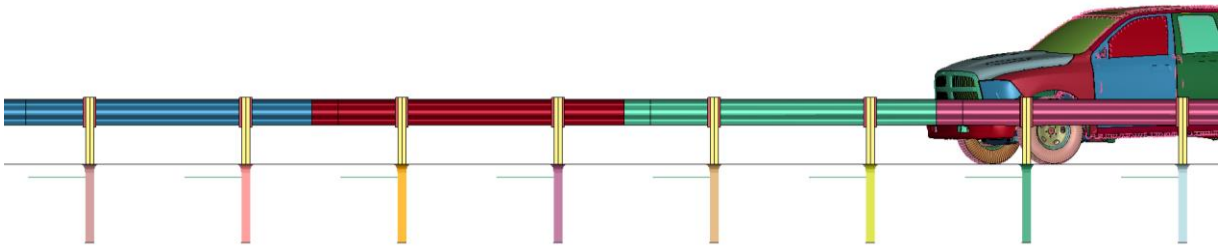

Time = 0 ms

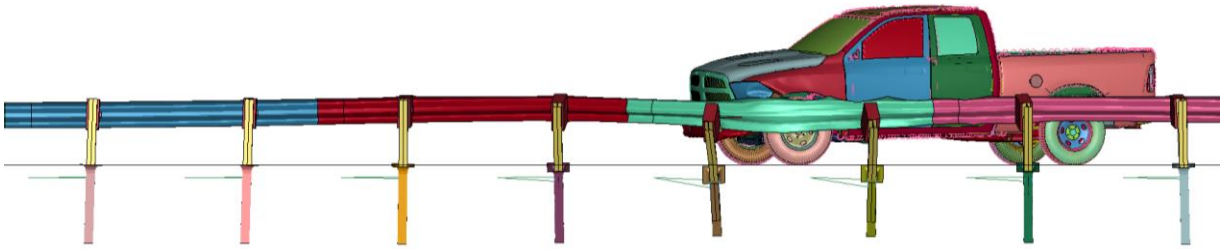

Time = 120 ms

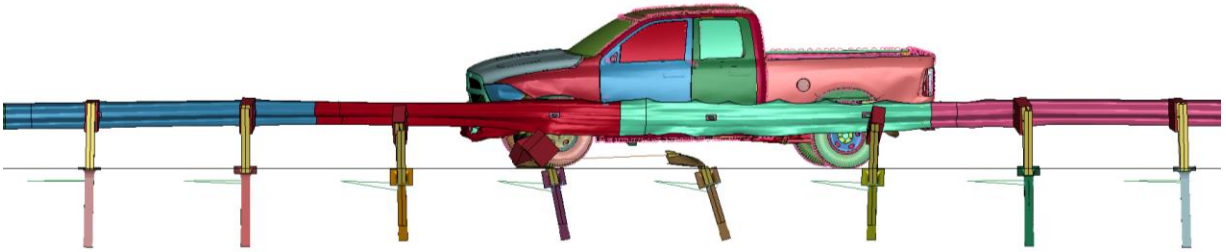

Time = 240 ms

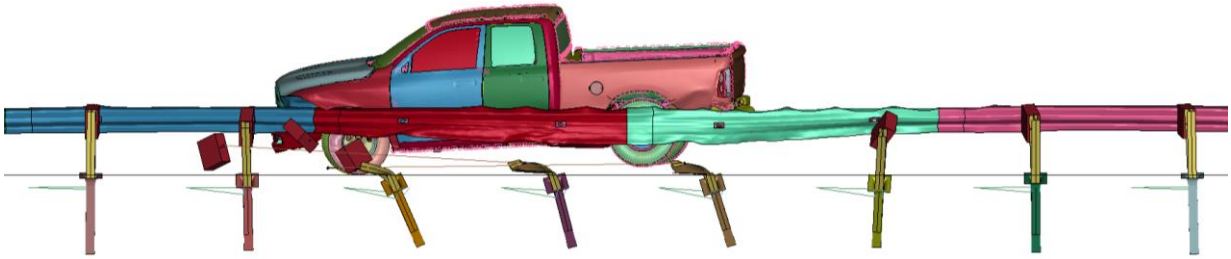

Time = 360 ms

Time = 480 ms

Figure 113. Sequential Images, MGS with Shallow Post Embedment of 28 in., Full-Post Spacing, and Lower-Bound Soil Strength at TL-3 Impact Conditions

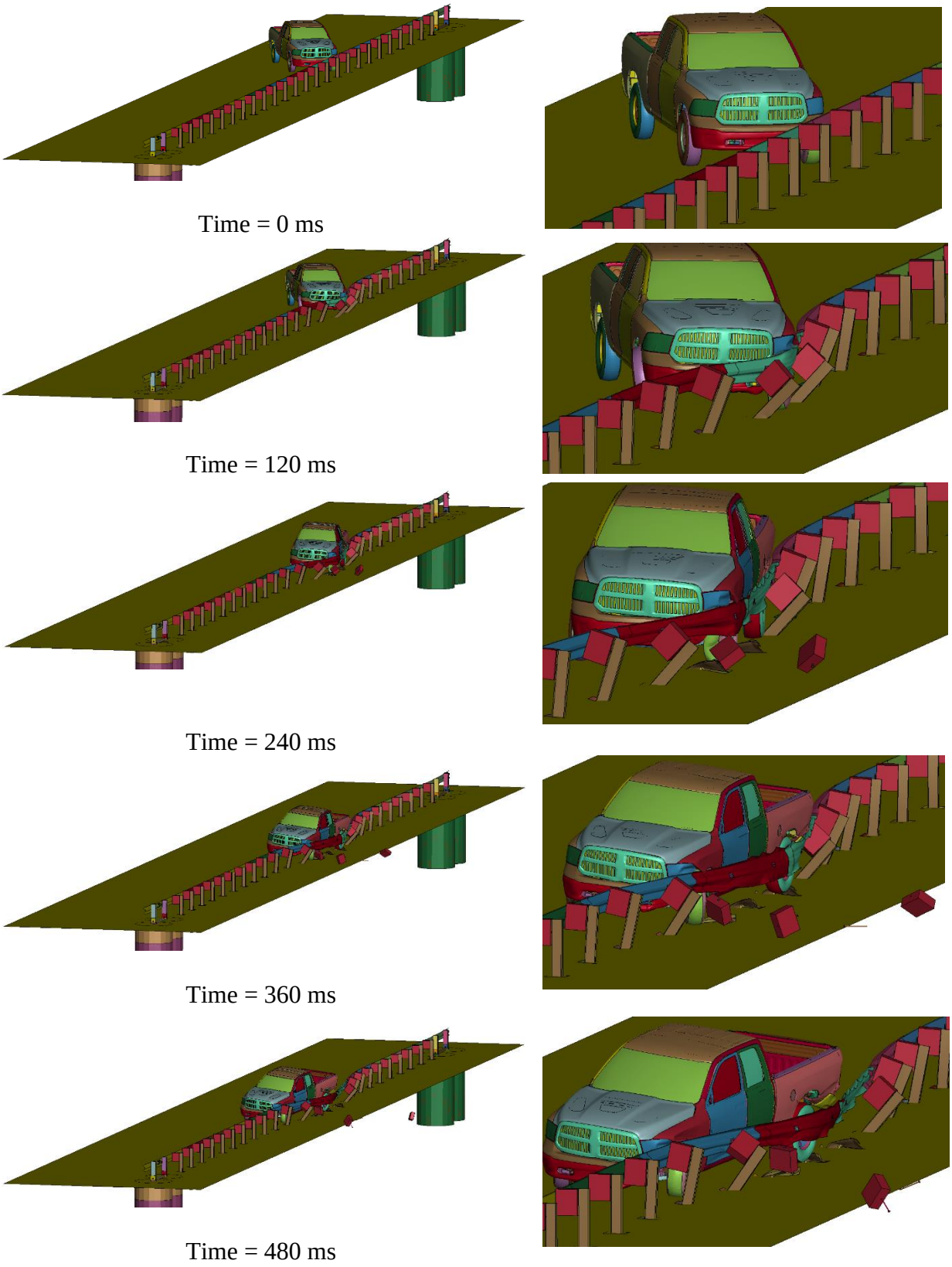

Figure 114. Sequential Images, MGS with Shallow Post Embedment of 28 in., Full-Post Spacing, and Lower-Bound Soil Strength at TL-3 Impact Conditions (Isometric View)

A summary of TL-2 simulation results, including dynamic deflection and working width, for the MGS with shallow embedment, standard post spacing, and lower-bound soil strength is shown in Table 21. The Euler angles and occupant risk values were well within the limit set in MASH.

Table 21. TL-3 Simulation of MGS with Shallow Post Embedment of 28 in., Full-Post Spacing, and Lower-Bound Soil Strength

Evaluation Criteria		Shallow Embedment of 28 in.	MASH 2016 Limits
OIV ft/s (m/s)	Longitudinal	-17.00 (-5.18)	±40 (12.20)
	Lateral	-14.23 (4.34)	±40 (12.20)
ORA g's	Longitudinal	-6.72	±20.49
	Lateral	-8.22	±20.49
Maximum Angular Displacement deg.	Roll	-3.34	±75
	Pitch	2.43	±75
	Yaw	-40.33	not required
THIV ft/s (m/s)		N/A	not required
PHD g's		N/A	not required
ASI		N/A	not required
Max. Dynamic Deflection in. (mm)		53.20 (1,351)	N/A
Working Width in. (mm)		74.30 (1,887)	N/A

6.4.3 MGS with Shallow Post Embedment and Half-Post Spacing

The Dodge Ram model impacted the MGS with shallow post embedment of 28 in. and half-post spacing 6 in. upstream from post no. 17 at a speed of 62 mph and an angle of 25 degrees, as shown in Figure 115. The vehicle was redirected out of the system with only minor tire snag on the posts. Twelve steel posts displaced during the impact, and four steel posts bent and sustained plastic deformation. Overall, the vehicle behavior during redirection was acceptable, and there was no indication of potential vehicle instabilities. Sequential photographs of the simulations are shown in Figures 116 through 118.

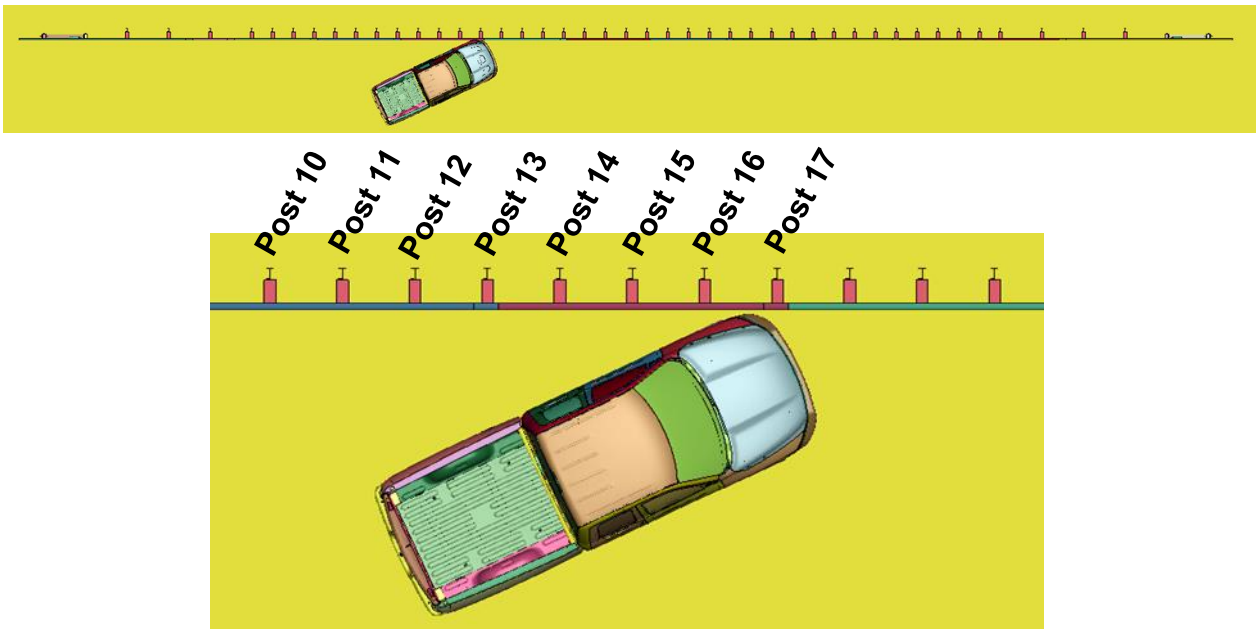

Figure 115. Dodge Ram Vehicle Model Impacting MGS with Shallow Post Embedment, Half-Post Spacing, and Lower-Bound Soil Strength at TL-3 Impact Conditions

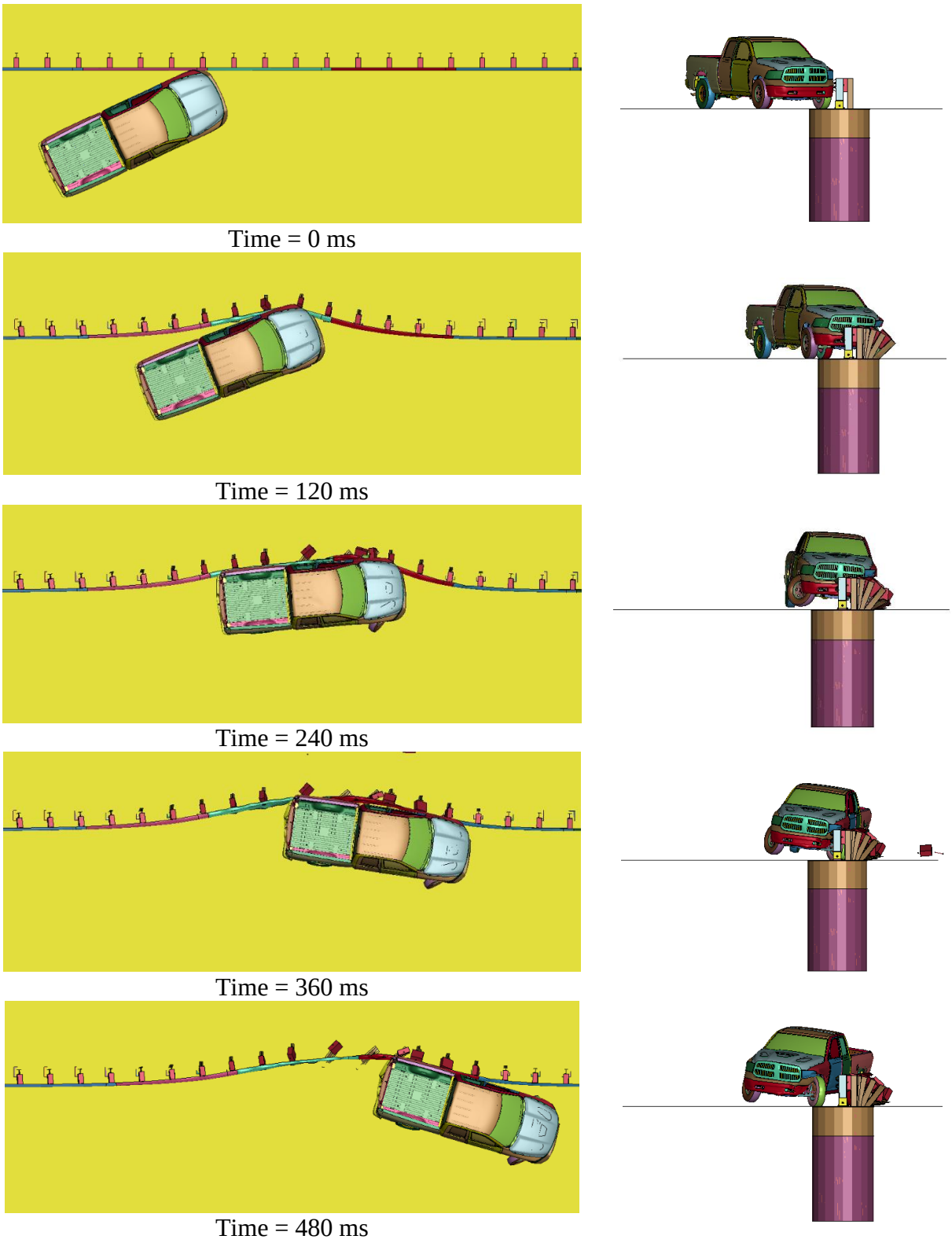

Figure 116. Sequential Images, MGS with Shallow Post Embedment of 28 in., Half-Post Spacing, and Lower-Bound Soil Strength at TL-3 Impact Conditions

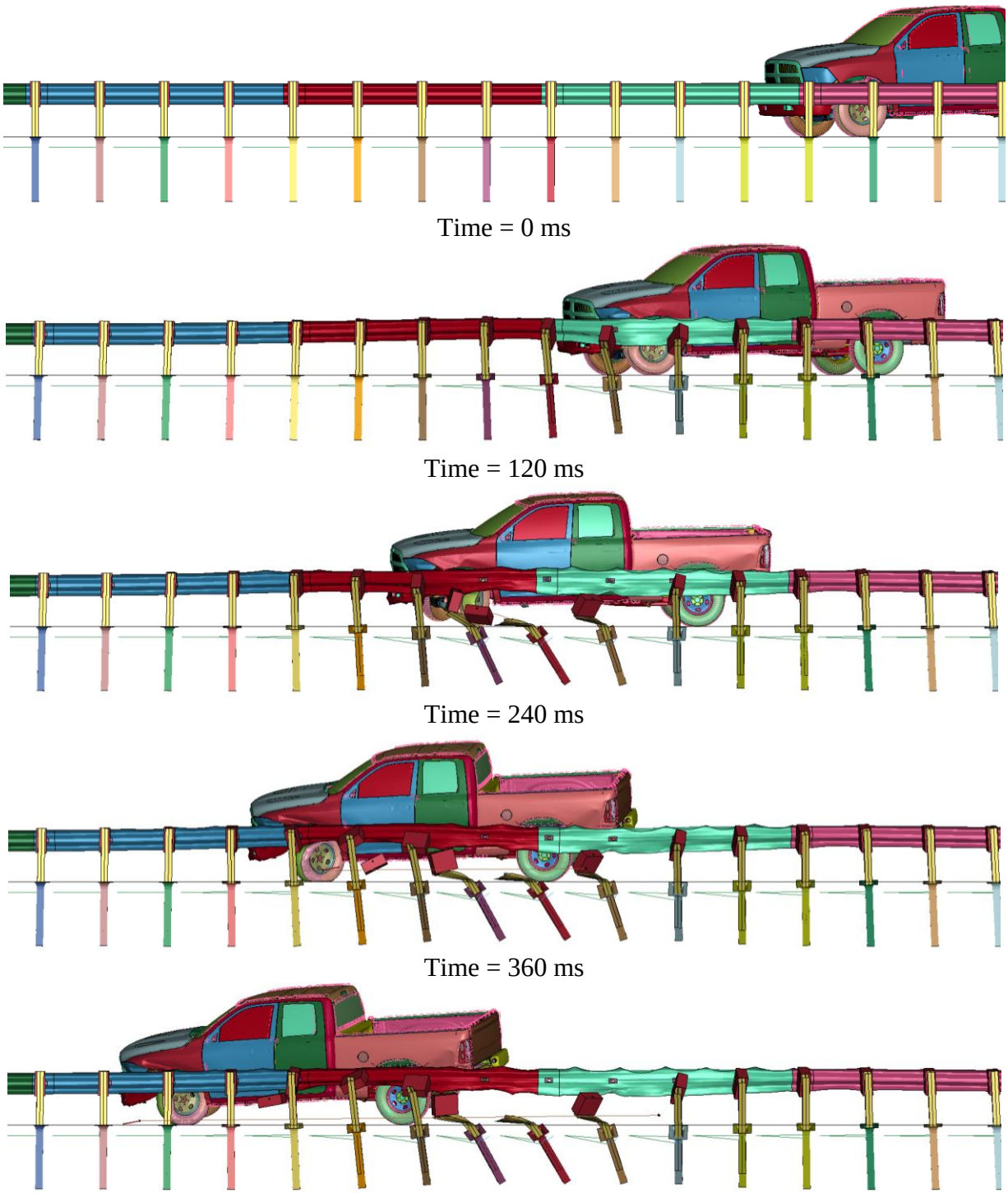

Figure 117. Sequential Images, MGS with Shallow Post Embedment of 28 in., Half-Post Spacing, and Lower-Bound Soil Strength at TL-3 Impact Conditions

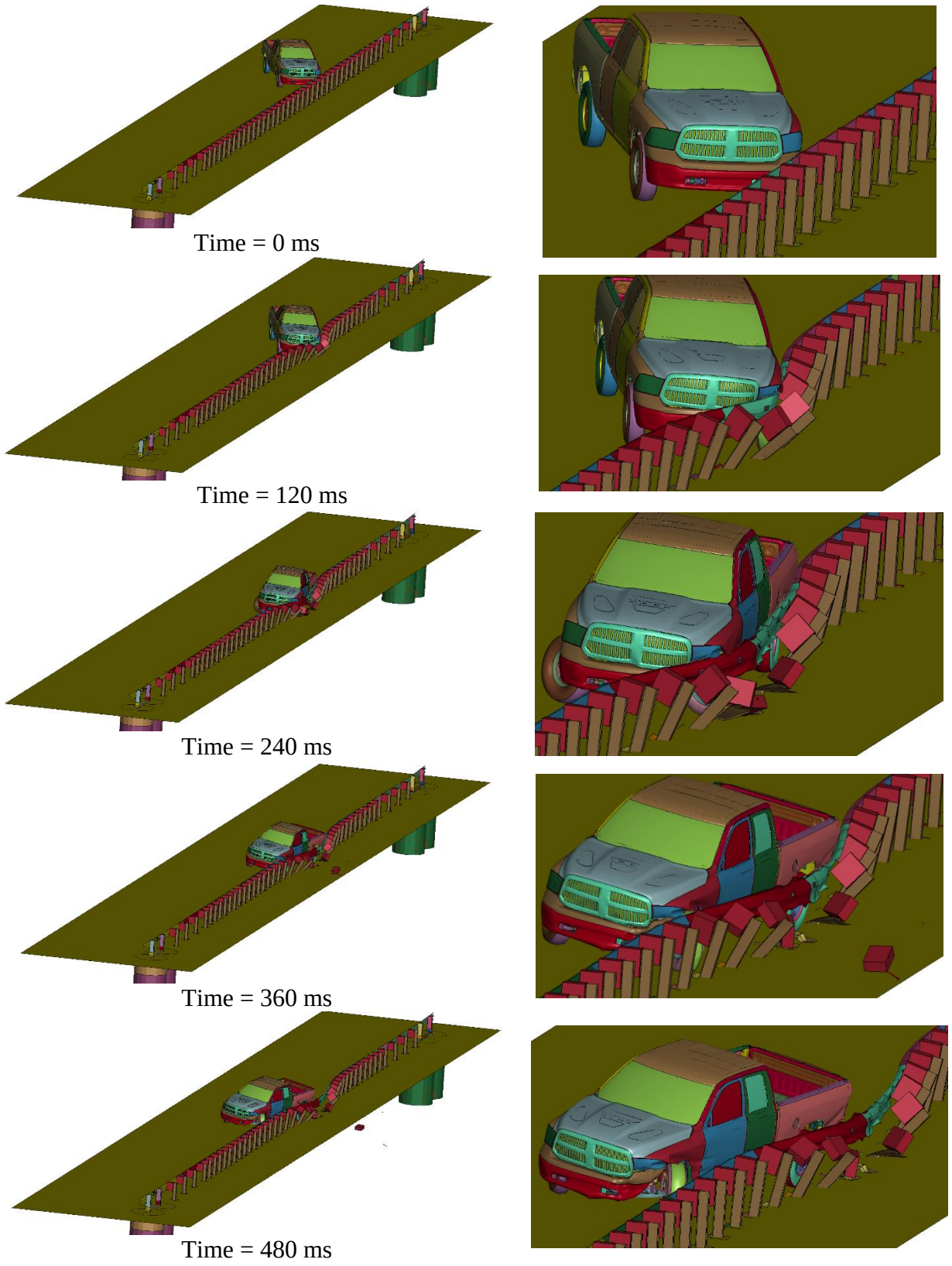

Figure 118. Sequential Images, MGS with Shallow Post Embedment of 28 in., Half-Post Spacing, and Lower-Bound Soil Strength at TL-3 Impact Conditions (Isometric View)

A summary of TL-3 simulation results, including dynamic deflection and working width, for the MGS with shallow embedment, half-post spacing, and lower-bound soil strength is shown in Table 22. The Euler angles and occupant risk values were well within the limit set in MASH.

Table 22. TL-3 Simulations of Shallow Post Embedment of 28 in., Half-Post Spacing, and Lower-Bound Soil Strength

Evaluation Criteria		Shallow Embedment of 28 in.	MASH 2016 Limits
OIV ft/s (m/s)	Longitudinal	-18.50 (-5.64)	±40 (12.20)
	Lateral	-16.12 (4.91)	±40 (12.20)
ORA g's	Longitudinal	-7.43	±20.49
	Lateral	-10.08	±20.49
Maximum Angular Displacement deg.	Roll	-8.85	±75
	Pitch	-2.20	±75
	Yaw	-41.96	not required
THIV ft/s (m/s)		N/A	not required
PHD g's		N/A	not required
ASI		N/A	not required
Max. dynamic Deflection in. (mm)		40.94 (1,040)	N/A
Working Width in. (mm)		56.78 (1,442)	N/A

6.4.4 MGS with Shallow Post Embedment and Quarter-Post Spacing

The Dodge Ram model impacted the MGS with shallow post embedment of 28 in. and quarter-post spacing at post no. 29 at a speed of 62 mph and an angle of 25 degrees, as shown in Figure 119. The vehicle was redirected with only minor tire snag on the posts. Sixteen steel posts displaced during the impact, and six steel posts experienced minor plastic damage. Overall, the vehicle behavior during redirection was acceptable, and there was no indication of potential vehicle instabilities. Sequential photographs of the simulation are shown in Figures 120 through 122.

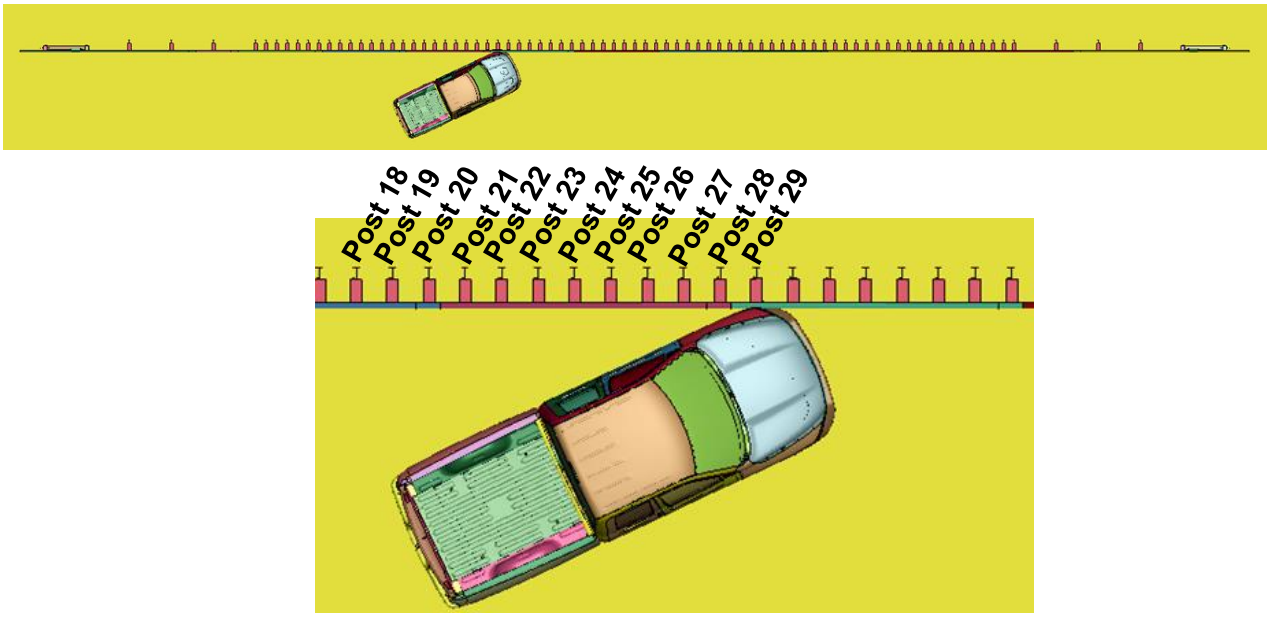

Figure 119. Dodge Ram Vehicle Model Impacting MGS with Shallow Post Embedment, Quarter-Post Spacing, and Lower-Bound Soil Strength at TL-3 Impact Conditions

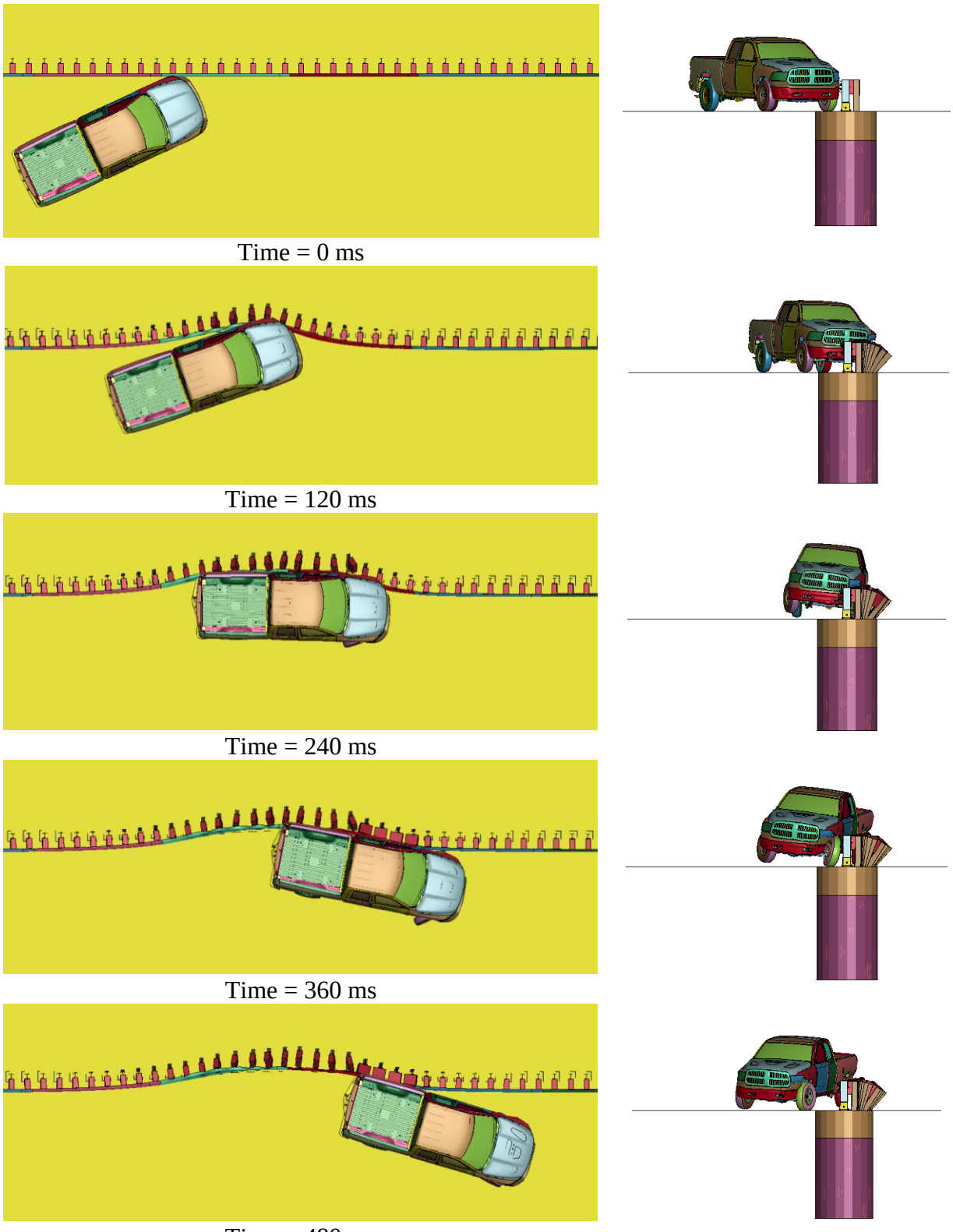

Figure 120. Sequential Images, MGS with Shallow Post Embedment of 28 in., Quarter-Post Spacing, and Lower-Bound Soil Strength at TL-3 Impact Conditions

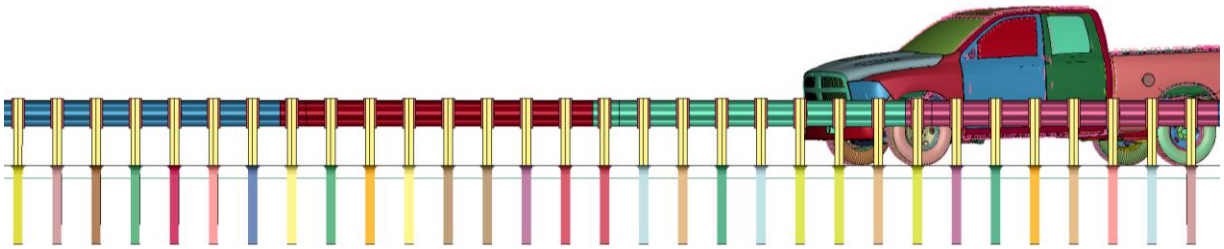

Time = 0 ms

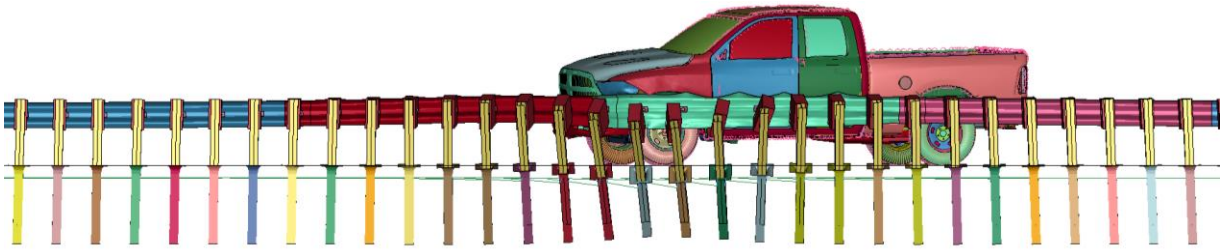

Time = 120 ms

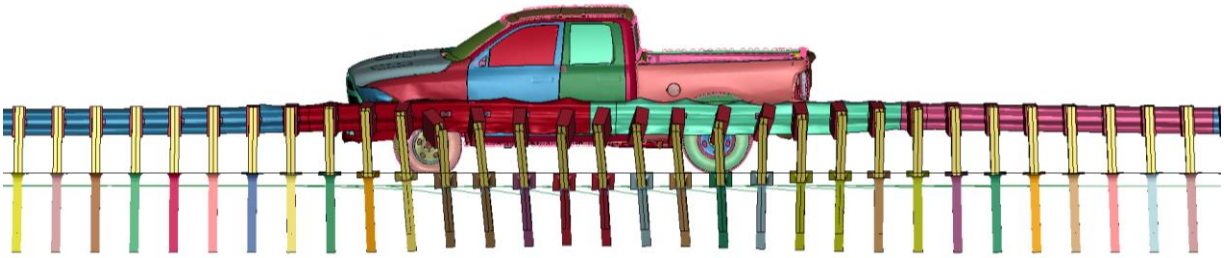

Time = 240 ms

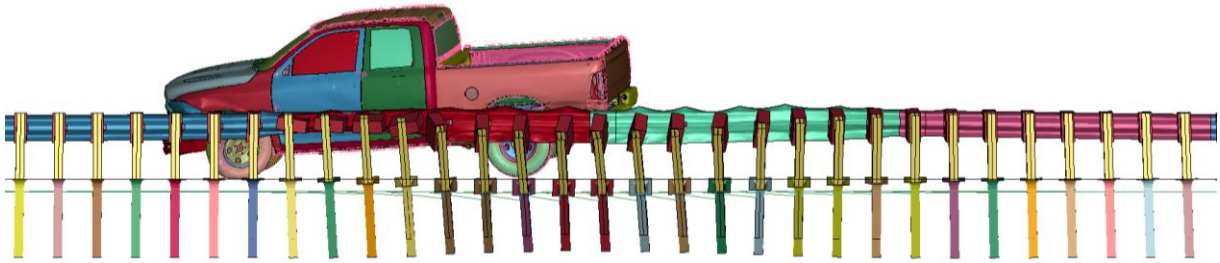

Time = 360 ms

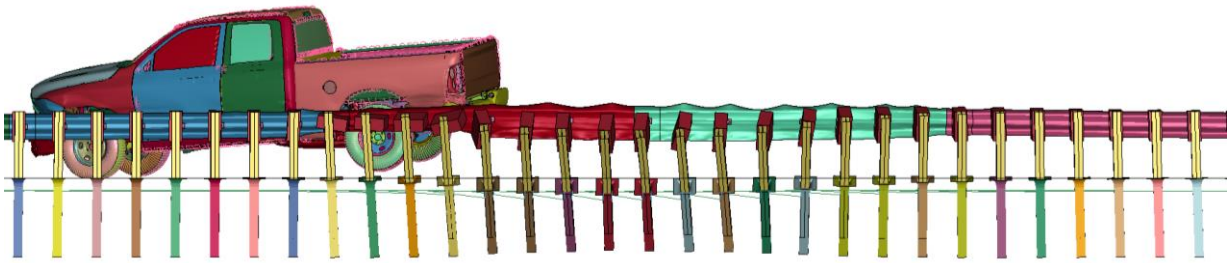

Time = 480 ms

Figure 121. Sequential Images, MGS with Shallow Post Embedment of 28 in., Quarter-Post Spacing, and Lower-Bound Soil Strength at TL-3 Impact Conditions

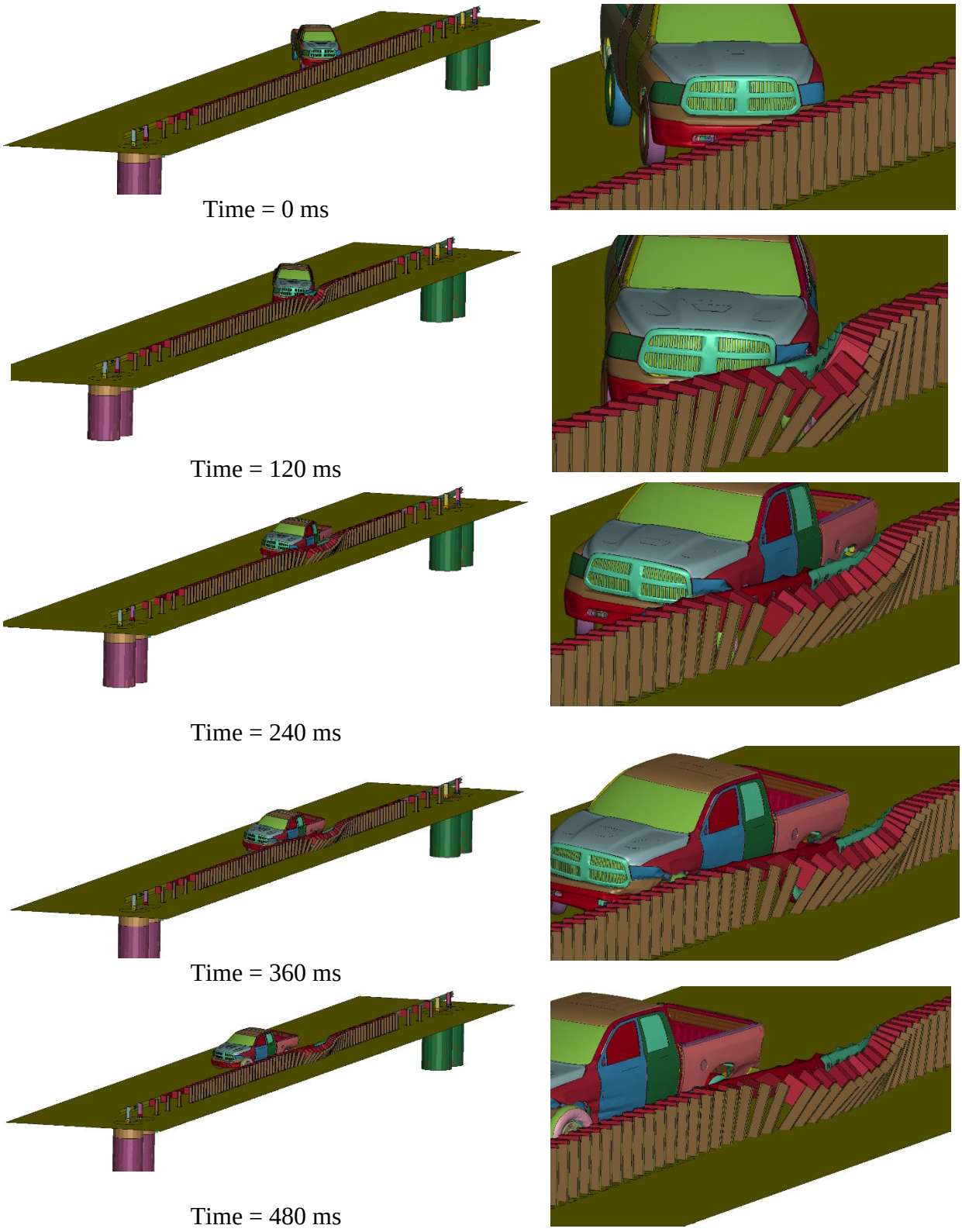

Figure 122. Sequential Images, MGS with Shallow Post Embedment of 28 in., Quarter-Post Spacing, and Lower-Bound Soil Strength at TL-3 Impact Conditions (Isometric View)

A summary of TL-3 simulation results, including dynamic deflection and working width, for the MGS with shallow embedment, quarter-post spacing, and lower-bound soil strength is shown in Table 23. The Euler angles and occupant risk values were well within the limit set in MASH.

Table 23. TL-3 Simulation Results of MGS with Shallow Post Embedment, Quarter-Post Spacing, and Lower-Bound Soil Strength

Evaluation Criteria		Shallow Embedment of 28 in.	MASH 2016 Limits
OIV ft/s (m/s)	Longitudinal	-16.55 (-5.04)	±40 (12.20)
	Lateral	-17.13 (-5.22)	±40 (12.20)
ORA g's	Longitudinal	-8.43	±20.49
	Lateral	-9.31	±20.49
Maximum Angular Displacement deg.	Roll	-7.16	±75
	Pitch	2.74	±75
	Yaw	-41.62	not required
THIV ft/s (m/s)		N/A	not required
PHD g's		N/A	not required
ASI		N/A	not required
Max. dynamic Deflection in. (mm)		31.50 (800)	N/A
Working Width in. (mm)		55.12 (1,400)	N/A

6.4.5 Discussion

The simulated dynamic deflection and working width for MGS with reduced post embedment and reduced post spacing with lower-bound soil strength at TL-3 impact conditions are summarized in Table 24. The MGS with shallower post embedment and quarter-post spacing had the lowest dynamic deflection of 31.5 in., while the MGS with shallower post embedment and full-post spacing had the highest dynamic deflection of 53.2 in. in lower-bound soil strength at TL-3 impact conditions. The baseline MGS model has the maximum dynamic deflection of 47.33 in. in the case of lower-bound soil strength at TL-3 impact conditions. As previously noted, lower-bound soil strength represents the soil with minimum acceptable soil strength. Therefore, the dynamic deflection and working width of MGS obtained from lower bound soil strength simulations were believed to be conservative.

Table 24. Summary of Results for MASH TL-3 MGS Simulation with Lower-Bound Soil Strength

Evaluation Criteria	Standard Post Embedment & Full-Post Spacing	Shallow Post Embedment			MASH 2016 Limits
		Full-Post Spacing	Half-Post Spacing	Quarter-Post Spacing	
Max. Dynamic Deflection in. (mm)	47.33 (1,202)	53.20 (1,351)	40.94 (1,040)	31.50 (800)	N/A
Working Width in. (mm)	65.93 (1,675)	74.30 (1,887)	56.78 (1,442)	55.12 (1,400)	N/A

6.5 MASH TL-3 Simulations with Upper-Bound Soil

The MGS with upper-bound soil was analyzed at TL-3 impact conditions (i.e., impact speed of 62 mph and angle of 25 degrees), using the impact points determined per MASH 2016 [1]. A total of four cases were investigated, with two embedment depths (i.e., standard embedment of 40 in. and shallow embedment of 28 in.) and three post spacings (i.e., full-, half-, and quarter-post spacing).

6.5.1 MGS with Standard Post Embedment and Full-Post Spacing

The Dodge Ram model impacted the MGS with standard post embedment and full-post spacing 34 in. upstream from post no. 12 at a speed of 62 mph and an angle of 25 degrees, as shown in Figure 123. The vehicle was redirected with only a minor tire snag on the posts. Five steel posts displaced during the impact, and five steel posts bent and sustained plastic deformation. Overall, the vehicle behavior during redirection was acceptable, and there was no indication of potential vehicle instabilities. Sequential photographs of the simulation are shown in Figures 124 through 126.

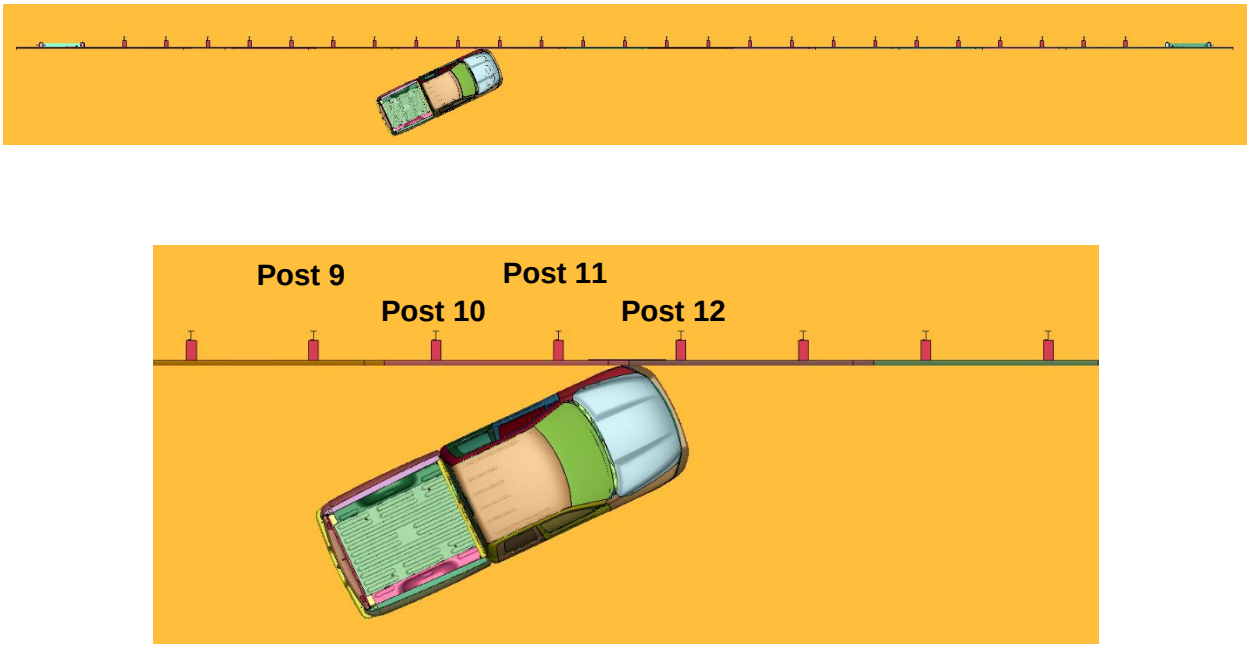

Figure 123. Dodge Ram Vehicle Model Impacting MGS with Standard Post Embedment, Full-Post Spacing, and Upper-Bound Soil Strength at TL-3 Impact Conditions

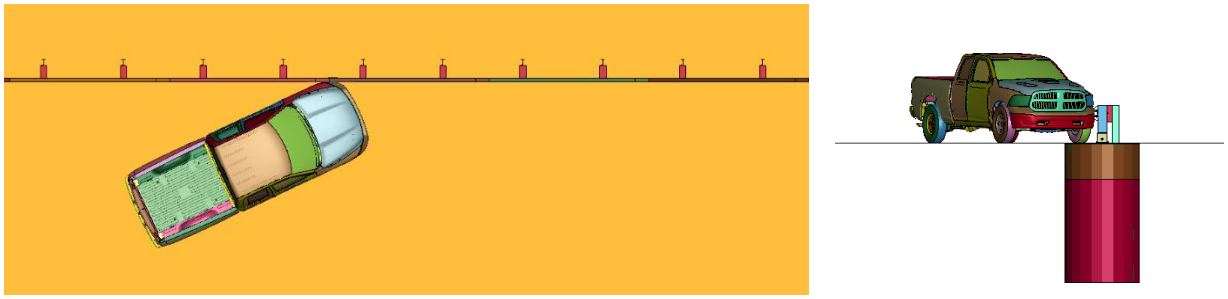

Time = 0 ms

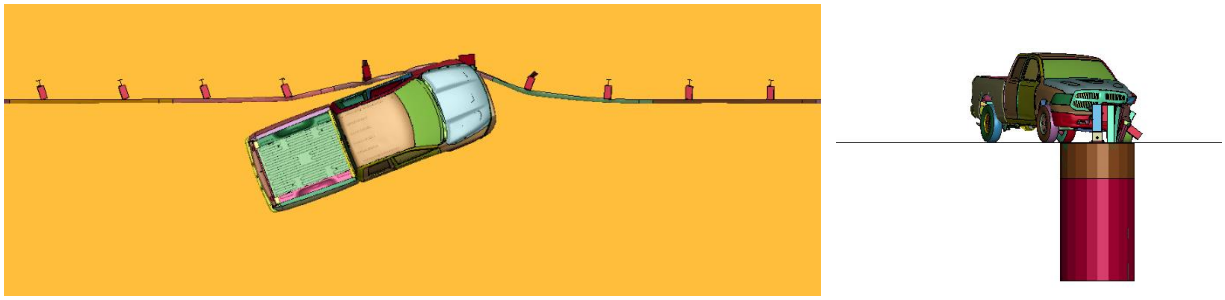

Time = 120 ms

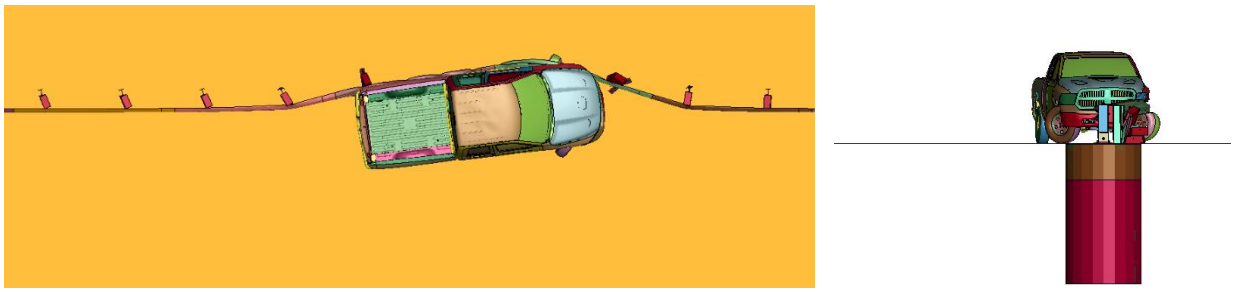

Time = 240 ms

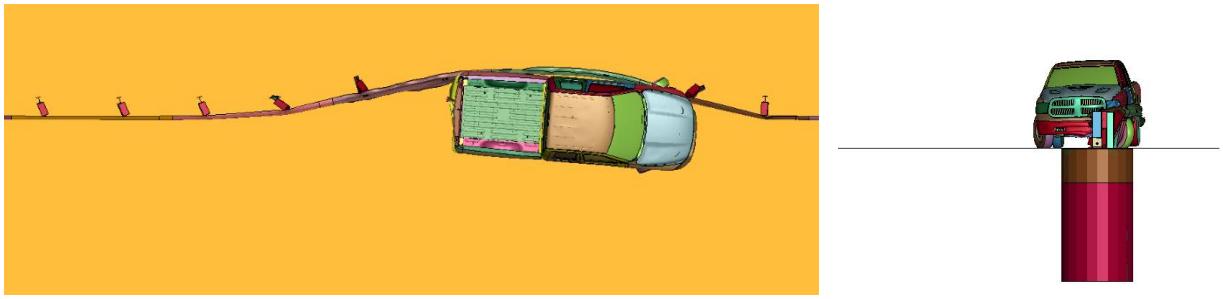

Time = 360 ms

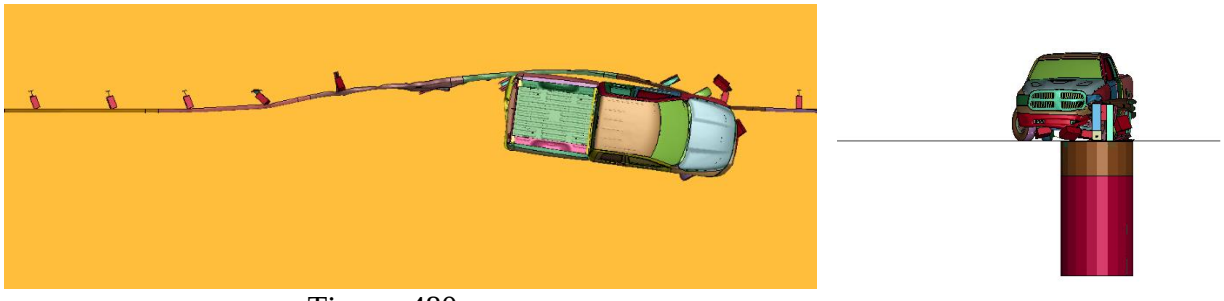

Time = 480 ms

Figure 124. Sequential Images, MGS with Standard Post Embedment, Full-Post Spacing, and Upper Bound Soil Strength at TL-3 Impact Conditions

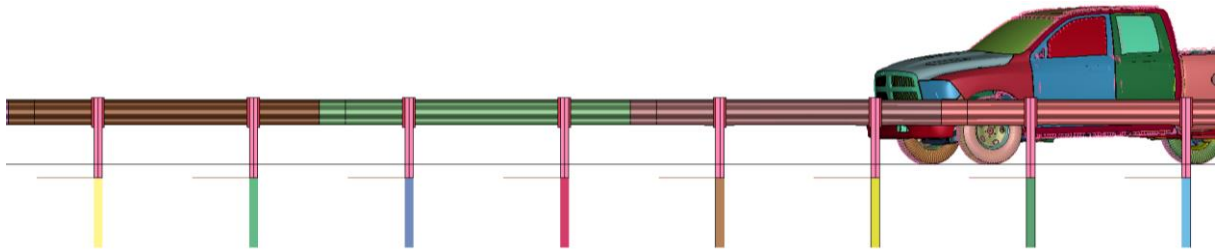

Time = 0 ms

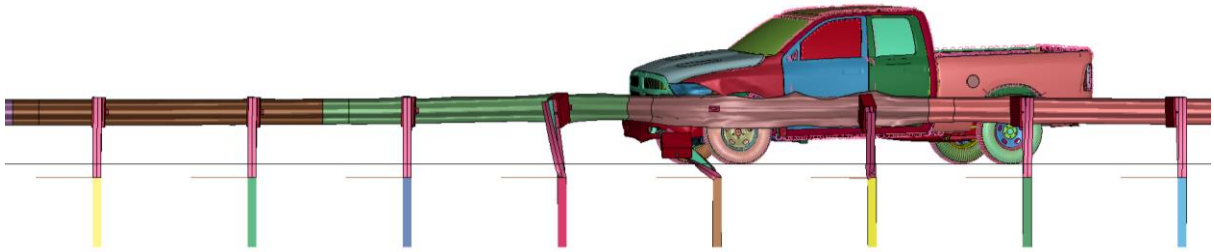

Time = 120 ms

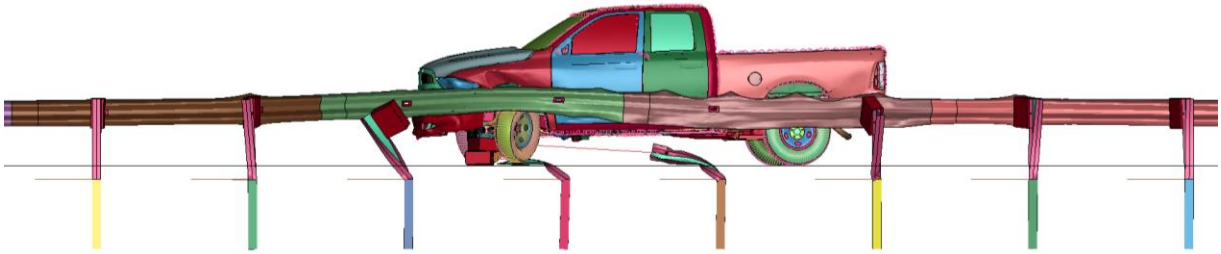

Time = 240 ms

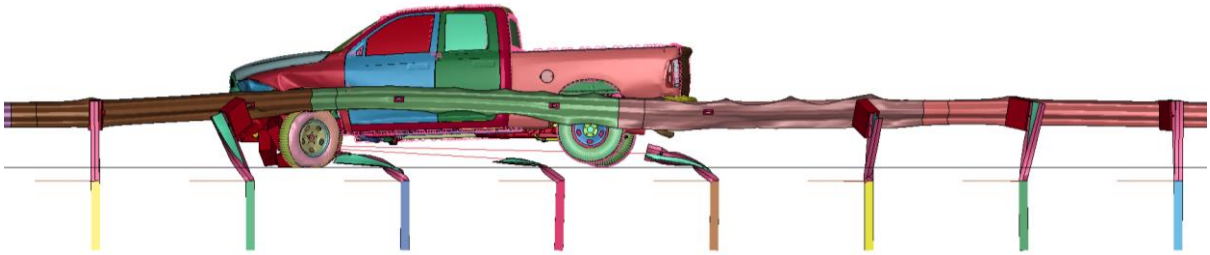

Time = 360 ms

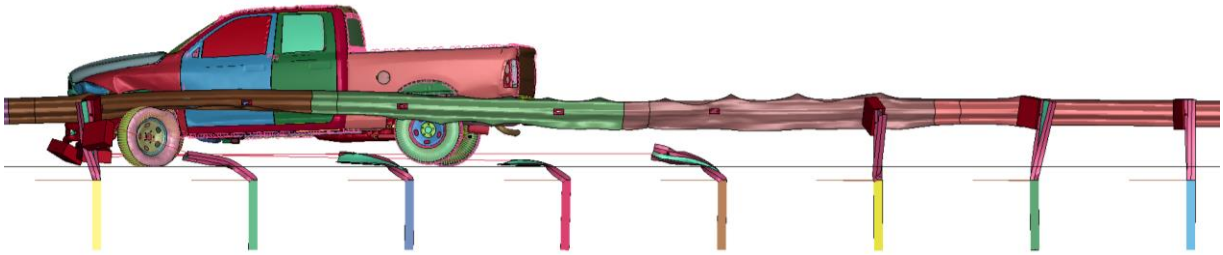

Time = 480 ms

Figure 125. Sequential Images, MGS with Standard Post Embedment, Full-Post Spacing, and Upper-Bound Soil Strength at TL-3 Impact Conditions

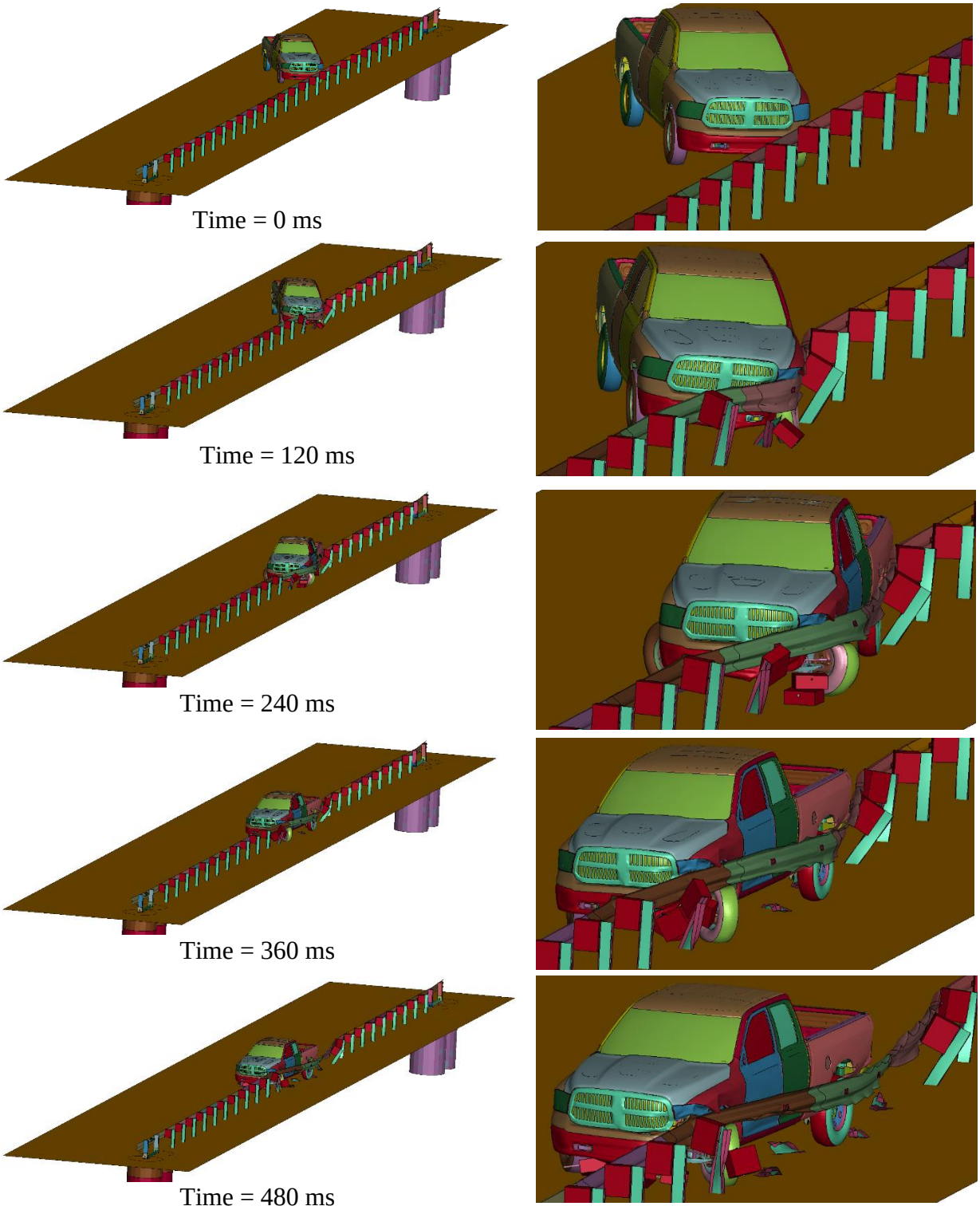

Figure 126. Sequential Images, MGS with Standard Post Embedment, Full-Post Spacing, and Upper-Bound Soil Strength at TL-3 Impact Conditions (Isometric View)

A summary of TL-3 simulation results, including dynamic deflection and working width, for the MGS with standard embedment, full-post spacing, and upper-bound soil strength is shown in Table 25. The Euler angles and occupant risk values were well within the limit set in MASH.

Table 25. TL-3 Simulation Results of MGS with Standard Post Embedment, Full-Post Spacing, and Upper-Bound Soil Strength

Evaluation Criteria		Standard Embedment: 40 in.	MASH 2016 Limits
OIV ft/s (m/s)	Longitudinal	-17.52 (-5.34)	±40 (12.20)
	Lateral	-14.32 (-4.36)	±40 (12.20)
ORA g's	Longitudinal	-7.16	±20.49
	Lateral	-7.22	±20.49
Maximum Angular Displacement deg.	Roll	3.07	±75
	Pitch	-2.14	±75
	Yaw	-33.00	not required
THIV ft/s (m/s)		N/A	not required
PHD g's		N/A	not required
ASI		N/A	not required
Max. Dynamic Deflection in. (mm)		42.91 (1,090)	N/A
Working Width in. (mm)		48.19 (1,224)	N/A

6.5.2 MGS with Shallow Post Embedment and Full-Post Spacing

The Dodge Ram model impacted the MGS with shallow post embedment and full-post spacing 17 in. downstream from post no. 11 at a speed of 62 mph and an angle of 25 degrees, as shown in Figure 127. The vehicle was redirected with only minor tire snag on the posts. Six steel posts displaced during the impact, and five steel posts bent and sustained plastic deformation. Overall, the vehicle behavior during redirection was acceptable, and there was no indication of potential vehicle instabilities. Sequential photographs of the simulation are shown in Figures 128 through 130.

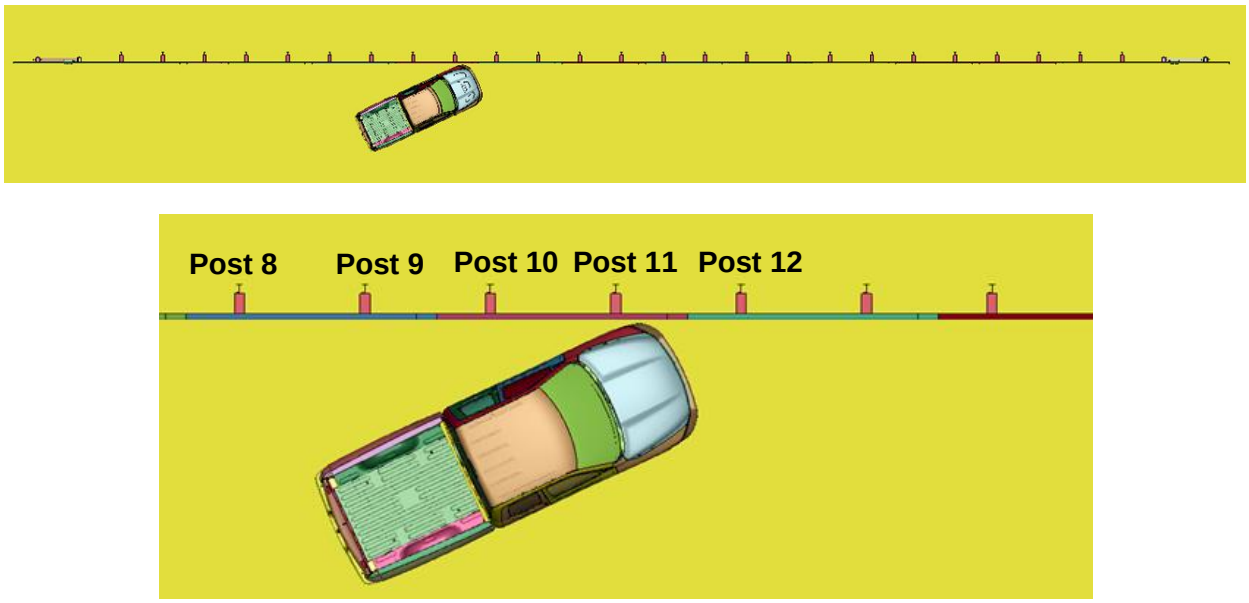

Figure 127. Dodge Ram Vehicle Model Impacting MGS with Shallow Post Embedment, Full-Post Spacing, and Lower-Bound Soil at TL-3 Impact Conditions

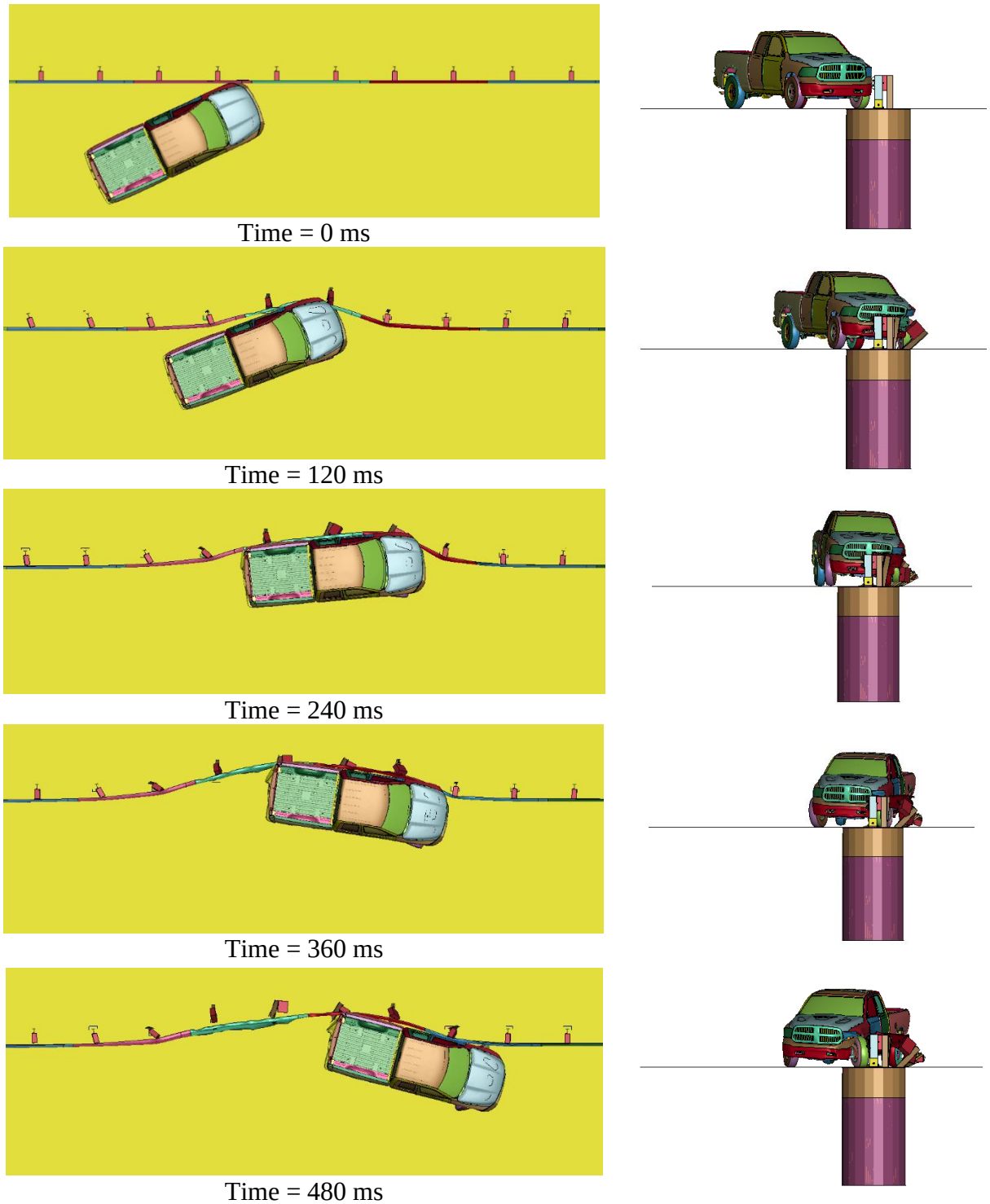

Figure 128. Sequential Images, MGS with Shallow Post Embedment of 28 in., Full-Post Spacing, Upper-Bound Soil Strength at TL-3 Impact Conditions

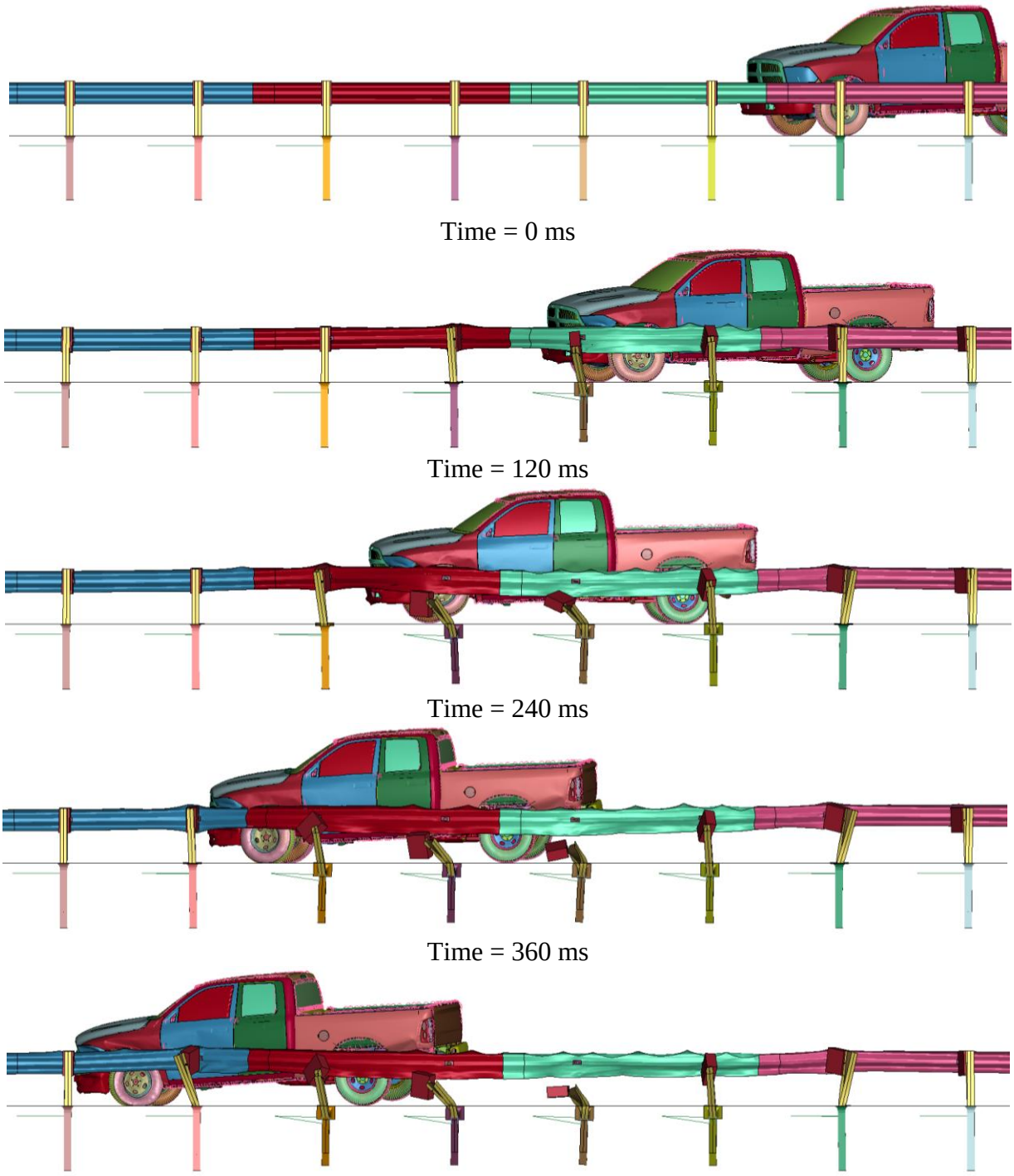

Figure 129. Sequential Images, MGS with Shallow Post Embedment of 28 in., Full-Post Spacing, Upper-Bound Soil Strength at TL-3 Impact Conditions

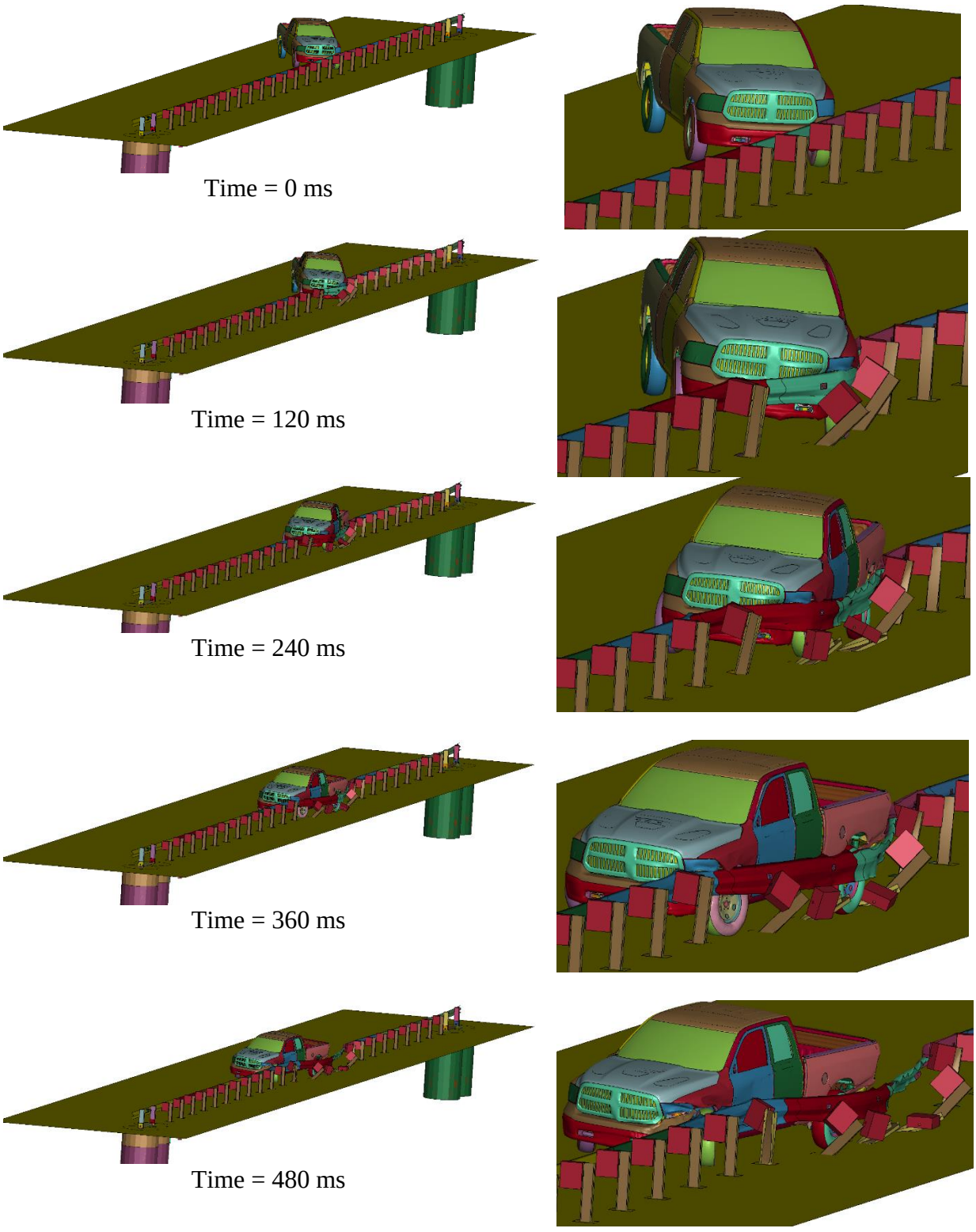

Figure 130. Sequential Images, MGS with Shallow Post Embedment of 28 in., Full-Post Spacing, Upper-Bound Soil Strength at TL-3 Impact Conditions (Isometric View)

A summary of TL-3 simulation results, including dynamic deflection and working width, for the MGS with shallow embedment, standard post-spacing, and upper-bound soil strength is shown in Table 26. The Euler angles and occupant risk values were well within the limit set in MASH.

Table 26. TL-3 Simulation Results of MGS with Shallow Post Embedment of 28 in., Full-Post Spacing, and Upper-Bound Soil Strength

Evaluation Criteria		Shallow Embedment of 28 in.	MASH 2016 Limits
OIV ft/s (m/s)	Longitudinal	-17.00 (-5.18)	±40 (12.20)
	Lateral	-14.23 (4.34)	±40 (12.20)
ORA g's	Longitudinal	-6.72	±20.49
	Lateral	-8.22	±20.49
Maximum Angular Displacement deg.	Roll	-3.34	±75
	Pitch	2.43	±75
	Yaw	-40.33	not required
THIV ft/s (m/s)		N/A	not required
PHD g's		N/A	not required
ASI		N/A	not required
Max. Dynamic Deflection in. (mm)		46.06 (1,170)	N/A
Working Width in. (mm)		63.18 (1,605)	N/A

6.5.3 MGS with Shallow Post Embedment and Half-Post Spacing

The Dodge Ram model impacted the MGS with shallow post embedment and half-post spacing 11 in. downstream from post no. 17 at a speed of 62 mph and an angle of 25 degrees, as shown in Figure 131. The vehicle was redirected with only minor tire snag on the posts. Seven steel posts displaced during the impact, and five steel posts bent and sustained plastic deformation. Overall, the vehicle behavior during redirection was acceptable, and there was no indication of potential vehicle instabilities. Sequential photographs of the simulation are shown in Figures 132 through 134.

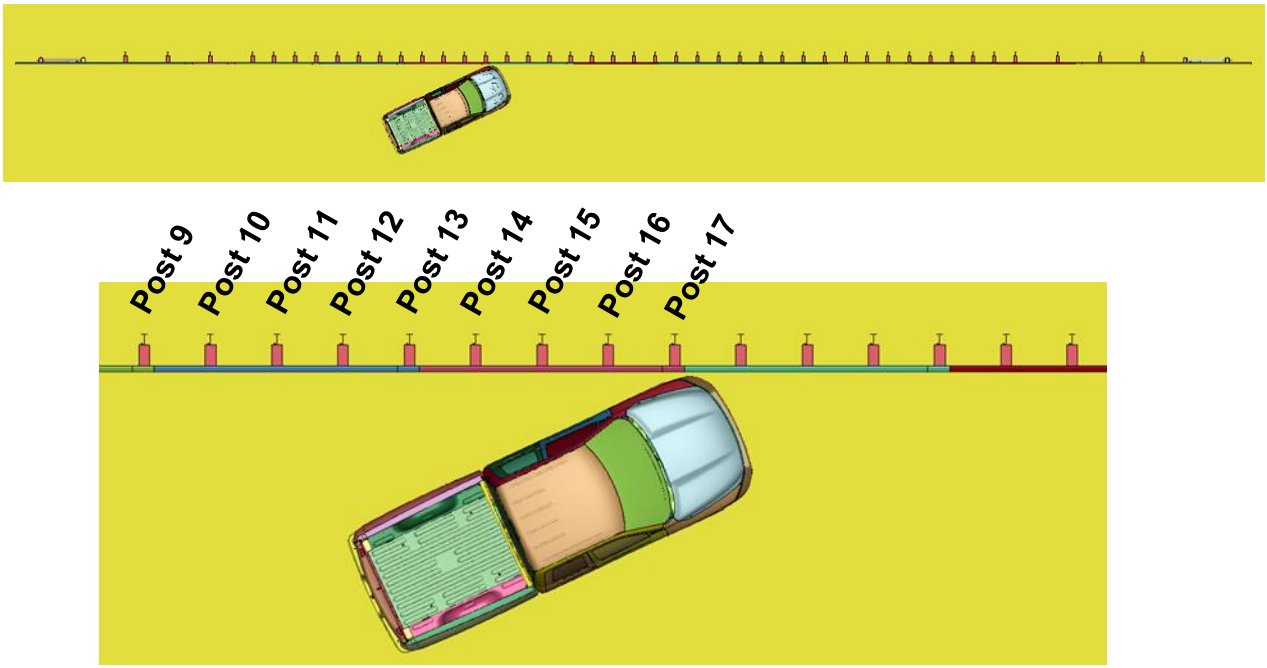

Figure 131. Dodge Ram Vehicle Model Impacting MGS with Shallow Post Embedment, Half-Post Spacing, and Upper-Bound Soil Strength at TL-3 Impact Conditions

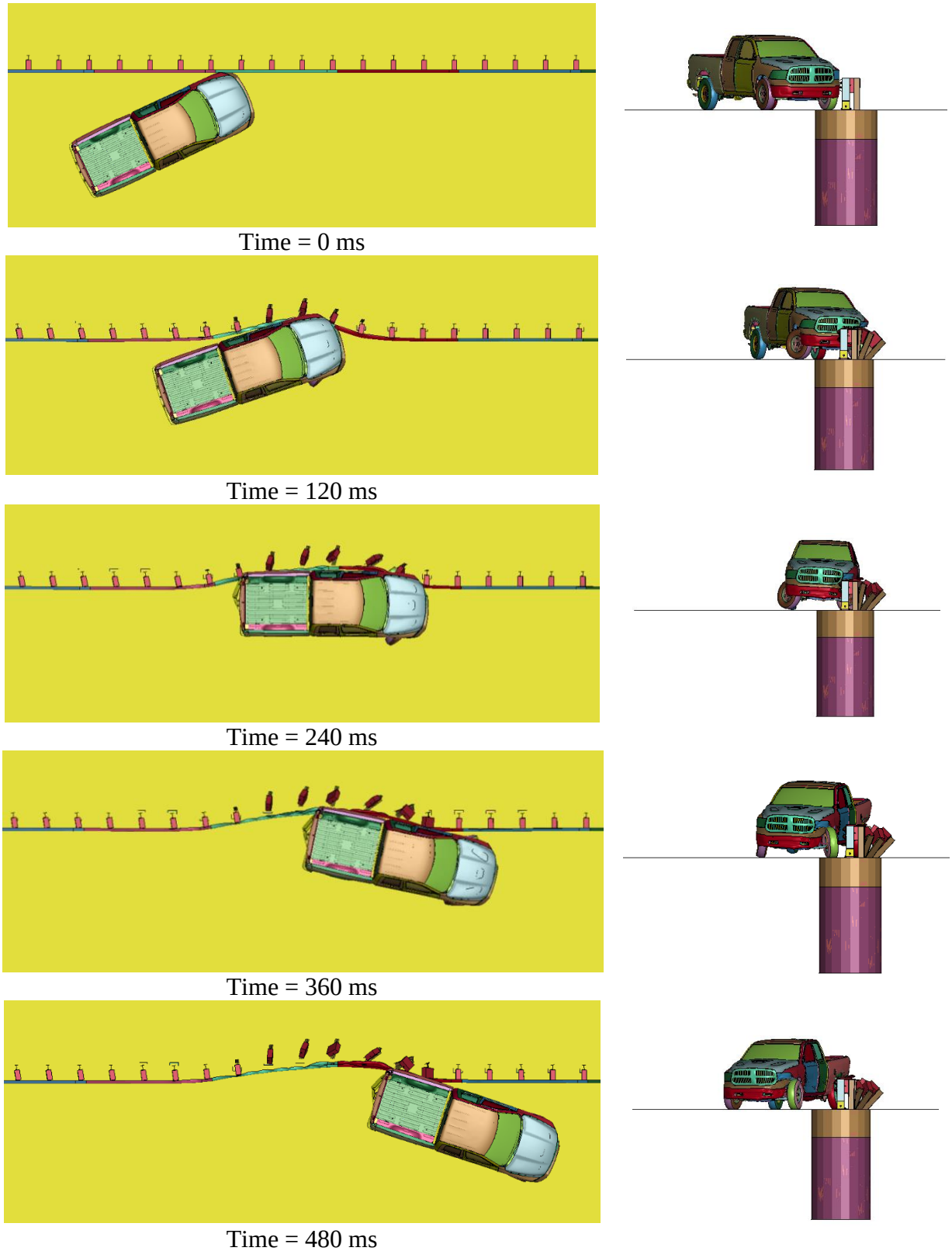

Figure 132. Sequential Images, MGS with Shallow Post Embedment of 28 in., Half-Post Spacing, and Upper-Bound Soil Strength at TL-3 Impact Conditions

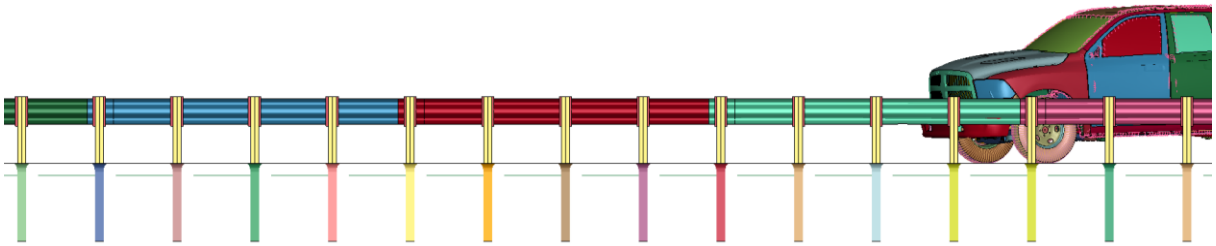

Time = 0 ms

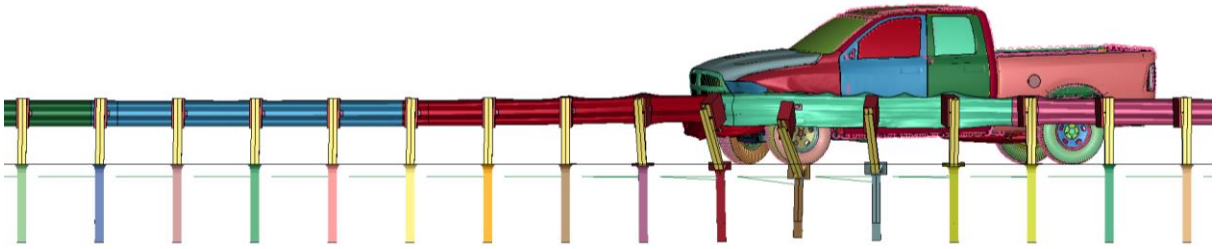

Time = 120 ms

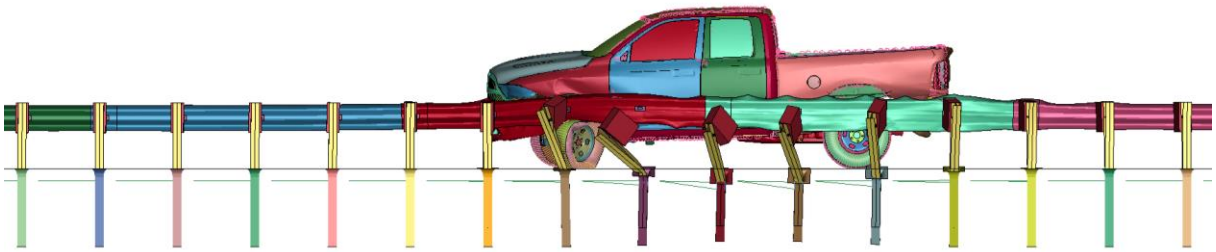

Time = 240 ms

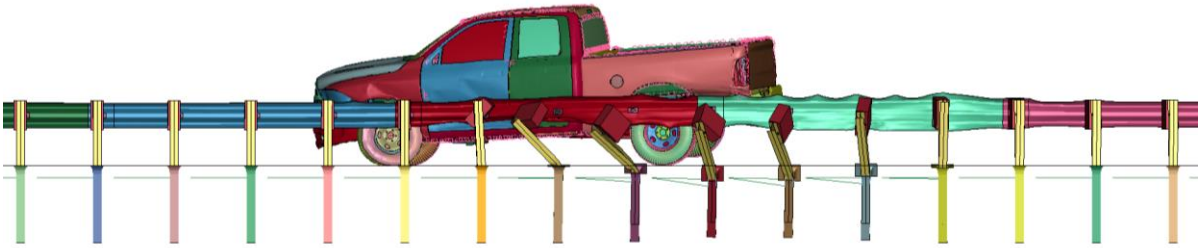

Time = 360 ms

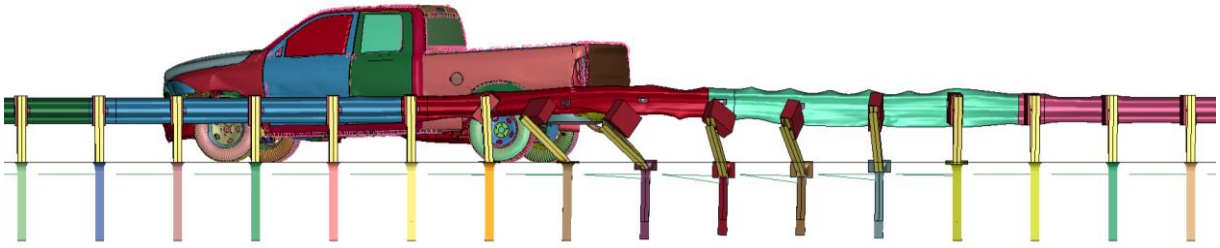

Time = 480 ms

Figure 133. Sequential Images, MGS with Shallow Post Embedment of 28 in., Half-Post Spacing, and Upper-Bound Soil Strength at TL-3 Impact Conditions

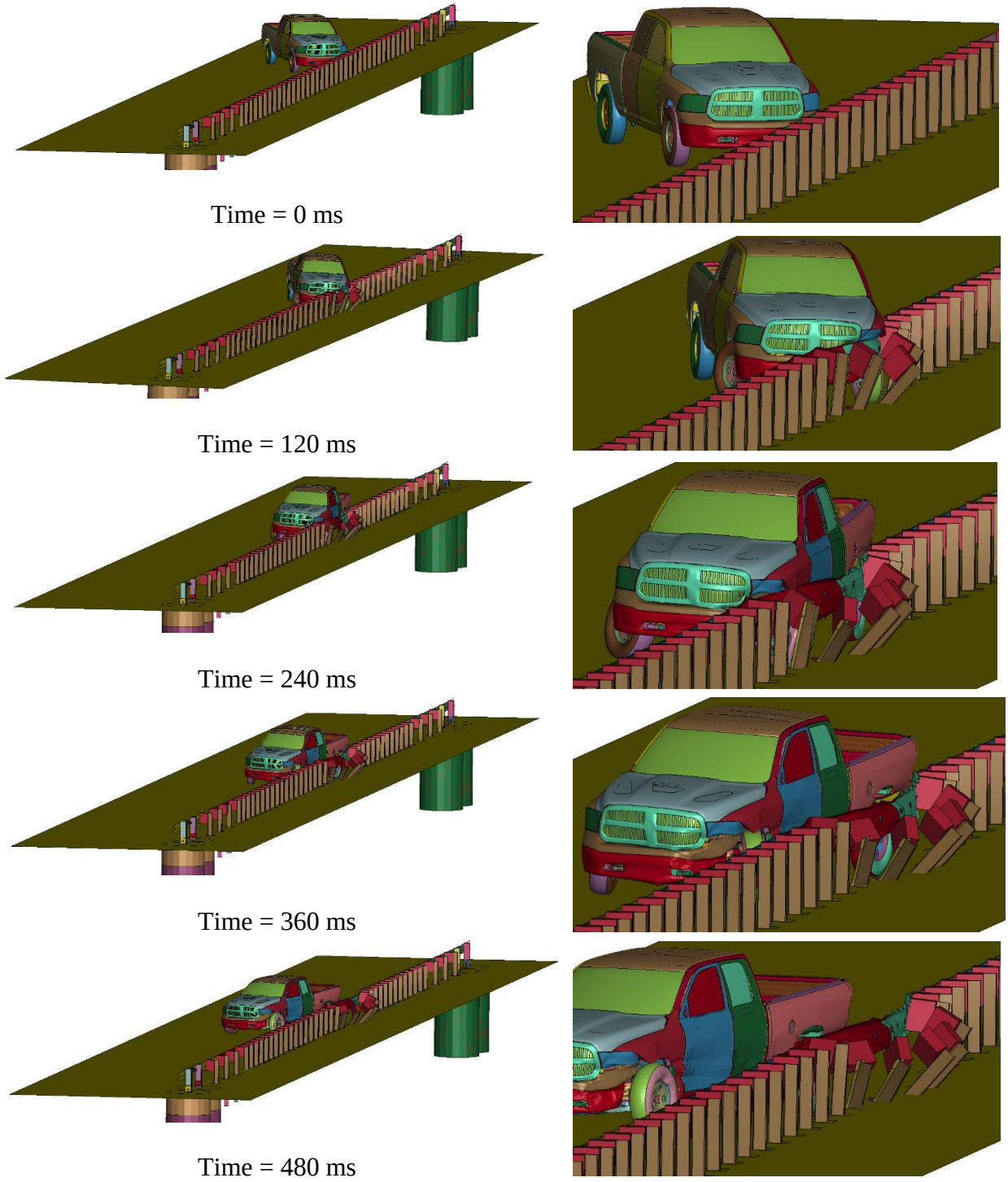

Figure 134. Sequential Images, MGS with Shallow Post Embedment of 28 in., Half-Post Spacing, and Upper-Bound Soil Strength at TL-3 Impact Conditions (Isometric View)

A summary of TL-3 simulation results, including dynamic deflection and working width, for the MGS with shallow embedment, half post spacing, and upper-bound soil strength is shown in Table 27. The Euler angles and occupant risk values were well within the limit set in MASH.

Table 27. TL-3 Simulation Results of MGS with Shallow Post Embedment of 28 in., Half-Post Spacing, and Upper-Bound Soil Strength

Evaluation Criteria		Shallow Embedment of 28 in.	MASH 2016 Limits
OIV ft/s (m/s)	Longitudinal	-19.13 (-5.83)	±40 (12.20)
	Lateral	-16.77 (-5.11)	±40 (12.20)
ORA g's	Longitudinal	-8.56	±20.49
	Lateral	-9.74	±20.49
Maximum Angular Displacement deg.	Roll	-2.85	±75
	Pitch	-1.99	±75
	Yaw	-43.37	not required
THIV ft/s (m/s)		N/A	not required
PHD g's		N/A	not required
ASI		N/A	not required
Max. dynamic Deflection in. (mm)		28.78 (731)	N/A
Working Width in. (mm)		52.55 (1,335)	N/A

6.5.4 MGS with Shallow Post Embedment and Quarter-Post Spacing

The Dodge Ram model impacted the MGS with shallow post embedment of 28 in. and quarter-post spacing 11 in. downstream from post no. 17 at a speed of 62 mph and an angle of 25 degrees, as shown in Figure 135. The vehicle was redirected out of the system with only minor tire snag on the posts. Seven steel posts displaced during the impact, and four steel posts bent and sustained plastic deformation. Overall, the vehicle behavior during redirection was acceptable, and there was no indication of potential vehicle instabilities. Sequential photographs of the simulation are shown in Figures 136 through 138.

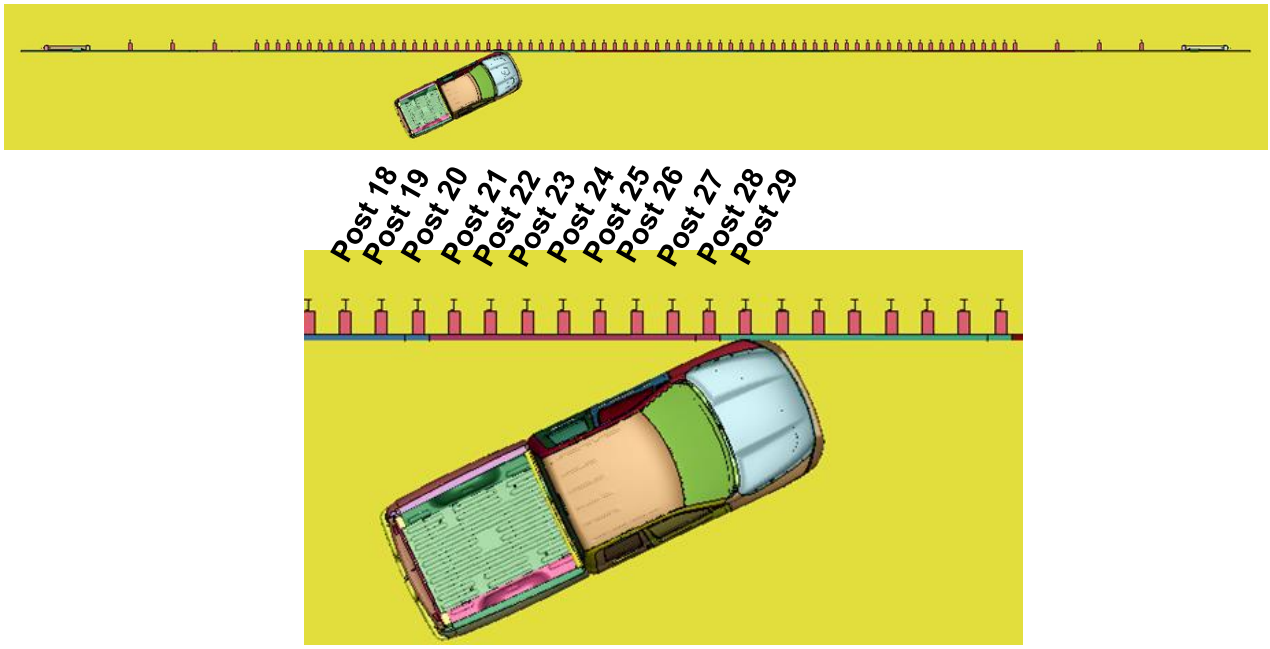

Figure 135. Dodge Ram Vehicle Model Impacting MGS with Shallow Post Embedment, Quarter-Post Spacing, and Upper-Bound Soil Strength at TL-3 Impact Conditions

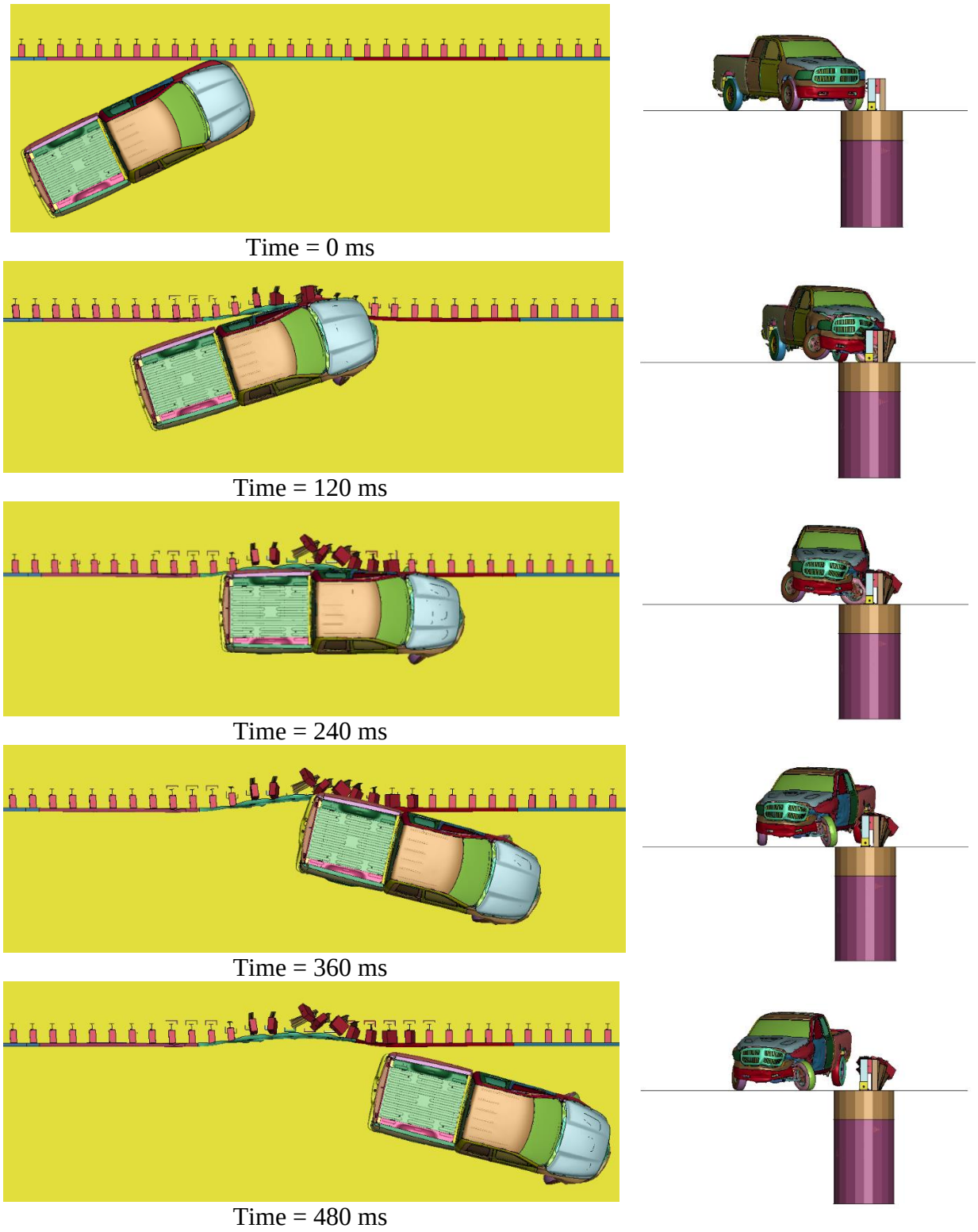

Figure 136. Sequential Images, MGS with Shallow Post Embedment of 28 in., Quarter-Post Spacing, and Upper-Bound Soil Strength at TL-3 Impact Conditions

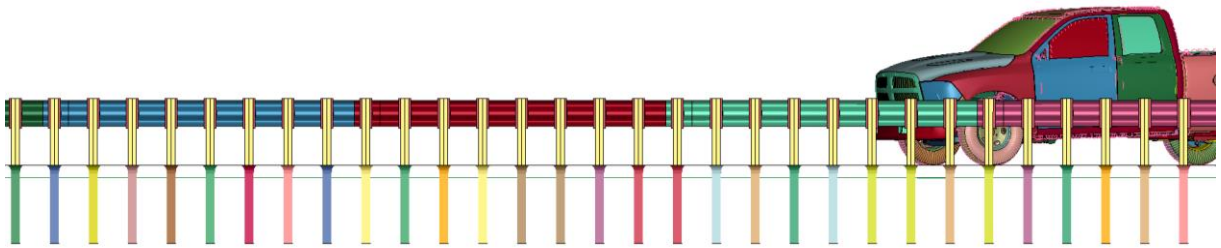

Time = 0 ms

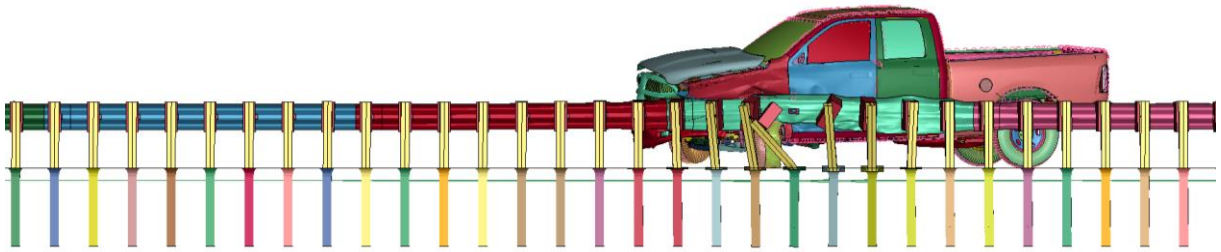

Time = 120 ms

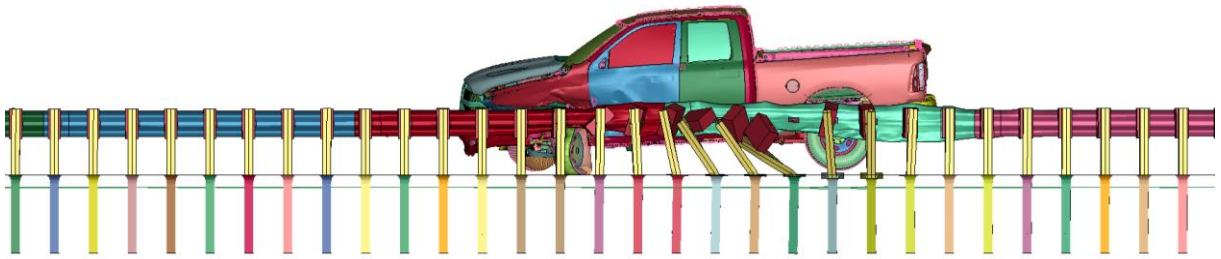

Time = 240 ms

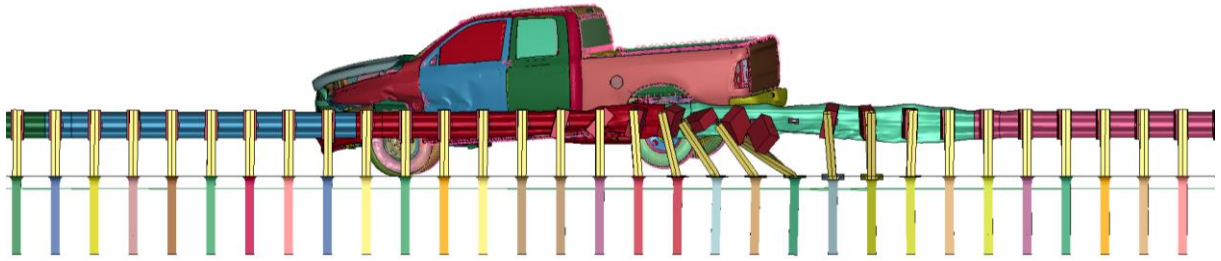

Time = 360 ms

Time = 480 ms

Figure 137. Sequential Images, MGS with Shallow Post Embedment of 28 in., Quarter-Post Spacing, and Upper-Bound Soil Strength at TL-3 Impact Conditions

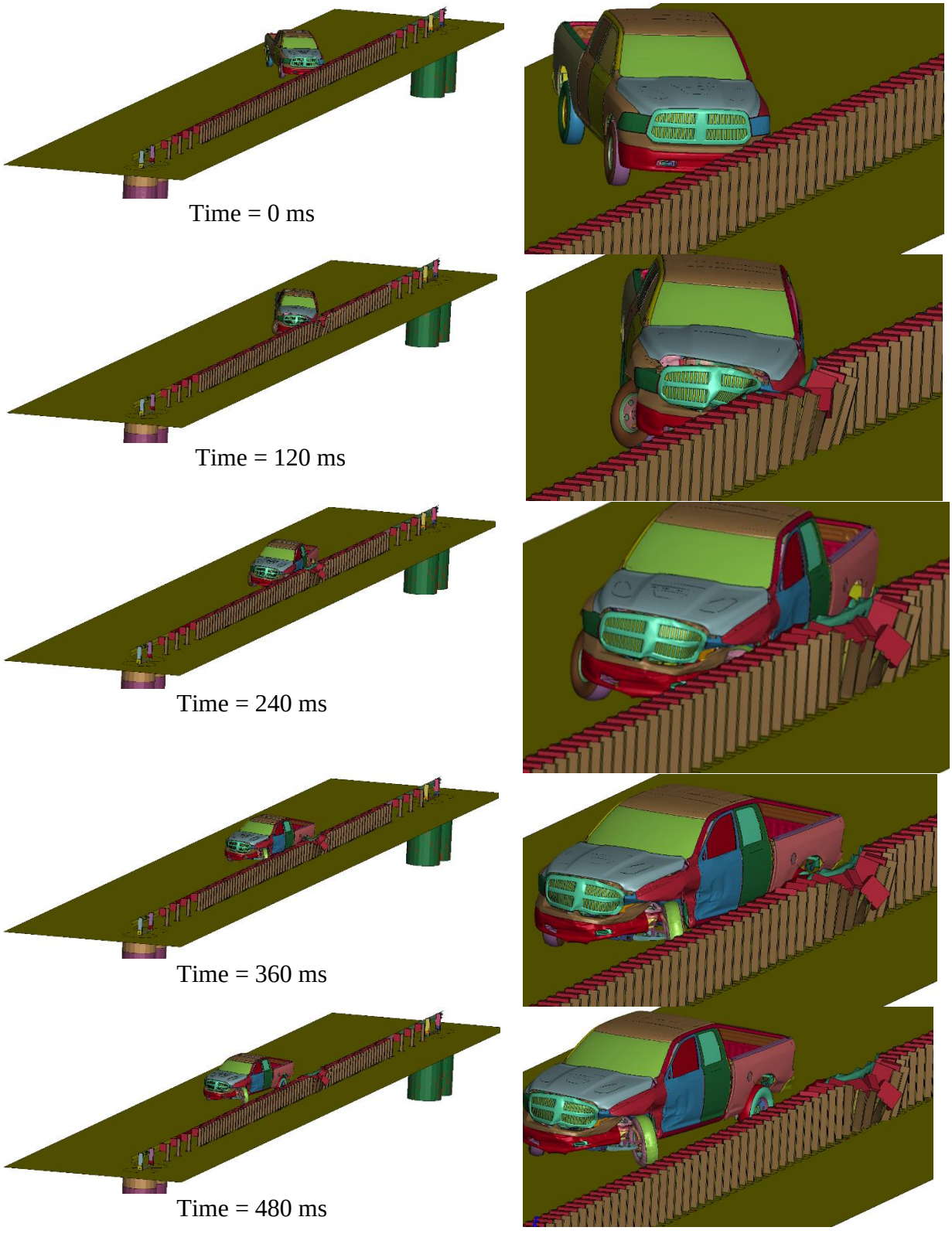

Figure 138. Sequential Images, MGS with Shallow Post Embedment of 28 in., Quarter-Post Spacing, and Upper-Bound Soil Strength at TL-3 Impact Conditions (Isometric View)

A summary of TL-3 simulation results, including dynamic deflection and working width, for the MGS with shallow embedment, quarter-post spacing, and upper-bound soil strength is shown in Table 28. The Euler angles and occupant risk values were well within the limit set in MASH.

Table 28. TL-3 Simulation Results of MGS with Shallow Post Embedment of 28 in., Quarter-Post Spacing, and Upper-Bound Soil Strength

Evaluation Criteria		Shallow Embedment of 28 in.	MASH 2016 Limits
OIV ft/s (m/s)	Longitudinal	-25.35 (-7.73)	±40 (12.20)
	Lateral	-20.17 (-6.15)	±40 (12.20)
ORA g's	Longitudinal	-15.11	±20.49
	Lateral	-8.54	±20.49
Maximum Angular Displacement deg.	Roll	-3.82	±75
	Pitch	-2.24	±75
	Yaw	-39.93	not required
THIV ft/s (m/s)		N/A	not required
PHD g's		N/A	not required
ASI		N/A	not required
Max. Dynamic Deflection in. (mm)		13.60 (345)	N/A
Working Width in. (mm)		33.78 (858)	N/A

6.5.5 Discussion

The simulated dynamic deflection and working width for MGS with reduced post embedment and reduced post spacing with upper-bound soil strength at TL-3 impact conditions are summarized in Table 29. The MGS with shallow post embedment and full-post spacing experienced the dynamic deflection of 46.06 in. and working width of 63.18 in., while the MGS with shallow post embedment and quarter-post spacing experienced a lower dynamic deflection of 13.6 in. and working width of 33.78 in.

The maximum dynamic deflection for the baseline MGS model with upper bound soil strength was 42.91 in. The relatively significant difference between the highest and lowest dynamic deflection was dependent on system stiffness (i.e., full- vs. half- vs. quarter-post spacing), post embedment depths (i.e., 28 in. vs. 40 in.), and soil strength.

As previously noted, the upper-bound soil strength represented stiffer and stronger MASH soil. Therefore, the dynamic deflection and working width of MGS installations in upper-bound soil simulations were believed to be non-conservative.

Table 29. MASH TL-3 Simulation Results for MGS with Upper-Bound Soil Strength

Evaluation Criteria	Standard Post Embedment & Full-Post Spacing	Shallow Post Embedment			MASH 2016 Limits
		Full-Post Spacing	Half-Post Spacing	Quarter-Post Spacing	
Max. Dynamic Deflection in. (mm)	42.91 (1,090)	46.06 (1,170)	28.78 (731)	13.60 (345)	N/A
Working Width in. (mm)	48.19 (1,224)	63.18 (1,605)	52.55 (1,335)	33.78 (858)	N/A

7 RECOMMENDATION FOR FULL-SCALE CRASH TESTING

A series of component bogie tests and LS-DYNA computer simulations were conducted to evaluate the use of the MGS with reduced post embedment and, if needed, with reduced post spacing to satisfy the TL-2 and TL-3 criteria of MASH. First, the bogie test results (i.e., test nos. LFCB-7 through LFCB-9 conducted on W6x16 posts) were used to develop simplified soil spring models for soil-embedded posts with reduced depth. Next, the updated curves were applied to replicate the bogie tests on W6x8.5 posts (i.e., test nos. LFCB-1 through LFCB-6). After a modeling refinement (i.e., elimination of sharp edges of soil tube model), the soil spring models could reasonably predict the soil-post behavior in bogie impacts. Next, the updated soil curves and updated soil tube shape were applied in the full MGS model. A series of LS-DYNA simulations were conducted on the MGS with reduced post embedment of 28 in. and standard embedment of 40 in. at TL-2 and TL-3 impact conditions. The MGS installations include full-, half-, and quarter-post spacing systems. Also, considering the variability of soil strength and its effect on soil-post behavior, in the particular case of reduced embedment, a lower bound and an upper bound were adopted for the soil strength curve. As such, the lower-bound soil strength was set based on the MASH soil limit and the upper bound soil strength was derived from the relatively strong and stiff soil used in the LFCB test series. As reported in Chapter 6, all simulations demonstrated smooth and stable vehicle capture and redirection, and all MASH criteria were met. However, models with standard post spacing displayed relatively large dynamic deflections.

Although the LS-DYNA models of the bogie tests were validated against the bogie test results, and the baseline MGS with 40-in. post embedment depth and full-post spacing were validated using past full-scale crash tests, these computer simulations have shortcomings. A major limitation is that the soil-spring model cannot predict posts rotating out of the soil when soil resistance is not sufficient for shallower posts, and the associated increase in barrier deflection. Additionally, the soil-spring model assumes the post bends or yields at a location about 6 in. below the ground line (where the soil springs were modeled), and assumes the post rotates at a point about two-thirds of post depth based on past test observations. Due to these uncertainties about the accuracy of the LS-DYNA models, any reduced post embedment depth MGS configurations identified through simulations need to be verified through full-scale crash testing. Additionally, it is unlikely that a significant reduction of post embedment for a guardrail system would be granted an FHWA eligibility letter with only computer simulations. If the states desire an FHWA letter or a more complete evaluation of the modified shallow embedment guardrail system, the second phase of this study is necessary. Phase II would consist of full-scale crash testing of the MGS configurations with reduced post embedment that are recommended through this study.

In order to recommend an MGS configuration with reduced post embedment depth for full-scale crash testing, a thorough comparison of MGS dynamic deflection and working width was conducted using the simulation results as well as past MGS full-scale crash tests. The aim was to determine the MGS configuration with the shallowest depth that would perform similarly to the baseline MGS (i.e., redirects vehicle with similar or less dynamic deflection/working width). The simulated dynamic deflections and working widths of the MGS with various post embedment depths and post spacings considering lower-bound and upper-bound soil strength at MASH TL-2 and TL-3 impact conditions are listed in Table 30.

Table 30. Simulated Dynamic Deflection and Working Width of MGS with Various Post Embedment Depths and Post Spacings, Lower-Bound and Upper-Bound Soil Strength at MASH TL-2 and TL-3 Impact Conditions

Item	Standard Embedment (40 in.) Full-Post Spacing (75 in.)	Shallow Embedment (28 in.) Full-Post Spacing (75 in.)	Shallow Embedment (28 in.), Half-Post Spacing (37.5 in.)	Shallow Embedment (28 in.) Quarter-Post Spacing (18.75 in.)
MASH TL-2, Lower-Bound Soil Strength				
Max. Dynamic Deflection (in.)	31.2	36.4	28.3	21.4
Working Width (in.)	51.9	55.2	50.2	44.7
MASH TL-2, Upper-Bound Soil Strength				
Max. Dynamic Deflection (in.)	25.0	24.2	15.2	7.4
Working width (in.)	36.1	45.8	37.3	28.8
MASH TL-3, Lower-Bound Soil Strength				
Max. Dynamic Deflection (in.)	47.3	53.2	40.9	31.5
Working Width (in.)	65.9	74.3	56.8	55.1
MASH TL-3, Upper-Bound Soil Strength				
Max. Dynamic Deflection (in.)	42.9	46.1	28.8	13.6
Working Width (in.)	48.2	63.2	52.6	33.8

As expected, the MGS dynamic deflection/working width (DD/WW) increased with a reduction in post embedment depth. Also, the MGS with reduced post spacing showed a decrease in dynamic deflection/working width as the system became stiffer. The simulations with the lower-bound soil model also had larger dynamic deflection/working width as compared to the ones with upper-bound soil. While these patterns were expected, the extent of these effects were not known. This simulated data was beneficial to compare the cases and the effect of various factors, such as post embedment depth, post spacing, and soil strength.

For a visual comparison, TL-2 simulated dynamic deflection/working width of the MGS with various post embedment depths and post spacings are shown in Figures 139 and 140, respectively. The four cases include the MGS with 40-in. deep posts (baseline) and the MGS with 28-in. deep posts at full-, half-, and quarter-post spacings. Note that there is no data available for the MGS crash tested under MASH TL-2 impact conditions, thus only simulated data is shown in Figures 139 and 140. For each MGS configuration, lower bound and upper bound values for DD/WW were shown. As such, the lower bound of DD/WW was associated with the upper-bound soil strength (i.e., strong and stiff soil used in the LFCB test series) and the upper bound of DD/WW was associated with the lower-bound soil strength (i.e., the MASH soil limit with the minimum acceptable soil strength). For example, for the baseline MGS, the simulated dynamic deflection with the upper bound of soil strength (i.e., "strong soil") was obtained at 25.0 in., while the dynamic deflection with the lower bound of soil strength (i.e., "MASH soil limit") was 31.2 in. Note that currently, there is no upper bound set for the soil strength in MASH. There may be concerns associated with extremely strong soil, which requires further research and is out of the scope of this study.

In Figure 139, the 31.2-in. maximum simulated dynamic deflection of the baseline MGS was set as the TL-2 deflection limit. As shown in Figure 139, the MGS with 28-in. deep posts and full-post spacing had a dynamic deflection ranging from 24.2 in. for strong soil and 36.4 in. for the MASH soil limit. The maximum dynamic deflection of 36.4 in. exceeded the maximum dynamic deflection of the baseline MGS of 31.2 in. Thus, the MGS with a 28-in. deep post at full-post spacing was not recommended. Note this does not mean this system would not pass MASH criteria. The simulations indicated that the predicted dynamic deflection of this system would be higher than that of the baseline MGS under TL-2 impact conditions.

For the MGS with 28-in. deep posts and half-post spacing, the simulated dynamic deflection ranged between 15.2 and 28.3 in., which compared well with the baseline MGS values. Thus, this system was expected to perform similarly to the MGS with standard post embedment at full-post spacing.

For the MGS with 28-in. deep posts and quarter-post spacing, the simulated dynamic deflection ranged between 7.4 and 21.4 in., which fell below the baseline MGS values. This system was expected to pass MASH TL-2 with lower deflection, but it was not recommended for full-scale crash testing as the reduced deflection may necessitate the need for a stiffness transition to the standard MGS, and the increased number of posts would add the cost.

A similar trend was observed for the working widths of these cases. As shown in Figure 140, the MSG with 28-in. deep posts and half-post spacing had a simulated dynamic deflection similar to the baseline MGS.

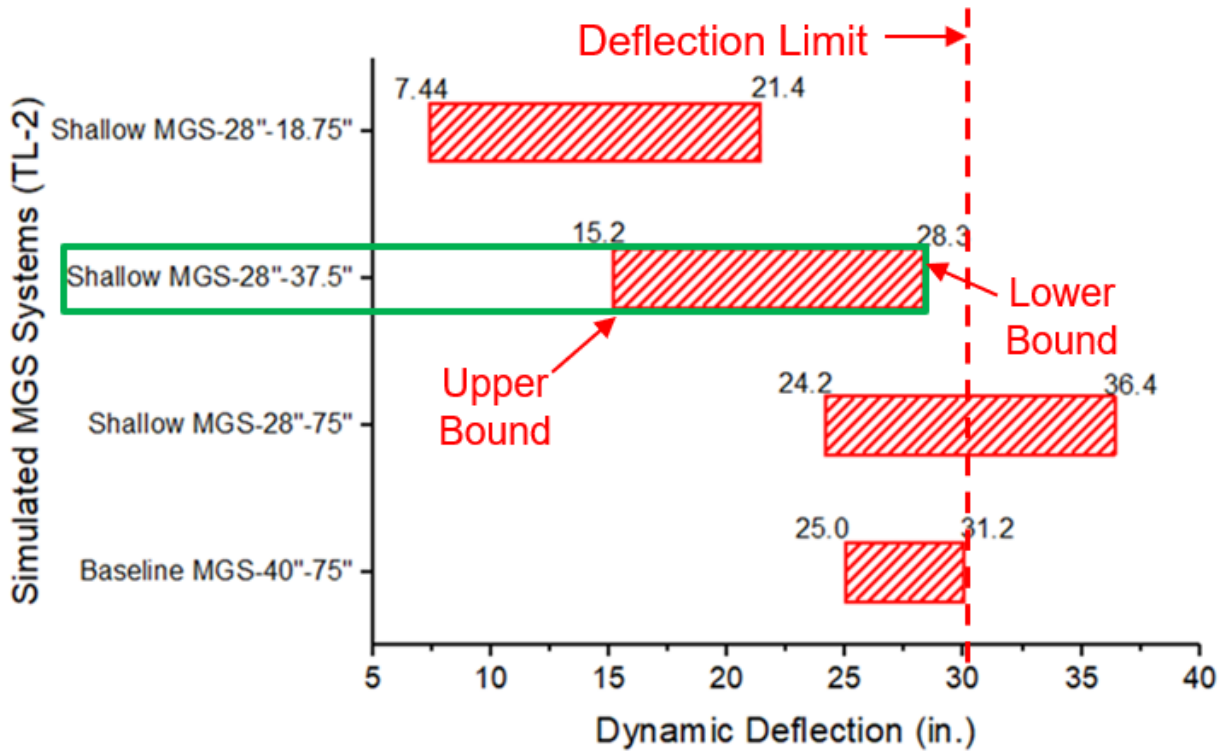

Figure 139. Dynamic Deflection for Simulated MGS Systems at MASH TL-2 Impact Conditions

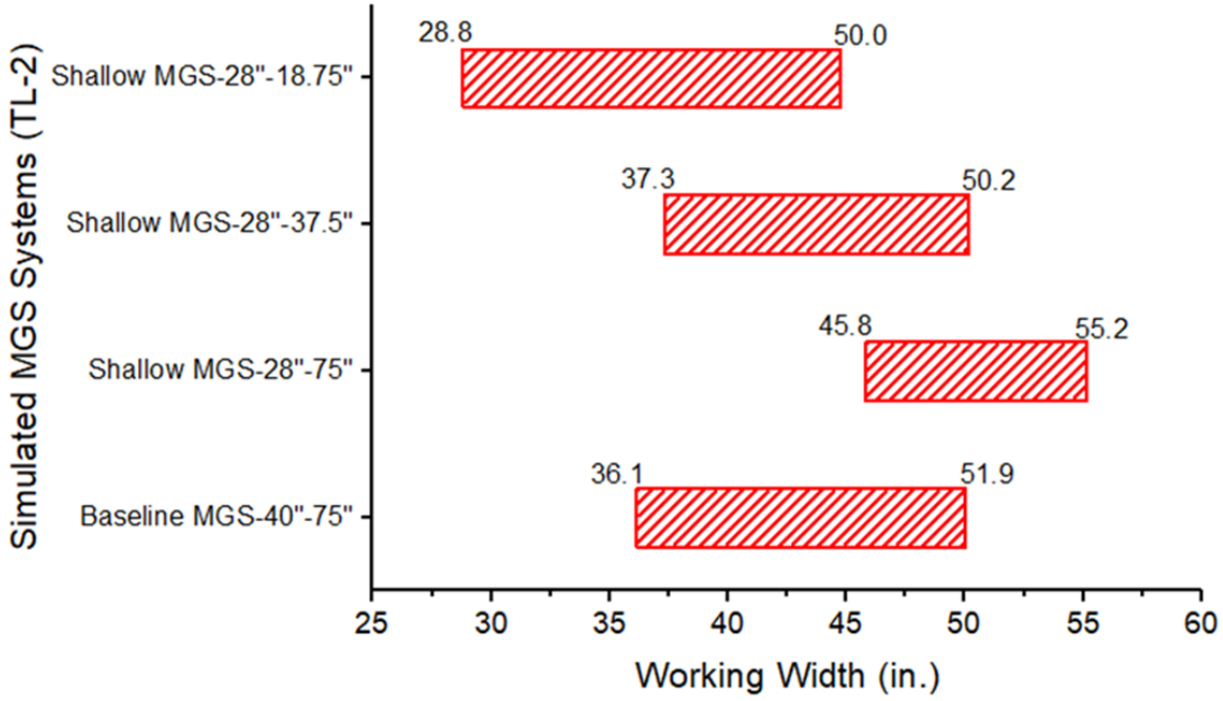

Figure 140. Working Width for Simulated MGS Systems at MASH TL-2 Impact Conditions

For MASH TL-3 impacts, the past MASH test designation no. 3-11 crash tests of the different versions of MGS were collected. Table 31 lists the relevant crash tests of the different versions of MGS with different post spacing.

Table 31. Dynamic Deflection and Working Width of Various Crash Tested, Standard Post Embedment MGS at MASH TL-3 Impact Conditions

Test No.	Post Spacing (in.)	Dynamic Deflection (in.)	Working Width (in.)	Remark
2214MG-2 [29]	75	43.0	48.6	Modified MGS – Update to NCHRP 350 test no 3-11
MGSMIN-1 [30]	75	42.2	48.8	75 ft long MGS, i.e., Minimum effective length for MGS
MGSWP-1 [31]	75	46.3	58.4	MGS with white pine wood posts
MGSSYP-1 [32]	75	40.0	53.8	MGS with southern yellow pine posts
MGSNB-1 [33]	75	34.1	43.2	Non-blocked MGS
ILT-1 [34]	75	44.1	47.3	With light pole behind MGS
690900-KES4 [35]	75	46.0	69.2	With 12-in. King MASH Composite Block on 31 in. MGS
690900-MON2 [36]	75	50.8	57.3	With Mondo Polymer 8 in. Composite Blockout
610211-01-2 [37]	18.75	19.5	37.1	Quarter-post spacing MGS, MASH
610211-01-3 [37]	37.5	25.6	37.3	Half-post spacing MGS, MASH
NPG-6 [38]	18.75	17.6	36.7	Quarter-post spacing MGS, NCHRP 350

In test no. 2214MG-2, which was conducted to the *Update to NCHRP Report 350* TL-3 impact conditions, the MGS had a dynamic deflection and working width of 43.0 and 48.6 in., respectively [29]. Test no. MGSMIN-1 evaluated the minimum effective guardrail length (i.e., the length-of-need) for the MGS. In this test, the 75-ft long MGS had dynamic deflection and working width of 42.2 and 48.8 in., respectively [30]. Two full-scale crash tests, test nos. MGSWP-1 and MGSSYP-1, were conducted on the MGS with white pine wood posts and southern yellow pine posts, respectively. In test no. MGSWP-1, the dynamic deflection and working width were 46.3 and 58.4 in., respectively [31]. In test no. MGSSYP-1, the dynamic deflection and working width

were 40.0 and 53.8 in., respectively [32]. The MGS without blockouts was crash tested in test no. MGSNB-1, which resulted in a dynamic deflection of 34.1 in. and a working width of 43.2 in. [33].

In another study, the combination of an MGS laterally offset 20 in. in front of a luminaire pole was crash tested in test no. ILT-1 to MASH TL-3 impact conditions to evaluate the minimum acceptable lateral offset between the luminaire pole and the back of the post. This crash test resulted in a dynamic deflection of 44.1 in. and a working width of 47.3 in. [34].

The MGS configurations with composite blockouts were also crash tested. In test no. 690900-KES4, the MGS was evaluated with 12-in. King MASH16 composite blockouts, resulting in a dynamic deflection of 46.0 in. and a working width of 69.2 in. [35]. In another study, the MGS with Mondo Polymer Technologies composite blockout with cut-outs (Model# GBl 4SH2) was evaluated, resulting in a dynamic deflection of 50.8 in. and a working width of 57.3 in. [36].

The crash test results of the MGS with reduced post spacing were collected and are shown in Table 31. The MGS with quarter-post spacing was crash tested in test no. 610211-01-2 and had a dynamic deflection of 19.5 in. and working width of 37.1 in. [37]. One full-scale crash test, test no. 610211-01-3, was conducted on MGS with half-post spacing under MASH TL-3 conditions, which failed due to the rail rupture caused by a localized interaction between the W-beam rail and the wood blockout. In continuation of this project, another full-scale crash test, test no. 610211-01-6, was conducted on the MGS with half-post spacing but with blockouts shortened from 14 in. to 10 in. This test resulted in a dynamic deflection of 25.6 in. and working width of 37.3 in. [37]. One full-scale crash test was conducted on the MGS with quarter-post spacing under NCHRP Report 350 TL-3 impact conditions. In this test, test no. NPG-6, dynamic deflection and working width were 17.6 and 36.7 in., respectively [38].

The past crash test results of the MGS with 40-in. deep posts and various post spacings were compiled with the simulated MGS dynamic deflection and working width at MASH TL-3 impact conditions, as shown in Figures 141 and 142. The cases include the MGS with 40-in. deep posts (baseline) and 28-in. deep posts at full-, half-, and quarter-post spacings. The red and blue boxes represent simulation and crash test results, respectively. Similar to TL-2 impacts, for TL-3 simulations of MGS configurations, a lower bound and an upper bound of DD/WW were considered which was associated with the upper bound (strong soil used in the LFCB test series) and an upper bound (MASH limit soil), respectively.

In past crash tests, different versions of MGS, including the MGS with composite blockouts, wood posts, and non-blocked MGS, had a relatively large range of dynamic deflection from 34.1 to 50.8 in., as shown in Figure 141.

The simulated dynamic deflection of MGS with standard post depth and full-post spacing ranged from 42.9 in. for the upper bound of strong soil and 47.3 in. for the lower bound of the MASH soil limit. Note that this range falls well within the crash test data, which ensures some confidence in the simulation results. Also, the simulated dynamic deflection range for the MGS with 40-in. deep posts is narrower than the MGS with shallower posts. In the MGS with 40-in. deep post, post failure and plastic hinge formation govern the behavior. Thus, the soil strength variation does not affect the deflection drastically. While for shallower posts, deflection varies

with soil strength to a greater extent, resulting in a larger dynamic deflection of 53.2 in. in the case of MASH soil limit.

As shown in Figure 141, for the MGS with 28-in. deep and full post spacing, the dynamic deflection of 53.2 in., associated with the MASH soil limit, exceeded the maximum dynamic deflection of the baseline MGS. Thus, 28-in. deep post MGS at full post spacing was not recommended for crash testing. However, it should be noted that this configuration may have potential to meet MASH TL-3 with an increased risk of failure and increased deflections.

For the MGS with 28-in. deep posts and half-post spacing, the simulated dynamic deflection ranged between 28.8 and 40.9 in., which compared well with the baseline MGS. Thus, this system was expected to perform similarly to the MGS with standard post embedment at full-post spacing.

In the MGS with 28-in. deep posts and quarter-post spacing, the simulated TL-3 dynamic deflection ranged between 13.6 and 31.5 in., which was below the baseline MGS. This system was expected to pass MASH TL-3 with lower deflection, but it was not recommended for full-scale crash testing as the reduced deflection may necessitate the need for a stiffness transition to the standard MGS, and the increased number of posts would add the cost.

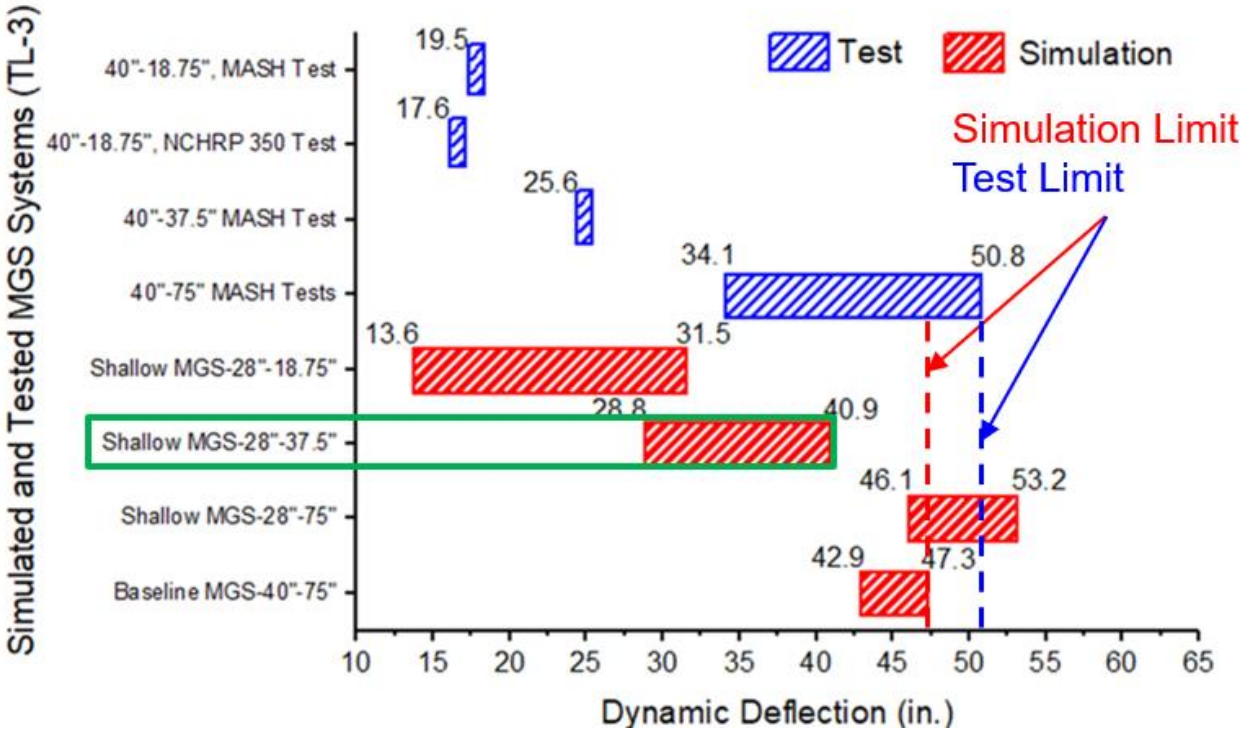

Figure 141. Dynamic Deflection for Simulated and MASH Crash-Tested MGS Systems at MASH TL-3 Impact Conditions

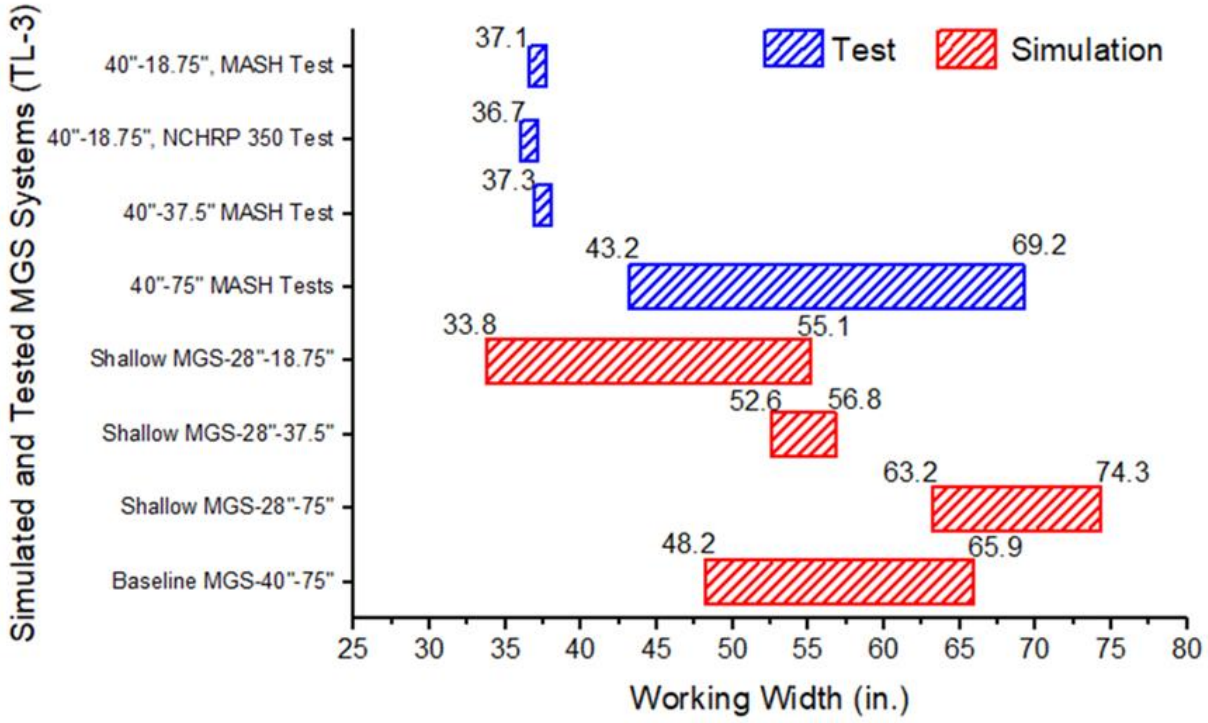

Figure 142. Working Width for Simulated and Crash-Tested MGS Systems at MASH TL-3 Impact Conditions

Based on the TL-2 and TL-3 simulation results and comparison of TL-3 crash test results of the MGS with various post spacings, the MGS with 28-in. deep and half-post spacing was anticipated to perform adequately under MASH TL-3 and TL-2 impacts. Thus, it is recommended for full-scale crash testing in future research. Note that since the same system is recommended for both TL-3 and TL-2 test levels, only one full-scale crash test under MASH test designation no. 3-11 would be necessary, as it is believed that a system meeting TL-3 criteria would perform safely under TL-2 impact conditions. If a future TL-3 crash test failed, the alternative would be a TL-2 evaluation of the configuration or a TL-3 evaluation of a modified system.

8 SUMMARY, CONCLUSIONS, AND RECOMMENDATIONS

The objective of this project was to evaluate the use of the MGS with reduced post embedment and reduced post spacing to satisfy MASH TL-2 and TL-3 impact safety requirements when installed over low-fill culverts. The investigation considered post embedment depths ranging between 28 in. and 40 in. It was desired to determine the shallowest post embedment MGS with full-post spacing, half-post spacing, and quarter post spacing that satisfied MASH TL-2 and TL-3 criteria for low-fill culverts and other applications.

A total of nine of dynamic component tests were conducted on W6x8.5 and W6x16 steel posts embedded in soil to determine the force vs. displacement and energy vs. displacement characteristics of MGS posts with reduced embedment depth and for calibration of LS-DYNA post-soil modeling. Test nos. LFCB-1 and LFCB-2 were conducted on W6x8.5 posts with a 36-in. embedment depth, while test nos. LFCB-3 and LFCB-4 were conducted on W6x8.5 posts with a 32-in. embedment depth. Test nos. LFCB-5 and LFCB-6 were conducted on the W6x8.5 posts with a 28-in. embedment depth. Test nos. LFCB-7, LFCB-8, LFCB-9 were conducted on W6x16 posts with 40-in., 34-in., and 28-in. embedment depths, respectively. All bogie tests on W6x8.5 steel posts resulted in plastic bending of the post below the ground except test no. LFCB-6. In all bogie tests on W6x16 posts, no damage occurred to the post, which provided improved data for isolating the post-soil forces for reduced embedment posts.

LS-DYNA computer models of the posts embedded in soil were developed and validated against the bogie test results. Modeling refinements were conducted to improve the prediction of post behavior in bogie impacts. Various soil tube concepts (i.e., straight flare, flared and curved, and various heights) were developed to replicate post bending and dynamic post-soil resistive forces. Comparison of the simulation results with the data from bogie test nos. LFCB-1 through LFCB-6 confirmed that the model with 6-in. height and 5-degree flare soil tube provided the best overall response.

An LS-DYNA model of the MGS with standard post embedment depth and full-post spacing (baseline model) was validated against test nos. 2214MG-2 and ILT-1 using the Dodge Ram vehicle model. The baseline simulation produced results that were comparable with the full-scale crash tests, and thus was used to evaluate the MGS installations with reduced post embedment and reduced post spacing at TL-2 and TL-3 impact conditions. Also, considering the variability of soil strength and its effect on soil-post behavior, in the particular case of reduced embedment, a lower bound and an upper bound were adopted for the soil strength curve. As such, the lower-bound soil strength was set based on the soil limit specification in MASH, and the upper bound was derived from the relatively strong and stiff soil used in the LFCB test series.

A series of simulations were performed with varied embedment depths and post spacings using both the upper and lower bound soil strengths in order to determine potential crashworthy, reduced embedment MGS configurations under MASH TL-2 and TL-3 impact conditions. Simulated MGS configurations were initiated with 28-in. embedment and standard, half, and quarter-post spacing. Deeper embedments were not planned for simulation unless none of the 28-in. embedment configurations were feasible. All of the 28-in. embedment simulation models indicated stable capture and redirection for TL-2 and TL-3 impacts. However, standard post spacing configurations generated relatively large barrier deflections as compared to the standard MGS system. Because the LS-DYNA post-soil model used in the study was not capable of

indicating or predicting shallow embedment posts rotating out of the soil under large displacements, the researchers elected to compare the simulated configurations with both baseline simulation models and available crash test data in terms of dynamic deflection and working width. The focus of these comparisons was to identify configurations that demonstrated dynamic deflections and working widths that were consistent with the range of dynamic deflections and working widths established in the baseline simulation models and existing crash tests of the MGS with standard post spacing and embedment. It was believed that reduced embedment configurations that had a dynamic deflection and working width closer to the standard MGS would have a higher chance of meeting future MASH full-scale crash testing and would be less likely to require a stiffness transition.

For TL-2 impact conditions, the MGS with a 28-in. embedment depth and half-post spacing had a simulated dynamic deflection that ranged between 15.2 and 28.3 in., which compared well with the baseline MGS range of 25 in. and 31.2 in. Thus, this system is expected to perform similarly to the MGS with standard post embedment at full-post spacing and was recommended for full-scale crash testing in future research.

Similarly, for TL-3 impact conditions, the MGS with a 28-in. embedment depth and half-post spacing had a simulated dynamic deflection that ranged between 28.8 and 40.9 in., which was similar to the standard MGS range of 34.1 in. and 50.8 in. (dynamic deflection range collected from the past crash tests) as well as the simulated baseline MGS range of 46.1 and 53.2 in. Thus, this system would perform similarly to the MGS with standard post embedment at full-post spacing and was recommended for full-scale crash testing in future research.

Since the same MGS configuration is recommended for both TL-3 and TL-2 test levels, only one full-scale crash test, MASH test designation no. 3-11, is deemed necessary to evaluate the modified MGS. It is assumed that successful crash testing under TL-3 would justify adequate performance at lower test levels. If the TL-3 test fails, the alternative would be TL-2 testing or a stiffer MGS (i.e., 28-in. quarter-post spacing).

Note that there is no need for a transition between the half-post and full-post spacing MGS systems with a shallow embedment depth of 28 in. as the stiffness and dynamic deflection of these two systems are very similar.

This research effort focused on the MGS with steel posts at reduced embedment depths. Since the MGS with wood posts have demonstrated a similar performance as compared to the steel-post MGS, it is believed that the recommendations made based on this study findings will be applicable to the MGS with wood posts. Note that a concern for wood posts embedded in extremely strong soil exists with wood-post MGS at any post embedment depth. Previous testing of wood post systems has shown that rapid fracture of wood posts can degrade the energy absorption of the barrier and can lead to rail rupture and pocketing.

Of another concern, frozen soil may adhere to the post and apply upward pressure when it expands. Deeper posts that extend below the frost line are less susceptible, but shallow posts may cause an issue. Thus, for states with extreme cold and a deep frost line, other MASH-compliant options for guardrails installed over low-fill structures such as long-span guardrails, strong-post guardrail attachments to the culvert slab, and weak-post guardrail systems anchored to the culvert slab or headwall may be more appropriate.

The simulations performed on the standard MGS with the upper and lower bound soil strength under both TL-2 and TL-3 impact conditions can provide guidance for end users on reasonable expected deflection and working width values for the MGS across a range of soil conditions. TL-2 simulated dynamic deflection of the standard MGS ranged from 25.0 in. (for upper-bound soil strength) to 31.2 in. (for lower-bound soil strength). The TL-2 simulated working width of the standard MGS ranged from 36.1 in. (for upper-bound soil strength) to 51.9 in. (for lower-bound soil strength). The TL-3 simulated dynamic deflection of the standard MGS ranged from 42.9 in. (for upper-bound soil strength) to 47.3 in. (for lower-bound soil strength). The TL-2 simulated working width of the standard MGS ranged from 48.2 in. (for upper-bound soil strength) to 65.9 in. (for lower-bound soil strength).

9 REFERENCES

1. *Manual for Assessing Safety Hardware (MASH), Second Edition*, American Association of State Highway and Transportation Officials (AASHTO), Washington, D.C., 2016.

2. Bielenberg, R.W., Faller, R.K., Rohde, J.R., Reid, J.D., Sicking, D.L., Holloway, J.C., Allison, E.M., and Polivka, K.A., *Midwest Guardrail System for Long-Span Culvert Applications*, Research Report No. TRP-03-187-07, Midwest Roadside Safety Facility, University of Nebraska-Lincoln, Lincoln, Nebraska, November 16, 2007.

3. Asadollahi Pajouh, M., Bielenberg, R.W., Schmidt-Rasmussen J.D., Bai, F., Faller, R.K., and Holloway. *Dynamic Testing and Evaluation of Culvert-Mounted, Strong-Post MGS to TL-3 Guidelines of MASH 2016*. MwRSF Research Report No. TRP-03-383-20-R1, Midwest Roadside Safety Facility, University of Nebraska-Lincoln, Lincoln, Nebraska, November 2, 2020.

4. Asadollahi Pajouh, M., Bielenberg, R.W., Schmidt-Rasmussen, J.D., and Faller, R.K. *Crash Testing and Evaluation of Culvert-Mounted Midwest Guardrail System.* Transportation Research Record, 2674(7), 161–171. https://doi.org/10.1177/0361198120921168

5. Polivka, K.A., Faller, R.K., Sicking, D.L., Rohde, J.R., Reid, J.D., and Holloway, J.C., *NCHRP 350 Development and Testing of a Guardrail Connection to Low-Fill Culverts*, Research Report No. TRP-03-114-02, Midwest Roadside Safety Facility, University of Nebraska-Lincoln, Lincoln, NE, November 1, 2002

6. Williams, W.F. and Menges, W.L., *MASH Test 3-11 of the W-beam Guardrail on Low-Fill Box Culvert*, Test Report No. 405160-23-2, Texas Transportation Institute, Texas A&M University, College Station, Texas, February 2012.

7. Thiele, J.C., Sicking, D.L., Faller, R.K., Bielenberg, R.W., Lechtenberg, K.A., Reid, J.D., and Rosenbaugh, S.K., *Development of a Low-Cost, Energy-Absorbing Bridge Rail*, Research Report No. TRP-03-226-10, Midwest Roadside Safety Facility, University of Nebraska-Lincoln, Lincoln, Nebraska, August 2010.

8. Thiele, J.C., Sicking, D. L., Lechtenberg, K.A., Reid, J.D., Faller R. K., Bielenberg, R.W. and Rosenbaugh, S.K. *Development of a Low-Cost, Energy-Absorbing Bridge Rail. Transportation Research Record No. 2262*. Transportation Research Board, National Research Council, Washington, D.C., 2011.

9. Faller, R.K., Rosenbaugh, S.K., Asadollahi Pajouh, M., *Top-Mounted Sockets for Weak-Post MGS on Culverts*, Research Report No. TRP-03-368-19, Midwest Roadside Safety Facility, University of Nebraska-Lincoln, Lincoln, Nebraska, October 2019.

10. Asadollahi Pajouh, M., Rosenbaugh, S.K., and Faller, R.K., Development and Evaluation of Top-Mounted Sockets for Weak-Post, Midwest Guardrail System on Culverts, Journal of Transportation Research Record, 10–21. https://doi.org/10.1177/03611981221089296

11. Hirsch, T.J., and Beggs, D., *Use of Guardrails on Low-Fill Bridge Length Culverts*, Research Report No. 405-2F, Texas A&M Transportation Institute, Texas A&M University, College Station, TX, August 1987.

12. Schmidt, T.L, Mongiardini, M., Bielenberg, R.W., Lechtenberg, K.A, Reid, J.D., and Faller, R.K., *Dynamic Testing of MGS W6x8.5 Posts at Decreased Embedment*, Final Report to the Nebraska Department of Roads, Transportation Research Report No. TRP-03-271-12, Midwest Roadside Safety Facility, University of Nebraska-Lincoln, Lincoln, Nebraska, December 17, 2012.

13. Ross, H.E., Sicking, D.L., Zimmer, R.A., and Michie, J.D., *Recommended Procedures for the Safety Performance Evaluation of Highway Features*, National Cooperative Highway Research Program (NCHRP) Report 350, Transportation Research Board, Washington, D.C., 1993.

14. *Manual for Assessing Safety Hardware (MASH)*, American Association of State Highway and Transportation Officials (AASHTO), Washington, D.C., 2009.

15. Julin, R.D., Reid, J.D., Faller, R.K., Mongiardini M., *Determination of the Maximum MGS Mounting Height - Phase II Detailed Analysis with LS-DYNA*, Research Report No. TRP-03-274-12, Midwest Roadside Safety Facility, University of Nebraska-Lincoln, Lincoln, December 5, 2012.

16. Asadollahi Pajouh, M., Julin, R.D., Stolle C.S., Reid, J.D., and Faller, R.K., *Rail Height Effects on Safety Performance of Midwest Guardrail System*, Journal of Traffic Injury Prevention, 19:2, 219-224, DOI: 10.1080/15389588.2017.1353687.

17. Society of Automotive Engineers (SAE), Instrumentation for Impact Test – Part 1 – Electronic Instrumentation, SAE J211/1 MAR95, New York City, New York, July 2007.

18. Hallquist, J.O., (2007). *LS-DYNA Keyword User's Manual*, LS-DYNA R7.1, Livermore, CA: Livermore Software Technology Corporation.

19. Asadollahi Pajouh, M., Schmidt, J.D., Bielenberg, R.W., Reid, J.D., and Faller, R.K., Simplified Soil-Pile Interaction Modeling under Impact Loading, *In Geotechnical Earthquake Engineering and Soil Dynamics Numerical Modeling and Soil-Structure Interaction* Reston, VA, American Society of Civil Engineers, pp. 269-280, 2018.

20. Julin, R.D., Reid, J.D., Faller, R.K., and Mongiardini, M., *Determination of the Maximum MGS Mounting Height – Phase II Detailed Analysis with LS-DYNA,* Final Report to the Midwest States' Regional Pooled Fund Program, Transportation Research Report No. TRP-03-274-12, Project No. TPF-5(193)-Year 20, Midwest Roadside Safety Facility, University of Nebraska-Lincoln, December 5, 2012.

21. Mongiardini, M., Ray, M., Plaxico, C., and Anghileri, M., *Procedures for Verification and Validation of Computer Simulations used for Roadside Safety Applications*, Final Report to the National Cooperative Highway Research Program (NCHRP), NCHRP Report No. W179, Project No. 22-24, Worcester Polytechnic Institute, 2010.

22. Julin, R.D., *Midwest Guardrail System LS-DYNA Model Comparison*, MwRSF Internal Report, Midwest Roadside Safety Facility, University of Nebraska-Lincoln, October 6, 2011.

23. Weiland, N.A., Stolle, C.S., Reid, J.D., Faller, R.K., Bielenberg, R.W., and Lechtenberg, K.A, *MGS Dynamic Deflections and Working Widths at Lower Speeds*, Final Report to the Midwest States' Regional Pooled Fund Program, Transportation Research Report No. TRP-03-314-15, Project No. TPF-5(193)-Year 24, Midwest Roadside Safety Facility, University of Nebraska-Lincoln, September 29, 2015.

24. Schmidt, J.D.., Reid, J.D., Bielenberg, R.W., and Faller, R.K, *Numerical Investigation of the Performance of Steel Guardrail Systems with Varied Mechanical Properties*, Final Report to the Advanced Coatings and Construction Solutions, MwRSF Research Report No. TRP-03-290-13, Midwest Roadside Safety Facility, University of Nebraska-Lincoln, July 25, 2013.

25. Mongiardini, M., Faller, R.K., Reid, J.D., Sicking, D.L., Stolle, C.S., and Lechtenberg, K.A., *Downstream Anchoring Requirements for the Midwest Guardrail System,* Report No. TRP-03-279-13, Midwest Roadside Safety Facility, University of Nebraska-Lincoln, Lincoln, Nebraska, October 28, 2013.

26. Mongiardini, M., Faller, R.K., Reid, J.D., and Sicking, D.L., *Dynamic Evaluation and Implementation Guidelines for a Non-Proprietary W-Beam Guardrail Trailing-End Terminal,* Paper No. 13-5277, Transportation Research Record No. 2377, Journal of the Transportation Research Board, TRB AFB20 Committee on Roadside Safety Design, Transportation Research Board, Washington D.C., pp. 61-73, January 2013.

27. Stolle, C.S., Reid, J.D., Faller, R.K., and Mongiardini, M., *Dynamic Strength of a Modified W-Beam BCT Trailing-End Termination,* Paper No. IJCR 886R1, Manuscript ID 1009308, International Journal of Crashworthiness, Taylor & Francis, Vol. 20, Issue 3, pp. 301-315, Published online February 23, 2015.

28. Vehicle Modeling, National Crash Analysis Center, George Washington University, Washington, D.C. Retrieved from: http://www.ncac.gwu.edu/research/reports.html, August 20, 2014.

29. Polivka, K.A., Faller, R.K., Sicking, D.L., Rohde, J.R., Bielenberg, R.W., and Reid, J.D. *Performance Evaluation of the Midwest Guardrail System – Update to NCHRP 350 Test No. 3-11 with 28" C.G. Height (2214MG-2)*, Report No. TRP-03-171-06, Midwest Roadside Safety Facility, University of Nebraska-Lincoln, Lincoln, 2006.

30. Weiland, N.A., Reid, J.D., Faller, R.K., Sicking, D.L., Bielenberg, R.W., and Lechtenberg, K.A., *Minimum Effective Guardrail Length for the MGS*, Report No. TRP-03-276-13, Midwest Roadside Safety Facility, University of Nebraska-Lincoln, Lincoln, 2013.

31. Stolle, C.J., Lechtenberg, K.A., Faller, R.K., Rosenbaugh, S.K., Sicking, D.L., and Reid, J.D. *Evaluation of the Midwest Guardrail System (MGS) with White Pine Wood Posts*, Report No. TRP-03-241-11, Midwest Roadside Safety Facility, University of Nebraska-Lincoln, Lincoln, 2011.

32. Gutierrez, D.A., Lechtenberg, K.A., Bielenberg, R.W., Faller, R.K., Reid, J.D., and Sicking, D.L., *Midwest Guardrail System (MGS) with Southern Yellow Pine Posts*, Report No. TRP-03-272-13, Midwest Roadside Safety Facility, University of Nebraska-Lincoln, Lincoln, 2013.

33. Schrum, K.D., Lechtenberg, K.A., Bielenberg, R.W., Rosenbaugh, S.K., Faller, R.K., Reid, J.D., and Sicking, D.L., *Safety Performance Evaluation of the Non-Blocked Midwest Guardrail System (MGS)*, Report No. TRP-03-262-12, Midwest Roadside Safety Facility, University of Nebraska-Lincoln, Lincoln, 2012.

34. Asadollahi Pajouh, M., Bielenberg, R.W., Schmidt, J.D., Lingenfelter, J., Faller, R.K., and Reid, J.D., *Placement of Breakaway Light Poles Located Directly Behind Midwest Guardrail System (MGS)*, Report No. TRP-03-361-17, Midwest Roadside Safety Facility, University of Nebraska-Lincoln, Lincoln, 2017.

35. Eckert B. R., Letter to Trinity Highway Products, LLC3617 Cincinnati Avenue, Rocklin, CA 95765, December 21, 2020. Retrieved from https://safety.fhwa.dot.gov/roadway_dept/countermeasures/reduce_crash_severity/barriers/pdf/b353.pdf.

36. Ellis M., Letter to Mondo Polymer Technologies, Inc, P.O Box 250, Reno, OH 45773, September 27, 2017. Retrieved from https://safety.fhwa.dot.gov/roadway_dept/countermeasures/reduce_crash_severity/barriers/pdf/b278a.pdf.

37. Kovar, J.C., Bligh R.P., Menges W. L., Schroeder G. E., Schroeder W., Wegenast S.A., Griffith B. L., and Kuhn, D.L., *MASH Crash Testing and Evaluation of the MGS Guardrail System with Reduced Post Spacing*, Report No. 610211-01, Texas A&M Transportation Institute, Texas A&M University, College Station, April 2022.

38. Polivka, K.A., Faller, R.K., Sicking, D.L., Reid, J.D., Rohde, J.R., Holloway, J.C., Bielenberg R.W., and Kuipers, B.D., *Development of the Midwest Guardrail System (MGS) for Standard and Reduced Post Spacing and in Combination with Curbs*, Report No. TRP-03-139-04. Midwest Roadside Safety Facility, University of Nebraska-Lincoln, Lincoln, 2004.

10 APPENDICES

Appendix A. Material Specifications

Table A-1. Bill of Materials, Test Nos. LFCB-1 through LFCB-6

Item No.	Description	Material Specification	Reference
a1	W6x8.5, 68" Long Steel Post	ASTM A992	H#55062395/02
a2	W6x8.5, 64" Long Steel Post	ASTM A992	H#55062395/02
a3	W6x8.5, 60" Long Steel Post	ASTM A992	H#55062395/02

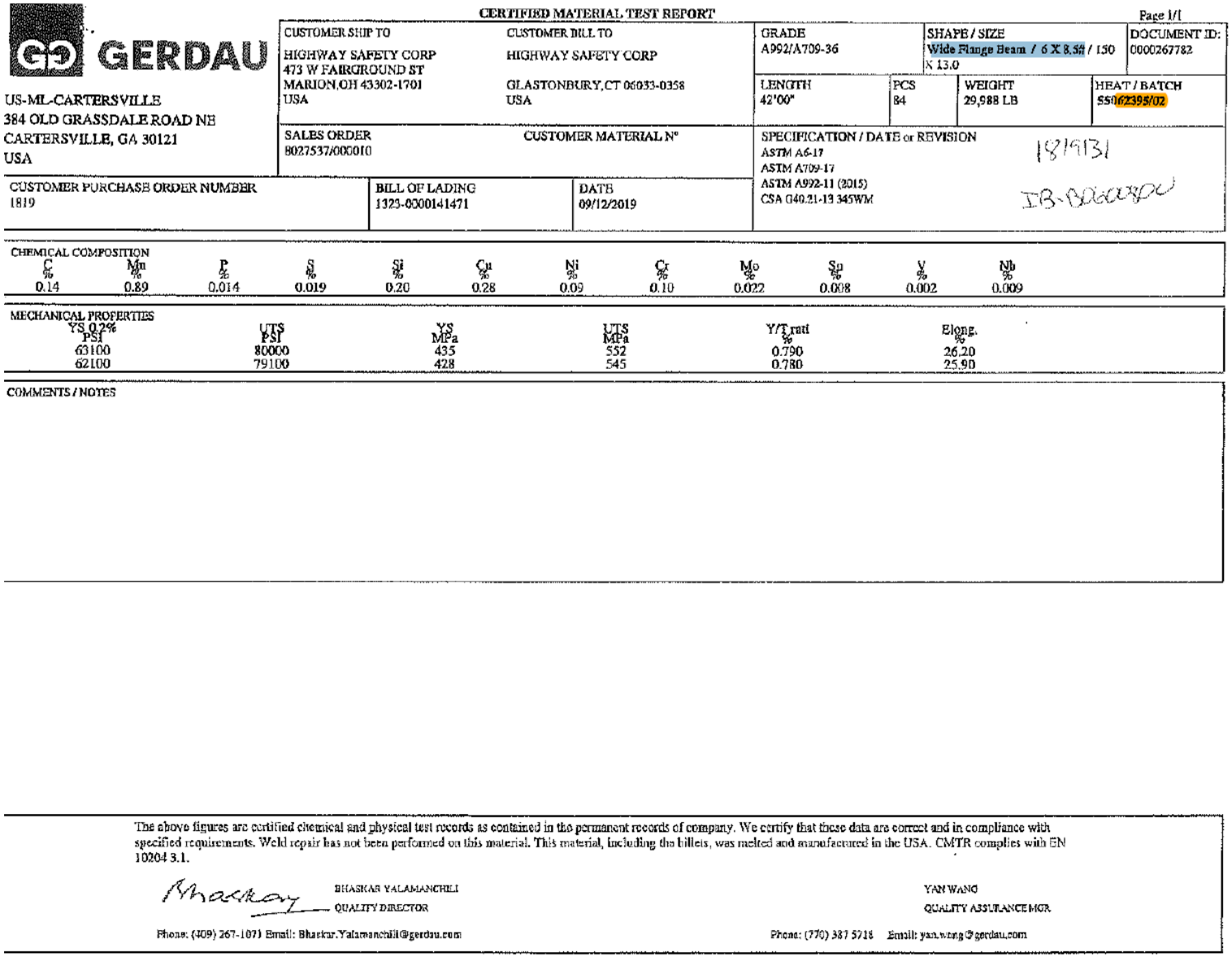

GERDAU

US-ML-CARTERSVILLE
384 OLD GRASSDALE ROAD NE
CARTERSVILLE, GA 30121
USA

CERTIFIED MATERIAL TEST REPORT

Page 1/1

CUSTOMER SHIP TO	CUSTOMER BILL TO
HIGHWAY SAFETY CORP 473 W FAIRGROUND ST MARION,OH 43302-1701 USA	HIGHWAY SAFETY CORP GLASTONBURY,CT 06033-0358 USA

GRADE	SHAPE / SIZE	DOCUMENT ID:
A992/A709-36	Wide Flange Beam / 6 X 8.5# / 150 X 13.0	0000267782

LENGTH	PCS	WEIGHT	HEAT / BATCH
42'00"	84	29,988 LB	55062395/02

SALES ORDER	CUSTOMER MATERIAL N°
8027537/000010	

SPECIFICATION / DATE or REVISION
ASTM A6-17
ASTM A709-17
ASTM A992-11 (2015)
CSA G40.21-13 345WM

1819131

CUSTOMER PURCHASE ORDER NUMBER	BILL OF LADING	DATE
1819	1325-0000141471	09/12/2019

CHEMICAL COMPOSITION

C %	Mn %	P %	S %	Si %	Cu %	Ni %	Cr %	Mo %	Sn %	V %	Nb %
0.14	0.89	0.014	0.019	0.20	0.28	0.09	0.10	0.022	0.008	0.002	0.009

MECHANICAL PROPERTIES

YS 0.2% PSI	UTS PSI	YS MPa	UTS MPa	Y/T ratio %	Elong. %
63100	80000	435	552	0.790	26.20
62100	79100	428	545	0.780	25.90

COMMENTS / NOTES

The above figures are certified chemical and physical test records as contained in the permanent records of company. We certify that these data are correct and in compliance with specified requirements. Weld repair has not been performed on this material. This material, including the billets, was melted and manufactured in the USA. CMTR complies with EN 10204 3.1.

BHASKAR YALAMANCHILI
QUALITY DIRECTOR
Phone: (409) 267-1071 Email: Bhaskar.Yalamanchili@gerdau.com

YAN WANG
QUALITY ASSURANCE MGR
Phone: (770) 387 5718 Email: yan.wang@gerdau.com

Figure A-1. W6x8.5 Steel Post, Test Nos. LFCB-1 through LFCB-6 (Item Nos. a1, a2, and a3)

Table A-2. Bill of Materials, Test Nos. LFCB-7 through LFCB-9

Item No.	Description	Material Specification	Reference
a1	W6x16, 72" Long Steel Post	ASTM A992	H#58039017/02 H#59091001/02
a2	W6x16, 66" Long Steel Post	ASTM A992	H#58039017/02 H#59091001/02
a3	W6x16, 60" Long Steel Post	ASTM A992	H#58039017/02 H#59091001/02

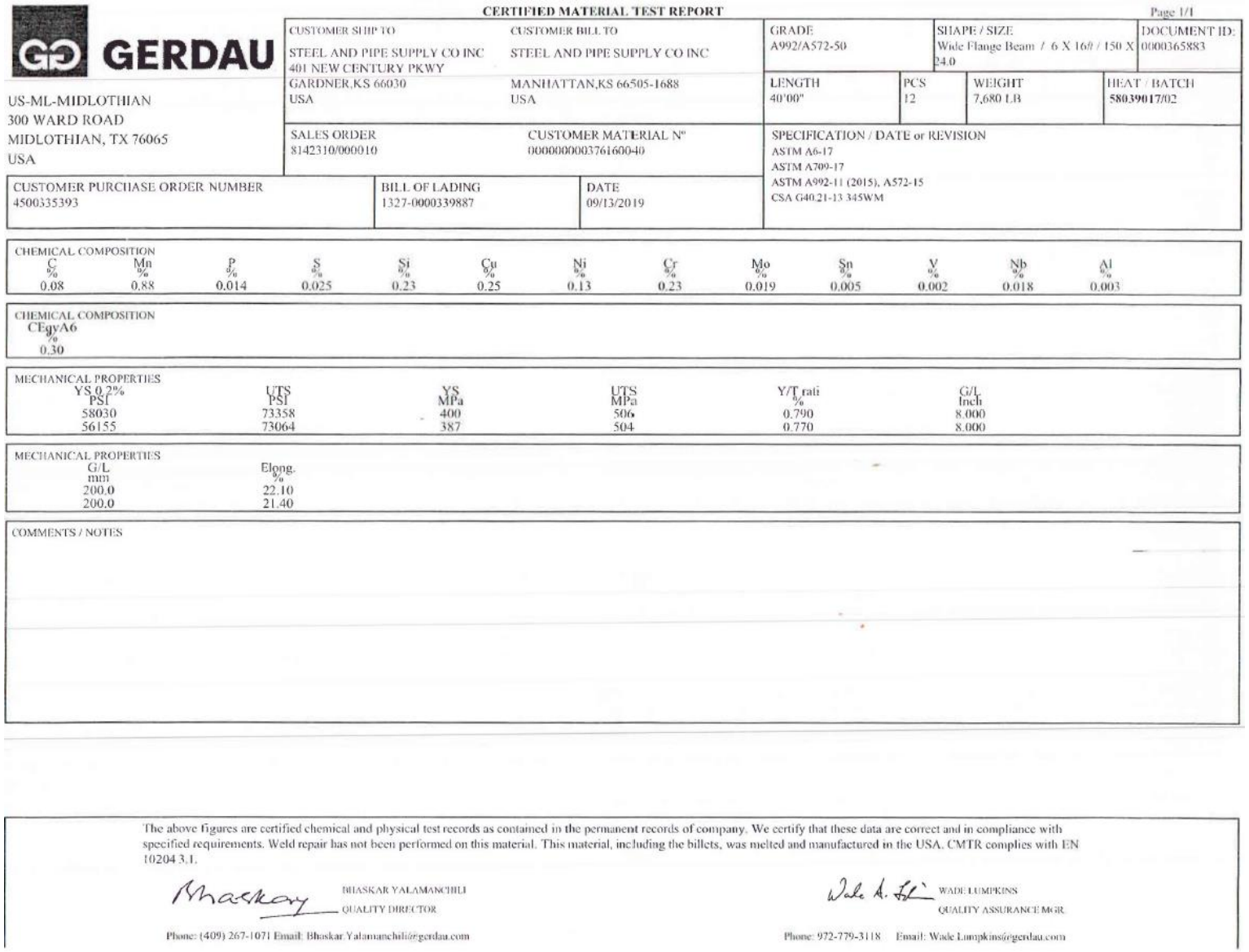

CERTIFIED MATERIAL TEST REPORT Page 1/1

GERDAU

US-ML-MIDLOTHIAN
300 WARD ROAD
MIDLOTHIAN, TX 76065
USA

CUSTOMER SHIP TO	CUSTOMER BILL TO
STEEL AND PIPE SUPPLY CO INC 401 NEW CENTURY PKWY GARDNER,KS 66030 USA	STEEL AND PIPE SUPPLY CO INC MANHATTAN,KS 66505-1688 USA

GRADE	SHAPE / SIZE	DOCUMENT ID:
A992/A572-50	Wide Flange Beam / 6 X 16# / 150 X 24.0	0000365883

LENGTH	PCS	WEIGHT	HEAT / BATCH
40'00"	12	7,680 LB	**58039017/02**

SALES ORDER	CUSTOMER MATERIAL N°
8142310/000010	000000000376160040

SPECIFICATION / DATE or REVISION
ASTM A6-17
ASTM A709-17
ASTM A992-11 (2015), A572-15
CSA G40.21-13 345WM

CUSTOMER PURCHASE ORDER NUMBER	BILL OF LADING	DATE
4500335393	1327-0000339887	09/13/2019

CHEMICAL COMPOSITION

C %	Mn %	P %	S %	Si %	Cu %	Ni %	Cr %	Mo %	Sn %	V %	Nb %	Al %
0.08	0.88	0.014	0.025	0.23	0.25	0.13	0.23	0.019	0.005	0.002	0.018	0.003

CHEMICAL COMPOSITION

CEgvA6 %
0.30

MECHANICAL PROPERTIES

YS 0.2% PSI	UTS PSI	YS MPa	UTS MPa	Y/T rati %	G/L Inch
58030	73358	400	506	0.790	8.000
56155	73064	387	504	0.770	8.000

MECHANICAL PROPERTIES

G/L mm	Elong. %
200.0	22.10
200.0	21.40

COMMENTS / NOTES

The above figures are certified chemical and physical test records as contained in the permanent records of company. We certify that these data are correct and in compliance with specified requirements. Weld repair has not been performed on this material. This material, including the billets, was melted and manufactured in the USA. CMTR complies with EN 10204 3.1.

BHASKAR YALAMANCHILI
QUALITY DIRECTOR
Phone: (409) 267-1071 Email: Bhaskar.Yalamanchili@gerdau.com

WADE LUMPKINS
QUALITY ASSURANCE MGR
Phone: 972-779-3118 Email: Wade.Lumpkins@gerdau.com

Figure A-2. W6x16 Steel Post, Test Nos. LFCB-7 through LFCB-9 (Item Nos. a1, a2, and a3)

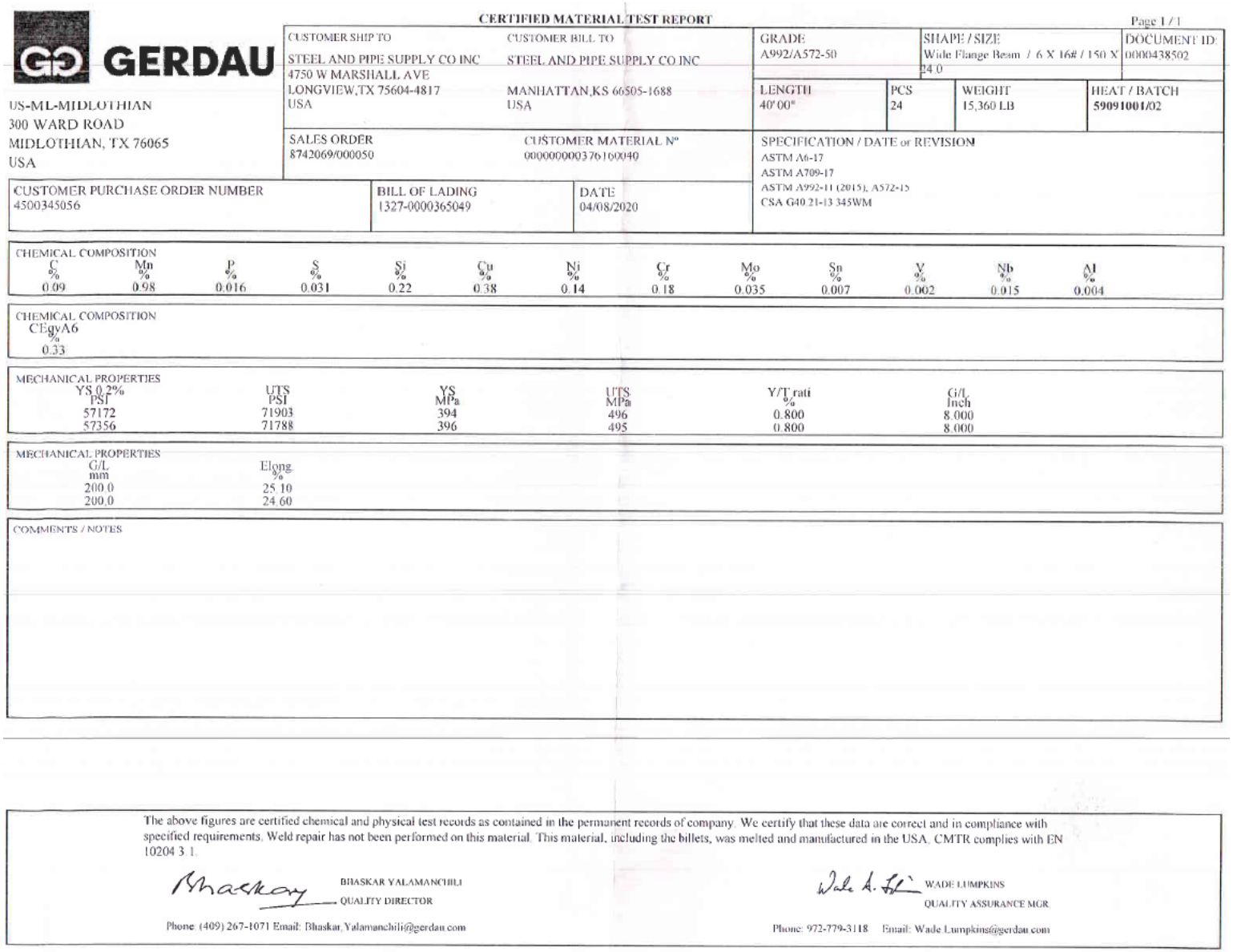

GERDAU

CERTIFIED MATERIAL TEST REPORT

Page 1 / 1

US-ML-MIDLOTHIAN
300 WARD ROAD
MIDLOTHIAN, TX 76065
USA

CUSTOMER SHIP TO
STEEL AND PIPE SUPPLY CO INC
4750 W MARSHALL AVE
LONGVIEW,TX 75604-4817
USA

CUSTOMER BILL TO
STEEL AND PIPE SUPPLY CO INC
MANHATTAN,KS 66505-1688
USA

GRADE	SHAPE / SIZE	DOCUMENT ID
A992/A572-50	Wide Flange Beam / 6 X 16# / 150 X 24'0	0000438502

LENGTH	PCS	WEIGHT	HEAT / BATCH
40'00"	24	15,360 LB	59091001/02

SALES ORDER: 8742069/000050

CUSTOMER MATERIAL N°: 000000000376160040

SPECIFICATION / DATE or REVISION
ASTM A6-17
ASTM A709-17
ASTM A992-11 (2015), A572-15
CSA G40.21-13 345WM

CUSTOMER PURCHASE ORDER NUMBER: 4500345056

BILL OF LADING: 1327-0000365049

DATE: 04/08/2020

CHEMICAL COMPOSITION

C %	Mn %	P %	S %	Si %	Cu %	Ni %	Cr %	Mo %	Sn %	V %	Nb %	Al %
0.09	0.98	0.016	0.031	0.22	0.38	0.14	0.18	0.035	0.007	0.002	0.015	0.004

CHEMICAL COMPOSITION

CEgvA6 %
0.33

MECHANICAL PROPERTIES

YS 0.2% PSI	UTS PSI	YS MPa	UTS MPa	Y/T rati %	G/L Inch
57172	71903	394	496	0.800	8.000
57356	71788	396	495	0.800	8.000

MECHANICAL PROPERTIES

G/L mm	Elong %
200.0	25.10
200.0	24.60

COMMENTS / NOTES

The above figures are certified chemical and physical test records as contained in the permanent records of company. We certify that these data are correct and in compliance with specified requirements. Weld repair has not been performed on this material. This material, including the billets, was melted and manufactured in the USA. CMTR complies with EN 10204 3.1.

BHASKAR YALAMANCHILI
QUALITY DIRECTOR
Phone: (409) 267-1071 Email: Bhaskar.Yalamanchili@gerdau.com

WADE LUMPKINS
QUALITY ASSURANCE MGR.
Phone: 972-779-3118 Email: Wade.Lumpkins@gerdau.com

Figure A-3. W6x16 Steel Post, Test Nos. LFCB-7 through LFCB-9 (Item Nos. a1, a2, and a3)

Appendix B. Bogie Test Results

The results of the recorded data from each accelerometer for every dynamic bogie test are provided in the summary sheets found in this appendix. Summary sheets include acceleration, velocity, and deflection vs. time plots as well as force vs. deflection and energy vs. deflection plots.

MIDWEST ROADSIDE SAFETY FACILITY

Bogie Test Summary

Test Information

Test Description:	Reduced Embedment Post For Shallow Fill Culvert
Test Number:	LFCB-1
Test Date:	3/31/2020
Failure Type:	Rotation in soil and post hinging

Post Properties

Post Type:	Steel
Post Size:	W6x8.5
Post Length:	68
Embedment Depth:	36
Orientation:	Strong Axis - 90 Degrees

Soil Properties

Gradation:	102019
Moisture Content:	NA
Compaction Method:	HE8

Bogie Properties

Impact Velocity:	20.62 mph	(30.24 ft/s)
Impact Height:	25	
Bogie Mass:	1865 lb	

Data Acquired

Accelerometer:	SLICE-1
Camera Data:	AOS-9, PAN-6

Test Results Summary

Event Duration:	0.1381	sec
Max. Deflection:	31.7	in.
Peak Force:	14.8	k
Initial Linear Stiffness:	5.1	k/in.
Total Energy:	264.5	k-in.

	@ 5"	@ 10"	@ 15"	@20"
Average Force (k)	10.62	11.12	11.05	10.59
Energy (k-in.)	53.1	111.2	165.8	211.9

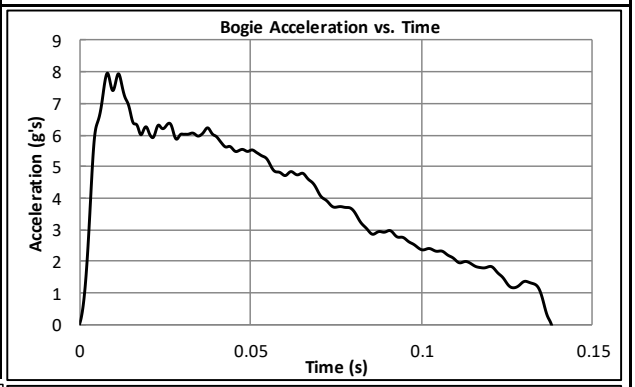

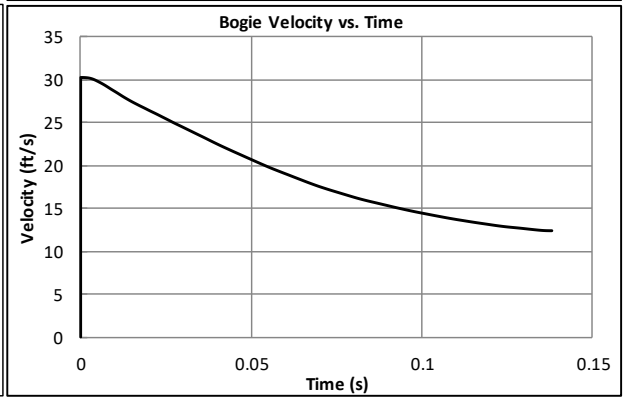

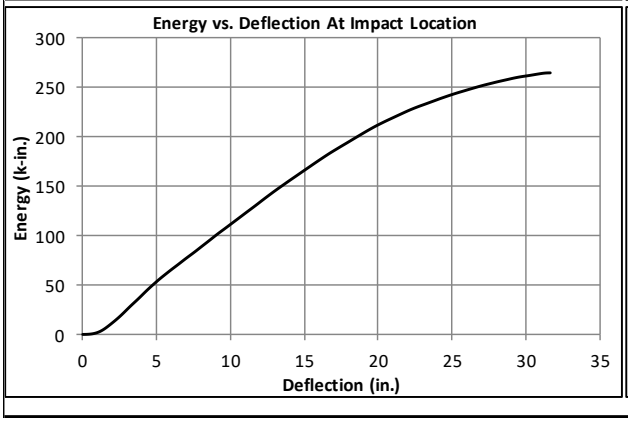

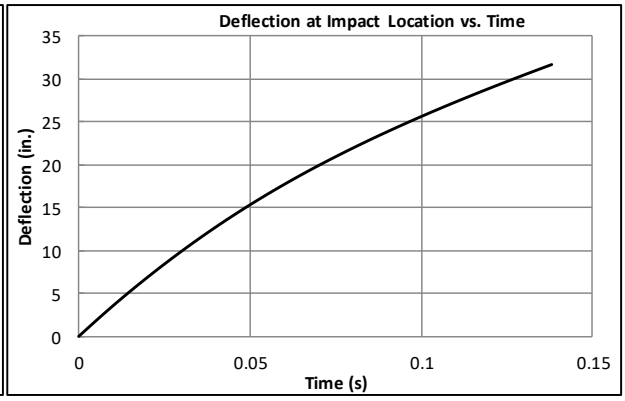

Figure B-1. Test No. LFCB-1 Results (SLICE-1)

MIDWEST ROADSIDE SAFETY FACILITY

Bogie Test Summary

Test Information

Test Description:	Reduced Embedment Post For Shallow Fill Culvert
Test Number:	LFCB-1
Test Date:	3/31/2020
Failure Type:	Rotation in soil and post hinging

Post Properties

Post Type:	Steel
Post Size:	W6x8.5
Post Length:	68
Embedment Depth:	36
Orientation:	Strong Axis - 90 Degrees

Soil Properties

Gradation:	102019
Moisture Content:	NA
Compaction Method:	HE8

Bogie Properties

Impact Velocity:	20.62 mph	(30.24 ft/s)
Impact Height:	25	
Bogie Mass:	1865 lb	

Data Acquired

Accelerometer:	SLICE-2
Camera Data:	AOS-9, PAN-6

Test Results Summary

Event Duration:	0.1393	sec
Max. Deflection:	32.0	in.
Peak Force:	14.3	k
Initial Linear Stiffness:	5.0	k/in.
Total Energy:	264.3	k-in.

	@ 5"	@ 10"	@ 15"	@20"
Average Force (k)	10.33	10.89	10.93	10.49
Energy (k-in.)	51.6	108.9	164.0	209.9

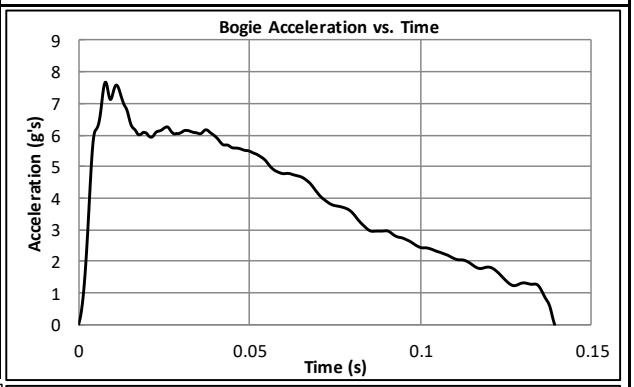

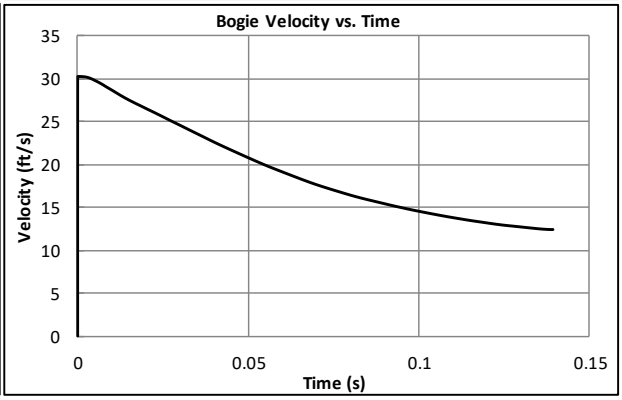

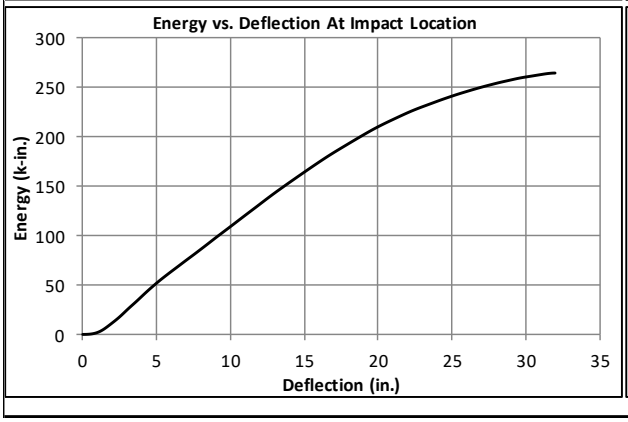

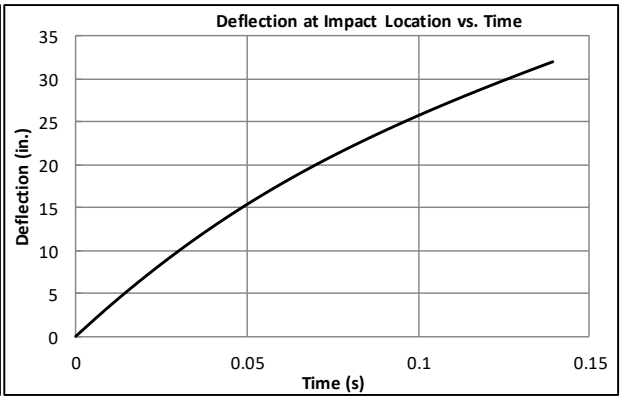

Figure B-2. Test No. LFCB-1 Results (SLICE-2)

MIDWEST ROADSIDE SAFETY FACILITY

Bogie Test Summary

Test Information

Test Description:	Reduced Embedment Post For Shallow Fill Culvert
Test Number:	LFCB-2
Test Date:	3/31/2020
Failure Type:	Rotation in soil and post hinging

Post Properties

Post Type:	Steel
Post Size:	W6x8.5
Post Length:	68
Embedment Depth:	36
Orientation:	Strong Axis - 90 Degrees

Soil Properties

Gradation:	102019
Moisture Content:	NA
Compaction Method:	He8

Bogie Properties

Impact Velocity:	22.26 mph	(32.64 ft/s)
Impact Height:	25	
Bogie Mass:	1865 lb	

Data Acquired

Accelerometer:	SLICE-1
Camera Data:	AOS-9, PAN-6

Test Results Summary

Event Duration:	0.1040	sec
Max. Deflection:	30.5	in.
Peak Force:	15.7	k
Initial Linear Stiffness:	5.3	k/in.
Total Energy:	225.3	k-in.

	@ 5"	@ 10"	@ 15"	@20"
Average Force (k)	11.00	11.61	11.19	9.98
Energy (k-in.)	55.0	116.1	167.9	199.7

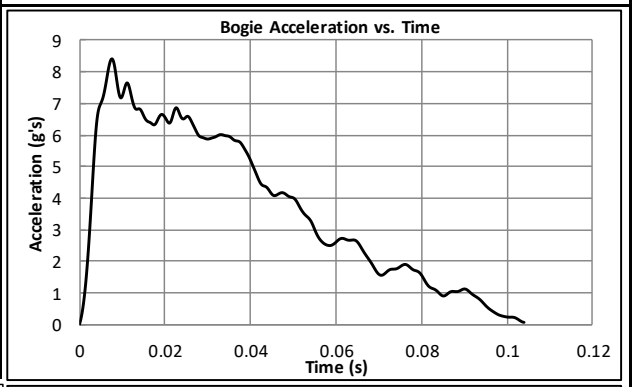

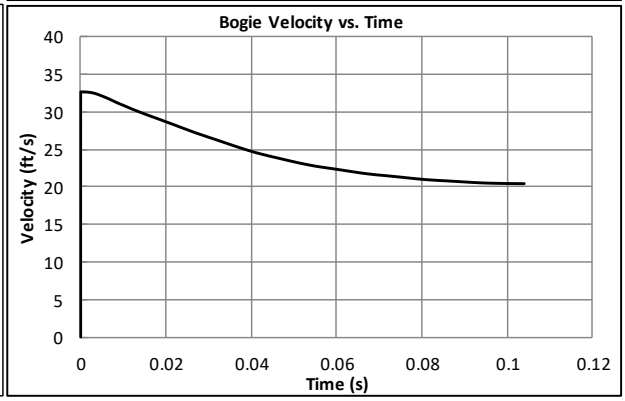

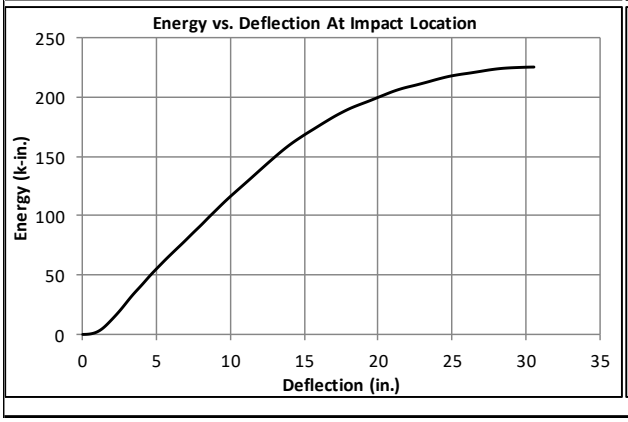

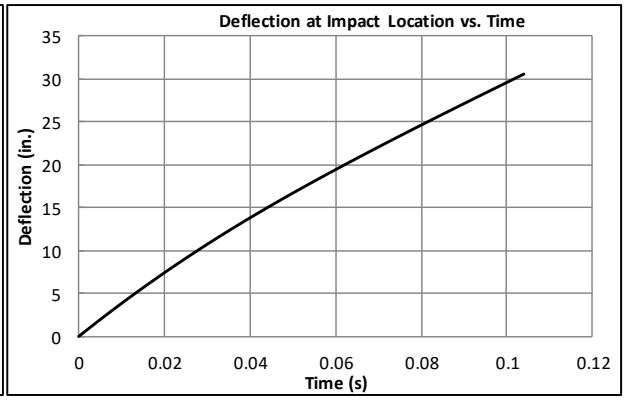

Figure B-3. Test No. LFCB-2 Results (SLICE-1)

MIDWEST ROADSIDE SAFETY FACILITY

Bogie Test Summary

Test Information

Test Description:	Reduced Embedment Post For Shallow Fill Culvert
Test Number:	LFCB-2
Test Date:	3/31/2020
Failure Type:	Rotation in soil and post hinging

Post Properties

Post Type:	Steel
Post Size:	W6x8.5
Post Length:	68
Embedment Depth:	36
Orientation:	Strong Axis - 90 Degrees

Soil Properties

Gradation:	102019
Moisture Content:	NA
Compaction Method:	He8

Bogie Properties

Impact Velocity:	22.26 mph	(32.64 ft/s)
Impact Height:	25	
Bogie Mass:	1865 lb	

Data Acquired

Accelerometer:	SLICE-1
Camera Data:	AOS-9, PAN-6

Test Results Summary

Event Duration:	0.1040	sec
Max. Deflection:	30.5	in.
Peak Force:	15.7	k
Initial Linear Stiffness:	5.3	k/in.
Total Energy:	225.3	k-in.

	@ 5"	@ 10"	@ 15"	@20"
Average Force (k)	11.00	11.61	11.19	9.98
Energy (k-in.)	55.0	116.1	167.9	199.7

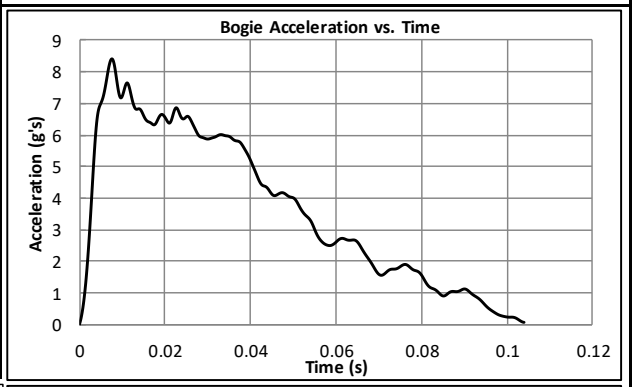

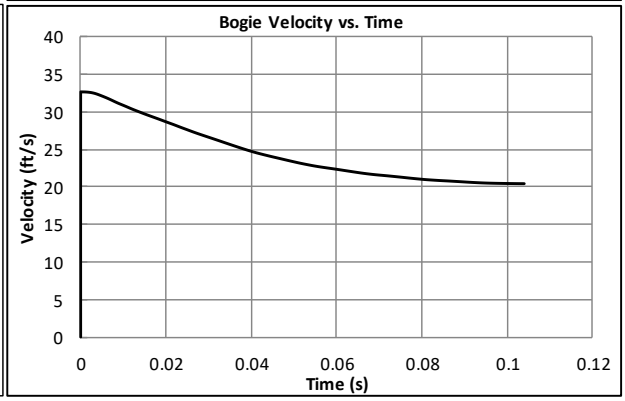

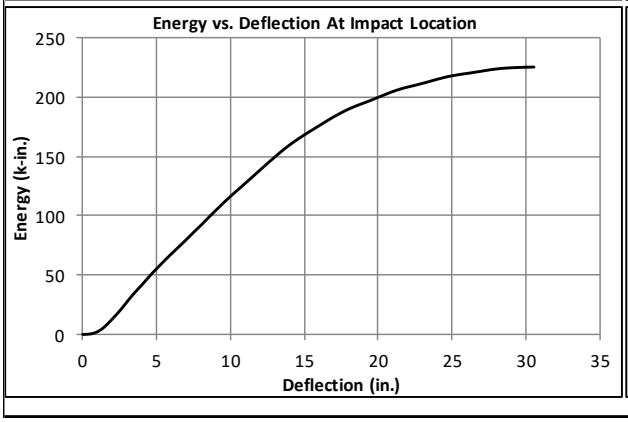

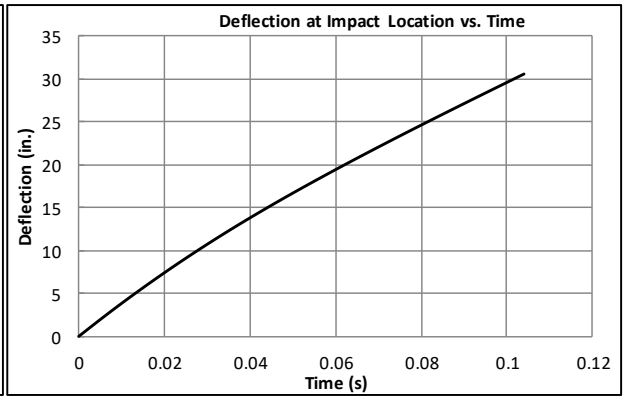

Figure B-4. Test No. LFCB-2 Results (SLICE-2)

MIDWEST ROADSIDE SAFETY FACILITY

Bogie Test Summary

Test Information

Test Description:	Reduced Embedment Post For Shallow Fill Culvert
Test Number:	LFCB-3
Test Date:	4/2/2020
Failure Type:	Rotation in soil and post hinging

Post Properties

Post Type:	Steel
Post Size:	W6x8.5
Post Length:	64
Embedment Depth:	32
Orientation:	Strong Axis - 90 Degrees

Soil Properties

Gradation:	102019
Moisture Content:	N/A
Compaction Method:	HE8

Bogie Properties

Impact Velocity:	20.41 mph	(29.94 ft/s)
Impact Height:	25	
Bogie Mass:	1865 lb	

Data Acquired

Accelerometer:	SLICE-1
Camera Data:	AOS-9, PAN-6

Test Results Summary

Event Duration:	0.1426	sec
Max. Deflection:	31.2	in.
Peak Force:	15.8	k
Initial Linear Stiffness:	6.4	k/in.
Total Energy:	265.7	k-in.

	@ 5"	@ 10"	@ 15"	@20"
Average Force (k)	11.40	11.80	11.47	10.71
Energy (k-in.)	57.0	118.0	172.0	214.1

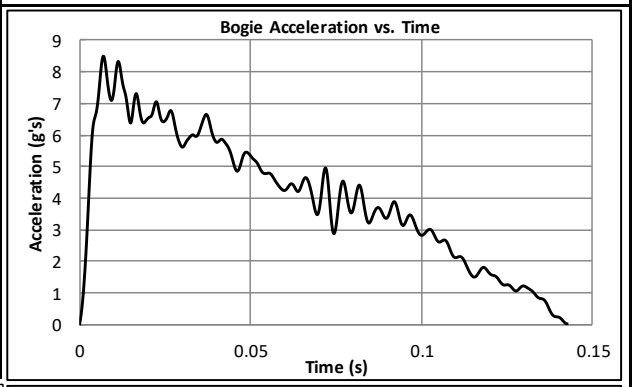

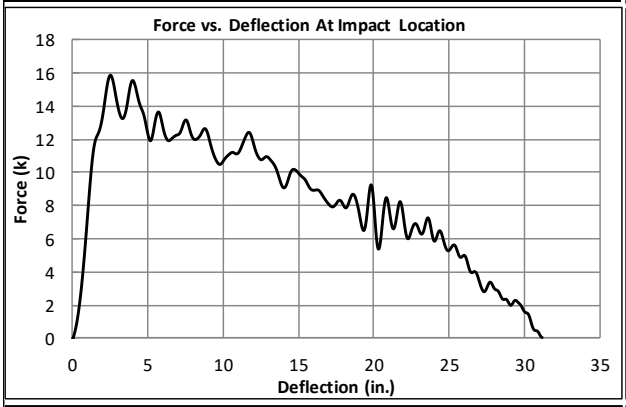

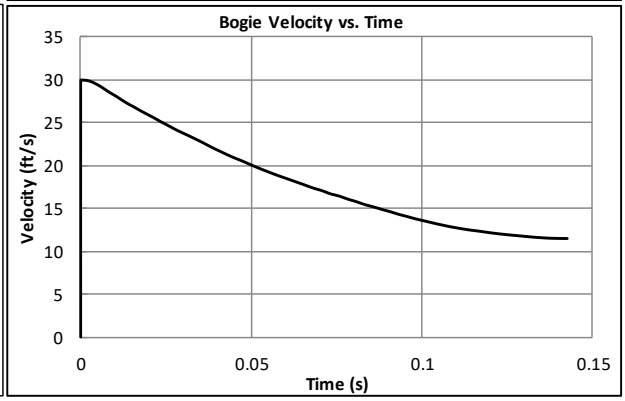

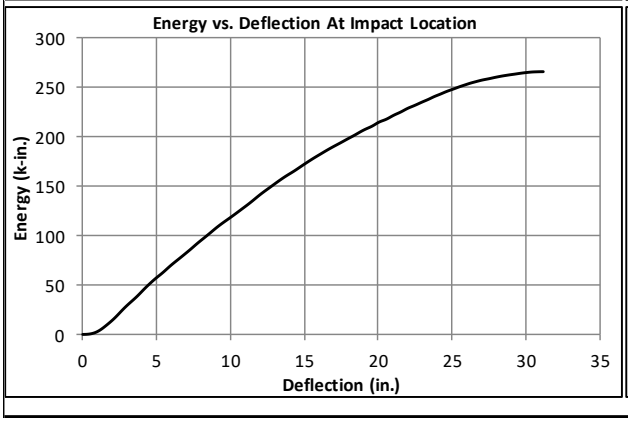

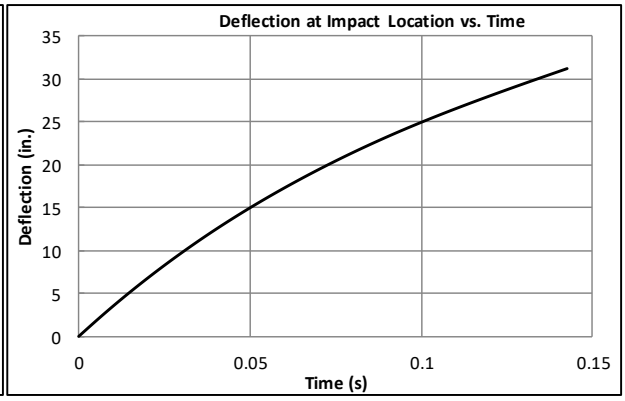

Figure B-5. Test No. LFCB-3 Results (SLICE-1)

MIDWEST ROADSIDE SAFETY FACILITY

Bogie Test Summary

Test Information

Test Description:	Reduced Embedment Post For Shallow Fill Culvert
Test Number:	LFCB-3
Test Date:	4/2/2020
Failure Type:	Rotation in soil and post hinging

Post Properties

Post Type:	Steel
Post Size:	W6x8.5
Post Length:	64
Embedment Depth:	32
Orientation:	Strong Axis - 90 Degrees

Soil Properties

Gradation:	102019
Moisture Content:	N/A
Compaction Method:	HE8

Bogie Properties

Impact Velocity:	20.41 mph	(29.94 ft/s)
Impact Height:	25	
Bogie Mass:	1865 lb	

Data Acquired

Accelerometer:	SLICE-2
Camera Data:	AOS-9, PAN-6

Test Results Summary

Event Duration:	0.1527	sec
Max. Deflection:	32.8	in.
Peak Force:	14.9	k
Initial Linear Stiffness:	5.5	k/in.
Total Energy:	267.2	k-in.

	@ 5"	@ 10"	@ 15"	@20"
Average Force (k)	10.58	11.36	11.15	10.48
Energy (k-in.)	52.9	113.6	167.2	209.6

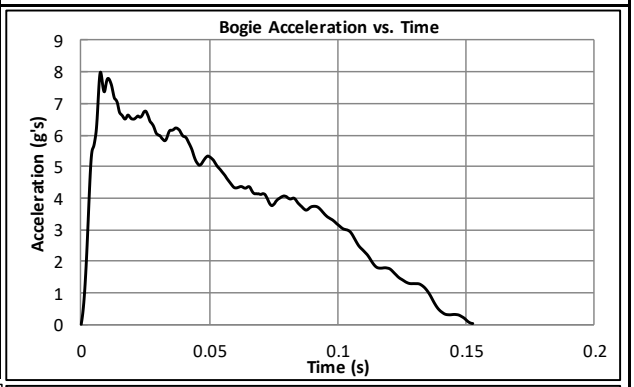

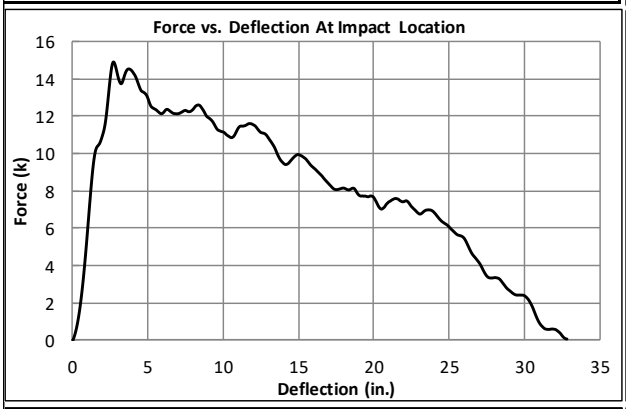

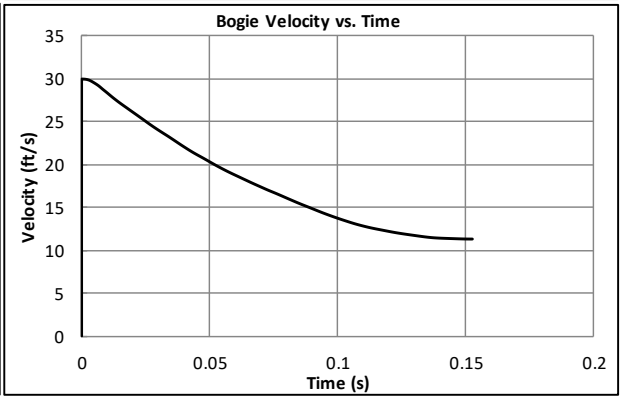

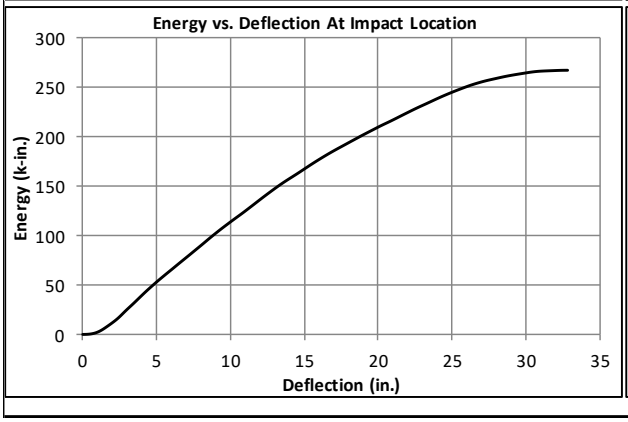

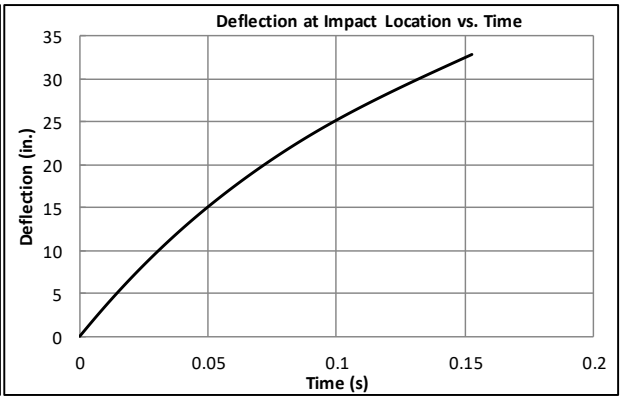

Figure B-6. Test No. LFCB-3 Results (SLICE-2)

MIDWEST ROADSIDE SAFETY FACILITY

Bogie Test Summary

Test Information

Test Description:	Reduced Embedment Post For Shallow Fill Culvert
Test Number:	LFCB-4
Test Date:	4/2/2020
Failure Type:	Rotation in soil and post hinging

Post Properties

Post Type:	Steel
Post Size:	W6x8.5
Post Length:	64
Embedment Depth:	32
Orientation:	Strong Axis - 90 Degrees

Soil Properties

Gradation:	102019
Moisture Content:	N/A
Compaction Method:	HE8

Bogie Properties

Impact Velocity:	20.25 mph	(29.7 ft/s)
Impact Height:	25	
Bogie Mass:	1865 lb	

Data Acquired

Accelerometer:	SLICE-1
Camera Data:	AOS-9, PAN-6

Test Results Summary

Event Duration:	0.1418	sec
Max. Deflection:	30.4	in.
Peak Force:	17.3	k
Initial Linear Stiffness:	6.7	k/in.
Total Energy:	258.1	k-in.

	@ 5"	@ 10"	@ 15"	@20"
Average Force (k)	12.11	12.39	12.01	11.07
Energy (k-in.)	60.6	123.9	180.1	221.3

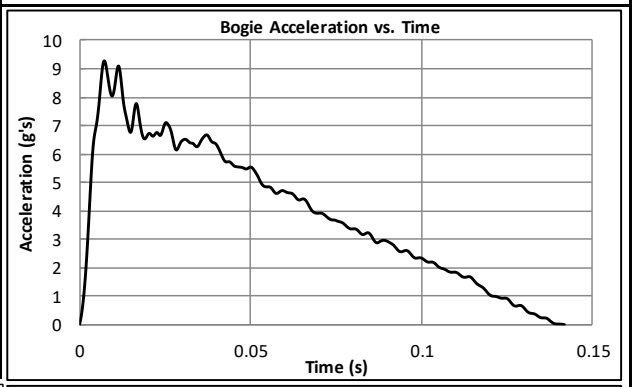

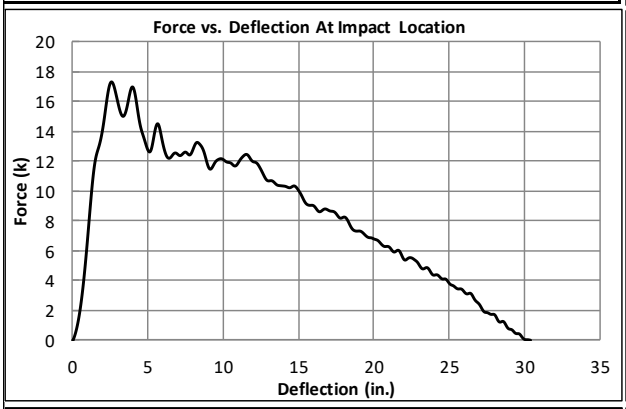

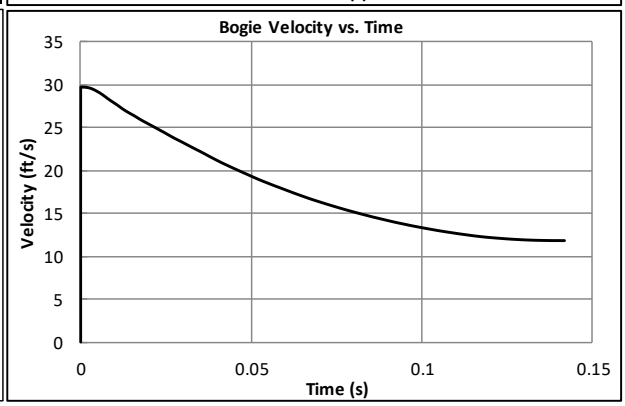

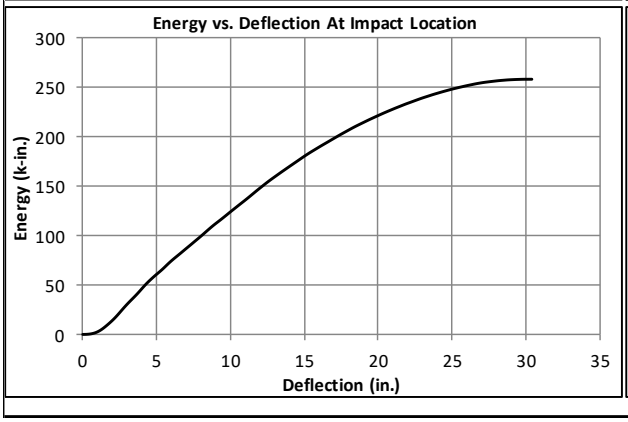

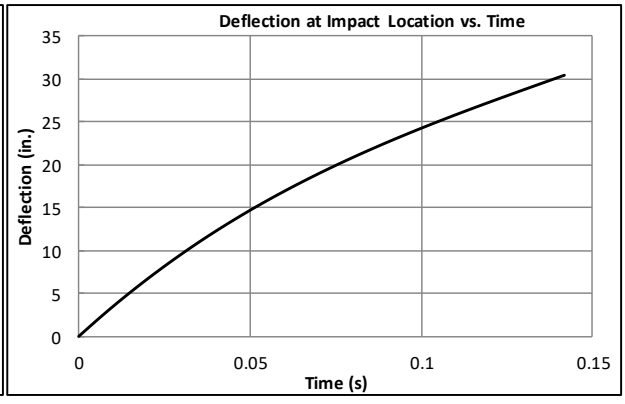

Figure B-7. Test No. LFCB-4 Results (SLICE-1)

MIDWEST ROADSIDE SAFETY FACILITY

Bogie Test Summary

Test Information

Test Description:	Reduced Embedment Post For Shallow Fill Culvert
Test Number:	LFCB-4
Test Date:	4/2/2020
Failure Type:	Rotation in soil and post hinging

Post Properties

Post Type:	Steel
Post Size:	W6x8.5
Post Length:	64
Embedment Depth:	32
Orientation:	Strong Axis - 90 Degrees

Soil Properties

Gradation:	102019
Moisture Content:	N/A
Compaction Method:	HE8

Bogie Properties

Impact Velocity:	20.25 mph	(29.7 ft/s)
Impact Height:	25	
Bogie Mass:	1865 lb	

Data Acquired

Accelerometer:	SLICE-2
Camera Data:	AOS-9, PAN-6

Test Results Summary

Event Duration:	0.1454	sec
Max. Deflection:	31.3	in.
Peak Force:	16.4	k
Initial Linear Stiffness:	6.0	k/in.
Total Energy:	256.1	k-in.

	@ 5"	@ 10"	@ 15"	@20"
Average Force (k)	11.63	12.03	11.75	10.86
Energy (k-in.)	58.2	120.3	176.3	217.1

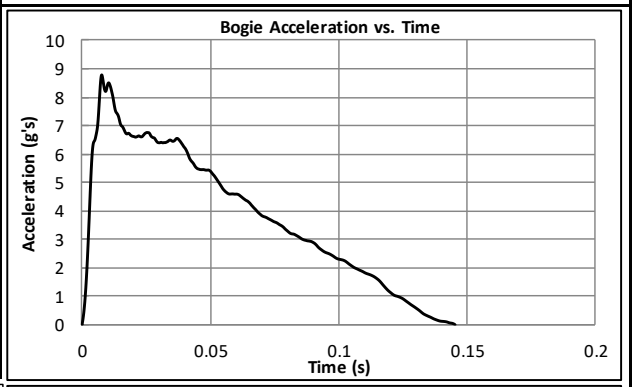

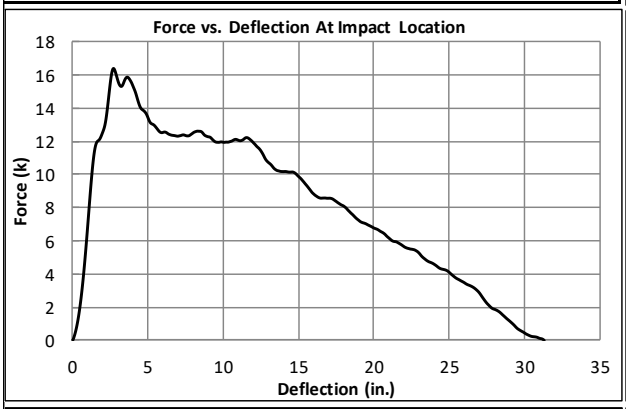

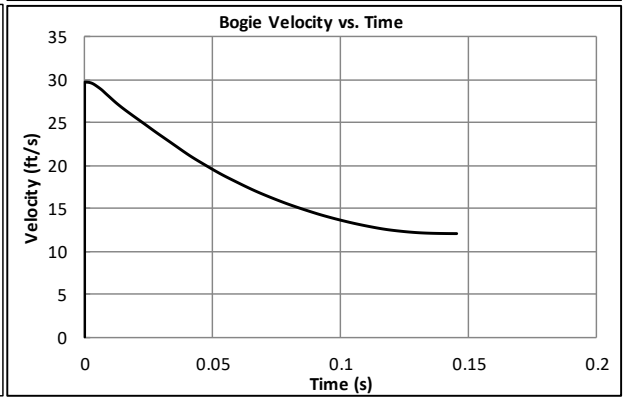

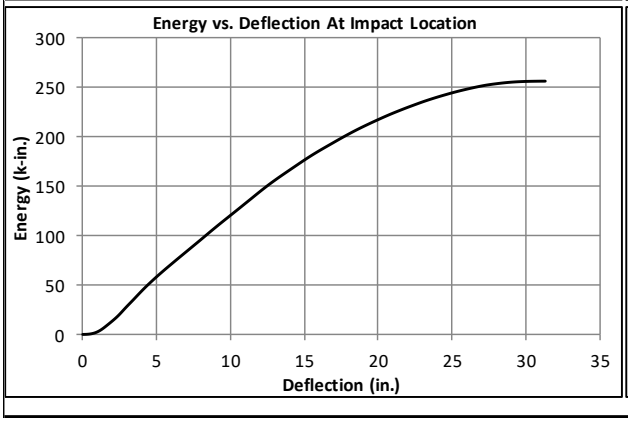

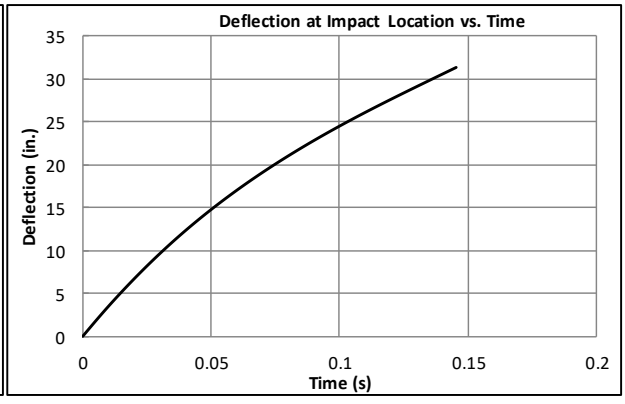

Figure B-8. Test No. LFCB-4 Results (SLICE-2)

MIDWEST ROADSIDE SAFETY FACILITY

Bogie Test Summary

Test Information

Test Description:	Reduced Embedment Post For Shallow Fill Culvert
Test Number:	LFCB-5
Test Date:	4/8/2020
Failure Type:	Rotation in soil and post hinging

Post Properties

Post Type:	Steel
Post Size:	W6x8.5
Post Length:	60
Embedment Depth:	28
Orientation:	Strong Axis - 90 Degrees

Soil Properties

Gradation:	102019
Moisture Content:	N/A
Compaction Method:	HE8

Bogie Properties

Impact Velocity:	22.68 mph	(33.26 ft/s)
Impact Height:	25	
Bogie Mass:	1865 lb	

Data Acquired

Accelerometer:	SLICE-1
Camera Data:	AOS-9, PAN-6

Test Results Summary

Event Duration:	0.1121	sec
Max. Deflection:	32.9	in.
Peak Force:	17.6	k
Initial Linear Stiffness:	5.1	k/in.
Total Energy:	237.7	k-in.

	@ 5"	@ 10"	@ 15"	@20"
Average Force (k)	11.25	12.51	11.93	10.48
Energy (k-in.)	56.2	125.1	178.9	209.7

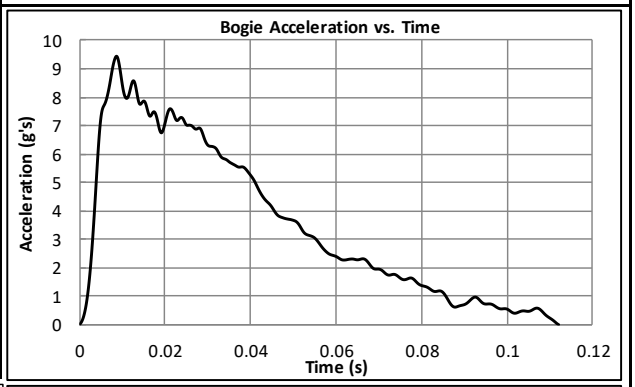

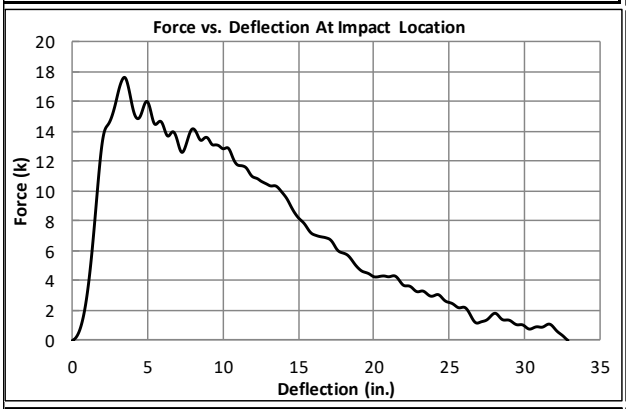

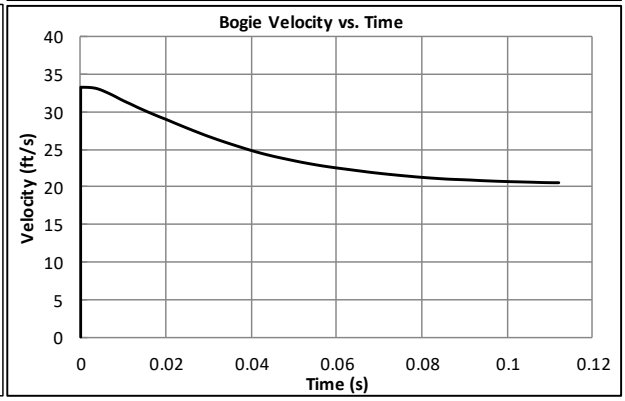

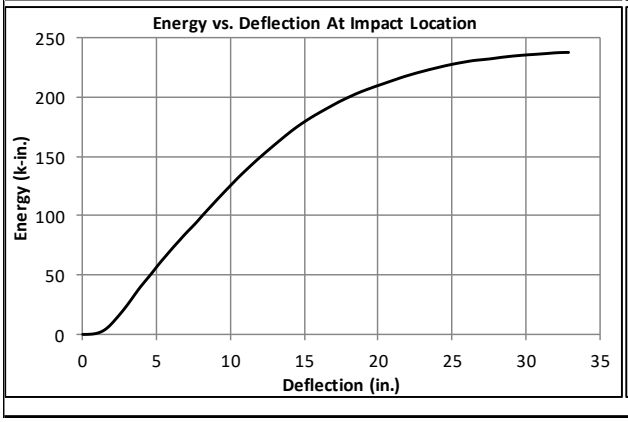

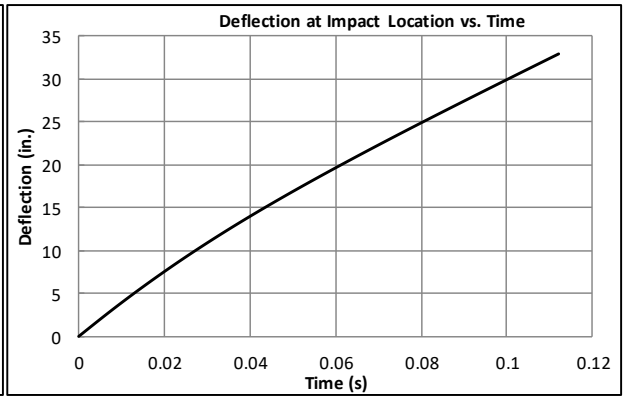

Figure B-9. Test No. LFCB-5 Results (SLICE-1)

MIDWEST ROADSIDE SAFETY FACILITY

Bogie Test Summary

Test Information

Test Description:	Reduced Embedment Post For Shallow Fill Culvert
Test Number:	LFCB-5
Test Date:	4/8/2020
Failure Type:	Rotation in soil and post hinging

Post Properties

Post Type:	Steel
Post Size:	W6x8.5
Post Length:	60
Embedment Depth:	28
Orientation:	Strong Axis - 90 Degrees

Soil Properties

Gradation:	102019
Moisture Content:	N/A
Compaction Method:	HE8

Bogie Properties

Impact Velocity:	22.68 mph	(33.26 ft/s)
Impact Height:	25	
Bogie Mass:	1865 lb	

Data Acquired

Accelerometer:	SLICE-2
Camera Data:	AOS-9, PAN-6

Test Results Summary

Event Duration:	0.1252	sec
Max. Deflection:	36.5	in.
Peak Force:	17.3	k
Initial Linear Stiffness:	5.3	k/in.
Total Energy:	233.4	k-in.

	@ 5"	@ 10"	@ 15"	@20"
Average Force (k)	10.97	12.00	11.54	10.21
Energy (k-in.)	54.8	120.0	173.1	204.2

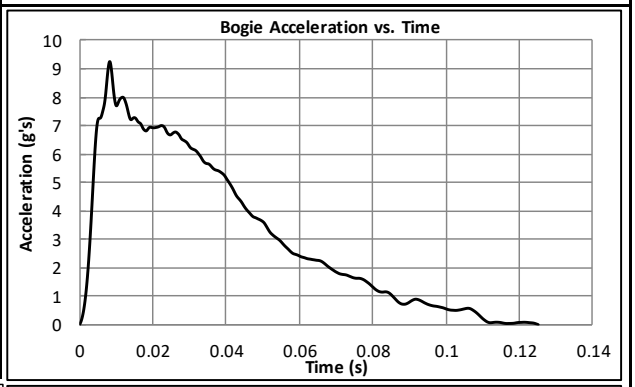

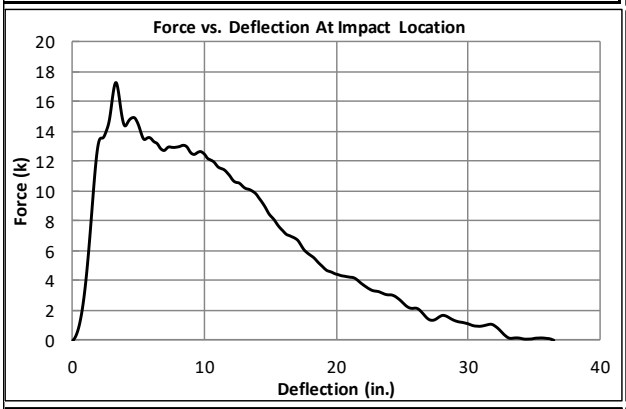

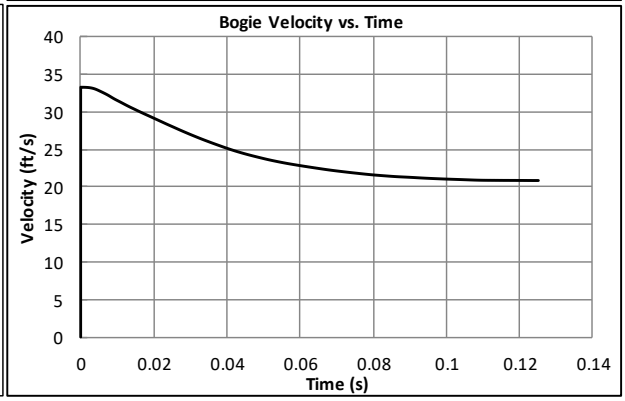

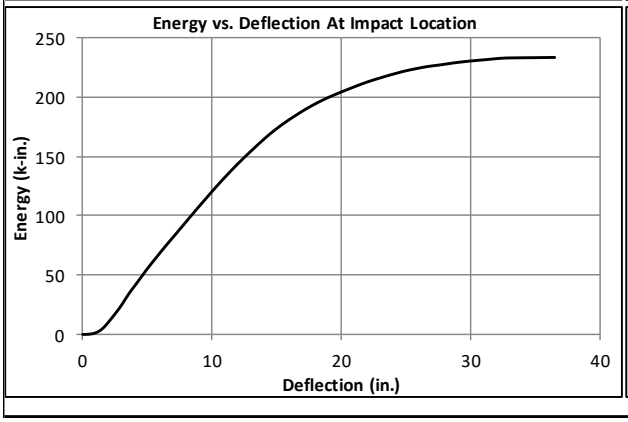

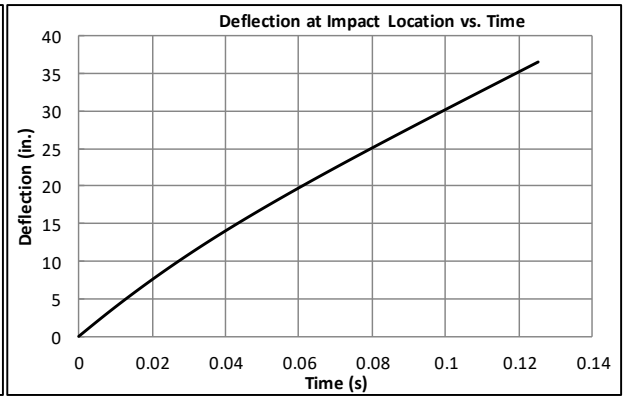

Figure B-10. Test No. LFCB-5 Results (SLICE-2)

MIDWEST ROADSIDE SAFETY FACILITY

Bogie Test Summary

Test Information

Test Description:	Reduced Embedment Post For Shallow Fill Culvert
Test Number:	LFCB-6
Test Date:	4/8/2020
Failure Type:	Rotation in soil and post hinging

Post Properties

Post Type:	Steel
Post Size:	W6x8.5
Post Length:	60
Embedment Depth:	28
Orientation:	Strong Axis - 90 Degrees

Soil Properties

Gradation:	102019
Moisture Content:	N/A
Compaction Method:	HE8

Bogie Properties

Impact Velocity:	20.81 mph	(30.52 ft/s)
Impact Height:	24.75	
Bogie Mass:	1865 lb	

Data Acquired

Accelerometer:	SLICE-1
Camera Data:	AOS-9, PAN-6

Test Results Summary

Event Duration:	0.1190	sec
Max. Deflection:	34.5	in.
Peak Force:	11.4	k
Initial Linear Stiffness:	2.6	k/in.
Total Energy:	162.1	k-in.

	@ 5"	@ 10"	@ 15"	@20"
Average Force (k)	8.70	8.93	8.25	7.22
Energy (k-in.)	43.5	89.3	123.8	144.4

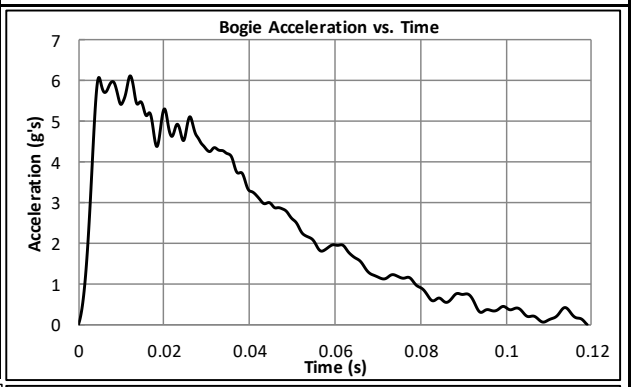

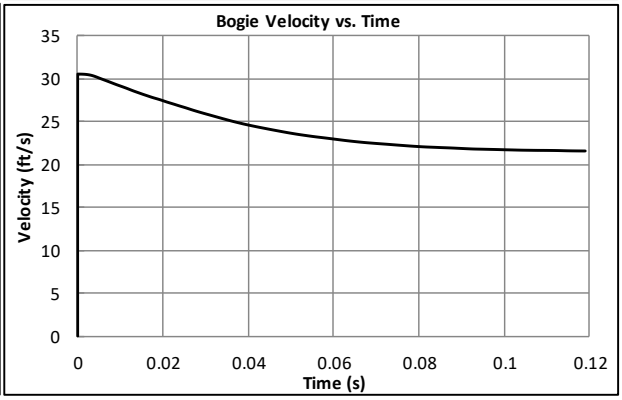

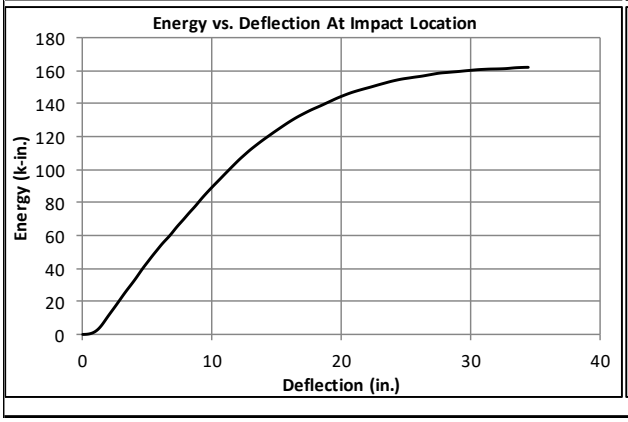

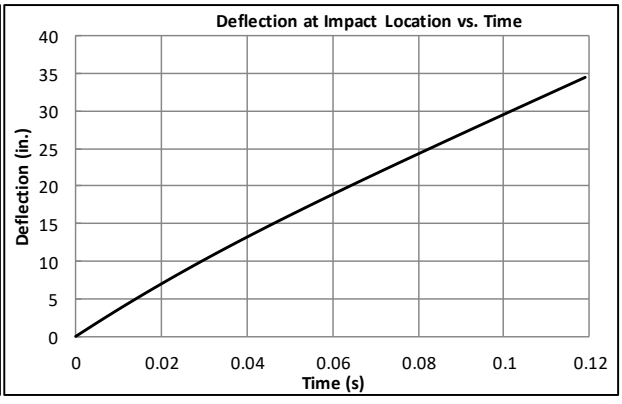

Figure B-11. Test No. LFCB-6 Results (SLICE-1)

MIDWEST ROADSIDE SAFETY FACILITY

Bogie Test Summary

Test Information

Test Description:	Reduced Embedment Post For Shallow Fill Culvert
Test Number:	LFCB-6
Test Date:	4/8/2020
Failure Type:	Rotation in soil and post hinging

Post Properties

Post Type:	Steel
Post Size:	W6x8.5
Post Length:	60
Embedment Depth:	28
Orientation:	Strong Axis - 90 Degrees

Soil Properties

Gradation:	102019
Moisture Content:	N/A
Compaction Method:	HE8

Bogie Properties

Impact Velocity:	20.81 mph	(30.52 ft/s)
Impact Height:	24.75	
Bogie Mass:	1865 lb	

Data Acquired

Accelerometer:	SLICE-2
Camera Data:	AOS-9, PAN-6

Test Results Summary

Event Duration:	0.1180	sec
Max. Deflection:	34.9	in.
Peak Force:	11.1	k
Initial Linear Stiffness:	4.0	k/in.
Total Energy:	150.2	k-in.

	@ 5"	@ 10"	@ 15"	@20"
Average Force (k)	7.98	8.19	7.68	6.73
Energy (k-in.)	39.9	81.9	115.2	134.6

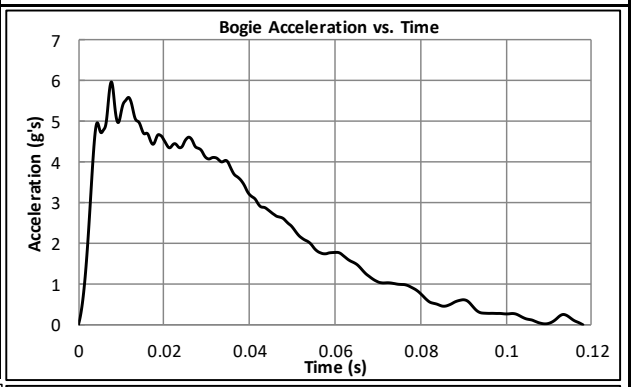

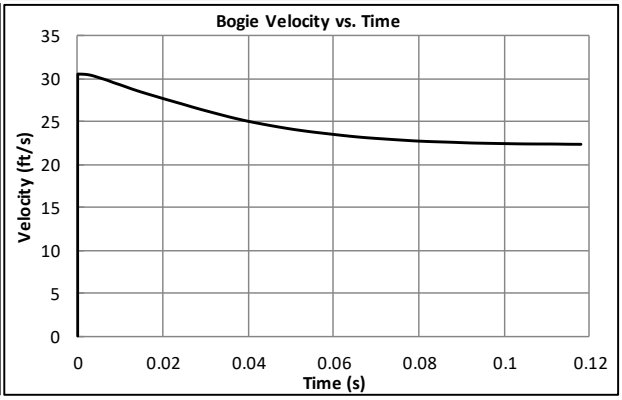

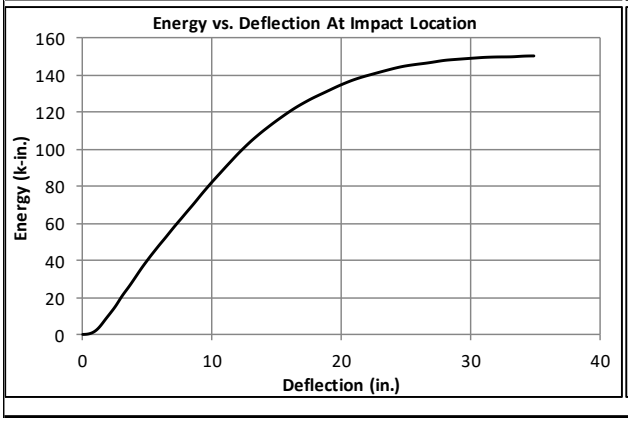

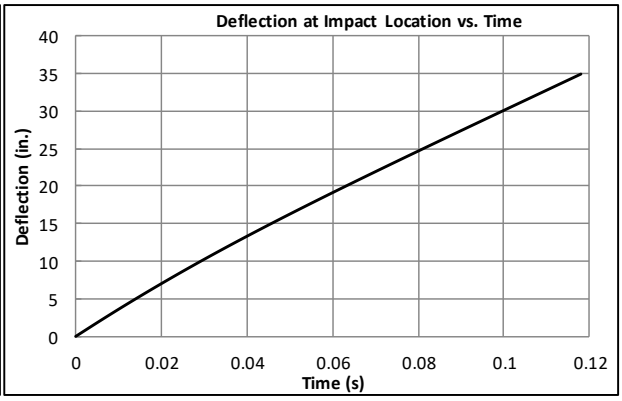

Figure B-12. Test No. LFCB-6 Results (SLICE-2)

MIDWEST ROADSIDE SAFETY FACILITY

Bogie Test Summary

Test Information

Test Description:	Reduced Embedment Post For Shallow Fill Culvert
Test Number:	LFCB-7
Test Date:	6/9/2020
Failure Type:	Rotation in soil

Post Properties

Post Type:	Steel
Post Size:	W6x16
Post Length:	72
Embedment Depth:	40
Orientation:	Strong Axis - 90 Degrees

Soil Properties

Gradation:	102019
Moisture Content:	N/A
Compaction Method:	HE8

Bogie Properties

Impact Velocity:	20.23 mph	(29.67 ft/s)
Impact Height:	24.75	
Bogie Mass:	1873 lb	

Data Acquired

Accelerometer:	SLICE-1
Camera Data:	AOS-9, PAN-6

Test Results Summary

Event Duration:	0.2061	sec
Max. Deflection:	28.5	in.
Peak Force:	23.4	k
Initial Linear Stiffness:	9.0	k/in.
Total Energy:	303.3	k-in.

	@ 5"	@ 10"	@ 15"	@20"
Average Force (k)	17.76	17.25	15.28	13.34
Energy (k-in.)	88.8	172.5	229.3	266.8

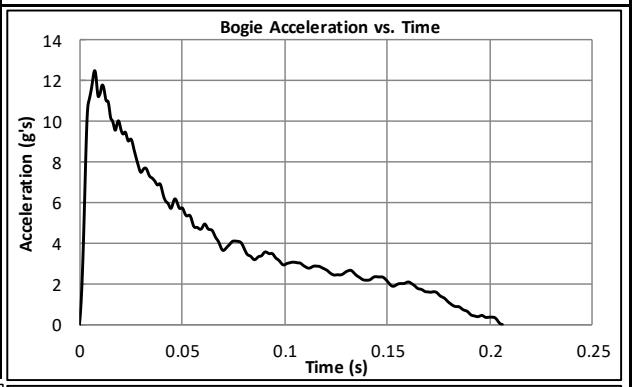

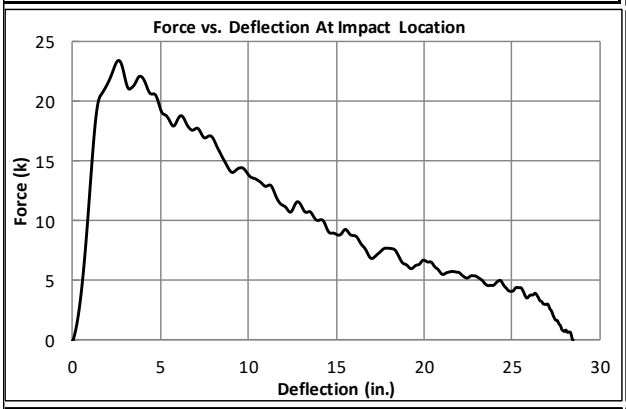

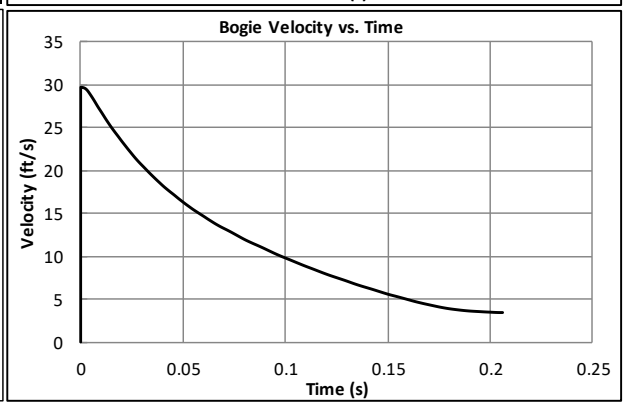

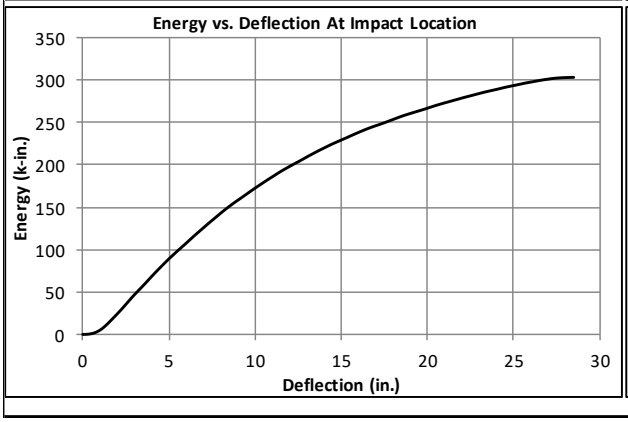

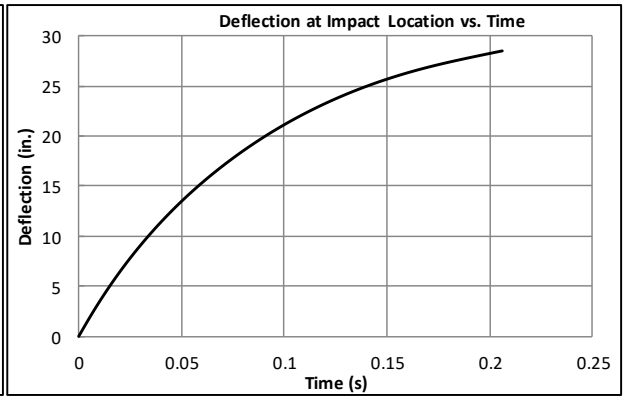

Figure B-13. Test No. LFCB-7 Results (SLICE-1)

MIDWEST ROADSIDE SAFETY FACILITY

Bogie Test Summary

Test Information

Test Description:	Reduced Embedment Post For Shallow Fill Culvert
Test Number:	LFCB-8
Test Date:	6/9/2020
Failure Type:	Rotation in soil

Post Properties

Post Type:	Steel
Post Size:	W6x16
Post Length:	66
Embedment Depth:	34
Orientation:	Strong Axis - 90 Degrees

Soil Properties

Gradation:	102019
Moisture Content:	N/A
Compaction Method:	HE8

Bogie Properties

Impact Velocity:	20.96 mph	(30.74 ft/s)
Impact Height:	24.75	
Bogie Mass:	1873 lb	

Data Acquired

Accelerometer:	SLICE-1
Camera Data:	AOS-9, PAN-6

Test Results Summary

Event Duration:	0.1512	sec
Max. Deflection:	33.1	in.
Peak Force:	18.5	k
Initial Linear Stiffness:	10.5	k/in.
Total Energy:	277.2	k-in.

	@ 5"	@ 10"	@ 15"	@20"
Average Force (k)	12.24	13.03	12.55	11.62
Energy (k-in.)	61.2	130.3	188.2	232.4

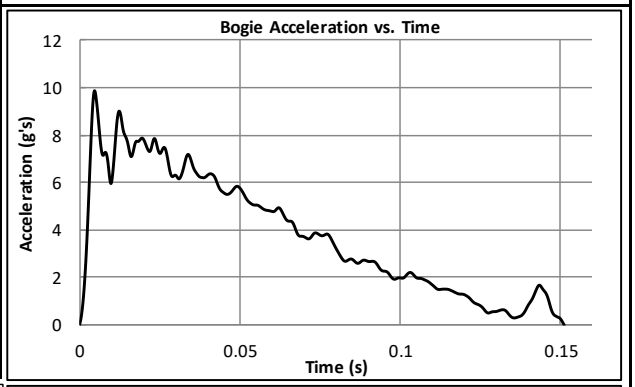

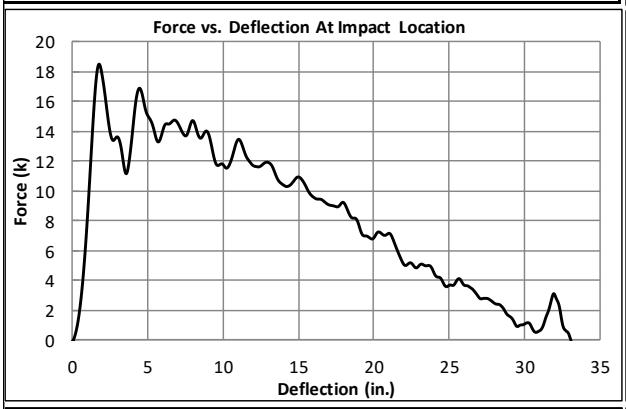

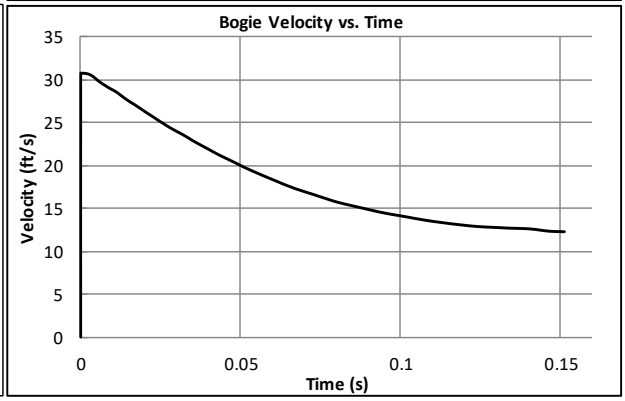

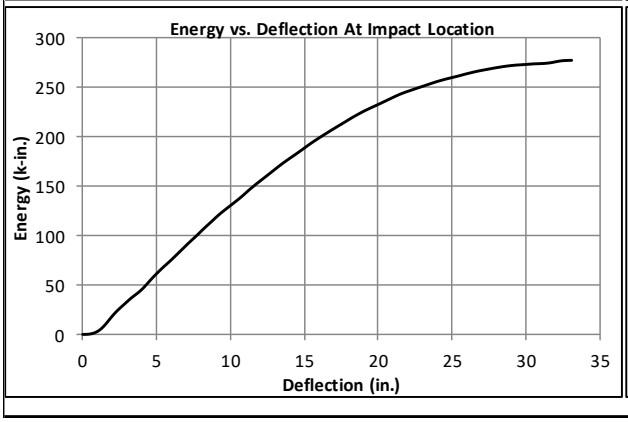

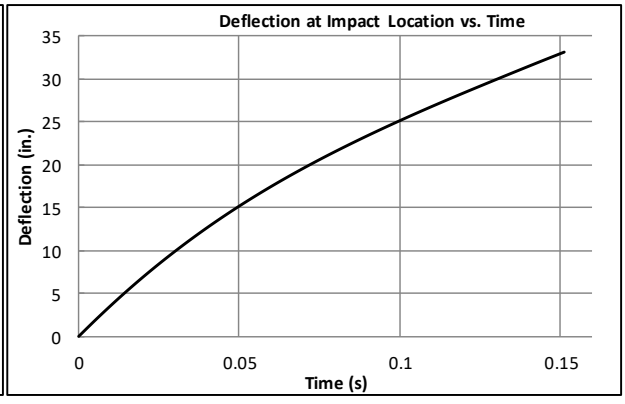

Figure B-14. Test No. LFCB-8 Results (SLICE-1)

MIDWEST ROADSIDE SAFETY FACILITY

Bogie Test Summary

Test Information

Test Description:	Reduced Embedment Post For Shallow Fill Culvert
Test Number:	LFCB-9
Test Date:	6/9/2020
Failure Type:	Rotation in soil

Post Properties

Post Type:	Steel
Post Size:	W6x16
Post Length:	60
Embedment Depth:	28
Orientation:	Strong Axis - 90 Degrees

Soil Properties

Gradation:	102019
Moisture Content:	N/A
Compaction Method:	HE8

Bogie Properties

Impact Velocity:	21.04 mph	(30.86 ft/s)
Impact Height:	24.75	
Bogie Mass:	1873 lb	

Data Acquired

Accelerometer:	SLICE-1
Camera Data:	AOS-9, PAN-6

Test Results Summary

Event Duration:	0.1194	sec
Max. Deflection:	34.2	in.
Peak Force:	15.7	k
Initial Linear Stiffness:	9.3	k/in.
Total Energy:	181.4	k-in.

	@ 5"	@ 10"	@ 15"	@20"
Average Force (k)	10.35	10.17	8.99	7.73
Energy (k-in.)	51.7	101.7	134.9	154.6

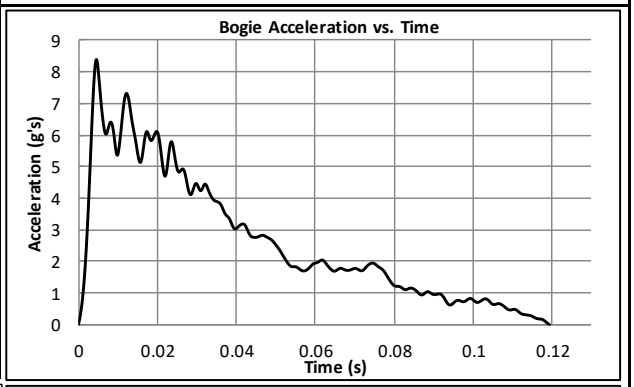

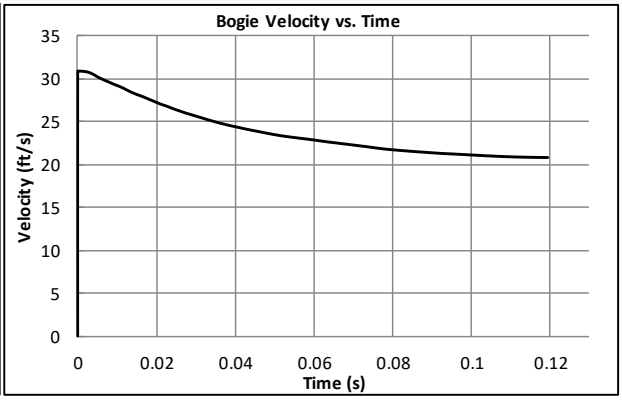

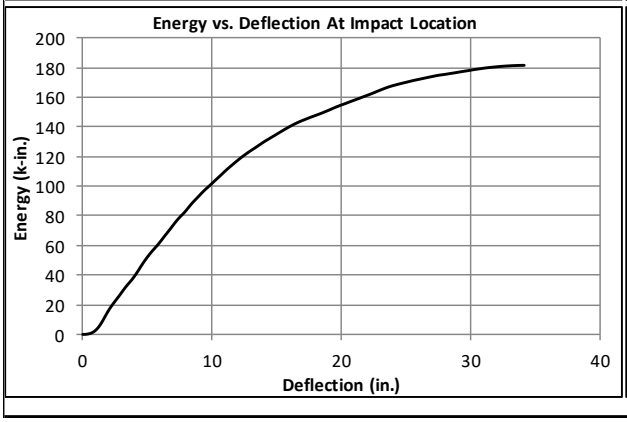

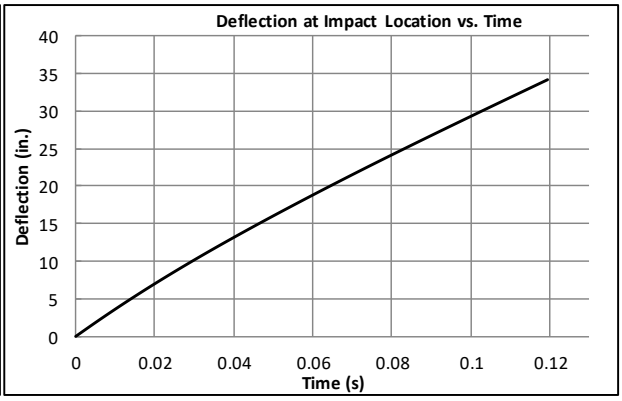

Figure B-15. Test No. LFCB-8 Results (SLICE-1)

Appendix C. Advanced Post-Soil Impact Modeling Using Adaptive Coupling of Finite Element Method and Smoothed Particle Hydrodynamics

C.1. Introduction

LS-DYNA finite element analysis is the primary numerical modeling tool used for development and evaluation of roadside safety features. Although LS-DYNA has been used often and successfully by roadside safety researchers and engineers, there still remain several limitations for its use that are solely based on the inability to focus on basic modeling.

In order for MwRSF researchers to continue to advance the state-of-the-art for LS-DYNA modeling within the roadside safety community as well as to enhance MwRSF's analysis capabilities for future Midwest Pooled Fund projects, MwRSF has previously requested that the Midwest Pooled Fund Program member states provide a limited amount of funds to be allocated annually for these advanced modeling and simulation efforts.

Recently, MwRSF has worked toward development of improved soil modeling in LS-DYNA in support of various Midwest Pooled Fund Program research projects. This has included development of alternative soil modeling methods, including the erosion method, Multi-Material Arbitrary Lagrangian-Eulerian (MM-ALE) method, adaptive coupling of Finite Element Method (FEM) and Smoothed Particle Hydrodynamics (SPH), and hybrid SPH-FEM method that have improved our ability to simulate dynamic loading of posts and other structures in soil with a variety of geometries and embedment depths as well as soil conditions. LS-DYNA Modeling Enhancement funding was applied to one those advanced soil modeling techniques, i.e., the adaptive FEM-SPH method, in support of this research project. It was believed that adoption of this soil modeling method for that project would improve the analysis of design for this research project and provide insight into future soil modeling efforts.

This appendix provides a summary of research efforts conducted using the adaptive FEM-SPH method for modeling and simulating laterally impacted post-soil systems, i.e., test nos. LFCB-1 through LFCB-4.

C.2. Principle of Adaptive Coupling of FEM-SPH Method

The FEM has been extensively used to analyze dynamic impact problems for the past several decades. Although the FEM has demonstrated its capabilities for a wide range of roadside safety engineering problems, the method is not always adequate when mesh distortions become severe during large deformations. Severely distorted elements may cause very small integration time increments. Therefore, the simulations may not proceed efficiently. One remedy for this problem is to delete severely distorted elements from the computation using an element erosion algorithm [1]. This feature enables the FEM to be used for large deformation dynamics problems, including impact, blast, or explosion. With the erosion method, the nodal masses can be retained; however, the deleted elements do not carry any stresses.

In the early 1990s, particle-based numerical algorithms began to appear in the field of solid mechanics. Since then, particle-based methods, such as the SPH method, have been refined and applied to analyze various engineering problems [2]. One of the SPH method's desirable characteristics is that the particles carry all variables (i.e., mass, position, velocity, internal energy, stress, and strain). This feature is often referred to as collocation characteristics and enables the simulation of large deformation problems [3]. Even though the SPH method's computational efficiency is not generally as good as FEM for impact problems with small deformations or until

the elements are severely distorted, the SPH method is robust, accurate, and efficient for dynamic impact problems involving large deformations [2].

An alternative computational approach is to combine the FEM and SPH methods using an adaptive algorithm, such that SPH particles replace highly strained or deleted solid elements. This computational method is often referred to as the adaptive coupling of FEM and SPH methods. An adaptive change means the change of discretization method, i.e., FEM to SPH, when certain criteria are satisfied, i.e., element erosion criteria. The method has been developed primarily for hypervelocity impact and penetration problems [2]. For these types of large deformation problems, FEM suffers from the necessity of deleting or eroding elements at some level of large deformations, and the SPH method suffers from long CPU time. Therefore, the adaptive coupling of the FEM and SPH method could be a powerful computational tool for modeling and simulating large deformation of granular soils during impacts.

One class of adaptive coupling techniques, which consists of embedding the SPH particles inside the conventional solid elements, is proposed in this study to model the fluid-like behavior of MASH strong soil during post impacts. The simulation starts with the FEM solid elements. As time progresses and plastic deformation increases, the heavily distorted solid elements are deleted from the computation. The SPH particles remain on deleting the solid element at suitable damage and the principal failure strain state, replacing the solid element with a discrete particle formulation in the large deformation zone. In this study, the damage and maximum principal failure strain were the elimination criteria utilized as the adaptivity threshold. For one-to-one enrichment, the SPH particle was located at the center of each solid soil element.

The adaptive FEM-SPH method is still an unfamiliar modeling approach among many roadside safety engineers and researchers. No to limited research has been reported on applying the adaptive FEM-SPH method for simulating the dynamic interaction between roadside safety structures and soil foundations. These circumstances can be enhanced if more researchers start investigating the adaptive coupling of the FEM and SPH methods.

C.3. Model Development and Simulation Details

This chapter aims to document the advanced soil modeling techniques for undertaking dynamic post-soil interaction under vehicular impacts. The new modeling technique is based on a large-deformation numerical method, advanced constitutive models, and dynamic contact algorithms. In each post-soil impact model, components, such as FE elements, SPH particles, constitutive models, boundary conditions, and load applications, need to be defined. In this section, these modeling details and components of the adaptive FEM-SPH method are explained in detail.

C.3.1. Constitutive Models

MASH Strong Soil

Choosing an appropriate granular soil constitutive model to reproduce soil behavior under dynamic impact environments is always challenging. Steel posts are often installed into MASH strong soil during crash testing of soil-based barrier systems. In order to accurately represent MASH strong soil behavior during post impacts, a rheological soil model (i.e., FHWA soil model

[18]) available within the LS-DYNA simulation platform was adopted. The fundamental theoretical basis of the FHWA soil model is presented in reference [4].

The FHWA soil model is specifically developed to model dense and rapid granular flows of compacted road-base material, also known as NCHRP Report 350 strong soil [13], used in crash testing of soil-based roadside safety structures. It should be noted that the NCHRP Report 350 strong soil is most similar to MASH strong soil. This constitutive model has been identified as the most suitable and comprehensive soil model within LS-DYNA hydrocode for incorporating elasto-plastic soil behavior, including the effects of confinement, strain rate, strain softening, and pore water pressure [5-6].

The baseline MASH strong soil input parameters were obtained from previous study [4]. The MASH strong soil input parameters used in this paper are shown in Table C-1. Details regarding the selection and determination of input parameter values for the MASH strong soil are discussed in reference [4]. Additionally, a detailed discussion was provided on the range of values of the FHWA soil model input parameters for computational modeling of dynamic impact post-soil interaction problems that typically involve MASH strong soil [4].

Table C-1. Input parameters for MASH strong soil [4]

Item	Soil Parameter	Value
Basic parameters	Specific gravity, G_s	2.65
	Water content, w (%)	3.4
	Density of soil, ρ_{soil} (kg/mm^3)	1.9e-06
	Density of water, ρ_{water} (kg/mm^3)	1.0e-06
Elasticity parameters	Bulk modulus, K (MPa)	20.0
	Shear modulus, G (MPa)	12.0
Yield parameters	Friction angle, ϕ_{peak} (degrees)	45.0
	Cohesion, c (kPa)	5.0
	Eccentricity parameter, e	0.7
	Modified MC surface coefficient, a (kPa)	3.7
Viscoplasticity parameters	Viscoplasticity parameter, γ	1.0e-03
	Viscoplasticity parameter, η	2.0
Strain softening parameters	Volumetric strain at initial damage threshold, ξ_0	1.0e-05
	Void formation energy, G_f	6.0e-08
	Residual friction angle, ϕ_{res} (degrees)	15.0

Steel Post

The most widely used and recommended material model in LS-DYNA for modeling metals under dynamic impact environments, the Piecewise-Linear Plasticity model [18], was adopted to model the stresses and strains in the steel posts. This material model is based on elasto-plasticity

and handles strain-rate effects using the Cowper-Symonds strain-rate model [7]. It includes the von Mises yield criterion, the associated flow rule, and isotropic strain hardening [18]. The material properties, such as Young's modulus, Poisson's ratio, and the effective stress vs. effective plastic strain curve for the steel tube posts were obtained from tensile tests conducted on samples taken from ASTM A992 steel posts at MwRSF and reported in references [8-9], were used as input data for the Piecewise-Linear Plasticity model.

C.3.2. Element Formulations, Volume Integration, and Hourglass Control

MASH Strong Soil

The adaptive coupling of mesh-based and mesh-free particle methods, based on the SPH method, was adopted to model the MASH strong soil during post impacts. Specifically, the technique of LS-DYNA, i.e., ADAPTIVE_SOLID_TO_SPH [18], was implemented. The soil was modeled using the classical Lagrangian, one-point quadrature, hexahedral elements, which were converted to discrete particles based on SPH formulation when the erosion criteria were satisfied. The FHWA soil model was initially assigned to the soil part with only solid elements and kept with the SPH particles. When the element erosion criteria were met, the solid elements were converted into SPH particles with a respective equivalent mass [18].

In the FHWA soil model, DAMLEV is the damage value (i.e., between 0 and 1.0) that causes element erosion of the soil elements [18]. At the same time, the EPSMAX is the maximum principal failure strain at which the soil element is deleted. Thus, in order for the soil element to be deleted, both EPSMAX and DAMLEV must be exceeded. Therefore, DAMLEV and EPSMAX were set equal to the maximum damage for incorporating element erosion into the soil model. As discussed in detail in reference [4], the maximum damage allowed in the soil element was related to the peak friction angle and residual friction of the MASH strong soil. These element erosion values were utilized as the adaptivity threshold for the simulation of various post-soil systems subjected to lateral impact loading

Steel Post

Plane stress shell elements were utilized for the I-shaped or wide flange (i.e., W152x12.6 and W152x23.6) posts to minimize the computational cost associated with increasing the time step. In the LS-DYNA simulation platform, many element formulations exist for plane stress shell elements. Among them, the default element type is Beltyschko-Tsay's formulation [18]. This element is very robust and economical [10]. However, hourglass modes appear when employing this shell element formulation; since, the one-point quadrature rule is used in the plane of the element. These hourglass modes need to be suppressed using hourglass control. In this study, the so-called very fast, fully integrated shell, which is very efficient and does not require hourglass control, was employed for the plane stress shell elements

C.3.3. Contact Algorithms

The AUTOMATIC_NODE_TO_SURFACE contact type was employed to model the contact between the bogie vehicle (neoprene impact head) and steel (post) interaction. A static and dynamic friction coefficient of 0.1 was applied to model the friction interaction between the neoprene impact head and the post. In dynamic impact simulations, it is often recommended to set

static and dynamic friction coefficients equal to avoid potential numerical instabilities and a higher frequency contact [18]. A penalty-based, two-way, ERODING_SURFACE_TO_SURFACE contact type was implemented to model the interaction between the post and soil. The sliding contact between the post and soil utilized a static coefficient of friction suggested by Yoshimi and Kishida [11] and Uesugi and Kishida [12]. Static and dynamic friction coefficients were set equal to avoid potential numerical stabilities and a higher frequency contact.

The contact between the post (i.e., finite elements) and the SPH particles was modeled with the AUTOMATIC_NODE_TO_SURFACE contact algorithm, as recommended in the reference [18]. The previously noted static coefficient of friction was utilized to model the sliding contact between the (steel) post and MASH strong soil SPH particles. The dynamic and static coefficients of friction were set equal.

C.3.4. Boundary Condition

The most suitable boundary condition that can be applied to the four exterior faces and the bottom surface of the soil domain was the Boundary Non-Reflecting (BNR) boundary condition. The BNR boundary condition enables the exterior and bottom boundaries of the soil domain to represent an infinite soil medium where shock waves from post impacts continue to propagate without reflection of both displacements and stresses. Thus, the BNR boundary condition on the computational domain was utilized for all simulations. Unlike standard boundary constraints where rotations and displacements are fixed, the BNR condition does not constrain rotations and displacements. Instead, conditions and equations are defined internally within the solver to characterize the computational domain as an infinite medium [18].

C.3.5. Load Application

The load application consisted of two stages to combine the gravity load, which is a static load, and the impact load, which is instead a transient load. In the first stage, the explicit dynamic relaxation feature was employed to apply gravity slowly to the post-soil systems. Upon completion of the dynamic relaxation or initialization stage, the model was stabilized, and the impact load was applied to the computational model of the post-soil system. In order to apply impact load, the bogie vehicle was assigned with an initial velocity that corresponded to the initial velocity of the bogie vehicle immediately before impacting the post-soil systems in the physical impact tests.

C.3.6. Validation of Adaptive FEM-SPH Method

The many assumptions involved in the successive steps of idealization, discretization, and modeling material behavior were validated by comparing the modeling results against physical impact test data from test nos. LFCB-1 through LFCB-4. As noted previously, the physical impact tests included W6x8.5 post-soil systems with embedment depths of 36 in. and 32 in. embedded in stiffer/stronger MASH strong soil.

The following sections describe the computational models developed using the adaptive FEM-SPH method to simulate test nos. LFCB-1 through LFCB-4. The force vs. displacement and energy vs. displacement responses at the impact height were utilized to assess the accuracy, robustness, and versatility of the adaptive FEM-SPH method. Model acceleration data was obtained from a node at the center of gravity of the bogie vehicle and processed similarly to the

physical impact test data. Newton's second law was used to obtain impact forces. The energy dissipated by the post-soil system was obtained by integrating areas under the force vs. displacement curves. The average force was calculated by dividing the energy by displacement.

C.4. Modeling Test Nos. LFCB-1 and LFCB-2 Using Adaptive FEM-SPH Method

This section details the numerical simulation conducted to evaluate the capability of the computational tool to simulate the impact behavior of standard guardrail posts embedded in soil. Test nos. LFCB-1 and LFCB-2, conducted on a 68-in. long, W6x8.5 steel post embedded 36 in. into stiffer MASH strong soil were modeled using the adaptive FEM-SPH method. Results obtained from the impact test and numerical simulation were compared and discussed.

C.4.1. Model Geometry, Set-Up, and Initial Conditions

Computational model geometry, set-up, and initial conditions of a laterally impacted W6x8.5 steel post embedded in MASH strong soil are shown in Figure C-1. For one-to-one enrichment, the SPH particles were situated at the center of each solid soil element.

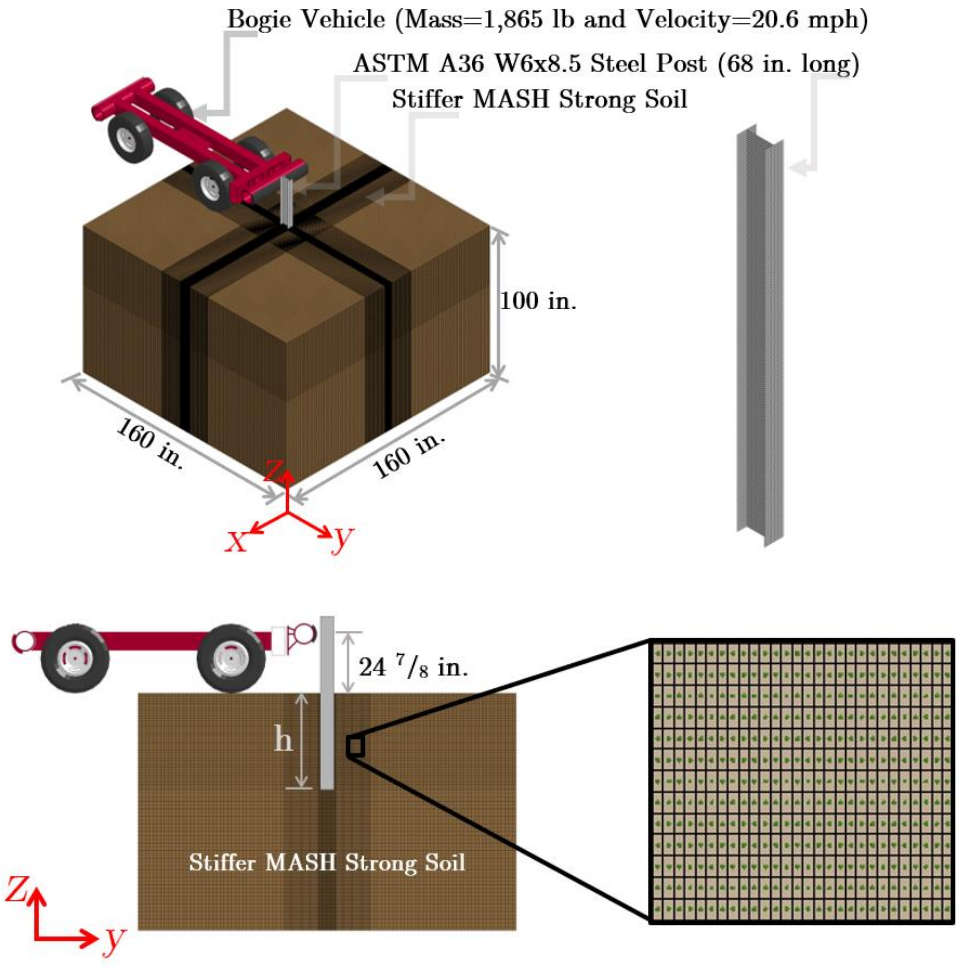

Figure C-1. Computational Model Geometry, Set-Up, and Initial Conditions of W6x8.5 Post Embedded in MASH Soil with Embedment h = 36 in.

C.4.2. Comparison Between Simulated and Physical Impact Test

Quantitative comparisons focused on force vs. displacement and energy vs. displacement responses. A good agreement between the simulated and physical impact test results can be observed in Figure C-2. The energy vs. displacement curves for both the simulation and physical impact test were similar in both shape and magnitude. The most important results for comparison purposes were average force at 5, 10, 15, and 20 in., post displacement (measured at the impact height). Average force at different post displacements was deemed helpful for designing and analyzing real-life, soil-based barrier systems under vehicle impacts [13].

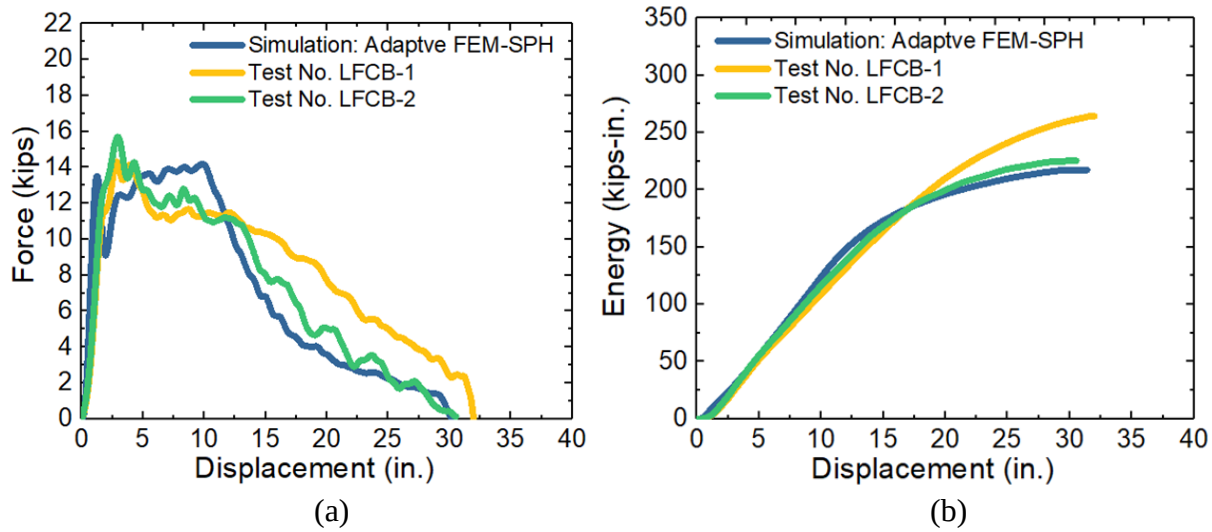

Figure C-2. Comparison of Simulated and Physical Impact Test Results: (a) Force vs. Displacement; and (b) Energy vs. Displacement

Average force comparison between test nos. LFCB-1 and LFCB-2 and simulation at post displacements of 5, 10, 15, and 20 in. is provided in Table C-2. The average forces at post displacements of 5, 10, 15, and 20 in. from the numerical simulation were within 1.9%, 10.7%, 5.5%, and 1.0%, respectively, when compared to the average (average forces) of the impact tests. Results from simulated dynamic impact events within 20% of a test are considered reasonable [21]. Thus, these results were deemed reasonable and satisfactory for the complex, dynamic impact post-soil interaction problem.

Table C-2. Average Force Comparison between Simulation and Test Nos. LFCB-1 and LFCB-2 at Post Displacements of 5, 10, 15, and 20 in.

Item	Average Force (kips)			
	at 5 in.	at 10 in.	at 15 in.	at 20 in.
Test No. LFCB-1	10.5	10.8	10.6	9.8
Test No. LFCB-2	11.1	11.6	11.2	10.0
Test Average	10.8	11.2	10.9	9.9
Simulation: Adaptive FEM-SPH Method	11.0	12.4	11.5	9.8

Qualitative comparisons focused on pile deformations during bogie impact and on permanent set after each test. Post-impact photographs from test nos. LFCB-1 and LFCB-2 were compared with images from the simulation, as shown in Figure C-3. This comparison indicated that the computational model appears to predict global behavior well, as ascertained via a study of deformed shapes and the location of regions where local buckling and plastic material response were observed. When the final deformed shape of the pile was compared to model predictions, as shown in Figure C-3, largely similar permanent set and localized plastic deformations were observed.

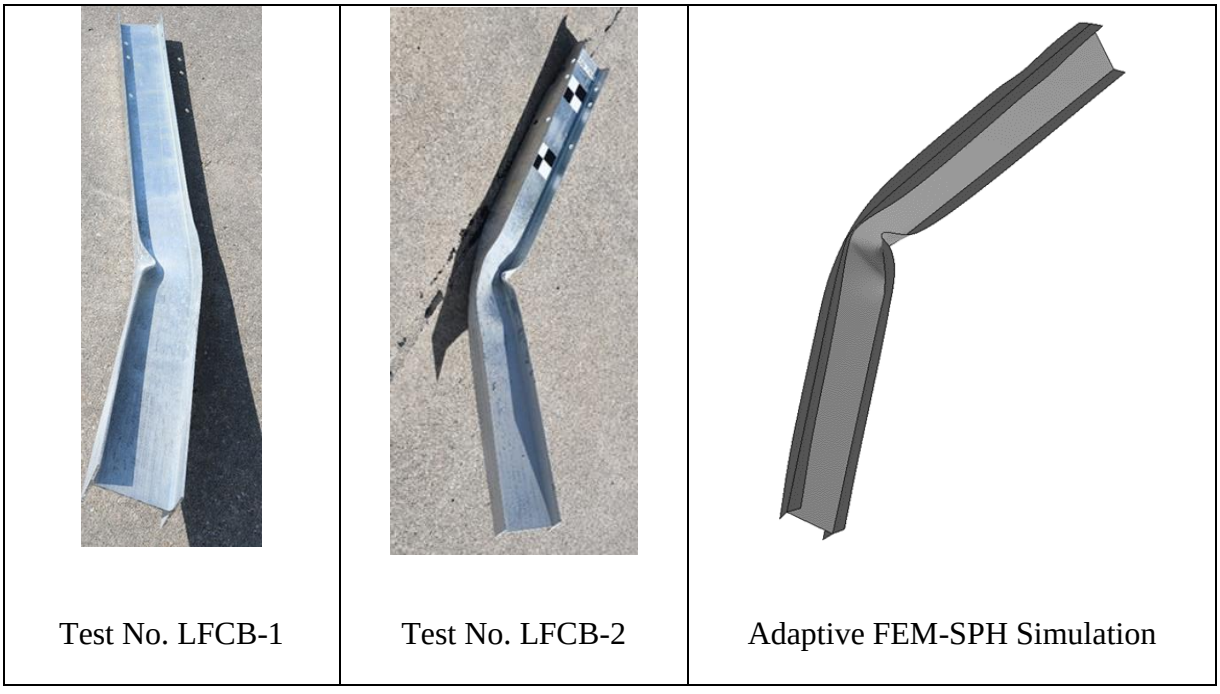

Test No. LFCB-1 | Test No. LFCB-2 | Adaptive FEM-SPH Simulation

Figure C-3. Post-Impact Photographs of Buckled W6x8.5 Steel Post, Physical Impact Test (i.e., Test Nos. LFCB-1 and LFCB-2) and Simulation using Adaptive FEM-SPH Method

C.4.3. Discussion of Results

The maximum dynamic bending moment produced by the lateral impact exceeded the yield moment of the post section, as shown in Figure C-4. As such, the lateral impact capacity of a W6x8.5 post (with embedment depth of 36 in.) embedded in MASH strong soil was primarily governed by the post characteristics. This type of failure mechanism was the so-called "flexible" or "long" pile mechanism in traditional geotechnical engineering. As shown in Figure C-4, a plastic hinge was formed. Hence, the impact resistance of the post-soil system was dependent on the dynamic yield moment of the post. This dynamic yield moment was reached before full mobilization of the dynamic soil resistance.

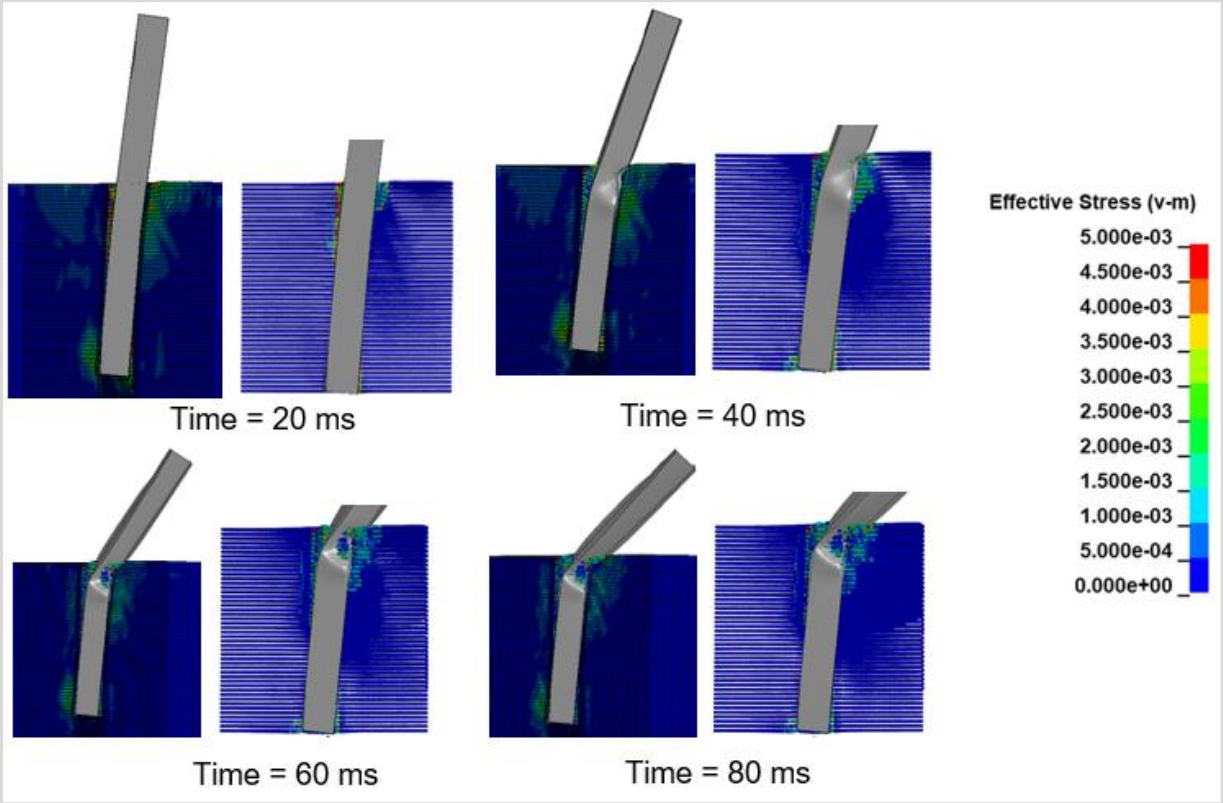

Figure C-4. Stress Distribution within MASH Soil in Laterally Impacted W6x8.5 Post

C.5. Modeling Test Nos. LFCB-3 and LFCB-4 Using Adaptive FEM-SPH Method

A numerical simulation of a bogie impacting a 64-in. long, W6x8.5 steel post embedded in stiff MASH strong soil was conducted to assess the predictive capability of the adaptive FEM-SPH technique for modeling reduced embedment depth response. Test nos. LFCB-3 and LFCB-4, which were conducted on a W6x8.5 steel post with a reduced embedment (i.e., 32 in.) and embedded in stiffer MASH strong soil were selected for comparison purposes. The following sections provide comparisons between simulated and physical impact tests and a discussion of results.

C.5.1. Model Geometry, Setup, and Initial Conditions

Computational model geometry, set-up, and initial conditions for 64-in. long, W6x8.5 steel post embedded in stiff MASH strong soil are shown in Figure C-5. The post was embedded 32 in. into stiff MASH strong soil and the volume was modeled with the adaptive FEM-SPH method.

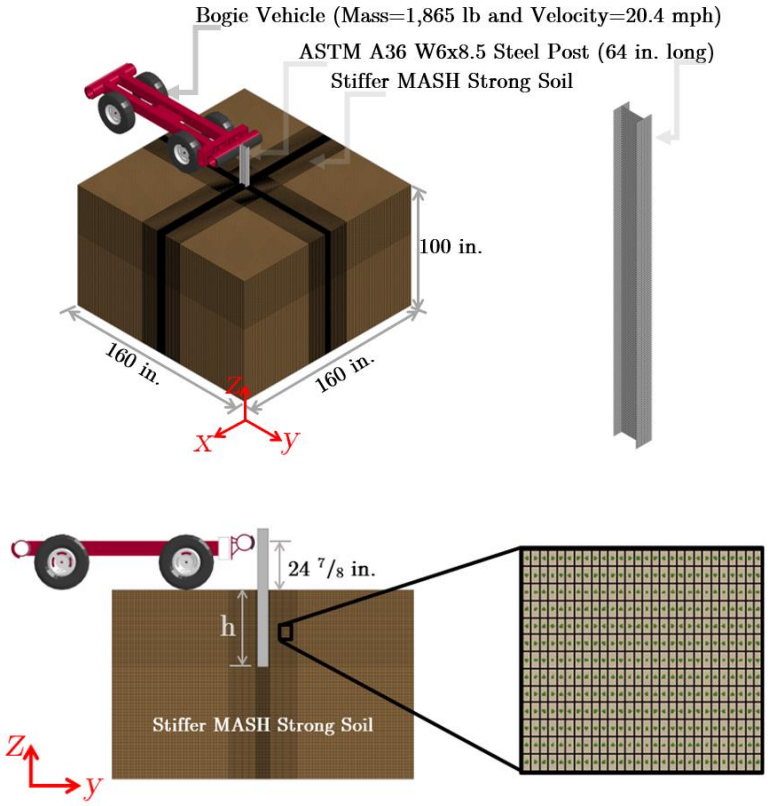

Figure C-5. Computational Model Geometry, Set-Up, and Initial Conditions of W6x8.5 Post Embedded in MASH Strong Soil with Embedment h = 32 in.

C.5.2. Comparison Between Simulated and Physical Impact Test

Simulation results were compared against results from test nos. LFCB-3 and LFCB-4 as shown in Figure C-6. Comparisons were focused on force vs. displacement, energy vs. displacement, and average force vs. displacement responses. Good agreement between the simulated and experimentally obtained responses can be observed in Figure C-6. The numerical model captured well the experimentally measured responses of the post-soil system.

An average impact force comparison at 5, 10, 15, and 20 in. of post displacement at the impact point was used to assess the accuracy of the computational technique. Average force comparison between test nos. LFCB-3 and LFCB-4 and simulation is provided in Table C-3.

The average forces at post displacements of 5, 10, 15, and 20 in. from the numerical simulation were within 4.2%, 7.4%, 6.7%, and 6.3%, respectively, when compared to the average

(average forces) of the impact tests. The simulation forces agreed with physical impact test results with a maximum error of 7.4% at a post displacement of 10 in.

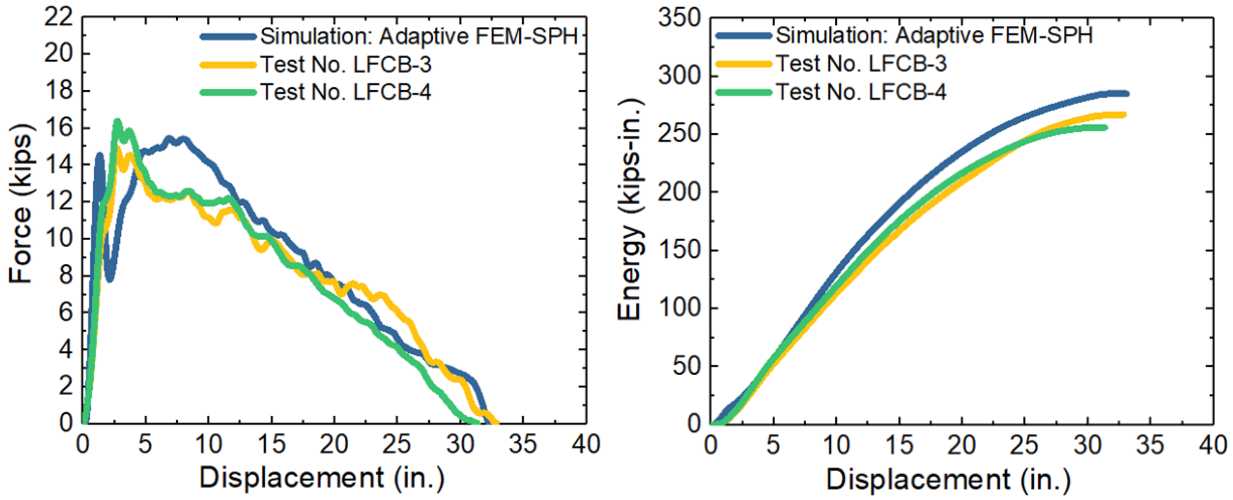

(a) (b)

Figure C-6. Comparison of Simulated and Physical Impact Test Results: (a) Force vs. Displacement; and (b) Energy vs. Displacement

Table C-3. Average Force Comparison between Simulation and Test Nos. LFCB-3 and LFCB-4 at Post Displacements of 5 in., 10 in., 15 in., and 20 in.

Item	Average Force (kips)			
	at 5 in.	at 10 in.	at 15 in.	at 20 in.
Test No. LFCB-1	11.6	12.0	11.7	11.0
Test No. LFCB-2	12.2	12.4	12.0	11.1
Test Average	11.9	12.2	11.9	11.1
Simulation: Adaptive FEM-SPH Method	11.4	13.1	12.7	11.8

Qualitative comparisons focused on the dynamic response of a pile-soil system during bogie impact. Figure C-7 shows the comparison and indicates that the computational model appears to predict global behavior well as ascertained via a study of post-impact pile behavior where the elastic response of the pile was observed. When the final deformed shape of the pile was compared to model predictions, as shown Figure C-7, largely similar post-impact responses between the impact test and simulated test were observed.

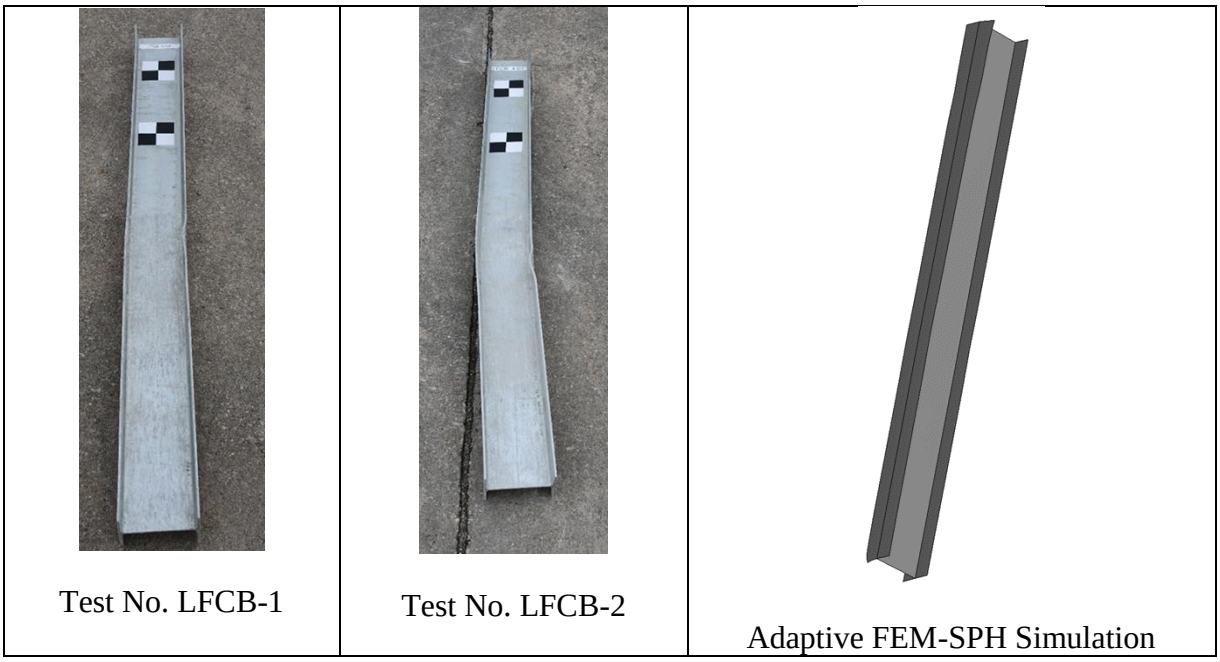

Figure C-7. Post-Impact Photographs of Buckled W6x8.5 Steel Post, Physical Impact Test (i.e., Test Nos. LFCB-1 and LFCB-2) and Simulation Using Adaptive FEM-SPH Method

C.5.3. Discussion of Results

As shown in Figure C-8, the dynamic impact response of a 68-in. long, W6x8.5 ASTM A992 steel post embedded in a stiff MASH strong soil was primarily governed by soil failure rather than post yielding. The maximum dynamic yield moment in the post was smaller than the yield moment of the post section. Thus, rigid rotation occurred, as illustrated in Figure C-8. Besides, Figure C-8 shows the stress distributions at each time-sequential in the MASH strong soil, represented by the solid elements and SPH particles on the left side. In contrast, the stress distribution pattern in the SPH soil particles that replaced the eroded solid soil elements is illustrated on the right side.

The lateral impact load on the post was initially carried by the soil close to the ground surface, as shown in Figure C-8. After the initial phase of lateral impact loading, the soil close to the ground surface deformed plastically and transferred the lateral impact load to the entire post embedment. Soil failure occurred when the ultimate lateral dynamic resistance of the soil along the length of the post was exceeded, as shown in Figure C-8. The post rotated about the center of rotation point, resulting in dynamic soil resistance to the front of the post below the rotation point and behind the post above the rotation point. Eventually, the W6x8.5 post failed by rotation when the resistance of the soil above and below the rotation point was exceeded, as illustrated in Figure C-8.

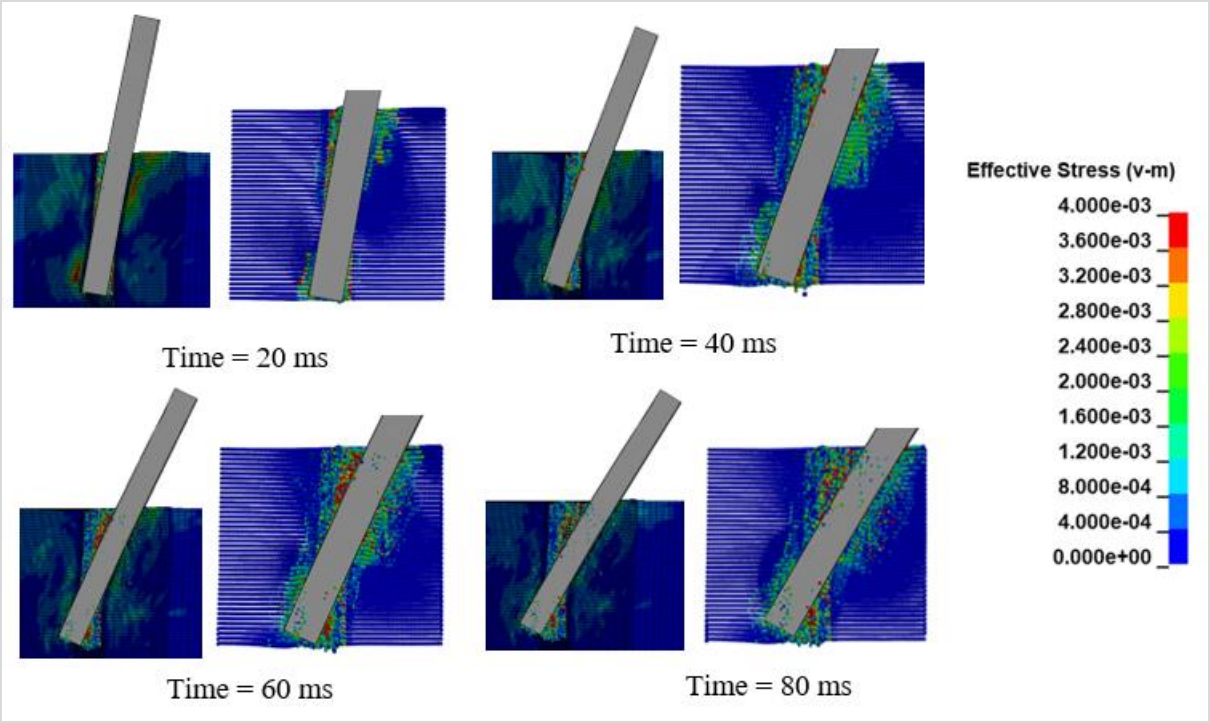

Figure C-8. Stress Distribution within MASH Strong Soil in Laterally Impacted W152x12.6 Post

C.6. Summary and Conclusion

A numerical simulation technique based on the adaptive coupling of FEM and SPH methods was employed for modeling the impact dynamics of posts embedded in stiffer MASH strong soil for test no. LFCB-1 through LFCB-4. An important aspect in evaluating the predictive capability of the adaptive FEM-SPH method was the accuracy of numerical simulation results in determining the force vs. displacement and energy vs. displacement responses of the post-soil system. Comparisons of results from simulation and physical impact tests were discussed. The results presented in this chapter allow the following conclusions to be drawn:

- The robustness, accuracy, and versatility of the adaptive FEM-SPH technique was successfully demonstrated for modeling shallower embedment (i.e., 32 in. and 36 in.) guardrail posts embedded in soil.

- It was found that the adaptive FEM-SPH technique can simulate both “long” or “flexible” and “short” or “rigid” post failure mechanisms.

- The dynamics of lateral impacts into post-soil systems can be modeled accurately with the adaptive FEM-SPH method. The simulated results highlighted the experimentally measured responses. The force vs. displacement and energy vs. displacement responses predicted by the adaptive FEM-SPH method proved to be within less than 10% of the physical impact test data for important range of actual performance. Overall, the percentage difference between the simulated test using the proposed method and

physical impact test were within post-soil impact testing variations observed between ant two similar impact tests.

- The presented results indicated the potential of the adaptive FEM-SPH method for the numerical analysis of the post-soil impact problem. The validated computational models can be used to study the effects of various parameters, including embedment depth, impact condition, and various soil conditions into the dynamic post-soil interaction problem.

The methodology presented in this chapter has been primarily demonstrated for modeling and simulating dynamic bogie testing of post-soil systems. Further research is needed to incorporate this method into full-scale, soil-embedded roadside safety structures to allow improved investigation into the influence of various factors, including soil properties, post embedment depths, terrain conditions, and other factors on soil-based roadside safety structures when subjected to vehicular impacts. Additionally, more work needs to be completed to numerically evaluate the dynamic impact response of full-scale, soil-embedded, roadside safety structures with slopes and high-water tables using the adaptive FEM-SPH method.

C.7 References

1. Luccioni, B., Aráoz, G., and Labanda, N., *Defining Erosion Limit for Concrete*. International Journal of Protective Structures, 4(3), pp. 315-340, 2013.

2. Johnson, G., Beissel, S., and Gerlach, C., *Another Approach to a Hybrid Particle-Finite Element Algorithm for High-Velocity Impact,* International Journal of Impact Engineering, 38(5), pp. 397-405, 2011.

3. Johnson, G., Stryk, R., and Beissel, S., *SPH for High Velocity Impact Computations*, Computer Methods in Applied Mechanics and Engineering, 139(1-4), pp. 347-373, 1996.

4. Yosef, T., *Development of Advanced Computational Methodologies and Guidelines for Modeling Impact Dynamics of Post-Granular Soil Systems*, Ph.D. Dissertation, University of Nebraska-Lincoln, 2021.

5. Saleh, M., and Edwards, L., *Evaluation of Soil and Fluid Structure Interaction in Blast Modelling of the Flying Plate Test*. Journal of Computers & Structures, 151, pp. 96-114, 2015.

6. Linforth, S., Tran, P., Rupasinghe, M., Nguyen, N., Ngo, T., Saleh, M., Odish, R., and Shanmugam, D., *Unsaturated Soil Blast: Flying Plate Experiment and Numerical Investigations*. International Journal of Impact Engineering, 125, pp. 212-228, 2019.

7. Cowper, G., and Symonds, P., *Strain Hardening and Strain-Rate Effects in the Impact Loading of Cantilever Beams.* Report No. 28, Brown University Division of Applied Mathematics, Providence, Rhode Island, 1957.

8. Schrum, K., Sicking, D.L, Faller, R.K., and Reid, J.D., *Predicting the Dynamic Fracture of Steel via a Non- Local Strain Energy Density Failure Criterion*, Final Report to Federal Highway Administration, MwRSF Research Report No. TRP-03-311-14, Midwest Roadside Safety Facility, University of Nebraska-Lincoln. 2014.

9. Meyer, D., Ammon, T.J., Bielenberg, R.W., Stolle, C.S., Holloway, J.C., and Faller, R.K. *Quasi-Static Tensile and Dynamic Impact Testing of Guardrail Components,* Report to the U.S. Army Surface Deployment and Distribution Command Traffic Engineering Agency, Transportation Research Report No. TRP-03-350-17, Midwest Roadside Safety Facility, University of Nebraska-Lincoln, 2017.

10. Belytschko, T., Lin, J., and Chen-Shyh, T., *Explicit algorithms for the nonlinear dynamics of shells.* Journal of Computer Methods in Applied Mechanics and Engineering, 42(2), pp. 225-251, 1984.

11. Yoshimi, Y., and Kishida, T., *A Ring Torsion Apparatus for Evaluating Friction between Soil and Metal Surfaces,* Geotechnical Testing Journal, 4(4), p. 145, 1981.

12. Uesugi, M., and Kishida, H., *Frictional Resistance at Yield between Dry Sand and Mild Steel,* Soils and Foundations, 26(4), pp. 139-149, 1986.

13. Homan, D., Thiele, J., Faller, R.K., Rosenbaugh, S.K., Rohde, J.R., Arens, S., Lechtenberg, K.A., Sicking, D.L., and Reid, J.D., *Investigation and Dynamic Testing of Wood and Steel Posts for MGS on a Wire-Faced, MSE Wall*, Final Report to the Federal Highway Administration, Research Report No. TRP-03-231-11, Midwest Roadside Safety Facility, University of Nebraska-Lincoln, 2012.

END OF DOCUMENT